Molecular mechanism of early metastatic breast cancer dissemination

Dissertation

zur Erlangung des Doktorgrades der Naturwissenschaften (Dr. rer. nat.)
der Fakultät für Biologie und Vorklinische Medizin der
Universität Regensburg

vorgelegt von

Hedayatollah Hosseini

aus Ahwaz, Iran

2016

Das Promotionsgesuch wurde eingereicht am

14.Dec. 2016

Die Arbeit wurde angeleitet von

Herr Prof. Dr. Christoph A. Klein

Untershrift:

Contents

1 Introduction

1.1 Metastasis

Metastasis is a multistage process during which malignant cells spread from the primary tumor to distant organs (Récamier, 1829; Talmadge and Fidler, 2010). Despite significant improvements in diagnosis and therapies, 90% of deaths from cancer are due to metastases that are resistant to conventional therapies (Fidler, 2003; Weigelt et al., 2005). Therefore, there are many gaps in our knowledge about metastasis. Understanding molecular players and processes involved in metastasis should lead to effective, targeted approaches to prevent and treat cancer metastasis.

During last decades many attempts have been allotted to unravel underlying mechanisms of metastasis and only few recent discoveries led to some mechanistic aspects of the process (Hanahan and Weinberg, 2011; Talmadge and Fidler, 2010; Valastyan and Weinberg, 2011). All molecular findings and supporting clinical data suggest a stepwise cascade for carcinoma invasion-metastasis including (1) local invasion of primary tumor cells through surrounding extracellular matrix (ECM) and stromal cell layers, (2) intravasation of cancer cells into the lumen of blood vessels, (3) surviving circulation within the vasculature, (4) arresting at distant organ sites, (5) extravasation into the parenchyma of distant tissues, (6) surviving in distant possible hostile microenvironments, and (7) reinitiating their proliferative programs at metastatic sites, in order to form micrometastases, and followed by generation of macroscopic, clinically detectable neoplastic growths (the step often referred to as ''metastatic colonization''; Figure 1) (Chaffer and Weinberg, 2011; Fidler, 2003; Valastyan and Weinberg, 2011). Since we are going to investigate mechanisms of dissemination in early and late course of tumour development, local invasion as the first distinctive step comes to the main focus.
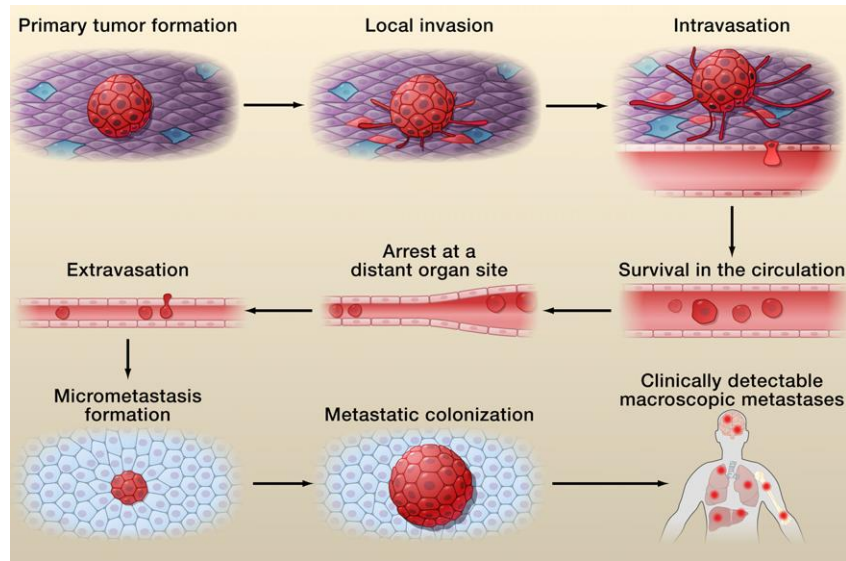
Figure 1. Cascade of metastasis. Clinically detectable metastases represent the end products of a complex series of cell-biological events, which are collectively termed the invasion-metastasis cascade. During metastatic progression, tumor cells exit their primary sites of growth (local invasion, intravasation), translocate systemically (survival in the circulation, arrest at a distant organ site, extravasation), and adapt to survive and thrive in the foreign microenvironments of distant tissues (micrometastasis formation, metastatic colonization). Carcinoma cells are depicted in red (Valastyan and Weinberg, 2011).

1.2 Local invasion and migration

During local invasion, cancer cells must acquire the ability to migrate and invade which implies an alteration in the genetic programs and phenotypic characteristics of cancer cells. In addition, cancer cells in the primary site are surrounded by a complex microenvironment comprising numerous cells including endothelial cells of the blood and lymphatic circulation, stromal fibroblasts and a variety of bone marrow-derived cells including macrophages, myeloid-derived suppressor cells, different types of monocytes and mesenchymal stem cells (Joyce and Pollard, 2009). It is increasingly apparent that crosstalk between cancer cells and cells of the neoplastic stroma is involved in the acquired capability for invasive growth and metastasis (Egeblad et al., 2010; Qian and Pollard, 2010; Joyce and Pollard, 2009; Kalluri and Zeisberg, 2006). Hence, local invasion on one hand depends on the phenotype and genotype of tumor cells and on the other hand is an outcome of crosstalk between cancer cells and microenvironment (Chiang and Massague, 2008).

Another component of tumor microenvironment is extra-cellular matrix (ECM). Interaction of ECM with cancer cells plays important role during local invasion and migration of cancer cells. When cancer cells grow at the primary sites, they interact with the adjacent ECM

and initiate binding via adhesion molecules (Hynes, 2002). Depending on the cell type and ECM substrate, focal contact assembly and migration can be regulated by different components of ECM such as integrins which connected the ECM to the cytoskeletons of cells (Friedl and Wolf, 2003). Suggesting, depending on the genotype of cells and composition of microenvironment, cancer cells can use different types of migration comprised of amoeboid and mesenchymal migration and in a singular or a multicellular process. Moreover, microinvasion can also happen as a result of protrusion of cells from the proliferative tumor (Friedl and Alexander, 2011).

When epithelial-derived tumors metastasize, the basal membrane is the first barrier that invading cells have to breach into. For breaching through the basal membrane, mechanisms and players all are conserved across species as well as cancer cells (Sherwood, 2006). Maybe the best characterized cell migration and invasion program shared between normal development and cancer is EMT (epithelial to mesenchymal transition) which is also conserved across species. The EMT emerged from abundant observations that demonstrated downregulation of E-cadherin in human carcinomas (Berx and van Roy, 2009), goes along with changes in the expression of genes encoding other cell-to-cell and cell-to-ECM adhesion molecules (Cavallaro and Christofori, 2004). These changes were found to confer abilities to invade, to resist apoptosis, and to disseminate (Hanahan and Weinberg, 2011; Mani et al., 2008; Polyak and Weinberg, 2009). This mechanism is similar to what was originally described for the normal early embryonic development (Micalizzi et al., 2010). Hence, it was not surprising when researchers found that molecular pathways classically associated with EMT, including Snail/Slug, Twist, Six1, Cripto, TGF-β, and Wnt/β-catenin, are highly conserved across species (Micalizzi et al., 2010; Nieto, 2013). Moreover, carcinoma cells that have passed through an EMT show stem-like state. It was speculated that stem cell character is critical in dissemination and launching new colonies of cancer cells in distant site (Chaffer and Weinberg, 2011).

1.3   Cancer stem cells in metastasis

A successful metastasis requires not only a local invasion, but also a property to support cancer cell growth in the primary site and the metastatic niche. Even among heterogeneous tumors only subsets of cells which are known as cancer stem cells (CSCs) support a proliferation hierarchy (Beck and Blanpain, 2013). They are defined as cancer cells able to initiate tumor growth in host

organs and differentiate into non-CSC (Clarke and Fuller, 2006; Palmer et al., 2012). The current CSC concept holds that disease relapse and later progression is largely due to the intrinsic therapy resistance of CSC, and. therefore, a successful eradication of cancer is only possible if the applied therapies are able to target CSC (Gupta et al., 2009).

There are several reasons that favor the view that cancer stem cells are the main migratory population in the primary site and the ultimate metastatic cells in the distant site: (1) Metastases of most carcinomas recapitulate the hierarchy and organization of their primary tumours (Brabletz et al., 2005); (2) Cells that have undergone EMT demonstrate CSC-like characteristics (Chaffer and Weinberg, 2011). It has also been shown that CSC spontaneously undergo Mesenchymal-Epithelial Transition (MET) which helps extravasation in the distant sites (Mani et al., 2008); (3) Signaling pathways regulating stemness (e.g. Wnt/β-catenin) are selectively expressed in the migratory front of tumors (Brabletz et al., 2005); (4) Migration of stem cells not only has a pivotal role during embryogenesis, but adult stem cells (also known as tissue stem cells) can also increase their migratory activity when their microenvironment is altered. For example, these cells play a key role in tissue damage repair - tissue injury activates developmental programs by activating adult stem cell migration to the site of damage (Imitola et al., 2004; Scadden, 2006); (5) It has frequently been observed that metastatic cells are carrying stem cell signatures. For example in breast cancer it was shown that there was similarity between gene expression profiles of breast cancer stem cells and the normal mammary stem cells (MaSCs). Interestingly, the stem cell phenotype is dominant in the metastatic lesion and disseminated cancer cells (Balic et al., 2006; Lawson et al., 2009). Therefore, it may be a plausible hypothesis that metastatic cancer cells are stem like cells.

1.4   Mammary gland development and breast cancer

The mammary gland, which distinguishes mammals from all other animals, works as an organ to produce and secrete milk for nourishing offsprings. The full development of this organ happens after birth (Inman et al., 2015). Terminal end buds (TEBs) are the main structures seen at the birth. TEBs are club-shaped structures comprising an outer layer of cap cells and a multilayered inner core of cells called body cells, appear at the tips of the ducts and start to invade the fat pad. After birth, mammary development is arrested until puberty, when extensive elongation of the

ducts and secondary branching takes place. Upon hormonal induction during puberty, proliferation within the TEBs results in ductal elongation and lumen formation. Consequently, TEBs disappear because of the limits of the fat pad space and ceasing of growth (Watson and Khaled, 2008).

The tissue architecture of mammary gland consists of different cell types: epithelial cells that form the ductal network of the gland; adipocytes, which constitute the fat pad and in which the ductal network is embedded; vascular endothelial cells, which make up the blood vessels; stromal cells, including fibroblasts; and a variety of immune cells. The epithelium in the mammary gland can be divided into two types: luminal and basal. The luminal epithelium forms the ducts and the secretory alveoli, whereas the basal epithelium consists essentially of myoepithelial cells (Sternlicht, 2005). These two types of epithelium form a bi-layered structure of simple epithelium that is embedded within the fatty stroma (Figure 2; (Watson and Khaled, 2008)). Comparative molecular studies of different normal mammary epithelial gene expression signatures and different subtypes of breast cancer have suggested that distinct cells of origin may give rise to the different subtypes (Visvader and Stingl, 2014).
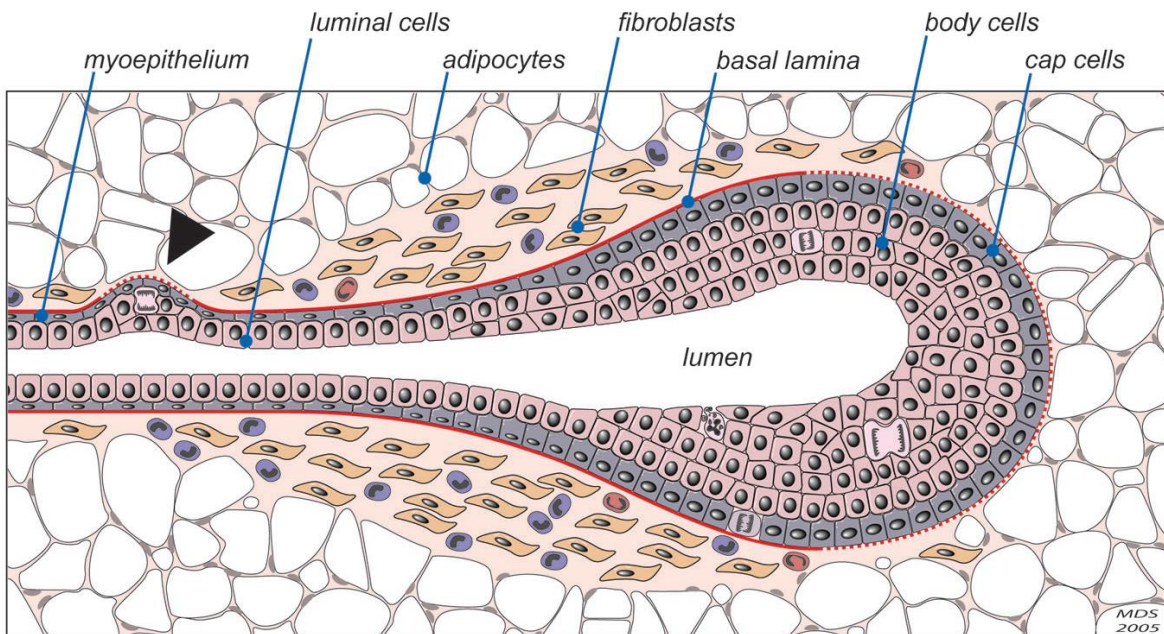
Figure 2. **Schematic diagram depicting the salient architectural features of TEBs and their subtending ducts, including their fibroblast-rich stromal collar and high mitotic index.** Though there is no evidence that normal ductal cells ever cross the basal lamina, thinning of the basement membrane (dotted lines) does seem to occur at the tips of invading ducts as a result of their partial enzymatic degradation and/or incomplete *de novo* synthesis. Stromal macrophages and eosinophils are also depicted (Sternlicht, 2005).

Extensive lineage tracing studies in mammary gland have been performed to define mammary stem cell (MaSC) population. The latest results suggested that the pubertal gland contains several different stem and progenitor cell populations, including bipotent stem cells that give rise to both the luminal and myoepithelial cells of the duct, or mono potent which give rise to luminal and alveolar cells alone.(Inman et al., 2015). The importance of MaSC became evident when it was seen that the MaSC/basal signature is most closely aligned with the expression profile of more aggressive subtypes of breast cancer (Shehata et al., 2012). Interestingly, mouse MaSCs are ER/PgR negative, and are localized in the basal compartment of mouse mammary epithelium in close proximity of ER/PgR positive mature luminal epithelial cells. It has been suggested that MaSCs need hormone receptor expressing cells for their expansion (Asselin-Labat et al., 2006).

Progesterone, estrogen and their nuclear receptors play essential roles during mammary gland morphogenesis. However, they are differently acting on mammary epithelial cells. While estrogen is mostly responsible for elongation of ducts (Ciarloni et al., 2007), progesterone induces side branching and expansion of epithelial structure into the mammary fat pad (Brisken, 2013). Progesterone induces mouse MaSC proliferation and expansion via RANKL (Figure 3; (Brisken, 2013; Joshi et al., 2010)). Furthermore, progesterone inhibits tight junction formation and terminal differentiation in mammary epithelial cells. The progressive reduction of PgR expression that occurs during late pregnancy has also been suggested to contribute to the onset of lactation and terminal differentiation of mammary epithelial cells (Ismail et al., 2002). It has been speculated that the impact of progesterone on MaSCs expansion and proliferation targets them for further cell transformation events leading to breast cancer (Joshi et al., 2010). The expansion of the MaSC pool by progesterone has been also suggested as underlying mechanism of the observation that menstrual cycling predisposes to breast cancer (Asselin-Labat et al., 2010).
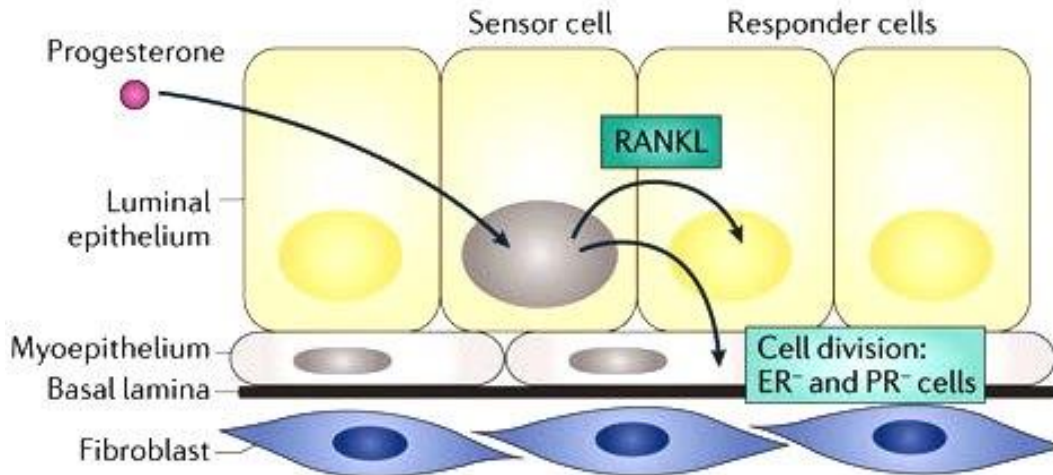
Figure 3. Models of cell-intrinsic and paracrine mechanisms of progesterone induced cell proliferation in the mouse mammary epithelium. A hormone receptor (HR)[+] cell is indicated by a grey nucleus. Progesterone induces the expression of receptor activator of nuclear factor-κB (NF‑κB) ligand (RANKL) secretion, which triggers the proliferation of adjacent HR^{−} cells. (Brisken, 2013).

Steroid hormone receptors, PgR (progesterone receptor) and ER-α (estrogen receptor alpha) also serve as markers of breast cancer subtypes. These subtypes were originally identified by gene expression studies, which confirmed the fundamental distinction between hormone receptor positive and negative cancers. Nuclear hormone receptor negative subtypes comprise triple-negative cancer (negative for HER2/ERα/PgR), the basal-like subtype, and cancers with Her2 gene amplification. Nuclear receptor positive subtypes comprise the luminal types which are further divided into luminal A and B (Bombonati and Sgroi, 2011) and form the majority of breast cancers. Luminal A tumours express ERα and/or PgR and differ to luminal B with higher proliferation rate (as frequently assessed by Ki-67 staining) or HER2 expression levels. Patient prognosis differs for various subtypes. Luminal A subtype has an overall good prognosis, and can be treated by hormone therapy. Her2-amplified breast cancers have a poor prognosis and are treated by targeted therapy using trastuzumab or lapatinib. However, no specific therapy is currently available for the other subtypes, although the prognosis of basal and luminal B tumors is poor (Adelaide et al., 2007; Bombonati and Sgroi, 2011; Williams et al., 2009).

Her2 and triple negative breast cancer are enriched with stem-like (May et al., 2011; Velasco-Velazquez et al., 2011). Consistently, it was shown that expression of Her2 induces stemness in mammary epithelial cells (Ginestier et al., 2007; Korkaya et al., 2008), which is partly mediated via the canonical NF-κB pathway and RANKL (Liu et al., 2010a). RANKL is a direct regulated target gene of progesterone (Brisken, 2013). Moreover, it was shown that

progesterone and its receptor modulate Her2 signalling and induce Her2 nuclear translocation (Beguelin et al., 2010). Therefore, progesterone on one hand regulates mammary gland side branching and migration of epithelial cells into the fat pad and on the other hand may regulate stemness in a crosstalk with Her2.

1.5   Early versus late dissemination of cancer cells

Until to date, many functional studies addressing mechanisms of metastasis used cell lines derived from advanced tumours or metastases. This appears to be justified as long as late metastatic dissemination from large tumours is the prevailing concept of metastasis (Fearon and Vogelstein, 1990; Hanahan and Weinberg, 2000). The late dissemination model holds that the majority of aberrations accumulate within the primary tumour before additional genetic hits lead to metastatic spread (Fearon and Vogelstein, 1990; Jones et al., 2008). Though intriguing at first sight this concept is inconsistent with some clinical and experimental observations. For example, it is well known that small tumours can indeed seed metastases and T1 stage (i.e. small) tumours diagnosed with metastasis at primary presentation are not such a rare event in clinical settings. Since it has been convincingly deduced from large epidemiological and imaging studies of breast cancer that growth of metastases takes several years (Engel et al., 2003), T1M1 (patients already diagnosed with primary tumours and suffering metastasis) stage cancers must have seeded cells when they were composed of less than $10^5 - 10^6$ tumour cells (Klein and Holzel, 2006). In addition, "cancer of unknown primary", a condition where metastasis is detected in the absence of a detectable primary tumour, comprises about 5% of all hospitalized cancer patients, and therefore is as frequent as esophageal cancer (Abbruzzese et al., 1994; van de Wouw et al., 2002). Therefore, cancer cells should have departed the primary lesion very early and before the acquisition of fully malignant phenotypes.

More empirical evidences come from the analysis of DCCs isolated from bone marrow before and after manifestation of metastasis. Genetic data indicated that DCCs from the two stages (M0, without metastasis, and M1, with metastasis) of metastatic spread differ (Klein et al., 2002; Schmidt-Kittler et al., 2003) and it was suggested that they might have disseminated early and evolved in parallel to the primary tumor (Figure 4; (Klein, 2009)). Subsequently, studies in transgenic mouse models (Eyles et al., 2010; Hüsemann et al., 2008; Rhim et al., 2012) and in

patients with in-situ carcinomas (Banys et al., 2012; Hüsemann et al., 2008; Sanger et al., 2011) corroborated this concept.
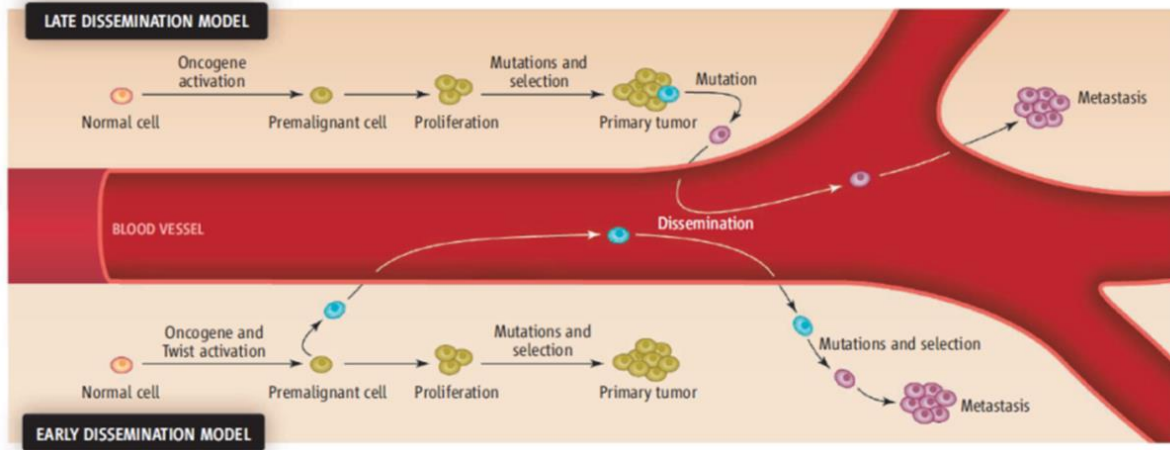
Figure 4. Evolution of malignancy. (Top) The late metastasis model places selection of genetic and epigenetic alterations mostly inside the primary tumor. If so, late-disseminating cells are genetically similar to the primary tumor, which can be used as a surrogate marker to choose a drug against disseminated tumor cells. (Bottom) By contrast, early-disseminated tumor cells accumulate such alterations at distant sites and diverge genetically from the primary tumors. Consequently, they may respond differently to drugs that are administered systemically (Klein, 2008).

1.6 Balb-NeuT as a mouse model for early dissemination

The ERBB2 (also known as HER2) receptor is a tyrosine kinase receptor that belongs to the epidermal growth factor receptor (EGFR) family. The rat homologue of the *ERBB2* gene is called the *NEU* gene and was originally identified from chemically-induced neuroblastomas1 (Schechter et al., 1984). Amplification of *ERBB2* has been observed in 20–30% of sporadic human breast cancers and, correlates with poor patient outcome (Slamon et al., 1987; Slamon et al., 1989). HER2 overexpression and amplification is also seen in subsets of gastric, esophageal, and endometrial cancers and also associated with poor prognosis (Mimura et al., 2005; Morrison et al., 2006; Yano et al., 2006). Moreover, when breast cancer patients with *HER2* amplification were treated with trastuzumab (Herceptin), a neutralizing monoclonal ERBB2 antibody, prolonged disease-free survival were observed when compared to control patients (Robert et al., 2006).

After first hints indicated a prominent role of Her2 in breast cancer, transgenic animal models for study breast cancer related Her2 subtype were generated. Transgene regulation via the

mouse mammary tumour virus-long terminal repeat (MMTV-LTR) promoter was ideally suited for this purpose, as it directs the high-level expression of a transgen specifically in the mammary epithelium (Sinn et al., 1987). These attempts resulted in different ERBB2-driven breast cancer murine models with different growth kinetics of tumors. It was speculated that these differences are due to the type of insert (wild type or activated mutant form), the background of host strains and some technical differences such as insertion site and copy number of inserts (Ursini-Siegel et al., 2007).

The over-expression of wild type *Neu* resulted in mammary tumors with a long latency about 1 year (Muller et al., 1988). Thus, researchers shifted to the use of an activated form of *Neu* (NeuT). The first NeuT mice were generated by Philip Leder's Group in FVB mouse strain (Muller et al., 1988). Tumors of this model were arising in a stochastic fashion in different organs other than mammary gland and, therefore, Libero Clerici's group tried to overcome that problem by changing vector construct and strain of mice. They changed to CD1 strain and generated a new NeuT model, but tumor onset was not similar in the following generations as well as some problems in the fertility of transgenic mice (Lucchini et al., 1992). Guido Forni's group developed the Balb-NeuT mouse model for the first time by breeding transgenic CD1 random-bred breeder male mouse with BALB/c females (Boggio et al., 1998). They generated a BALB/c background mouse model carrying the mutated rat HER-2/neu oncogene (Tg-NeuT; amino acid 664 Val→Glu) driven by the MMTV promoter. This mouse model is known as one of the fastest Her2-driven breast tumor forming model (Figure 5) with a constant onset of tumors in offsprings and little involvement of other organs. However, MMTV–NEU mice models serve not only as a simple breast cancer model, but also many studies used and are using these models in concert with additional transgenic animals, to identify key candidate genes and correlated signaling involved in various biological processes in tumor biology (Ursini-Siegel et al., 2007).
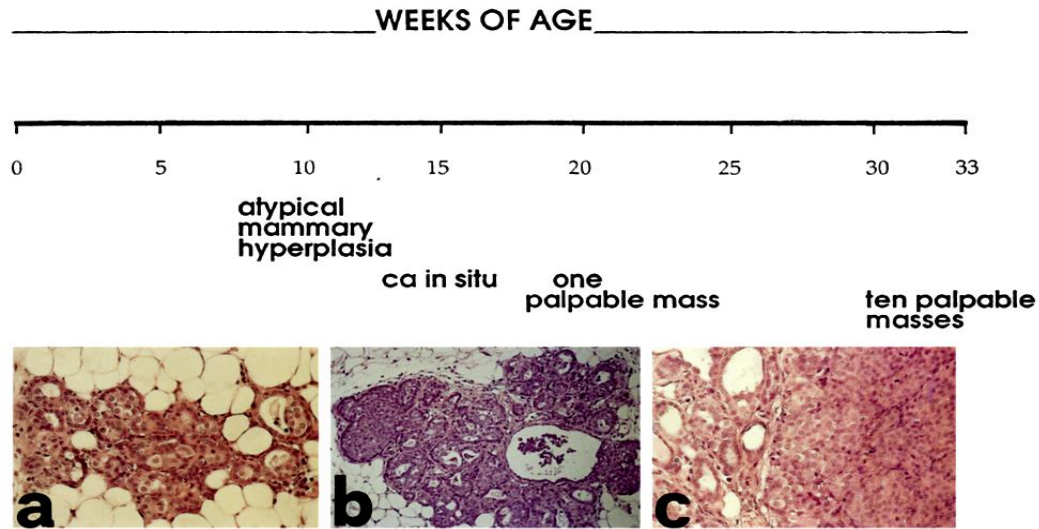
Figure 5. Progression of HER-2/*neu* carcinogenesis in untreated Balb–NeuT. Histology shows that ductular atypical hyperplasia (*a*) is already evident and widely distributed in all mammary glands at 3 weeks of age. This hyperplasia progresses to carcinoma in situ (*b*) between weeks 13 and 17, and then to an invading lobular carcinoma (*c*) (Boggio et al., 1998).

1.7 Aim of work

Although, many studies support the concept of early dissemination of cancer cells, the concept of parallel progression of primary tumors and metastasis is still under debate (Valastyan and Weinberg, 2011). That is because experimental data derived from cell lines suggest metastasis to be a consequence of increasing aggressiveness and loss of differentiation, acquisition of epithelial-mesenchymal transition and genetic deterioration. Therefore, it is unclear how early-disseminated, "normal-like" cancer cells should be able to successfully overcome critical metastatic steps (Valastyan and Weinberg, 2011) unlike late disseminating cancer cells thought to be similar to primary tumor cells. Based on previous data from the Balb-NeuT model and patients, this work aims to elucidate underlying mechanisms responsible for early dissemination of tumor cells in breast cancer.

In the Balb-NeuT model, we previously noted that dissemination was not only an early event but also observed that the frequency of DCCs in bone marrow did not increase with tumor size (Figure 6; (Hüsemann et al., 2008)).

17
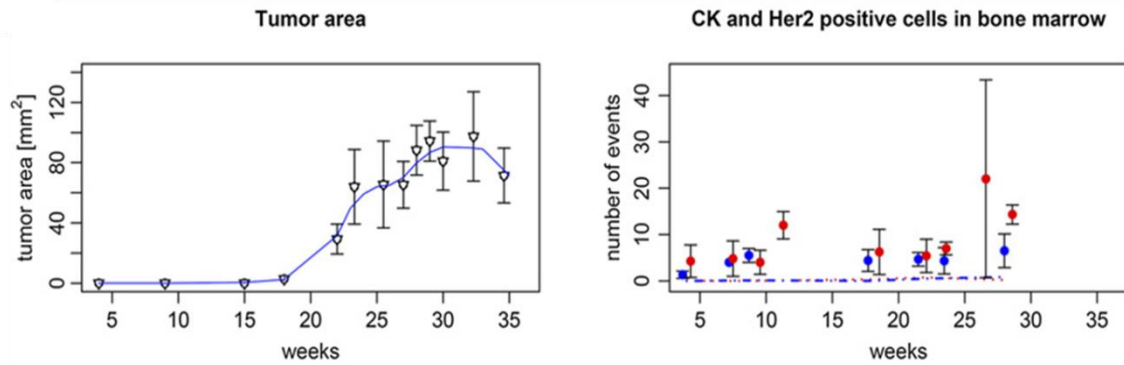
Figure 6. Progression of local and systemic disease in Balb-NeuT mice over time. Left panel: Increase of tumor area. Right panel: number of CK+ (red dots) and HER-2+ (blue dots) cells per 5 x 10^5 bone marrow. Number of disseminated cancer cells does not increase by increasing tumor size (Hüsemann et al., 2008).

The same was true for breast cancer patients, suggesting that both in mice and men seeding propensity is relatively (i.e. related to the number of tumor cells) lower in large as compared to small cancers. Moreover, even in breast cancer patients without histologically invasive cancers but pre-invasive lesions such as atypical ductal hyperplasia (ADH) or in situ carcinomas (DCIS), we could detect DCCs in bone marrow as in mice (Hüsemann et al., 2008). Therefore, this project was designed to address several critical questions in this regard:

1) How do breast cancer cells disseminate in very early stage before tumor manifestation?
2) To what extent are early disseminated cancer cells fit to colonize and form metastasis?
3) Which mechanism reduces metastatic seeding from advanced stages of cancer growth?
4) What is the relevance of our findings to human data and disease courses in breast cancer?

2 Materials and Methods

2.1 Methods

2.1.1 Animal Experiments

2.1.1.1 Maintenance

Balb-NeuT transgenic mice were obtained through collaboration with Dr. Guido Forni and maintained in our facilities according to the European Union guidelines. All animal experiments were performed according to the EU and national institutional regulations (Government of Upper Palatinate, 55.2-2532.1-27/14). Mice were screened at 3 to 4 weeks of age for hemizygosity (neuT$^+$/neuT$^-$), and negative littermates served as wild-type BALB/c mice controls. Mammary glands of Balb-NeuT female mice were inspected twice a week and arising tumors were measured in two perpendicular diameters.

2.1.1.2 Surgery

Mice were anaesthetized with Midazolam 5mg/kg, Fentanyl 0,05mg/kg, Medetomidin 0,5mg/kg i.p. Thorax and abdomen were shaved, and skin was incised from caudal to cranial region in the midline. For sphere injection experiments, 50 spheres (see section 2.1.3.4 for sphere generation) were mixed with matrigel (final concentration was 40%) and injected into the fourth right mammary gland of BALB/c mice. In case of tissue transplantation, a piece (approximately 1 mm^3) of donor mammary tissue from 4-week-old Balb-NeuT mice or PT (21-23 week-old) was implanted in the cleared mammary fat pad of recipient mice. The skin was closed by a suture using polygelatin string and anesthesia was antagonized with Flumazenil 0,5mg/kg, Atipamezol 2,5mg/kg, Naloxon 1,2mg/kg s.c.. Postoperative analgesia was achieved by Buprenorphin (0,1 mg/kg) s.c.. Curative surgery or sacrifice of mice was done when the diameter of tumors was between 5-10 mm.

2.1.1.3 Mice dissection

Mice were sacrificed by asphyxiation with CO_2 or by cervical dislocation. The organs of interest were either embedded in paraffin (see section 2.1.1.5 for paraffin embedding tissue) or used for snap freezing (see section 2.1.1.6 for tissue snap frizzing). The following organs were preserved for the later immunohistochemical analysis: 1) mammary glands, 2) tumors, 3) lungs, 4) liver and 5) spleen. Bone marrow was prepared by the protocol described in the next section (section 2.1.1.4).

2.1.1.4 Bone marrow preparation for staining

Tibias and femurs were collected either from BALB/c or Balb-NeuT in PBS or basal medium. The soft tissue surrounding the bones was removed. Epiphyses were cut with scissors to flush out the bone marrow. Using a 26G needle and 1 ml syringe the bone marrow was flushed out into a 50 ml tube. Alternatively, for some experiments the flushed bones were put into a mortar to break the bones using mortar and pestle. The broken bones were washed with 1x PBS to collect the remaining bone marrow cells after flushing. Afterwards, the cells were pooled and centrifuged at 200x g for 10 min. The supernatant was discarded and the pellet was resuspended in 9 ml of 1x PBS. The cell suspension was slowly and carefully overlaid onto 6 ml of 65% percoll in a 15 ml tube to form a layer and centrifuged for 20 min at 1000x g to remove erythrocytes. The interphase was then carefully collected using a 5 ml pipette and transferred into a new 50 ml tube. The tube was filled up with 1x PBS and centrifuged for 10 min at 500x g for washing the cells. The cells were resuspended in 5 ml of 1x PBS and counted. Finally, 5×10^5 cells were dropped on adhesion slides.

2.1.1.5 Extent of dissemination relative to tumour area

Data were taken from reference (Hüsemann et al., 2008). Briefly, gland/tumour areas were calculated from 270 mammary glands/tumours of 27 mice assuming the shape of an ellipse/circle for each tumour. The tumour area of mammary glands without palpable (i.e. not measurable by a caliper) tumours was set to 0.1 mm^2 (i.e. assuming a diameter of 350 µm of a total, circular hyperplastic lesion within a mammary gland) for lesions from week 4 to week 9 old mice and 0.4 mm^2 for week 11 mice. The adjustment for week 11 was based on a microscopic evaluation

revealing an about fourfold increase in hyperplastic lesions. CK positive cells from 27 mice were calculated as the mean of single disseminated cells per 10^6 BM cells.

2.1.1.6 Paraffin embedding of murine tissue samples

The dissected tissue samples were fixed in a 4% paraformaldehyde (PFA) solution for 12 h. Following fixation, the samples were washed 3 times in 1x PBS. The major obstacle during the tissue sectioning represents residual water in the embedded tissue. Therefore, dehydration of the paraffin embedded samples was achieved by series of washing steps in alcohol (70%, 85% and 100% ethanol, each step 1 hour). Then the fixed and dehydrated tissue was washed twice for 30 min in 100% xylene. This step serves not only the removal of alcohol from the tissue, but also facilitates the penetration of the paraffin during the subsequent embedding. After three incubation steps with paraffin (parablast embedding media), tissues were embedded. Paraffin embedded tissue is stored at room temperature.

2.1.1.7 Tissue snap freezing

Tissue were labeled appropriately and packed in aluminum foils. Then, they were drawn in 50 ml falcon filled with 2-methyl butane. Falcon tube has carefully been placed into the liquid nitrogen. Complete freeze is achieved at ~60 seconds (90 seconds maximum for larger specimens). Finally, samples were removed and stored in -80^{0}C freezer. These samples have been used for RNA extraction or IHC staining.

2.1.2 Laser Microdissection and microarray analysis

Laser microdissection was performed to dissect metastatic lesions from lung, primary tumors, epithelial layers of mammary glands of Balb-NeuT mice at the time point of EL, and BALB/c mice at different age. Small pieces summing up to 10^5 μm^2 for each sample were catapulted into a cap with 10 μl paramagnetic oligo-dT bead suspension and lysis buffer. The extraction of mRNA and microarray experiments were performed as described previously (Hartmann and Klein, 2006).

2.1.3 Cell culture experiments

2.1.3.1 Cell lines

All used cell lines, characteristics and media are listed in section 2.2.8. Cell lines were preserved in liquid nitrogen in appropriate medium containing 5% DMSO. They were propagated until 70% confluence apart from the cases when the experimental strategy implied differently. Cell lines were detached using Trypsin/EDTA and re-plated in an appropriate cell density. All cells were incubated at 37°C with 5% CO_2 and were routinely tested for mycoplasma and were found to be negative.

2.1.3.2 Cell culture treatments

Steroid hormones (progesterone, aldosterone, β-estradiol, testosterone, and hydrocortisone) were dissolved in ethanol. Rankl and Wnt4 were dissolved according to the manufacturer's instructions. Cells were cultured 24 hours before treatment in appropriate densities. The desired concentration of that given hormone or factors were prepared in fresh media and added to the cultured cells only after cells were washed 2 times with PBS. These treatments were repeated for three times in each 24 hours interval. Cells were washed 2 times with PBS and fresh media containing additives were added. Three hours after last treatment, cells were washed 2 times with PBS and harvested with cell scraper for RNA or protein extraction.

2.1.3.3 Cell density experiments

TUBO cells were cultured in 3 x 10^4 cells/cm^2 for high density and 5.2 x 10^3 cells/cm^2 for low density experiments. PT primary cells were cultured in 10.6 x 10^4 cells/cm^2 for high density and 2.2 x 10^3 cells/cm^2 for low density experiments. Criterions for human cell lines, was 100% confluency for high density and 20-30% confluency for low density. For hormone treatment and comparisons between low and high density experiments, cells were incubated for 76 h and fresh hormone treatment as well as washing (PBS 2x) was done in 24 h intervals. I avoided changing medium and washing steps during incubation of cells when miRNA analyses were aim of experiment. In migration experiments 10^4 cell/well were seeded (24 well migration chambers) for low density and 5 x 10^4 cell/well for high density. For migration experiments (see section 2.1.5) low density was 1 x 10^4 cells per well (24 well plate) and high density was 5 x 10^4 cell per well.

For sphere culture experiments (see section 2.1.3.5) low density was 10^3 cells/ml and high density was 10^4 cell/ml.

2.1.3.4 Primary cultures

Mammary glands were collected either from BALB/c or Balb-NeuT in a 50 ml tube with PBS. The tissue was minced with surgical blades to small pieces and digested in basal medium (DMEM/F12, 100 nM HEPES buffer, 10 mg/ml insulin, 0.5% BSA and 0.5x penicillin/streptomycin) with 200 U/ml collagenase, 10 ng/ml EGF and 200 U/ml hyaluronidase. The tissue was digested for 1.5-2 hours at 37° C in the incubator mixed every 1 hour. The digested tissue was transferred to a 50 ml tube. After a first centrifugation step of 1 min at 80 g to isolate the organoids the supernatant was collected into a new 50 ml tube and centrifuged at 200 g for 3 min to isolate mammary epithelial cells (MEC) which are in the pellet fraction. The supernatant consist of fibroblastic cells. Cells were re-suspended in DMEM medium (for primary 2D culturing) or basal medium (for sphere culturing), counted and cultured in appropriate densities in plates.

2.1.3.5 Sphere culture

The epithelial cells isolated after digestion were re-suspended in basal medium and subsequently cultured in a density of 5×10^4 cells/ml in ultra- low adherent plates coated with 1.2% poly-HEMA. Sphere culture medium was basal medium supplemented with 2% B27, 10 µg/ml EGF, 10 ng/ml bFGF, 20 ng hIL6 (a gift of Dr. Stefan Rose-John Christian-Albrechts-University, Kiel, Germany), 4 ng/ml heparin, 5 ng/ml Gro-α, and in case of progesterone treatment with 10 nM progesterone. Sphere cultures were incubated at 37°C with 5% CO_2 and 7% O_2 and spheres were screened after 10 days. Size and number of mammospheres was inspected under light microscope and measured using Zeiss Axiovision software after 10-14 days.

Sphere assay for cell lines was performed similarly. Cultured cells were tripsinized and dissociated to single cell suspension. Then, cells were re-suspended in basal medium and seeded in appropriate densities in poly-HEMA coated plates. Size and number of spheres was inspected under light microscope and measured using Zeiss Axiovision software after 3-5 days.

2.1.3.6   Preparation of poly-HEMA and low attachment plates

To prepare coating solution, 2.4 g of poly-hydroxy-ethyl-methyl-acrylate (poly-HEMA) were added to 20 ml of 95% ethanol and put on a shaker at 65° C to dissolve for ~8 hours. To the above dissolved poly-HEMA, 80 ml of 95% ethanol was added and mixed. The prepared solution could be stored indefinitely at 4° C. Poly-HEMA solution was added to the cell culture dishes at a final density of 0.8 mg/cm (w/v). The plates were dried overnight in a sterile hood with lids slightly opened. The poly-HEMA-coated plates can be stored indefinitely until use at +4° C.

2.1.3.7   Sphere counting

Spheres were counted after 10-14 days for primary cells and 3-5 days for cell lines. Only spheres with size bigger than 50 μm were counted. Sphere counting for cell lines were done by screening whole plates in10X magnification of microscope. In case of primary cell culture when number of spheres increased to thousand or more (i.e. progesterone or Wnt4/Rankl treatment), each plate were centrifuged in 1000 g for 5 minutes. Sphere pellet was resuspended in 1 ml PBS and 20 μl of sphere suspension was taken while pipetting was processing by 1ml pipettor. That was done in triplicates for each plate and the 20 μl sphere suspension were spread as one strip-line in the surface of one empty culturing plate. The average number of spheres in all strip-lines multiplied to factor 50 in order to estimate total number of spheres per plate.

2.1.3.8   Conditioned medium preparation

Cell media supernatant of confluent cultured cell has been collected in 50 ml tubes and centrifuged for 10 min at 1000xg to pellet cells and cell debris. The supernatant was sterile filtered through a 0.22 μm filter to remove any cells in the conditioned medium. The medium was used immediately or stored at -80° C until further use. Target cells for treatment were cultured 24 hours before.

2.1.3.9   Transwell assay

Transwell insert with a microporous membrane of 0.4 μm were used to separate the upper and lower compartments. The microporous membrane allows only soluble factors to pass through

between the compartments. EL cells were cultured in the lower chamber and PT cells were cultured in the upper chamber. Both were cultured in a density of 10^6 cells per well of 6 well plates (DMEM 10% FCS; Figure 7).
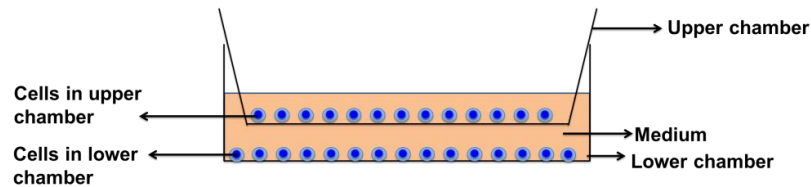
Figure 7. Schematic representation of transwell assay experimental setup.

2.1.4 Differentiation of mammosphere cells

Chamber slides were coated with a layer of 100 % matrigel. Then freshly isolated and digested single cells from mammary glands or primary tumors were seeded on the top of solidified Matrigel (Figure 8). The differentiation condition was as previously described (Debnath et al., 2003; Ghajar and Bissell, 2008). The formation of acini was monitored every 24 h for 4 weeks. The media was changed every 3 days. Additionally, a long time sphere culture was performed to evaluate differentiation. Spheres were kept in culture without passaging for 5 weeks but with adding fresh medium every week. The formation of acini like structures was used as criterion for differentiation. I recorded the time point when EL and PT cells formed acini structures upon control or progesterone treatment conditions.
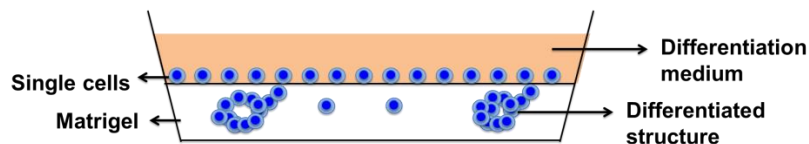
Figure 8. Schematic representation of differentiation assay experimental setup.

2.1.5 Migration/Invasion assays

2.1.5.1 3D Migration/Invasion assay

Transwell inserts (Corning; cat no: 3422) with 8 µm pores were coated with 40% matrigel. $4x10^4$ cells from cell lines and 10^5 cells isolated from tissue or spheres were resuspended in FCS-free medium before seeding. Cells were then seeded in 200 µl of FCS-free medium (DMEM) on the

top of matrigel layer and FCS medium (DMEM) was added to the lower chamber (Figure 9). For additional treatments both upper and lower media were supplemented with progesterone (10 nM), Wnt4 (5 ng/ml) or Rankl (50 ng/ml). After 72 hours incubation of cells isolated from mammospheres or freshly digested tissues, inserts were removed and cells were fixed with methanol (-20^0C for 10 min) and stained with trypan blue. Cells were counted from 3 fields (4x magnification) when visualized under the microscope.
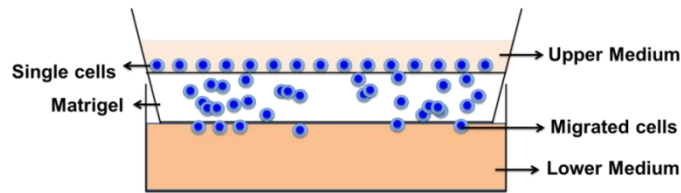
Figure 9. Schematic representation of migration/invasion assay experimental setup.

2.1.5.2 Stem cell migration assay

To evaluate stemness of migratory cells, we established new invasion-sphere formation assay where the cells were sandwiched between two layers of 40% matrigel in the upper chamber and the lower chamber was coated with poly-HEMA. Lower medium was mammosphere medium which has been described in sphere assay section (Figure 10). After 72 hours, inserts have been removed, fixed and stained with trypan blue for single cell migration analysis. 600 µl of fresh sphere medium was added to the lower chamber and cells incubated for 14 days until spheres were counted.
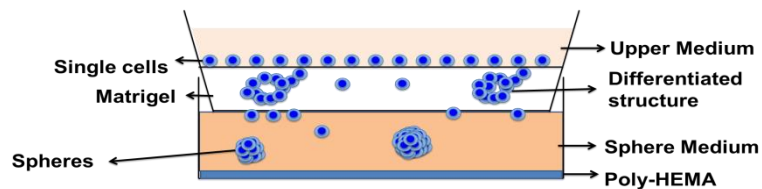
Figure 10. Schematic representation of migration-Sphere formation assay experimental setup.

2.1.6 Proliferation assay

Single cell suspensions were cultured in 96 well plates and proliferation was evaluated by XTT colorimetric assay kit (Roche; cat no: 11465015001) based on manufacturers instruction. Cell seeding concentration was 3000 cells/well which was done in 6 replications. The media were supplemented with investigated factors (see appropriate experiments) or hormones as well as vehicle and were changed every second day.

2.1.7 Staining

2.1.7.1 Haematoxylin and eosin staining

Paraffin embedded tissue was cut into 5 µm sections onto poly-L-lysine-coated slide. Sections were dewaxed in Xylol for 10 min twice and rehydrated first in 100% ethanol for 3 min and then in 80% ethanol for 3 min. The sections were washed in PBS for 1 min thrice and incubated with hematoxylin for 45 sec. The slides were rinsed in tap water for a short duration and washed in tap water for 30 min in a glass cuvette. Eosin (0.1%) was added to the tissue sections and after 2 min they were washed with ddH$_2$O for 1 min. The stained sections were dehydrated in 70% ethanol for 2 min, 100% ethanol for 2 min and finally in xylol for 15 min. Mounting gel was added to the tissue sections and a cover slip was placed carefully on the gel avoiding bubbles and were left to dry overnight.

2.1.7.2 Bone marrow staining for DTC detection

At least 10^6 cells per mouse were stained to detect positive cells. Blocking solution (5% rabbit serum in 1x TBS) was added to the slides to rehydrate the cells and to block unspecific binding of antibodies to the cells. After 20 min the blocking solution was discarded and primary antibody against CK 8 and 18 (all antibodies and working concentrations are listed in section 2.2.6) was added and incubated for 60 min. The primary antibody was discarded and slides were washed 3 times for 3 min in 1x TBS. Then slides were incubated with the secondary antibody for 25 min, and washed 3 times for 3 min in 1x TBS followed by incubation with ABC complex for 25 min. Finally, the development system of the BCIP/NBT for alkaline phosphatase enzymatic substrate was added for 10 min. The slides were washed 3 times for 3 min and screened for CK8/18 positive cells. The positive cells were typically violet-to-black in color. TUBO, a tumor cell line

derived from a murine primary mammary tumor of Balb-NeuT which expresses CK8/18, was used as a positive control.

2.1.7.3   Immunohistochemistry

For PgR and Her2 immunohistochemistry of tissues, 5 µm sections of paraffin blocks were collected onto poly-L-lysine-coated slides. Samples were dewaxed by two 5-min washes in xylene and rehydrated with graded alcohol by 5-min washes and a final wash in water. A standard Tris-EDTA buffer and pressure cooking was the antigen retrieval procedure and then sections were blocked in 0.3% H_2O_2 in TBS and 10% normal goat serum. Sections were incubated for 1 hour with primary antibody and after washing secondary antibody (Vector lab PK4001 or PK5000) was added based on manufacturers suggested dilution (see section 2.2.6). After washing with PBS, sections were stained using the ABC detection system (Vector laboratory) according to the manufacturer's instruction. Visualization was performed with chromogen reagent (Dako; cat no: 10046560) according to manufacture instructions.

2.1.7.4   Immunofluorescence staining

For staining of cells from monolayer cell culture, cells were seeded onto 24 well culture plates in appropriate density. After 72 hours incubation, cells were washed with PBS and fixed with 4% PFA for 10 minutes. Then, cells were permeabilized with 0.2% triton X100 followed by washing steps and blocking with 1% BSA, 5% serum of species of secondary antibody in PBS at room temperature for 1 hour, followed by incubation with primary antibody (see 2.2.6) for 1 h at room temperature. Cells were then washed three times with PBS and incubated with labeled secondary antibody (Jackson ImmunoResearch Laboratory Inc) for 1 h at room temperature. For a nuclear counterstain, cells were incubated for 10 min with DAPI 0.5 µg/ml (Sigma). For the staining of spheres in differentiation experiments, mammospheres were picked and transferred to a 24 well cell culture plate and incubated for 8 h in sphere medium in order to fix them to the surface. The subsequent protocol was as for monolayer cell culture staining. For staining of cells attached to the inserts from migration experiments, inserts were used directly after migration (see migration section), for blocking step and IF staining as monolayer cell culture staining. Images were captured on an Axio Vert 200M microscopy (Carl Zeiss Microscopy).

2.1.8 PCR

2.1.8.1 Quantitative PCR

All mRNA extractions were performed by RNeasy kit (Qiagen) according to manufacturer's instructions. For miRNA extraction miScript II RT Kit (Qiagen) was used. cDNA was generated using reverse transcriptase kits (Qiagen). Finally, 25 ng of cDNA was used for qPCR. Quantitative PCR was performed using a Light Cycler instrument (Roche) and Fast Start Master SYBR Green Kits (Roche). Data analysis was done using the RelQuant software (Roche) with a reference gene and a calibrator (reference) sample in every run. Mouse reference cDNA served as a positive control. Measurements that showed unspecific products in the melting curve analysis were discarded from further analysis. Expression levels are given relative to β-actin for gene expression analyses and RNU6 for miRNA analyses (for primers and their sequences see section 2.2.5). All primers were synthesized by Eurofins MWG Operon Company.

2.1.8.2 PCR

End-point PCR for different genes (see section 2.2.5 for primers and sequences) was done according to table 1 and under the program listed in table 2.

Table 1. **Ingredient of a PCR reaction**

Volume	Reagent
7,15 µl	Ultra-pure DEPC- water
1 µl	PCR buffer + dNTP
0,5 µl	Forward oligonucleotide (8 µM concentration)
0,5 µl	Reverse oligonucleotide (8 µM concentration)
0,25 µl	BSA
0,1 µl	Taq DNA-polymerase
0,5 µl	DNA

Temperature	Time
94 ^{0}C	2:00 min
58 ^{0}C	0:30 min
72 ^{0}C	2:00 min
94 ^{0}C	0:15 min
58 ^{0}C	0:30 min
72 ^{0}C	0:20 min
Repeat steps from step 4 to 6 (14 times)	
94 ^{0}C	0:15 min
58 ^{0}C	0:30 min
72 ^{0}C	0:20 min
Repeat steps from step 8 to 10 (24 times)	
72 ^{0}C	2:00 min
4 ^{0}C	∞

2.1.8.3 Agarose gel electrophoresis

Amplified products of the specific PCR were separated with gel electrophoresis, on1.5% agarose in TBE buffer with ethidium-bromide (0,5 µg/ml). Samples were mixed with a loading dye and loaded in the gel. PCR amplicons were separated at 160 V for 45 min.

2.1.9 Viral transduction

2.1.9.1 Construction of the lentiviral/Retroviral particles

The 293T cells were propagated in DMEM media supplemented with 10% FCS and L-glutamine. The transfection ability of the 293T cells depends on the culture conditions. Therefore, 6 x 10^6 cells were seeded in a 10 cm cell culture dishes 15h before the transfection. Transfection was performed once the cells reached 70% confluence. Transfection medium (DMEM; 10% FCS) containing 25 µM chloroquine was added 45 min before the start of transfection. Chloroquine's function is to block plasmids degradation in the endosome/lysosome system which increases transfection rate (Ciftci and Levy, 2001; Erbacher et al., 1996). Half an hour to two hours after chloroquine addition the medium was replaced by transfection mixture.

The composition of the transfection mixture was:

For PgR-B (Lentiviral) particles:

5 µg pMD2G (envelope plasmid),
20 µg psPAX2 (packaging plasmid),
20 µg lentiviral plasmid (GeneCopeia; Cat no: Z5911)

For Her2 (Retroviral) particles:

5 µg pCMV-VSV-G (envelope plasmid from Addgene),
20 µg pUMVC3 (packaging plasmid from Addgene),
20 µg lentiviral plasmid (pLXSN-NNeu was obtained from Dr. Lisa Petti, Albany Medical Center, Albany, NY) (Petti and Ray, 2000),

Then, water was added up to 250 µl, and finally 250 µl of 0.25 M $CaCl_2$ solution was added (see transfection solution). This mixture was diluted into 2x HEBS buffer solution (see transfection solution). The final volume of transfection was 1 ml for one 10 cm plate. The transfection mixture was added drop wise to HEK-293T cells. The medium was replaced 6h after the transfection mixture was added. The addition of the transfection mixture is taken as the start point of the S2 work. Therefore, all work was performed according to the safety recommendation prescribed for the S2 work. The viral particles were collected 48h and 72h post transfection and stored at -80^{0}C.

2.1.9.2 Transfection Solutions

$CaCl_2$ 0.5 M

36.75 g $CaCl_2$ $2H_2O$,
Add H_2O (twice distilled / Millipore, additionally sterilized) up to 100 ml.
Sterile filter and store at 4° C (3-6 months) or aliquot and store at -20° C for longer time.

2x HeBS

1.63 g NaCl
0.074 g KCl

1 ml 1M HEPES buffer

0.021 g Na_2HPO_4

Add distilled H_2O up to 90 ml

PH 7.05 adjusted with NaOH (at RT)

Fill up to 100 ml with H2O

Sterile filter and store at 4° C (3-6 months) or aliquot and store at -20° C for longer time.

After thawing to room temperature, pH was measured again

Chloroquine

25 mM stock solution in water (25µM final working concentration).

2.1.9.3   Determination of virus titer

Virus titer represents the number of the virus particles in 1 ml. Determination of the virus titer was performed using gradient treatment in target cell lines. Cells were propagated in a 12-well plate. The cells (4 x 10^4 cells/well) were plated and propagated overnight at 37 °C. On the next day, medium was removed, cells were washed and virus diluted in 1:10, 1:100, 1:1000, 1:10000 and added to the cells. After 24 hours, 10 µg/ml puromycin for lentiviral transduction and 1000 µg/ml G418 was added for retro viral transduction. Titer of the produced virus (Transforming Units per milliliter =TU/mL) was determined by the following equation:

Number of discrete colonies/ dilution factor= TU/mL

The best dilution is the one which is less or equal to the number of seeded cells, because that will avoid multiplicity of integration (MOI) in target cells.

2.1.9.4   The selective propagation of the transduced cells

Lenti-/retroviral vectors used for the stabile integration and expression of the PgR-B/Her2 contain genes for the puromycin (lentiviral particles for PgR-B) and neomycin (retroviral particles for Her2) resistance. Therefore, transduced cells have stable integrated and expressed gene for antibiotic resistance. Treatment of transduced cells with antibiotic depletes uninfected

cells. Positively transduced clones were expanded and screened for PgR and/or Her2 levels by western blot analysis and qPCR.

2.1.1 Western blot analysis

2.1.9.5 Protein extraction and quantification

Protein was extracted from cell lines or fresh tissues using lysis buffer (RIPA buffer; Sigma) supplemented with protease inhibitors (protease cocktail; Thermo scientific). For homogenization of tissue samples, they were punched with a piston in liquid nitrogen to become powder and then subjected for RIPA digestion. RIPA digestion was done in shaker at 4 °C for 15-30 minutes. After centrifugation of digested cells/tissues, they were centrifuged and supernatant used for protein measurement and western blotting. Protein quantification was subjected for BCA protein assay kit (Thermo scientific) and their concentrations were equalized by adding appropriate RIPA buffer.

2.1.9.6 Gel electrophoresis

Quantified protein lysates were mixed with SDS loading dye and heated for 10 minutes at 95°C to denature protein structures. Then, 30 µg proteins were loaded on SDS-PAGE gels. The composition of used gels can be seen in tables 3 and schematic set up of gel electrophoresis is shown in figure 11. Gel chambers and electrophoresis power supply were from Biorad (See list of devices in 2.2.4 section). Gels were running in constant 40 V and every 15-30 minutes have been checked until the blue dye run out of lower edge of gel. Composition of running buffer can be seen in table 4.

Table 3. **Composition of stacking and resolving gels**

Resolving gel	6%
H_2O	6,7 ml
3M Tris pH 9	1,3 ml
Acrylamid 30	2,3 ml
20 % SDS	50µl
TEMED	10µl
10% APS	50µl

Stacking gel	
H_2O	2,6 ml
1M Tris pH 6,8	420 µl
Acrylamid 30	550 µl
20 % SDS	17 µl
TEMED	5 µl
10% APS	33 µl
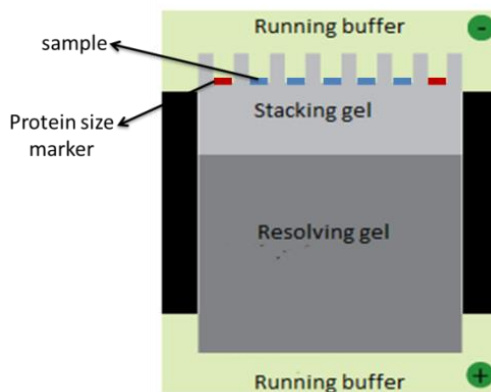
Figure 11. Schematic representation of the SDS PAGE setup. The upper part of gel is stacking and the lower is resolving gel. The stacking gel is needed to concentrate/pack all the proteins in one band, so that they will start migrating in the running gel all at the same time. The running gel allows separation of the proteins in the sample based on their molecular weight. Both side lanes were used for protein size marker which helps to predict the position of protein of interest. Upper and lower chambers were filled with running buffer (table 4) and proteins migrate from negative to positive pole.

Table 4.   SDS loading dye composition

Running Buffer	10X	1X
Glycine	288 g	28.8 g
Tris base	60.4 g	6.04 g
SDS	20 g SDS (200ml 10%SDS)	2 g
ddH2O	1.8 l	1 l

2.1.9.7   Semi Dry Blotting

Next, proteins have been transferred from gel onto a polyvinylidene difluoride membrane (Millipore, Billerica, MA, USA). That was semi dry method in which membrane coupled to gel and sandwiched between wet Whatmann paper papers. Composition of blotting buffer can be seen in table 5. Blotting was done at 20 V for 30 minutes. Then, membrane containing proteins were dried in air and strips (based on protein size marker roughly predicted that carry our protein of interest) have been cut.

Table 5.   Blotting buffer composition

5 x blotting buffer (2L)	1x Blotting buffer
125 mM Tris base (30,2 g /2 L)	200 ml 5 x buffer
1920 mm glycine (144 g /2 L)	600 ml Millipore
- - - - - - - - - - - - - -	200 ml methanol

2.1.9.8 Protein detection

Blocking of membrane was done with 6% skim milk for 2 hours on shaker in room temperature and immunoblotting with the primary antibodies was done overnight at 4 °C (for antibody concentration see section 2.2.6). Washing was done 3 times and 5 minute each with TBST (see table 6 for composition). It was followed by incubation with the horseradish peroxidase-conjugated secondary antibody for 30 minutes. The blots were visualized using substrate kit (GE Healthcare) and bands were visualized by Imagequant LAS 4000 (GE Healthcare).

Table 6.   **TBST buffer composition**

TBS 10x (concentrated TBS)	
24.23 g	Tris HCl
80.06 g	NaCl
800 ml	H_2O (dissolve)
make up to 1l by adding H_2O	
set PH at 7.6 and 2ml Tween 20 was added for 1x buffer	

2.1.10 miRNA analyses and sequencing

For exosomes isolation ultracentrifugation method was used as previously described (Thery et al., 2006). Exosomes pellet was resuspended in fresh medium and used for T47D cell line treatments and PgR expression was checked in different time points. For miRNA sequencing we used $4x10^6$ cells and exosomes were isolated from confluent TUBO cell line medium. The miRNA cloning and sequencing was done in the same way as described recently (Dueck et al., 2014). Briefly, all pooled samples were run in a MiSeq sequencer (Illumina) for 80 cycles single end run. In this sequencing run MiSeq reagent kit Version 3 was used. Data analysis was done using in house written scripts. Sequences were mapped - without any mismatches allowed - against murine miRNAs listed in miRBase version 20 (June 2013; www.mirbase.org). The minimum length of reads was set to 18 nt. Annotated miRNA-reads were normalized as RPM-Values regarding the total number of mapped reads in the respective library. Mimic miRNA were ordered from Eurofins MWG Operon company and all sequences are in section 2.2.7. For miRNA transfection we used reverse transfection protocols recommended by RNAiMAX (Life Technology) instruction and 50 nm concentration of miRNA.

2.1.11 Analysis of Breast Cancer Patients:

We analyzed data of 2239 patients from the Department of Oncology and Obstetrics, University of Tubingen. DCC status was assessed according to the Consensus protocol (Fehm et al., 2006), using the anti-cytokeratin antibody A45B/B3 and evaluating 2×10^6 bone marrow cells. PgR expression of primary tumors was categorized into PgR staining scores 0-1 for absent expression; 2-8 for intermediate expression and 9-12 for high expression. Her2 status of primary tumors was categorized into the staining score 0 for absence of Her2 staining (IHC negative); score 1 and score 2 without Her2 amplification (IHC positive) and into score 2 with Her2 amplification and 3 (which is known to be caused by Her2 amplification; FISH positive).

2.1.12 Bioinformatic and Statistical analysis

Statistical analyses and estimation of variation within each group of data were performed using GraphPad Prism V6. For *in vivo* experiments, sample size was estimated using G*Power (version 3). For each experiment, mouse numbers are given in the figures or the text. All *in vitro* and primary culture experiments were performed at least in triplicate and student's t-test was applied for comparisons. For comparison of qPCR results of EL-signature between different groups, gene wise t-test p-values were combined using Stouffer's method. For all other experiments we applied the D'Agostino-Pearson omnibus normality test. When sample size was sufficiently large (n≥8) and were not distributed normally according to the D'Agostino-Pearson test (p≤0.05) we applied the Mann-Whitney test. A linear regression test (F-test for slopes) was used to compare proliferation curves and tumour growth. For comparing numbers between different groups we applied Fisher's exact or if the sample numbers were at least 5 in each condition the chi-square test. All *p* values represent two tailed values. All p values and statistical tests are mentioned in the figures and legends. Genomatix (version 2.0) (https://www.genomatix.de) was used for signaling pathway analysis and oPOSSUM (version 1) (http://opossum.cisreg.ca/oPOSSUM3/) for transcription factor binding site (TFBS) enrichment. For miRNA binding enrichment we used DIANALAB (http://diana.cslab.ece.ntua.gr/) and for the identification of target miRNAs for single target genes the miRANDA software (http://www.microrna.org/microrna/home.do) was used.

2.2 Materials

2.2.1 Reagent

Product	Manufacturer	Cat. Number
2-Log DNA-Ladder 1kb	NEB	N32005
AB/AP-System	DAKO	AK-5000
AB/HRP-System	DAKO	PK-4000
AB-Serum	Bio-Rad	805315
Acetic acid	Merck, Darmstadt	100063
Agarose	Sigma-Aldrich	A3038
Aldostrone	Sigma-Aldrich	A9477-5mg
Amonium per-sulfate	Sigma-Aldrich	A3678
Ampicillin	AppliChem GmbH, Darmstadt	A0839
B27	Invitrogen	17504-44
BCIP/NBT	BioRad	1706432
B-estradiol	Sigma-Aldrich	E4389
bFGF	Sigma-Aldrich	F0291
Bovine serum albumin (BSA), 20 mg/ml	Roche	10711454001
Bromphenol blue	Sigma-Aldrich	B3269
BSA	Roche	1071145001
Chloroform	Sigma-Aldrich	25690
Chloroquine	Sigma-Aldrich	C6628
Cholera toxin	Sigma-Aldrich	C9903
Collagenase	Sigma-Aldrich	C0130
Collagenase Type I	CellSystems biotech	LS4196
Cortisone	Sigma-Aldrich	C2755-1g
DAB	DAKO	K3468
DAPI	Roche, Penzberg	32670
dATP, 100 mM	GE Healthcare	27-1850-04
dCTP, 100 mM	GE Healthcare	27-1860-04
DEPC-H_2O	Invitrogen	750023
dGTP, 100 mM	GE Healthcare	27-1870-04
Diluent C	Sigma-Aldrich	CGDIL-6x10 ml
DMEM	Pan-Biotech	P04-03500
DMEM/F12	Pan-Biotech	P04-41500
EGF	Sigma-Aldrich	E9644
Eosin	Sigma-Aldrich	54802

Ethanol absolute	J.T. Baker	8006
Ethidium bromide (1 %)	Sigma-Aldrich	E8751
Eukitt (Mounting gel)	Sigma-Aldrich	03989-100ML
Expand Long Template Enzyme Mix	Roche	11 759 060 001
FCS	PAN Biotech	P30-3702
Fetal bovine serum (FBS)	Pan Biotech, Aidenbach	P30-1506
Formaldehyde	Merck, Darmstadt	104003
Formamide	Merck, Darmstadt	344 205
Formamide, deionized	Sigma-Aldrich	F9037
Goat serum	DAKO	X0907
GRO-α	RnDsystems	275GR
Halt Protease inhbitor	Thermo scientific	1862209
Hematoxylin	Sigma-Aldrich	MHS16
Heparin	Sigma-Aldrich	H3149
Hyaluronidase Type IV-S	Sigma-Aldrich	H4272
Hybond ECL nitrocelelluse paper	GE Healthcare	RPN203E
Hydrocortisone	Sigma-Aldrich	H0888-1gr
Igepal	Sigma-Aldrich	I3021-50ML
Insulin	Sigma-Aldrich	I9278
Isopropanol	Fluka	59300-2.5ML
Levamasol	Sigma-Aldrich	L9756
L-Glutamin (200 mM)	Pan-Biotech	P04-80100
Matrigel	BD Biosciences	356231
Matrigel growth factor reduced, phenol red free	Corning	356231
Methanol	VW	1.06009.2500
Methyl cellulose	Sigma-Aldrich	M0512-100G
Mouse serum	DAKO	X0910
MseI 50 U/µl	New England Biolabs	R0525M
Nomegestrol acetate (NOMAC)	Sigma-Aldrich	SML0133-5MG
OPA Plus	Amersham Biosciences,	27-0901-02
Panscript Taq-Polymerase	PAN Biotec	MB-30010250
Paraformaldehyde	VW	104005
Penicillin/Streptomycin (10 U/µL)	Pan-Biotech	P1-010
Percoll	Amersham Biosciences	17089102
PKH26	Sigma-Aldrich	MINI26-1KT
Polyhema	Sigma-Aldrich	P3932
Precision Plus Protein Dual Color standards	Biorad	161-0374
Progestrone	Sigma-Aldrich	P8783-5gr
Protein Size Marker	New England Biolabs	P7702S

Proteinase K	Roche	3115828001
RIPA	Sigma-Aldrich	R0278
Rotipherase gel 30 (37:5:1)	Roth	3029.2
RPMI 1640	Pan-Biotech	P05-17500
SDS loading dye	RoTH	K929.1
Sodium citrate	Sigma-Aldrich	73894-100ML
T4 DNA Ligase	Roche	10799009001
TEMED	Roth	2367.3
Testostrone	Sigma-Aldrich	T15000-1G
Tween 20	Sigma-Aldrich	P9416
Xylol	Roth	9713.3
RNAiMAX	Life Technology	13778030
Polygelatin string	Ethicon, Germany	

2.2.2 Consumable

Product	Manufacturer	Cat. Number
Adhesion slides	Roth	H8701
Filter (0.22 μm)	Roth	P666.1
Syringe needles (26G)	Braun	C7181
Cell culture plates	Schubert and Weiss, OMNILAB	FALC351007
Cell culture flasks	Sarsted	831.810.302
Glass slides	Langenbrinc	03-0001
6 well plates	Greine	657160
Reaction tubes 1,5 ml	CLN Gmb	CLN-BÖT1.5
Reaction tubes 0,2 ml	Abgen	AB-0337
Transwell plates (10 cm, 0.4 μm pore)	Cornin	3419
6.5mm Transwell with 8.0μm Pore Polycarbonate Membrane Insert	Corning	3422
CaCl2	Sigma	C5080
NaCl	Sigma	S7653
Kcl	Sigma	P9541
HEPES	Sigma	H7523
Chloroquine		C6628

2.2.3 Kits

Name of kit	Manufacturer	Cat. Number
PKH26 general cell membrane labeling	Sigma-Aldrich	PKH26GL
DAB-System	DAKO	K3468
ABC-HRP-System	Vector Laboratories	PK-4000
MTT	Roche	11465007001
RNeasy mini-kit	Qiagen	74104
Revers trascript	Qiagen	205311
Pierce BCA protein assay	Thermo scientific	23227
ECL Detection kit for western blotting	GE Healthcare	RPN2109
Plasmid purification	Qiagen	12381
DNA Gel Extraction Kit	Qiagen	28706
DNA extraction Mini Kit	Qiagen	51304

2.2.4 Devices

Device	Company
Axio Imager Z1 Fluorescence microscope	Zeiss, Göttingen
Balance	Kern, Balingen
BenchMark Ultra	Ventana, USA
Capillary holder for micromanipulation	Eppendorf, Hamburg
Cell culture incubator	Heraeus, Hanau
Cell culture incubator	Heraeus, Hanau
Cell culture laminar flow	Heraeus, Hanau
Centrifuge	Heraeus, Hanau
Centrifuge	Eppendorf, Hamburg
Centrifuge, tabletop	Grant Bio, USA
Centrifuge, tabletop	Eppendorf, Hamburg
Cytospine Centrifuge	Hettich, USA
DM RXA Fluorescence microscope	Leica, USA
Cauterizer	Fine Science Tools, Hedelberg
FACS Canto II	BD Biosciences, USA
Electrophoresis gel chamber	Biostep, Jahnsdorf
Photometer, GeneQuant II	Pharmacia Biotech, USA
Laser micro-dissection microscope	P.A.L.M, Bernried
19 LSR II flow cytometer	BD Bioscience, USA
Magnetic stirrer	VELP Scientifica
MJ Research Peltier Thermal Cycler PTC-200	Bio-Rad
MJ Research Peltier Thermal Cycler Tetrad	Bio-Rad
Multipipette Stream	Eppendorf, Hamburg

Neubauer- Cell counter	Schubert und Weis, Munich
Optical microscope	Optech, Canada
Pipette controller	Brand, Wertheim
pH-meter	Eutech Instruments, The Netherlands
Pipettes (2 µl, 20 µl, 200 µl, 1000 µl)	Eppendorf, Hamburg
Power supply for gel chamber electrophoresis	MRC, Israel
Pump	KNF, Freiburg
StuartTM Scientific roller mixer	Stuart Scientific, UK
Thermo mixer	Eppendorf, Hamburg
UV illuminator	Intas, Gottingen
Vortex mixers	VELP Scientifica, Italy
Water bath	Memmert, Schwabach
Trans Blot SD cells	Bio-Rad
Mini-PROTEAN Tetra Cell	Bio-Rad
Cell culture incubator	Heraeus
Flourescence microscope	Leica
Heat block thermo mixer 5436	Eppendorf
Inverted microscope	Leica
Refrigerated centrifuge	Eppendorf
Micromanipulator Microinjector 5242,	Eppendorf
MJResearch Peltier Thermal Cycler PTC-200	Bio-Rad
Voltmeter EPS 200	Pharmacia Biotech
UV-screen	INTAS
Video camera	INTAS
Water bath	Memmert
Centrifuge	Eppendorf
Cytospin centrifuge	Hettich
Dissection tools for murine surgery	Heiland
Imagequant LAS 4000	GE Healthcare
Emax microplate reader	Molecular devices, LLC, US

2.2.5 Primers

Gene	5' Primer	3' Primer
AHNAK	GTCTTTGTTCAGGAGGTG	CCCATGGTATTCAGCAAC
Nfatc3	GGAGCAAACCAAAGCCTG	CTCGGCTACCTTCAGTTTC
Stac3	GATTCTTCCCTCCAAACTTC	TAACCACCAGCTTCATCTC
Zc3hav1	TTCTTCCACTCCTGTCCC	TTCTGCTCCACATCCTTC
Baz2a	AGTCTCTGGTAGTGGTGATG	TGCTTCATTCTCTTCCCAC
Nr3c2	CTTTCCGCCTGTCAATGC	TCATCTCCACACACCAAGCAG
Zfp780b	TGGATGCTACTCAGAAGGTC	CCTGTCTGTTTCTTCCTTCA
Nr3c1	CAAGGGTCTGGAGAGGACAA	TACAGCTTCCACACGTCAGC
B.actin	GTGACAGCATTGCTTCTGTG	TCTCAAGTCAGTGTACAGGC
Wint4	GCCATCGAGGAGTGCCAATAC	GCCACACCTGCTGAAGAGATG
PgR A&B	AAGCCAGTTTGAAGAGATG	ATTCAAGCAGTACAGGTGG
PgR B	AAAGGATCCGCAGGTTCTC	GGCGAGACTACAGACGACAC
Esr1(α)	CCTCCCGCCTTCTACAGGT	CACACGGCACAGTAGCGAG
AR	GAACTACATCAAGGAACTCG	TATGGGACTTGATTAGCAG
Esr2 (β)	TCTCTTCCCAGCAGCAGTC	GCATTCAGCATCTCCAGC
RANKL	CCTCACCATCAATGCTGC	TACGCTTCCCGATGTTTC
	Human Primers	
Gene	5' Primer	3' Primer
PgR A&B	CCAGCCAGAGCCCACAATAC	GTTGTGCTGCCCTTCCATTG
B.actin	TGGACATCCGCAAAGACCTG	GGGTGTAACGCAACTAAGTCAT
ER-α	TTGGCCAGTACCAATGACAA	GGCAGCTCTTCCTCCTGTTT

2.2.6 Antibodies

Name of antibody	Cat. Number	Manufacture	Working Concentration
β-actin antibody	A5441-.5ML	Sigma-Aldrich	1/20,000 for WB
PR (C-20)	sc-539	santa cruz Biotech	1/100
ER-α (MC-20)	sc-542	santa cruz Biotech	1/100 for WB
AR (N-20)	sc-816	santa cruz Biotech	1/100 for WB
ER-β (H-150)	sc-8974	santa cruz Biotech	1/100 for WB
NR3C2 (GR (p-20))	sc1002	santa cruz Biotech	1/100 for WB
NR3C1 (GR (M-20))	sc-1004	santa cruz Biotech	1/100 for WB
Sca1	130093222	militeny biotech	1/500 for WB
EpCAM-Alex647 (clone: G8.8)	118212	Biolegend	1/200 for WB
c-erbB-2 (Her2 (clone: PK)) for WB and IHC	DLN-12083	Dianova	1/500 for WB
Keratins K8/K18 (GP11)	GP11	Progen Biotechnik	1/200 for IHC
Rabbit IGg	Sc-2027	santa cruz Biotech	1/200 for IHC
Goat anti Rabbit-AF 488	A11017	Life Technologies	1/200 for IF
Goat anti mouse-Cy3	115-166-003	Jackson ImmunoResearch	1/200
Goat anti Guinea pig-Cy3	106-165-003	Jackson ImmunoResearch	1/200
Guinea Pig IgG	CR4	Sino Biologival Inc.	1/100
Anti mouse HRP	NA931	GE Healthcare	1/2000 for WB
Anti Rabbit HRP	NA934	GE Healthcare	1/2000 for WB
Anti Goat HRP	sc-2020	santa cruz Biotech	1/2000 for WB

2.2.7 miRNAs

miRNA	Ref Sequence	mimic miRNA	Mimic Sequence
mmu-miR-30a-5p	uguaaacauccucgacuggaag	mmu-miR-30a-5p F	TGTAAACATCCTCGACTGGAAG
		mmu-miR-30a-5p R	CTTCCAGTCGAGGATGTTTACA
mmu-miR-30a-3p	cuuucagucggauguuugcagc	mmu-miR-30a-3p F	CTTTCAGTCGGATGTTTGCAGC
		mmu-miR-30a-3p R	GCTGCAAACATCCGACTGAAAG
mmu-miR-21a-5p	uagcuuaucagacugauguuga	mmu-miR-21a-5p F	TAGCTTATCAGACTGATGTTGA
		mmu-miR-21a-5p R	TCAACATCAGTCTGATAAGCTA
mmu-miR-25-3p	cauugcacuugucucggucuga	mmu-miR-25-3p F	CATTGCACTTGTCTCGGTCTGA
		mmu-miR-25-3p R	TCAGACCGAGACAAGTGCAATG
mmu-miR-92a-3p	uauugcacuugucccggccug	mmu-miR-92a-3p F	TATTGCACTTGTCCCGGCCTG
		mmu-miR-92a-3p R	CAGGCCGGGACAAGTGCAATA
mmu-miR-340-5p	uuauaaagcaaugagacugauu	mmu-miR-340-5p-F	TTATAAAGCAATGAGACTGATT
		mmu-miR-340-5p-R	AATCAGTCTCATTGCTTTATAA
mmu-miR-9-5p	ucuuugguuaucuagcuguauga	mmu-miR-9-5p-F	TCTTTGGTTATCTAGCTGTATGA
		mmu-miR-9-5p-R	TCATACAGCTAGATAACCAAAGA
mmu-miR-92a-1-5p	agguuggggauuugucgcaaugcu	mmu-miR-92a-1-5p F	AGGTTGGGATTTGTCGCAATGCT
		mmu-miR-92a-1-5p R	AGCATTGCGACAAATCCCAACCT
mmu-miR-21a-3p	caacagcagucgaugggcuguc	mmu-miR-21a-3p F	CAACAGCAGTCGATGGGCTGTC
		mmu-miR-21a-3p R	GACAGCCCATCGACTGCTGTTG

2.2.8 Cell lines

Cell line	Species	Origion	Medium
TUBO	Mouse	Breast cancer A gift from Dr. Guido Forni , Department of Clinical and biological science, university of Turin, Italy	DMEM+20% FCS, 2mM L-Glutamat, 1%P/S
MM3MG	Mouse	Mouse Mammary normal epithelial cells from BALB/c background, ATCC: CRL-6376	DMEM+10% FCS, 2mM L-Glutamat, 1%P/S
MM3MG-Her2	Mouse	Normal Mammary epithelial cell line transduced with wild type Rat Her2	DMEM+10% FCS, 2mM L-Glutamat, 1%P/S + G418 (500 μg/ml)
SKBR3	Human	mammary gland/breast; derived from metastatic site: pleural effusion, ATCC® HTB-30™	RPMI 1640 + 10% FCS, 2mM L-Glutamat, 1% P/S + 1mM Napuruvat
MCF10A	Human	Normal Mammary epithelial cell line, ATCC® CRL-10317™	DMEM/ F12, 1% pen/Strep, 5% horse Serum, 20 ng/mL EGF, 0,5 μg/mL Hydrocortisone, 0,1 μg/mL cholera Toxin, 10 μg/mL insulin
4T1	Mouse	Tumorgenic cell line from spontaneous mammary tumors derived from BBALB/c. (A gift from Dr. Fred Miller, Michigan Cancer Foundation, Detroit USA)	DMEM+10% FCS, 2mM L-Glutamat, 1%P/S
MM3MG-PgR	Mouse	Normal Mammary epithelial cell line transduced with wild type human PgR B	DMEM+10% FCS, 2mM L-Glutamat, 1%P/S + Puromycin (10 μg/ml)
T47D	Human	mammary gland; derived from metastatic site: pleural effusion ATCC® HTB-133™	RPMI 1640 + 10% FCS, 2mM L-Glutamat, 1% P/S
MDA231	Human	mammary gland/breast; derived from metastatic site: pleural effusion, ATCC® HTB-26™	RPMI 1640 + 10% FCS, 2mM L-Glutamat, 1% P/S
BT474	Human	mammary gland; breast/duct ATCC® HTB-20™	DMEM+10% FCS, 2mM L-Glutamat, 1%P/S
MCF7	Human	mammary gland, breast; derived from metastatic site: pleural effusion, ATCC® HTB-22™	RPMI 1640 + 10% FCS, 2mM L-Glutamat, 1% P/S + 1mM Napuruvat
MDA361	Human	mammary gland/breast; derived from metastatic site: pleural effusion, ATCC® HTB-26™	DMEM+10% FCS, 2mM L-Glutamat, 1%P/S
HCC 1569	Human	mammary gland; breast, ATCC® CRL-2330™	RPMI 1640 + 10% FCS, 2mM L-Glutamat, 1% P/S
Cama	Human	mammary gland/breast; derived from metastatic site: pleural effusion, ATCC® HTB-21™	RPMI 1640 + 10% FCS, 2mM L-Glutamat, 1% P/S
HS578T	Human	mammary gland/breast, ATCC® HTB-126™	DMEM+10% FCS, 2mM L-Glutamat, 1%P/S
66cl4	Mouse	Tumorgenic cell line from spontaneous mammary tumors derived from BBALB/c. (A gift from Dr. Fred Miller, Michigan Cancer Foundation, Detroit USA)	DMEM+10% FCS, 2mM L-Glutamat, 1%P/S
67NR	Mouse	Tumorgenic cell line from spontaneous mammary tumors derived from BBALB/c. (A gift from	DMEM+10% FCS, 2mM L-Glutamat, 1%P/S

		Dr. Fred Miller, Michigan Cancer Foundation, Detroit USA)	
MDA-MB 175	Human	mammary gland; breast/duct; derived from metastatic site: pleural effusion, ATCC® HTB-25™	DMEM+10% FCS, 2mM L-Glutamat, 1%P/S
ZR751	Human	mammary gland; breast/duct; derived from metastatic site: pleural effusion, ATCC® HTB-132™	RPMI 1640 + 10% FCS, 2mM L-Glutamat, 1% P/S
Htert-HME	Human	Normal Mammary epithelial cell line, ATCC® CRL-10317™	DMEM/ F12, 1% pen/Strep, 5% horse Serum, 20 ng/mL EGF, 0,5 µg/mL Hydrocortisone, 0,1 µg/mL cholera Toxin, 10 µg/mL insulin
BT549	Human	mammary gland; breast/duct; derived from metastatic site: pleural effusion, ATCC® HTB-122	RPMI 1640 + 10% FCS, 2mM L-Glutamat, 1% P/S
HCC1806	Human	mammary gland; breast/duct; derived from metastatic site: pleural effusion, ATCC® HTB-132™	RPMI 1640 + 10% FCS, 2mM L-Glutamat, 1% P/S
HCC1937	Human	mammary gland; breast/duct; derived from metastatic site: pleural effusion, ATCC® HTB-2336™	RPMI 1640 + 10% FCS, 2mM L-Glutamat, 1% P/S
MDA231	Human	mammary gland; breast/duct; derived from metastatic site: pleural effusion, ATCC® HTB-26™	DMEM+10% FCS, 2mM L-Glutamat, 1%P/S
MDA468	Human	mammary gland; breast/duct; derived from metastatic site: pleural effusion, ATCC® HTB-132™	DMEM+10% FCS, 2mM L-Glutamat, 1%P/S

2.1.2 Special cell culturing media

Medium	Composition	Final conc
Basal medium	500 ml DMEM/F12	
	5 ml HEPES buffer 1 M	10 mM
	5 mlPen/Strep 100 unit/ml	1x
	BSA	0.50%
	500 µl Insulin 10µg/µl	10 µg/ml
Sphere medium	48.8 ml basal medium	
	1 ml B27 50X	1x
	50 µl EGF 10 ng/µl	10 ng/ml
	50 µl heparin 4 ng/µl	4 µg/ml
	20 µl bFGF 25 ng/µl	10 ng/ml
	25 µl GRO-α 10 ng/ml	5 ng/ml
	50 µl HIL-6 20 ng/µl	20 ng/ml
Differentiation Medium	25 ml Hams/F12	
	1.25 ml FCS	5%
	25 µl Insulin 10 mg/ml	10 µg/ml
	50 µl EGF 10 µg/ml	20 ng/ml
	125 µl Hydrocortisone 0.1 mg/ml	0.5 µg/ml
	250 µl Cholera Toxin 10 µg/ml	100 ng/ml
Digestion medium	10 ml Basal medium	
	100 µl hyaluronidase 10 mg/ml	100 U/ml
	100 µl collagenase 33 µg/ml	300 U/ml
	10 µl EGF 10 ng/µl	10 ng/ml

2.2 Abbreviation

bp	Base pair
BCIP	5-Bromo-4-chloroindol-3-ol dihydrogen phosphate ester mono-p-toluidinium salt
BM	Bone marrow
BSA	Bovine serum albumin
bFGF	Basic fibroblast growth factor
cDNA	Complementary deoxyribonucleic acid
CGH	comparative genomic hybridization
CM	Conditioned medium
CK	Cytokeratin
CSC	Cancer stem cell
DTC	Disseminated Tumor cell
DCC	Disseminated cancer cell
ddH2O	Deionized distilled water
DNA	Deoxyribonucleic acid
DMSO	Dimethyl sulphoxide
EGF	Epidermal growth factor
EpCAM	Epithelial cell adhesion molecule
FITC	Fluorescein isothiocyanate
GRO-α	Growth related oncogene-alpha
HE	Haematoxylin-Eosin
ICC	Immunocytochemistry
IgG	Immunoglobulin G
IHC	Immunohistochemistry
HIL-6	Hyper-interleukin-6
MEC	Mammary epithelial cells
MMTV	Mouse-mammary tumor virus
MRD	Minimal residual disease
PBS	Phosphate buffer saline
PCR	Polymerase chain reaction
PFA	Para-formaldehyde
RT	Room temperature
PR	progesterone receptor (Protein)
PgR	progesterone receptor (Gene)
ESR1/ER-α	Estrogen receptor alpha
ESR2/ER-β	Estrogen receptor Beta
Her2/Erbb2	erb-b2 receptor tyrosine kinase 2
Sca-1	Stem cell antigen-1
SDF-1	Stromal derived factor-1

TBM	Tumor bone marrow
TBS	Tris buffer saline
TMEC	Tumor mammary epithelial cells
TW	Transwell
UV	Ultra violet
WT, wt	Wild type
EL	Early lesion
PT	Primary tumor
Met	Metastasis

3 Results

3.1 Cancer cell dissemination starts at early stages in Balb-NeuT model

In Balb-NeuT mice activation of transgene starts at week 4 when menstrual cycles of mice starts and secreted progesterone activates MMTV promoter (Figure 12). From our previous works, we could detect disseminated cancer cells (DCC) shortly after activation of the Her2-transgene at puberty, i.e. between week 4 and 9. At this time point, lesions represent the morphology of Atypical Ductal Hyperplasia (Figure 12).
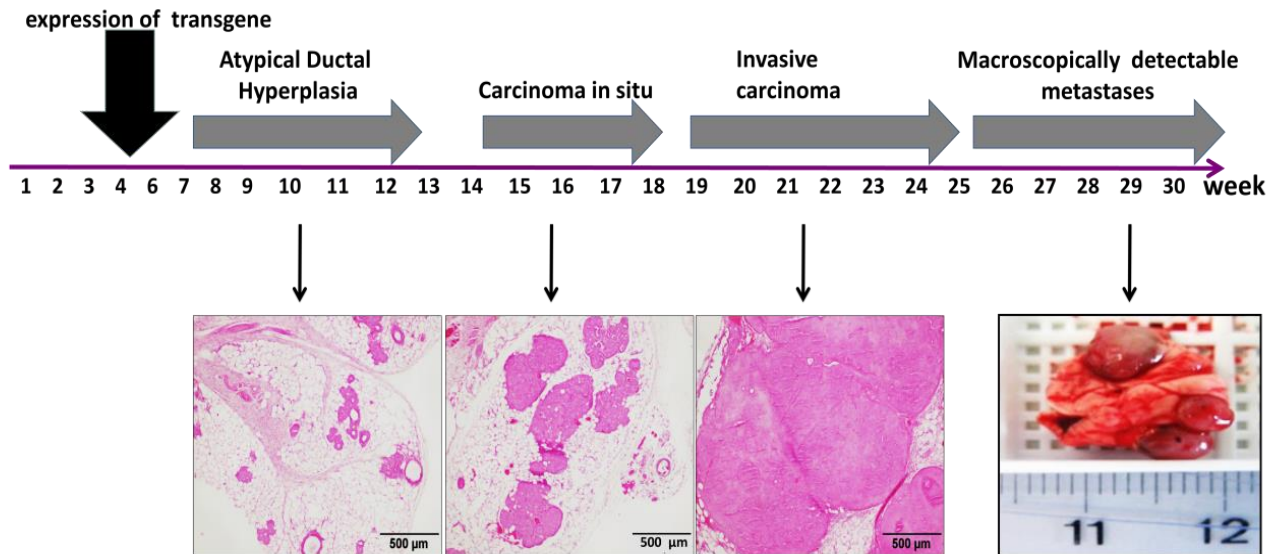
Figure 12. Time course of mammary tumor development in Balb-NeuT mice. From the 4th week of life, cells in the not yet completely formed ducts of the mammary glands express the protein product of Neu-T oncogene. From 7th to 12th week of life, expanding side buds give rise to atypical hyperplasia and from week 15th carcinoma *in situ* can be detected. These lesions grow to become invasive and palpable through the skin around the 19th week of life, and occupy the bulk of the subcutaneous fibro-adipose tissue from the armpits down to the sites of the two sets of five mammary glands on each side of the groin. Lung metastases are evident from the 27th week onwards.

To analyze seeding rate of cancer cells over the course of tumor development in this model, we analyzed number of DCCs in the bone marrow of mice. The number of seeded cancer cells were constant over the full observation period until mice had to be dissected (Hüsemann et al., 2008). Thus we hypothesize that increase in the number of cancer cells, by tumor growth, does not increase number of dissemination. In order to test that we measured gland or tumour areas from 270 mammary glands or tumours of 27 mice at different time points of Balb-NeuT

model. The tumour area of mammary glands without palpable (that is, not measurable by a caliper) tumours was set to 0.1 mm2 (that is, assuming a diameter of 350 μm of a total, circular hyperplastic lesion within a mammary gland) for lesions from 4–9-week-old mice and 0.4 mm2 for 11-week-old mice. The adjustment for 11-week-old mice was based on a microscopic evaluation showing an about 4-fold increase in hyperplastic lesions. Dissemination to the bone marrow was determined by the number of cytokeratin-positive cells per 10^6 bone-marrow cells. We plotted the tumor cell seeding relative to the total tumor area as a measure of cell numbers at risk to disseminate and found it to be maximal at early stages and to decline as the primary tumors grew (Figure 13). This is the time point that mostly we see ADH lesions (Figure 12), but it is difficult to surly claim no DCIS exist at this time point. Therefore, we use early lesions (EL) hereafter in the text to reflect all possible lesions at this time point.

The higher potency of dissemination at the EL time point drove our interests to disclose dissemination mechanism in these early lesions and study differences with late dissemination from advanced lesions.
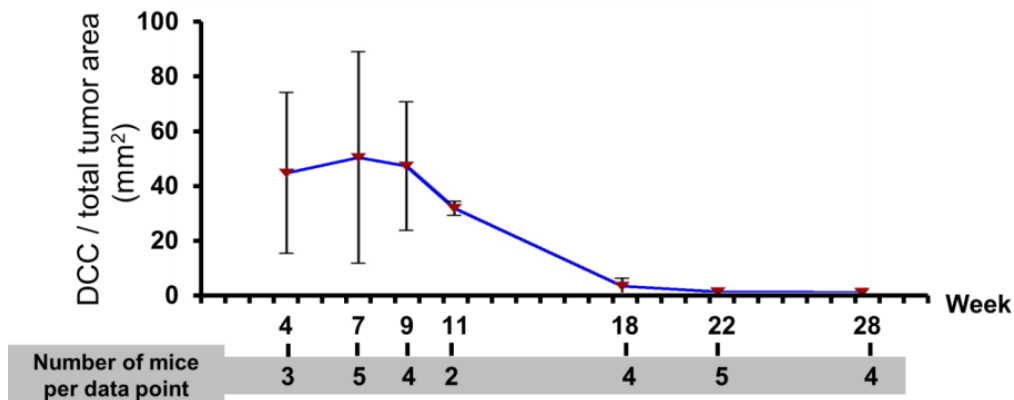
Figure 13. Dissemination over tumor area. Primary tumor growth and tumor cell dissemination to the bone marrow (BM) in Balb-NeuT mice over the time (Y-axis: displays the number of detected DCCs per 10^6 BM cells divided by the total tumor area in mm^2). Cancer cells were identified by anti-CK staining in bone marrow. The number of mice used per data point is written below the graph.

3.2 Progesterone and *Her2 s*ignaling regulate gene expression program of early lesions

3.2.1 Gene expression analyses revealed an exclusive expression profile for early lesions

In order to study early dissemination program, we compared expression program of early lesions, primary tumors, lung metastases of Balb-NeuT and normal mammary glands of BALB/c mice using microarray gene expression analyses. Laser microdissection was done and epithelial layers were dissected out from ductal structure or masses of tumor and metastasis. All samples, numbers and time points of sample collection are shown in table 7.

Table 7.   Samples used for gene expression analyses

Tissue	Mouse-strain	Age [weeks]	Number of mice	Number of samples
Normal mammary tissue	BALB/c	8 and 18	n = 7	n = 10
Early lesions (EL)	Balb-NeuT	9	n = 3	n = 7
Primary tumors (PT)	Balb-NeuT	27-29	n = 6	n =19
Lung Metastases (Met)	Balb-NeuT	27-29	n = 3	n = 7

First, a differentially expression profile has been generated for early lesions compared to each of the other stages (Figure 14; microarray analyses was done by Matthias Maneck from Computational diagnostics group, Institute of functional genomics, University of Regensburg). Then we cross-compared these three profiles and generated a gene expression profile unique to EL comprising 1278 gene transcripts. Next, this gene list was shortened to 300 genes by focusing on genes highly conserved between mouse and human (Supplementary Data 1). The conservation criterion was similarity in the regulatory sequences in both 3' and 5' of coding sequences between human and mouse. We checked if same miRNAs and transcription factors regulate these genes to be considered as conserved gene.
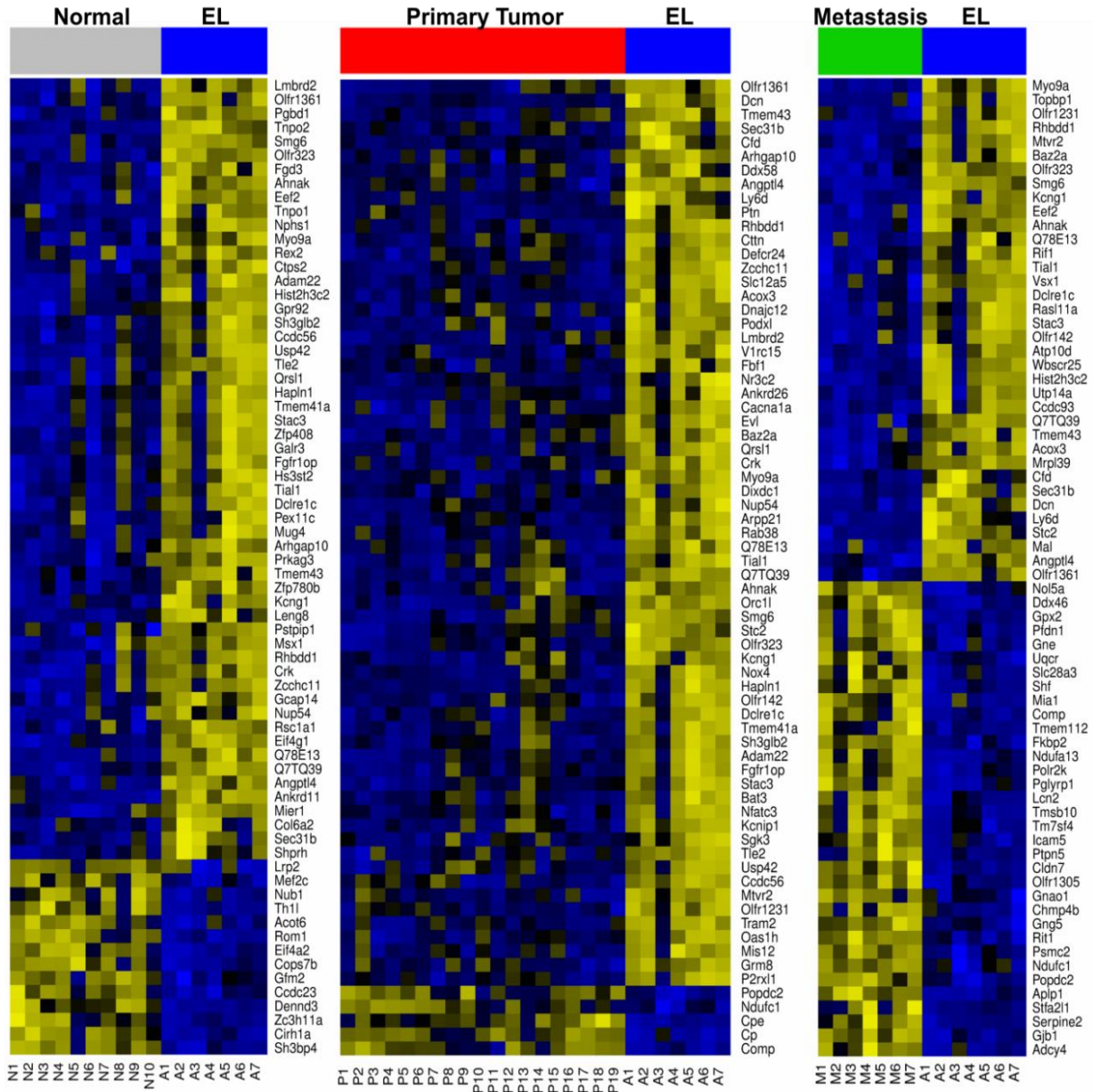
Figure 14. Microarray heatmaps. Heatmaps of genes differentially expressed between sample types (wt BALB/c non-transgenic mammary glands (normal, N1-10); Balb-NeuT Early lesions (EL, A1-7); Balb-NeuT primary tumors (PT, P1-19); lung metastases (Met, M1-7); yellow: strong expression; blue: low expression). This figure was generated by Matthias Maneck from Institute of functional genomics, University of Regensburg.

The gene list was further scrutinized for transcription factors (using oPOSSUM software version 1), and signaling pathway enrichment (Genomatix software version 2). The transcription binding enrichment showed that nuclear receptors family were prominent in the suggested list and interestingly, three members of steroid hormones including ESR, AR and NR3C1 were among them (Table 8).

Table 8.   oPOSSUM TF binding enrichment and role of nuclear receptors. A short list of genes specifically expressed in EL samples (300 genes, supplementary Data 1) was loaded into the oPOSSUM web based software (version 1). The 'TF class' column in this table indicates nuclear receptors as the main regulators of this profile. The 'Target gene hits' column indicates the number of genes from the 300 gene list which can be regulated by that specific transcription factor that is listed in the "TF binds to differentially expression profile" column. The 'Target gene non–hits' represents the number of genes from 300 gene-list that cannot be regulated by that specific transcription factor that is listed in the 'TF binds to differentially expression profile' column. The 'Target TFBS hits' represents total number of binding sites on the whole number of genes in the 'Target gene hits' column. Numbers of target TFBS hit are higher than target gene hits because one transcription factor can bind several times to a gene.

TFs bind to differentially expression profile	TF Class	Target gene hits	Target gene non-hits	Target TFBS hits
ESR1	NUCLEAR RECEPTOR	60	154	80
HNF1A	HOMEO	123	91	426
Pax4	PAIRED-HOMEO	62	152	88
NR3C1	NUCLEAR RECEPTOR	154	60	613
Ar	NUCLEAR RECEPTOR	77	137	107
RORA_2	NUCLEAR RECEPTOR	136	78	351
PPARG-RXRA	NUCLEAR RECEPTOR	32	182	36
RXRA-VDR	NUCLEAR RECEPTOR	45	169	53
PPARG	NUCLEAR RECEPTOR	9	205	10
NF-kappaB	REL	178	36	912
RORA_1	NUCLEAR RECEPTOR	186	28	991
NR2F1	NUCLEAR RECEPTOR	167	47	499
HNF4A	NUCLEAR RECEPTOR	183	31	934
SP1	ZN-FINGER, C2H2	198	16	2411

Similar results were obtained from the signaling pathways analyses. Steroid hormone receptors were among transcription factor regulators for all signaling pathways suggested by Genomatix software (Table 9). These analyses suggested steroid nuclear receptors and their regulated pathways as main candidate regulators of the EL-specific expression profile.

Table 9. Genomatix analyses and role of steroid hormone receptors. A shortlist of genes specifically expressed in EL samples (300 genes, supplementary Data 1) loaded into the Genomatix software (v2.0) to identify dominant signaling pathways or networks, which regulate these genes. Five different sub-tables were generated based on different criteria as provided in the heading of each table. The p-value indicates enrichment of the EL list in specific pathways or networks. The column entitled "number of involved genes" displays the number of genes from the expression profile of EL, which are involved in that particular signaling pathway or network. The rightmost five columns of each table display hormone nuclear receptors involved in that pathway or network. The (+) sign shows the involvement of steroid hormone receptors in the regulation of that given signaling pathway. Note that the progesterone receptor is not showing up in any of pathways possibly due to lacking information used by software or its indirect role acting via its paracrine factors.

5 top ranking canonical signal transduction pathways								
	p value	Number of involved genes	ER-α	ER-β	PgR	Nr3C1	Nr3c2	AR
MAP kinase	3.63 e-6	19				+		
FOXA2&A3 Network	7.13E-06	18				+	+	+
SMAD2&3 signaling	1.47E-05	20	+			+	+	+
P38 MAPK	4.71E-05	16	+			+	+	
TGFBR	1.54E-04	12	+				+	+
5 top ranking biological process networks (Gene ontology)								
	p value	Number of involved genes	ER-α	ER-β	PgR	Nr3C1	Nr3c2	AR
Transcription from RNA pol II promoter	1.57E-19	67	+	+		+	+	+
Positive regulation of transcription, DNA dependent	8.20E-19	56	+				+	+
Regulation of transcription from RNA pol II complex	1.26E-18	60	+				+	+
Positive regulation of RNA metabolic process	1.02E-17	56	+				+	+
Positive regulation of gene expression	1.97E-17	56	+				+	+
5 top ranking signal transduction pathways (literature mining)								
	p value	Number of involved genes	ER-α	ER-β	PgR	Nr3C1	Nr3c2	AR
Developmental	1.44E-05	22					+	
CEBP beta	1.44E-05	18	+				+	+
Histone deacetylase	2.72E-05	19	+				+	+
Differentiation	6.33E-05	26	+				+	
Nuclear receptor subfamily	7.03E-05	14	+			+	+	+

5 top ranking cellular component networks (Gene ontology)								
	p value	Number of involved genes	ER-α	ER-β	PgR	Nr3C1	Nr3c2	AR
Nucleoplasm	1.07E-11	56	+	+		+	+	+
Transcription factor complex	2.18E-10	22	+	+		+	+	+
Nucleus	2.38E-10	135	+	+		+	+	+
Nuclear lumen	4.38E-10	87	+	+		+	+	+
Nuclear part	5.27E-10	74	+	+		+	+	+
5 top ranking molecular function networks (Gene ontology)								
	p value	Number of involved genes	ER-α	ER-β	PgR	Nr3C1	Nr3c2	AR
Sequence specific DNA binding transcription factor activity	6.16E-31	71	+	+		+	+	+
Nucleic acid binding transcription factor activity	6.59E-31	71	+	+		+	+	+
Sequence specific DNA binding	1.17E-27	57	+	+		+	+	+
Sequence specific DNA binding RNA pol II transcription	9.28E-23	32	+	+		+	+	+
Regulatory region DNA binding	1.53E-22	37	+	+		+	+	+

Next, we checked the expression of all steroid hormone receptors in samples which used for microarray experiments (samples in Table 7). Our qPCR results showed all of them, except of ERα, were up-regulated in EL samples compared to Mets and PTs (Figure 15), which underlined obtained results of bioinformatics analyses (Tables 8 and 9).
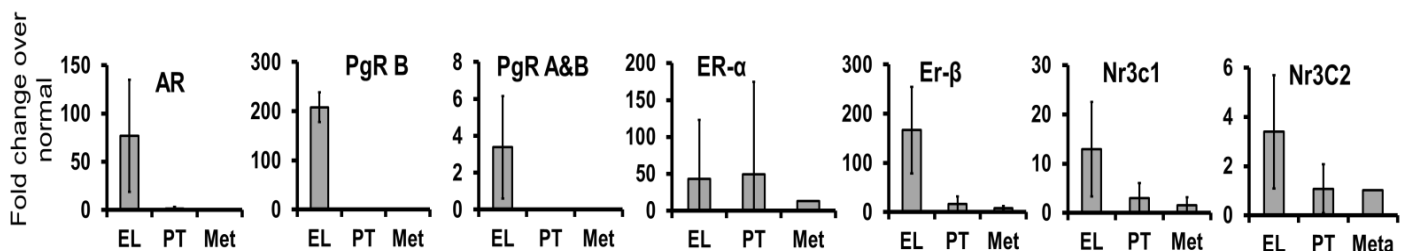
Figure 15. Quantitative PCR for mRNA expression of steroid hormone receptors in the microarray analyzed samples. Quantitative PCR for mRNA expression of all steroid hormone receptors in samples of EL, early lesions; PT, advanced primary tumor; Met, lung metastasis). All steroid hormone receptors except of ER-α are upregulated in EL samples compared to PTs and Mets. Samples are shown in Table 7 and are the same which used for gene expression analyses in Fig 14.

3.2.2 Progesterone as regulator of EL gene expression profile

To test whether steroid hormones induce the expression of genes characteristic for EL, we performed *in vitro* stimulation of mammary cells by steroid hormones. To monitor EL signature activation, five up-regulated genes in EL from microarray analyses were selected and used as surrogate markers of signature activation. Therefore, we used Nr3c1 as it had the highest number of target genes from the differentially expressed gene list (Table 8) and Nr3c2 that was the main one involved in governing pathways (Table 9). AHNAK, Baz2a and Nfatc3 were selected from the highly upregulated profile (supplementary Data 1). All surrogate markers comprising AHNAK, Baz2a, Nfatc3, Nr3c1 and Nr3c2, were first confirmed by qPCR for their induced expression in EL (Figure 16). The qPCR primers were designed between exons close to the 3' UTR of genes ant tried to cover all possible isoforms of target gene. All primers were tested for their efficiency and specificity of amplification. The specificity of amplification was checked by a single melting curve in the end of qPCR. The efficiency of each primer was checked by the efficiency calculator program of light cycler software.
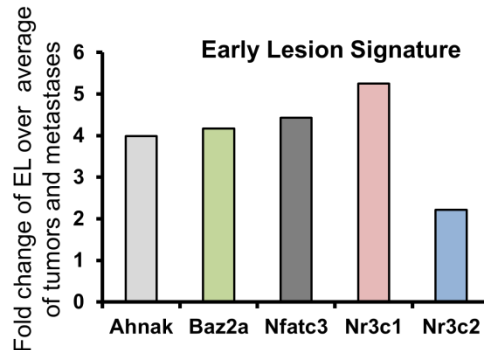
Figure 16. Early lesion signature. Five genes up-regulated genes in the EL samples were selected as EL surrogate signature (Fold change of each gene for EL over average expression of PTs and metastases). Samples are shown in Table 7 and are the same which used for gene expression analyses in Fig 14.

Then, primary cultures derived from mammary glands of 7-9 week old Balb-NeuT mice were exposed to all steroid hormones including estrogen, progesterone, aldosterone, cortisol, and testosterone. All mammary glands of mouse were pooled (three mice were used; see method section for primary culture) and cells were dissociated mechanically and enzymatically. Mammary epithelial cells were sorted by density centrifugation and cultured in the routine cell culture conditions. Hormones were added in different concentrations comprising 1, 10 and 100 nM. The experiment lasted 75 hours and fresh media plus fresh hormones were added every 24

hours. At the harvesting day, cells were treated with fresh media and hormones and harvested after 3 hours. After, RNA extraction (three samples for each condition) and c-DNA synthesize, qPCR was done (technical duplicate or triplicate per sample) to evaluate changes in the expression of genes of the EL signature in the treated samples compared to controls. Among all tested hormones, progesterone was the only steroid hormone that generated the EL surrogate signature constantly over different applied concentrations (Figure 17).
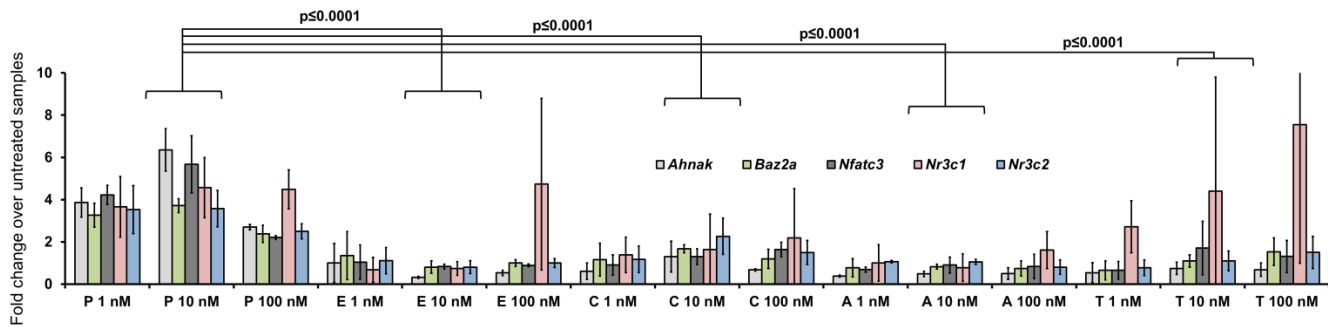
Figure 17. Hormone treatment of EL primary culture and qPCR evaluation of EL-signature. Hormone responsiveness of digested fresh tissue of 7-9 week old Balb-NeuT samples. Primary cultures (2.6×10^4 cells/cm^2) were treated with progesterone (P), estrogen (E), aldosterone (A), cortisol (C), and testosterone (T) in different concentrations (1, 10, and 100 nM) or vehicle (ethanol; untreated) for 75 hours. Only progesterone could induce expression of the complete EL signature. All p-values, Student's *t*-test and Stouffer's combined probability test; all error bars correspond to standard deviation (Mean ±SD).

After confirmation that progesterone induced the surrogate EL-signature, we next wanted to check if this induction effect is dependent on age and strain of mice (NeuT or wild type strain; 3 mice per condition pooled and three c-DNA samples were derived; qPCRs were done in duplicate or triplicate technical replication; see method section for sample preparation). Therefore, we compared hormone responsiveness of EL and PT cells as well as normal mammary epithelial cells from mice having the same age as mice with EL (week 9). Interestingly, only EL cells of 9-week old Balb-NeuT mice, but not wild type mammary cells or PT cells, were responding to treatment with up-regulation of the surrogate genes (Figure 18).
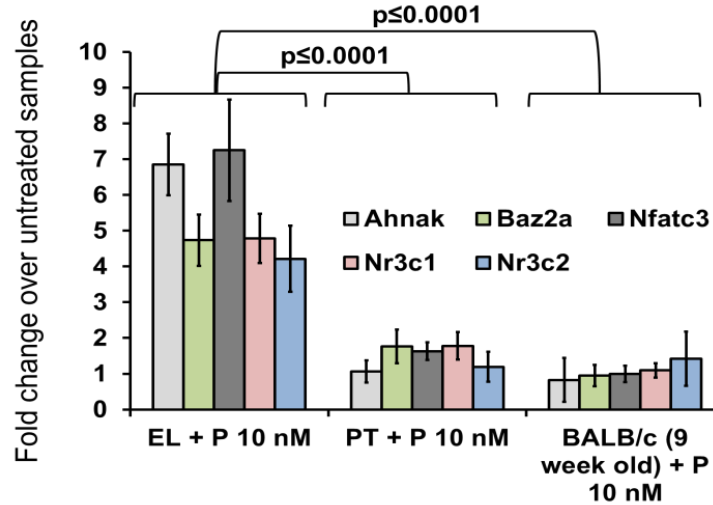
Figure 18. Hormone treatment of primary cultures from different tissues and qPCR evaluation of EL-signature. Progesterone induction of the EL signature (10 nm *vs.* ethanol vehicle) only in mammary cells from young transgenic mice. All p-values, Student's *t*-test and Stouffer's combined probability test; all error bars correspond to standard deviation (Mean ±SD).

These results suggested that response to progesterone is dependent on the expression of Her2 (only Balb-NeuT was responding) and may also be a stage-specific program (only EL was responding). To test this hypothesis, immunohistochemistry was done for progesterone receptor (PgR) and Her2 expression on the three tissue types. Early lesions showed the highest coincidence between PgR (strong expression) and Her2 (moderate expression) stained cells (Figure 19). Primary tumors completely lost PgR expression which explained why progesterone treatment could not induce the signature in these cells.
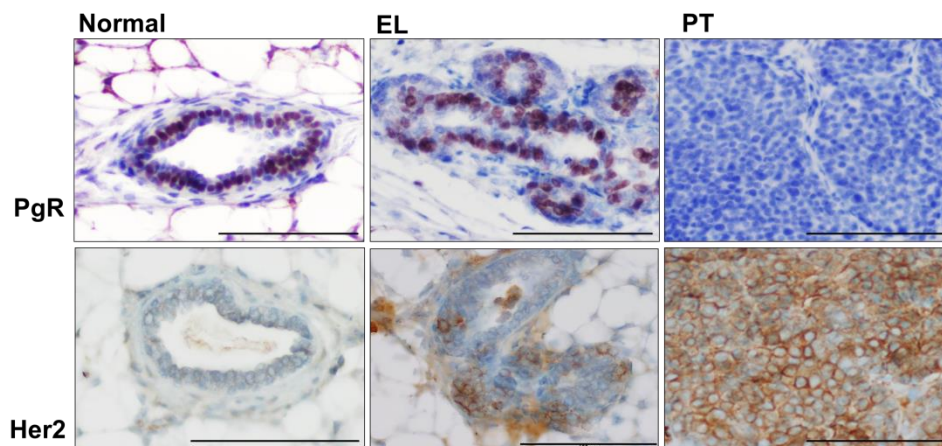
Figure 19. PgR and Her2 staining in tissues. Immunohistochemistry of PgR (nuclear; brown; upper panel) and Her2 (membrane; brown; lower panel; scale bar = 100 µm). Note that highest overlap between Her2 and PgR expression is in the EL stage. There is low expression of Her2 before EL and there is complete loss of PgR in the later stages.

3.2.3 Her2 and progesterone cooperate to generate EL signature

We asked if the EL surrogate signature was the consequence of MMTV-promoter-driven expression of Her2 in transgenic animals, because the MMTV-promotor is responding to progesterone. We checked TUBO cells, a cell line derived from a Balb-NeuT primary tumor, and additional BALB/c derived cell lines 4T1, 67NR and MM3MG to evaluate their gene expression response to progesterone exposure (10 nM progesterone; progesterone treatment condition was 75 h with 24 h intervals for washing and refreshing media). In addition to TUBO cells, 4T1 cells responded to progesterone by up-regulating the EL surrogate signature (Figure 20), indicating that the signature does not depend on the MMTV promoter driving Her2 because 4T1 cells are not transgenic for MMTV-driven Her2.
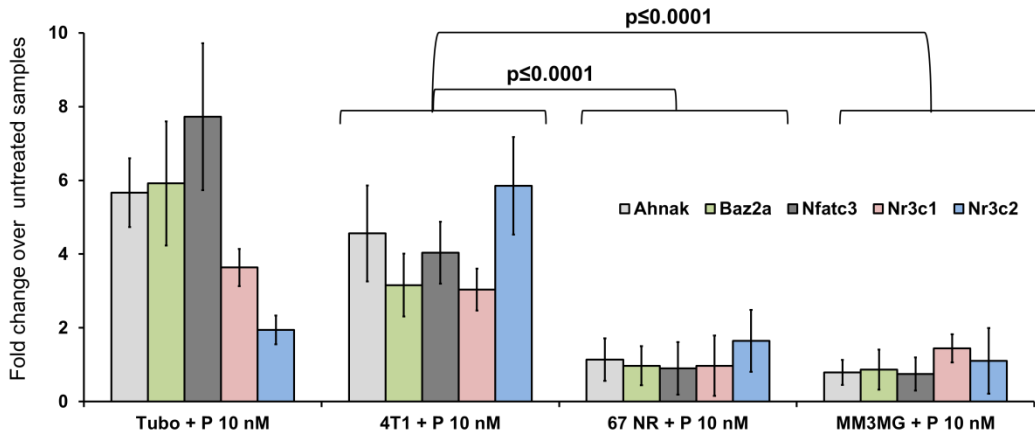
Figure 20. Cell line treatment with progesterone and qPCR evaluation of EL-signature. Progesterone induced the EL signature in TUBO and 4T1 cells (however, only in low cell density: 5.2×10^3 cells/cm^2), but not in 67NR and MM3MG cells. All p-values, Student's *t*-test and Stouffer's combined probability test; all error bars correspond to standard deviation (Mean ±SD).

Further investigation was done to find the differences of steroid hormone receptors and Her2 in the responding and non-responding cell lines at protein level. Protein blotting results revealed that the B form of PgR (PgR-B), the main isoform in mammary gland development and morphogenesis (Aupperlee et al., 2005; Fernandez-Valdivia et al., 2005; Mulac-Jericevic et al., 2003), and Her2 were only expressed in responding cell lines, i.e. 4T1 and TUBO (Figure 21 A). To further confirm that surrogate marker expression truly depends to the progesterone stimulation, TUBO cells were exposed to increasing concentrations of progesterone (1 nM - 100 nM) and noted a dose-dependent up-regulation of Nr3c1, Nr3c2, AR, and PgR (Figure 21 B). Likewise, progesterone induced Her2 expression in TUBO and 4T1 cells in a dose-dependent manner (Figure 21 B-C). These results also showed a concomitant upregulation of PgR and Her2

upon progesterone treatment similar to what has been observed in IHC results of EL which showed higher overlap between Her2 and PgR expression in this stage (Figure 19). Hence, we hypothesized that upregulation of Her2 is induced by PgR and to test that, I transduced the Her2 and PgR-B-negative MM3MG cells with PgR-B and observed an up-regulation of Her2 (Figure 21 D). Further corroboration was done by protein analysis of tissues where I observed that higher expression of PgR-B at 9 week old mammary glands, even wild type one, is correlated with slight upregulation of Her2 (Figure 21 E). ELs strongly express PgR and moderately express Her2 but advanced lesions completely lost PgR while Her2 was strongly expressed (Figure 21 E, Figure 19). Collectively, these results suggested that genetic program of early lesions in this model is governed by fine tune expression of Her2 and PgR and interplay between their signaling.
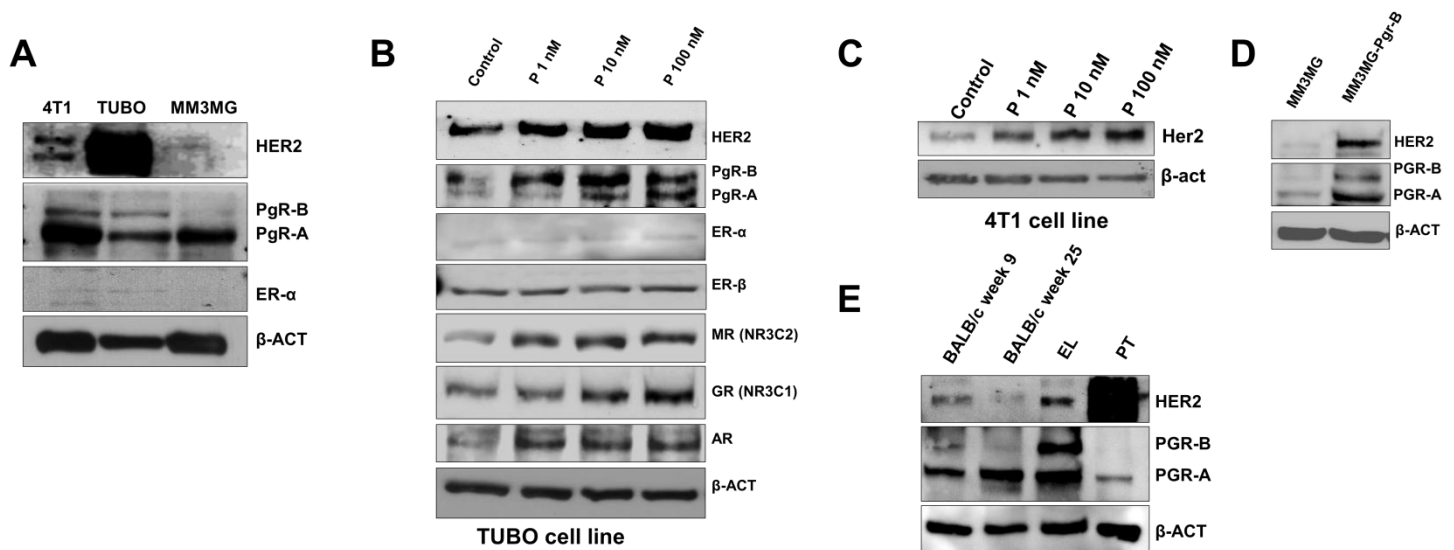
Figure 21. Protein analyses of steroid hormone receptors and Her2 (**A**) Western blot analyses of progesterone and estrogen receptors and Her2 in hormone responding (4T1 and TUBO) and non-responding (MM3MG) cell lines. Note the presence of Her2 and progesterone receptor B in 4T1 and TUBO cells as opposed to the non-responding MM3MG cells. (**B**) Progesterone treatment of TUBO cells and protein analyses for steroid hormone receptors and Her2, demonstrates up-regulation of Her2, Nr3c1, Nr3c2, AR and PgR by progesterone. (**C**) Progesterone treatment up-regulates Her2 in 4T1 cells. (**D**) Overexpression of PgR B in the MM3MG cell line up-regulates Her2 expression. (**E**) Higher expression of PgR-B in young mammary glands, up-regulates slightly Her2 expression. See supplementary data 4 for the original blotting figures.

3.3 Progesterone signaling regulates the migration program in EL and is linked to side branching and morphogenesis

3.3.1 Role of Progesterone in side branching and morphogenesis

We aimed to evaluate the link between progesterone-induced EL signature and the migratory behavior of cancer cells by performing *in vitro* migration/invasion assays. Because progesterone is known as the main regulator of mammary gland side branching and this function is mediated by progesterone-induced cytokines (Brisken et al., 2000; Brisken and O'Malley, 2010), Wnt4 and Rankl were included into the analysis. Accordingly, we checked their relevance by analyzing mRNA expression levels in fresh frozen samples (PT, 6 mice; EL, 4 mice; BALB/c 8 weeks old, 5 mice; BALB/c 25 week old, 4 mice; each mouse was used as one sample; qPCR was done as technical duplicate or triplicate for each sample) and found mRNA upregulation of these factors in EL samples which was in parallel to PgR expression (Figure 22 A). Next, we tested if the progesterone effect on EL signature works through these paracrine factors (3 mice per condition pooled and three c-DNA samples were derived; qPCRs were done in duplicate or triplicate technical replication; see method section for sample preparation). Interestingly, Wnt4 and Rankl can regenerate EL signature and their combined action resulted in strong responses (Figure 22 B).
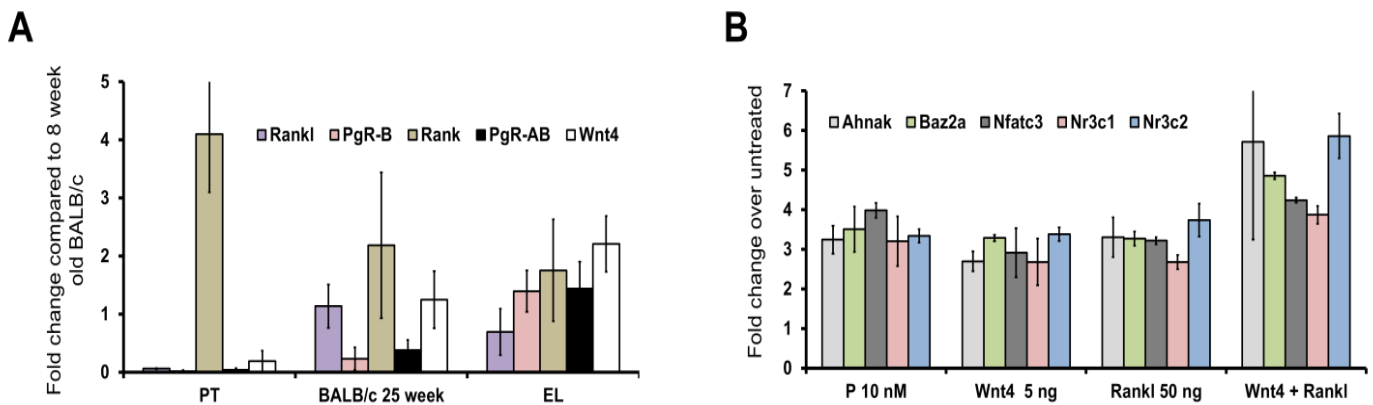
Figure 22. Wnt4 and Rankl are mediators of progesterone impacts (**A**) Quantitative PCR for PgR, Rank, Rankl and Wnt4, shows higher expression of PgR, Wnt4 and Rankl in EL compare to PT samples. Note strong expression of Rank in primary tumors. (**B**) Primary cultures of EL treated with progesterone, Wnt4 and Rankl. Wnt4 and Rankl also generate full EL signatures and act in an additive manner. All error bars correspond to standard deviation (Mean ±SD).

The observation that inducer (progesterone) and mediator (Wnt4 & Rankl) physiologically regulating side branching and morphogenesis, were also inducing the EL signature, encouraged us to hypothesize that mammary side branching mechanisms might be recruited in early lesions and exploited for migration and dissemination. To support this notion, we compared (collaboration with Julio A. Aguirre-Ghiso's lab from Mount Sinai School of Medicine, New York) the rate of PgR positive cells in ducts that are distal (advancing tree away from the nipple - more dynamic developmental tissue) and proximal to the origin (closer to the nipple - more stable differentiated ducts; 2 mice per age point; Figure 23 A) in wild-type mice. We found that the distal and more invasive part of the duct displayed a higher percentage of PgR$^+$ cells than the proximal ducts (Figure 23 A-B). This difference was evident at 5 weeks of age and clearer at 12 weeks when PgR$^+$ epithelial cells drop even more in the differentiated structures (Figure 23 B).
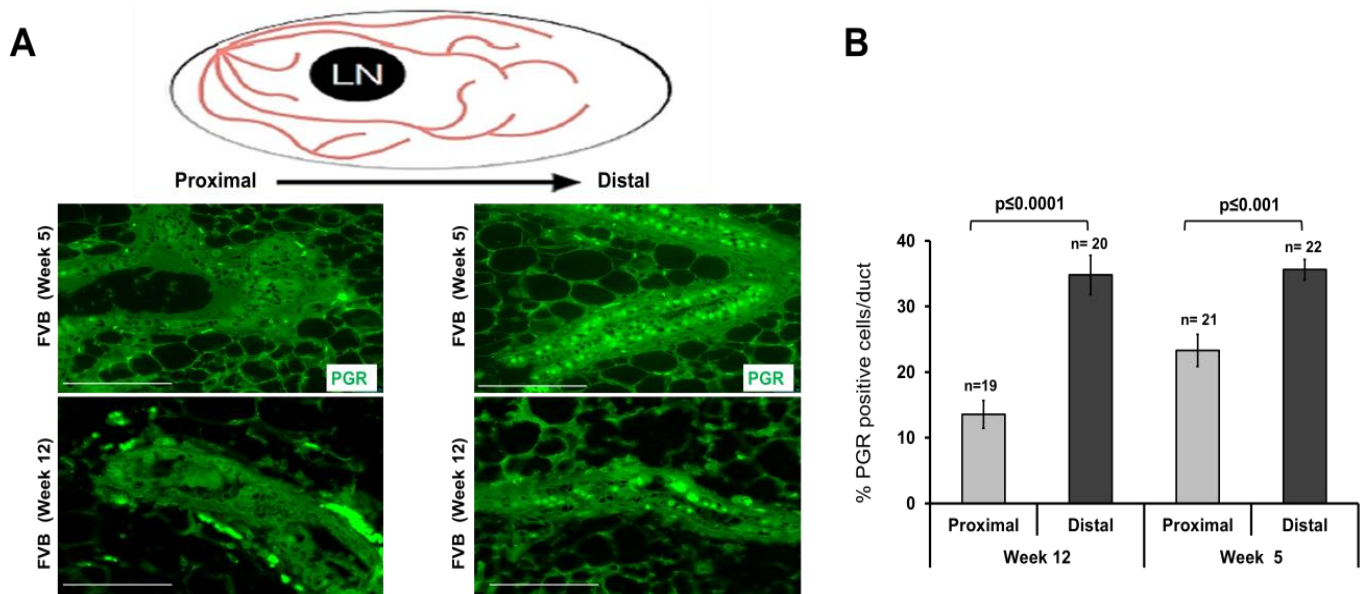
Figure 23. PgR staining in posterior anterior epithelial structures of mammary gland (**A**) PgR (green) staining at 5 weeks and 12 weeks of age (scale bar = 100 µm). (**B**) The percentage of PgR cells per duct was quantified using dye separation images (n=20 ducts, two mice/age group) in the proximal and distal portions of the gland (relative to the origin; LN, lymph node). All p values calculated based on Student's t-test; error bars correspond to standard error of the mean (Mean ±SEM) and numbers in the top of each column shows number of screened ducts (at least three mice for each time point). Note that LN was helping to assure about position of ducts as distal or proximal. This figure generated by Julio A. Aguirre-Ghiso's lab from Mount Sinai School of Medicine, New York.

3.3.2 Progesterone and its paracrine factors regulate *in vitro* migration of PT and EL cells

To test if the same players governing side branching and morphogenesis are also involved in migration of early lesion cells; we tested migration ability of these cells exposing to progesterone and induced paracrine factors. Cells were seeded on the top of a layer of 30% matrigel in the upper side of inserts of transwell plates. After 72 hours cells migrated to the lower side of insert fixed and stained with trypan-blue and visualized under the microscope. Migration events were evaluated for mammary epithelial cells from 9 (EL-derived) and 22 (PT-derived) week-old Balb-NeuT mice either directly isolated from tissues or obtained from dissociated mammosphere. The results from both approaches were very similar. Progesterone and its paracrine signals, Wnt4 and Rankl, induced migration of cells from EL-derived samples and suppressed it in cells from primary tumors (Figure 24 A, and B for tissue-derived cells and Figure 24 C, and D for sphere-derived cells; see supplementary data 3 for the raw numbers and replications). These results suggested that progesterone and its paracrine signals induced migration of EL similar to their induction of mammary side branching during mammary epithelial morphogenesis.
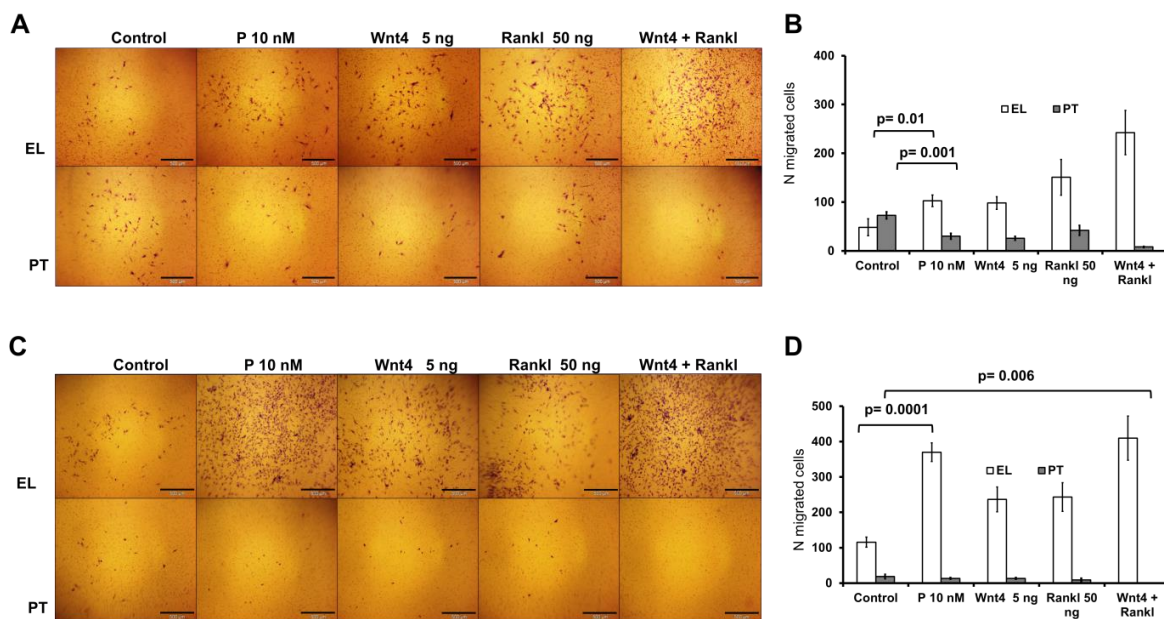
Figure 24. Role of progesterone and its paracrine factors in migration of EL and PT cells. Photomicrograph of migration assay and quantification. Trypan blue staining of EL and PT cells after migration (scale bars = represent 500 µm). Progesterone and its paracrine mediators Wnt4 and Rankl induce migration of EL but not PT cells. Cells were derived from tissue digestion (**A-B**) or sphere cultures after dissociation (**C-D**) and 1 x 10^5 cells were seeded in each migration well (24 well plate). Scale bars in panels A and C represent 500 µm. Panels B and C display the number of migrated cells. All p-values, student's t-test; all error bars correspond to standard deviation (Mean ±SD).

3.4 Progesterone signaling regulates migration, stemness, and proliferation of cancer cells

3.4.1 Higher sphere formation ability of young mammary epithelial cells

In addition to the motility and invasion, progesterone-induced paracrine signals are known to activate mammary stem cells (MaSCs) during mammary gland development. This and the notion that stem-like cells are regarded as prime candidates for metastasis founders, prompted us to explore the impact of progesterone-induced paracrine signals on MaSCs and progenitor cells. Mammary epithelial cells from 9 week-old Balb-NeuT and wild type mice and from primary Balb-NeuT-derived tumors were cultured under ultra-low adherent conditions in mammosphere medium (Liao et al., 2007), where the number of sphere-forming cells informs about cells with stemness potential (mammary epithelial cells from ≥3 mice were pooled and at least tree plate run for each condition). In order to prepare single cell suspension, dissected mammary glands or PTs were minced mechanically to small pieces and dissociate enzymatically using collagenase and hyaluronidase solved in basal medium. Single-cell suspensions were grown in the basal medium supplemented with B27, EGF, basic fibroblast growth factor (bFGF), heparin, Grow-α and HIL6 in 3 or 5 cm plates at a density of 50,000 cells/mL. After 10-14 days sphere bigger than 50 μm were counted as the mammospheres.

Consistent with previous reports on Her2-stimulated stemness and sphere formation (Ginestier et al., 2007; Korkaya et al., 2008), Balb-NeuT-derived samples displayed significantly higher number of spheres per plated cells than age-matched controls. Furthermore, we noted that 8 week-old BALB/c mammary cells produced higher sphere numbers than mammary cells from 25-week old BALB/c mice (Figure 25 A). However, EL samples produced by far the highest numbers of spheres. We therefore used Sca-1, as the relevant cancer stem cell marker in the Balb-NeuT model (Grange et al., 2008), and investigated its expression in normal glands and during malignant growth (done in collaboration with Piero Musiani from aging research centre, Gabriele d'Annunzio University Foundation, Italy). Interestingly, we noted an increase of Sca-1 expressing cells in the EL compared to the normal glands and a decrease of epithelial cells with Sca-1

expression as the tumours grew large. In advanced cancers Sca-1 appeared to be expressed almost exclusively by endothelial cells (Figure 25 B).
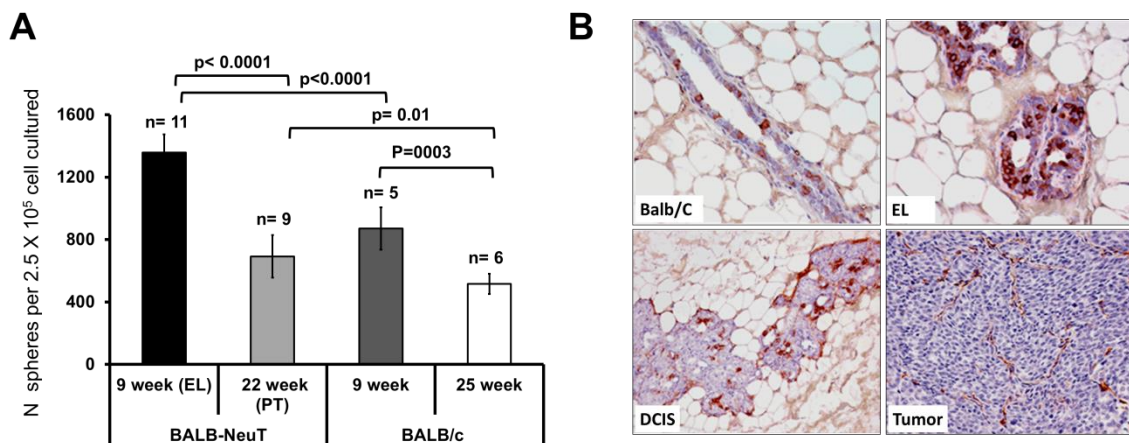
Figure 25. Age and Her2-transgene activity regulate stemness. (A) Her2-transgenic mammary cells form more mammospheres than control cells. The total number of spheres formed is also higher in 9 week-old mice compared to 22 (Balb-NeuT) and 25 (BALB/c) week-old mice with and without transgene. Numbers in the top of each column shows number of experiments (each experiment run with ≥3 mice). **(B)** IHC staining of Sca-1 as stem cell marker demonstrates diminishing of stem like cells during tumor development. In advanced tumours Sca-1 staining can be observed mostly in endothelial cells. All p-values, student's t-test; all error bars correspond to standard deviation (Mean ±SD). Sca-1 staining generated by Piero Musiani from aging research centre, Gabriele d'Annunzio University Foundation, Italy.

3.4.2 Higher expression of PgR in young mammary glands

To support the hypothesis that higher number of spheres in young mammary gland-derived cells is linked to the expression of PgR, IHC staining was performed for PgR in the FFPE samples at different time points of tumor development as done for sphere assay. Interestingly, by comparing the expression of PgR in wild type and transgenic mice of different age (week 4 vs. week 40), we noted a 75% reduction in PgR^{+} epithelial cells at higher age in wild type and a complete loss in PTs (Figure 26 A-B, and 22 A). This reduction paralleled the decreased expression of Wnt4 and Rankl, the prime PgR-induced paracrine signals (Figure 22 A). Therefore, expression of PgR and its paracrine factors is concurrent with expression of stemness markers at the mammary epithelial structures.
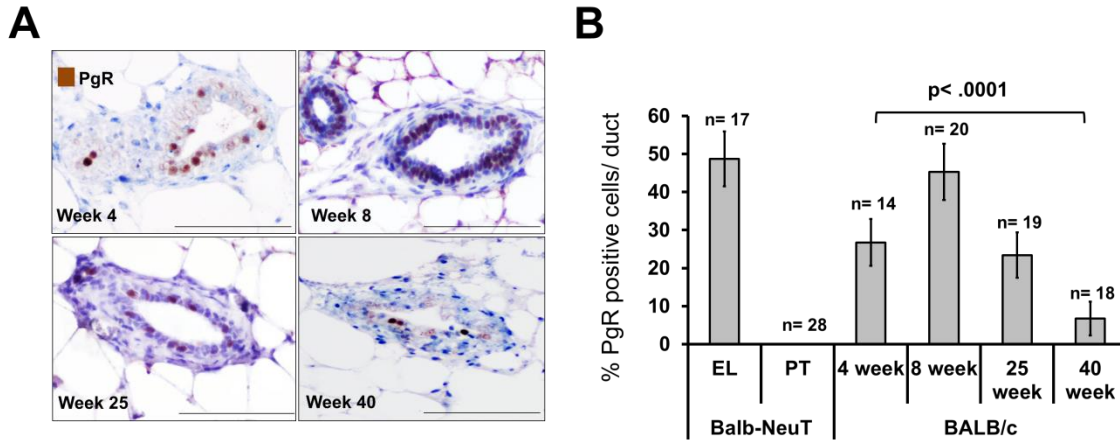
Figure 26. PgR IHC staining. (A-B) IHC staining shows higher expression PgR (brown staining) in epithelial structures of younger mammary glands compare to the older one in both transgene and wild type (scale bar = 100 μm). PGR expression was reduced by 75% in 40-week-old wild-type mammary gland compared to 4-week-old mice and disappeared in primary tumours (see also Figs 21 and 22). All p values, Student's t-test; n, number of ducts or glands (in early lesions and normal tissue) or visual fields in primary tumours; (at least three mice for each time point); all error bars correspond to standard deviation (Mean ±SD).

3.4.3 Progesterone-induced paracrine factors regulate stemness of PT and EL cells

Young mammary glands are enriched with PgR positive cells and express higher level of Wnt4 and Rankl compared to older mammary glands (Figures 22A and 26). In addition, they are more able to form spheres (Figure 25A). We therefore tested whether stimulation of sphere formation by progesterone can be recapitulated by the paracrine action of Wnt4 and Rankl. Indeed, EL derived cells responded to progesterone and Wnt4/Rankl with the increase of sphere formation (p= 0.01) whereas sphere formation from primary tumor samples was suppressed by Wnt4 and Rankl (p= 0.003; Figure 27; mammary cells from ≥3 mice pooled and ≥ 3 samples were used for sphere formation assay like 3.4.1). Therefore, sphere formation as a stemness trait of cancer cells in this model is regulated by progesterone signaling. Depend on the stage which cancer cells are derived from, progesterone signaling either induces (for EL cells) or suppresses (for PT cells) stemness.
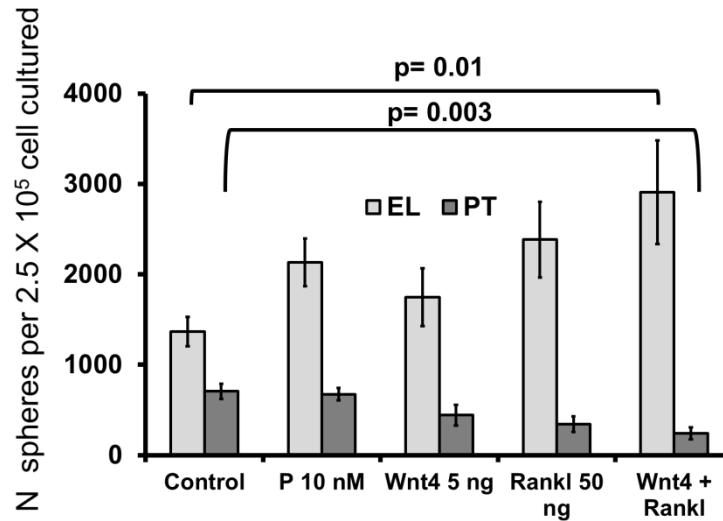
Figure 27. Role of progesterone and its paracrine factors in sphere formation of EL and PT cells. Progesterone and its paracrine factors induce sphere forming ability of EL and suppress it for PT cells. All p-values, student's t-test; all error bars correspond to standard deviation (Mean ±SD).

3.4.4 Stemness feature of migrating cells

The similarity of migration and stemness behavior of EL and PT cells in response to progesterone and induced paracrine signals, prompted us to test the stemness of migrating cells. EL or primary tumor derived cells were plated on matrigel that covered the membrane of a transwell chamber. After migration through matrigel, we counted mammosphere formation in the lower chamber, where we prevented cell adhesion by poly-HEMA coating of surface (Figure 28 A). After 72 hours of incubation, inserts were removed and stained. As before, EL samples displayed a higher number of migratory cells. Over the next 7 days, we could detect significantly higher numbers of spheres in the lower chambers of EL samples than of primary tumor samples (Figure 28 B and C). All steps, including migration (p=0.001; Student's t-test) and sphere formation (p=0.005; Student's t-test) were significantly induced by progesterone treatment. We conclude that progesterone induces migration of stem-like cells which might also encompass the ability of DCCs for distant outgrowth.
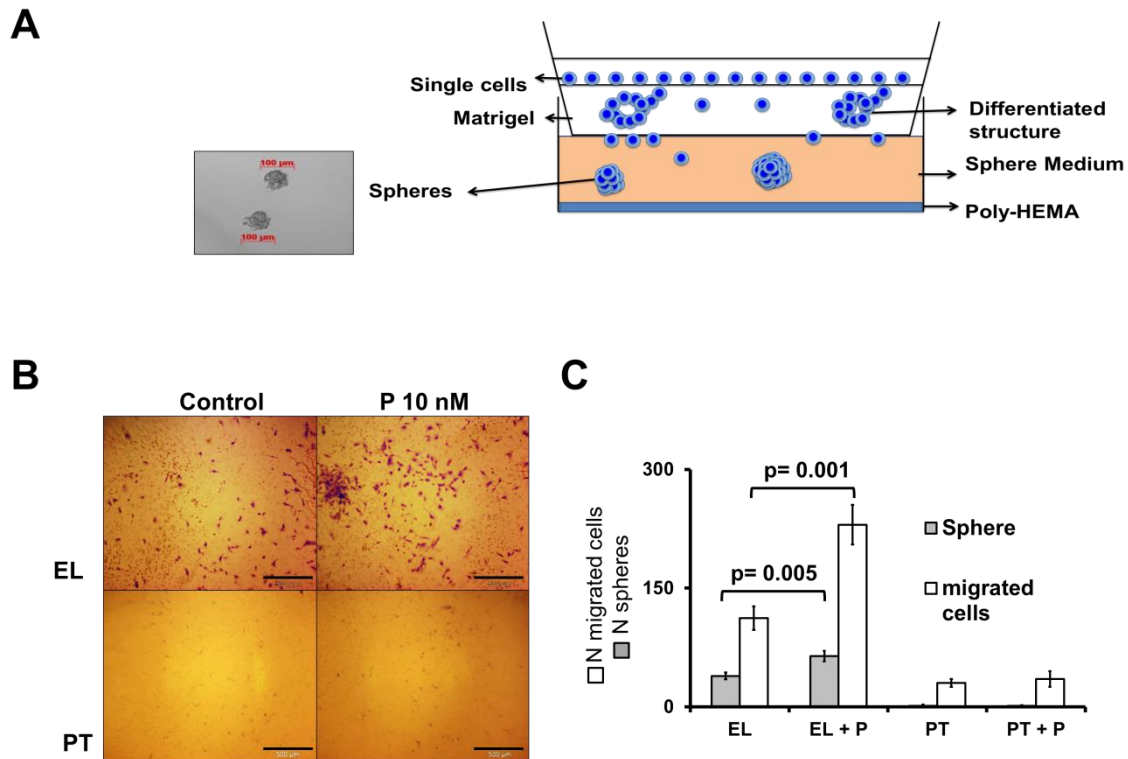
Figure 28. Migration and sphere formation assay. (**A**) Schematic of combined migration and sphere assay. The lower chamber is filled with serum-free sphere medium and bottom is covered with poly-hema to prevent adhesion and enable sphere formation. (**B-C**) Micrograph of migration-sphere formation assay (scale bar = 500 µm) and quantification. All p-values, student's t-test; all error bars correspond to standard deviation (Mean ±SD).

3.5 Her2 expression levels determine migratory vs. proliferative cellular responses

We found that progesterone stimulates migration and sphere formation via its paracrine factors. In addition we found while EL signature, migration and stemness depends on co-signaling of PgR and Her2, but strong expression of Her2 in PT cells changes these phenotypes. Therefore, we asked what role the expression level ("dose") of Her2 expression plays in this scenario.

3.5.1 Progesterone-induced paracrine factors act as inducer of stemness and migration for EL-like cells and supressor for PT-like cells

To test role of Her2 expression in this model, we transduced MM3MG cells, a normal mouse mammary epithelial cell line which weakly expresses Her2 and PgR (Figure 21 A), with PgR-B

or Her2 and assessed their sphere formation and migration abilities (similar to what described in 3.4.1-3; see method sections for more details). Overexpression of PgR-B (MM3MG-PgR B) decreased the migration of these cells but they were not responding to progesterone. Similarly, PgR overexpression reduced sphere formation of these cells (Figure 29 A-C). Conversely, Her2 overexpression increased sphere formation and migration of cells. Therefore, the migratory cells are PgR negative cells; either non-transduced cells (MM3MG) or Her2 (MM3MG-Her2) cells; those were selected to further test them for impact of progesterone signaling in migration and sphere formation.
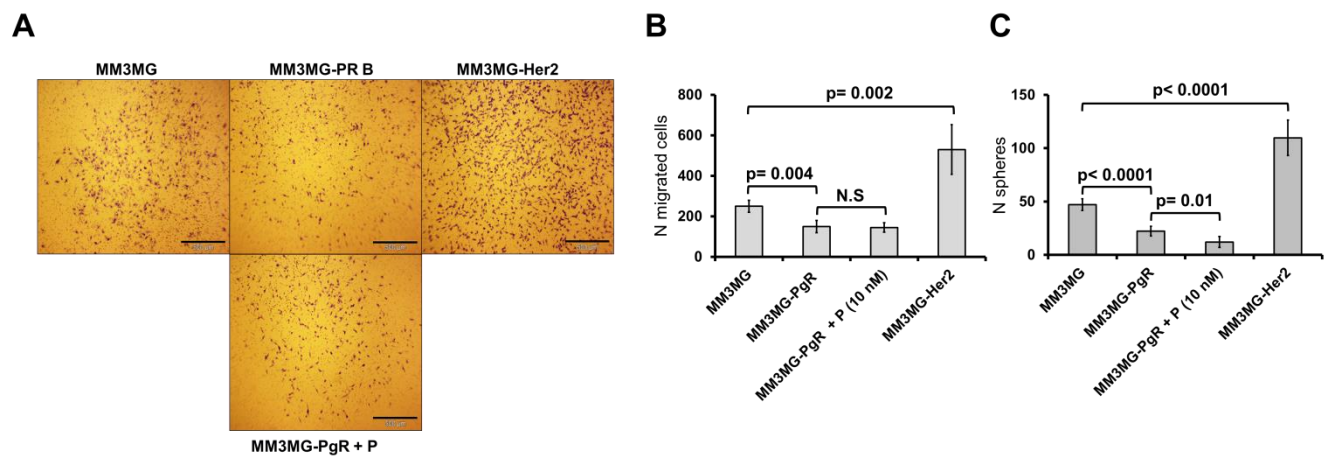
Figure 29. PgR and Her2 expression and evaluation of migration and sphere formation. (**A-B**) Overexpression of PgR-B in MM3MG cells reduced migration while Her2 overexpression (MM3MG-Her2) increased migration. Progesterone did not alter migration of PgR B-overexpressing cells (MM3MG-PgR B). (**D**) Overexpression of PgR-B in MM3MG cells reduced sphere formation ability while Her2 overexpression increased it. All p-values, student's t-test; N.S, not significant; all error bars correspond to standard deviation (Mean ±SD).

In the co-culture experiments, we observed that co-culturing of MM3MG with MM3MG-PgR or addition of Wnt4/Rankl to MM3MG cells induced their migration and addition of Wnt4/Rankl induced sphere-forming ability of MM3MG cells (Figure 30 A-C). In contrast, MM3MG-PgR cells or addition of Wnt4/Rankl suppressed migration of MM3MG-Her2 cells. The two cytokines also suppressed MM3MG-Her2 sphere formation (Figure 30 D-F). These results indicate that 1) MM3MG-Her2 cells behave like Balb-NeuT PT cells, 2) MM3MG cells behave like EL cells, 3) expression of PgR suppressing migration and sphere formation, but MM3MG-PgR cells can influence migration and sphere formation of neighboring cells.
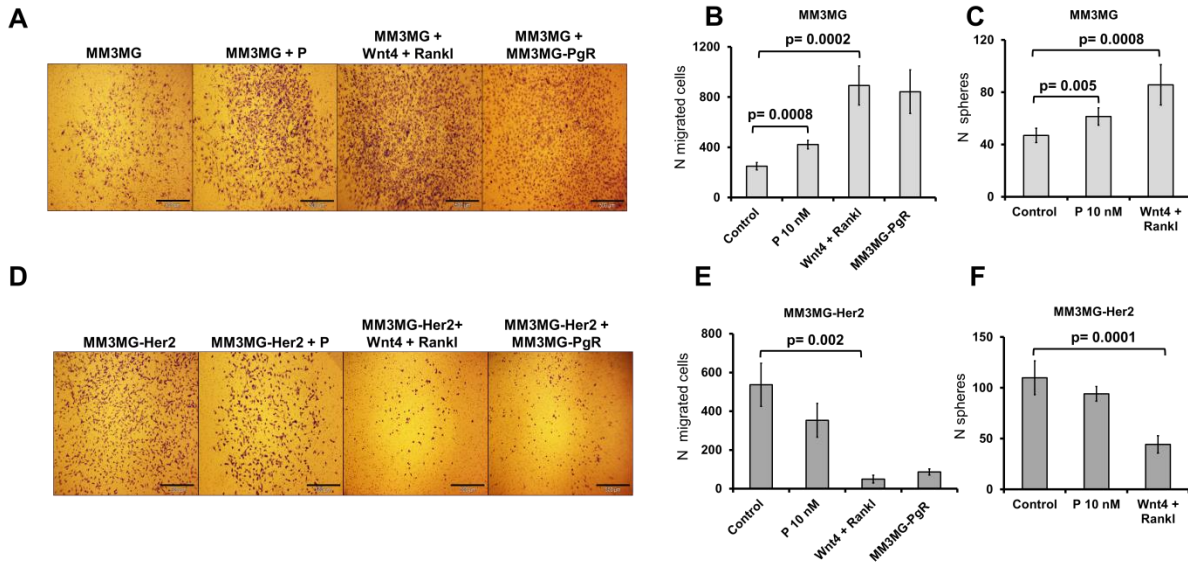
Figure 30. Migration and stemness of Her-negative and positive cells under activation of progesterone signaling (**A-B**) Migration of MM3MG cells after treatment with progesterone (P), Wnt4 + Rankl, or 1-to-1 mixing of MM3MG with MM3MG-PgRB cells. Progesterone or paracrine factors (Wnt4+Rankl) induce migration of MM3MG cells. Co-culture with MM3MG-PgRB increases migration of MM3MG cells. (**C**) Progesterone or Wnt4+Rankl induce sphere formation of MM3MG cells. (**D-E**) Migration assay for MM3MG-Her2 cells. MM3MG-Her2 cells after treatment with progesterone, Wnt4/Rankl, or mixing (1-to-1) with MM3MG-PgRB cells. Wnt4+Rankl suppress migration of MM3MG-Her2 cells. Also, presence of MM3MG-PgRB cells decreases migration. (**F**) Progesterone or Wnt4+Rankl suppress sphere formation of MM3MG-Her2 cells. All p-values, student's t-test; all error bars correspond to standard deviation (Mean ±SD).

To test that the effect of PgR$^+$ cells on neighboring cells goes via paracrine signals, we used neutralizing antibody against Rankl and chemical Wnt inhibitor (IWP2) in migration and sphere forming assays (migration and sphere assays for primary culture like what described in 3.4) of EL cells while they were simultaneously treated by progesterone. Interestingly, these inhibitors completely abrogated impact of progesterone on migration and stemness of EL cells (Figure 31).
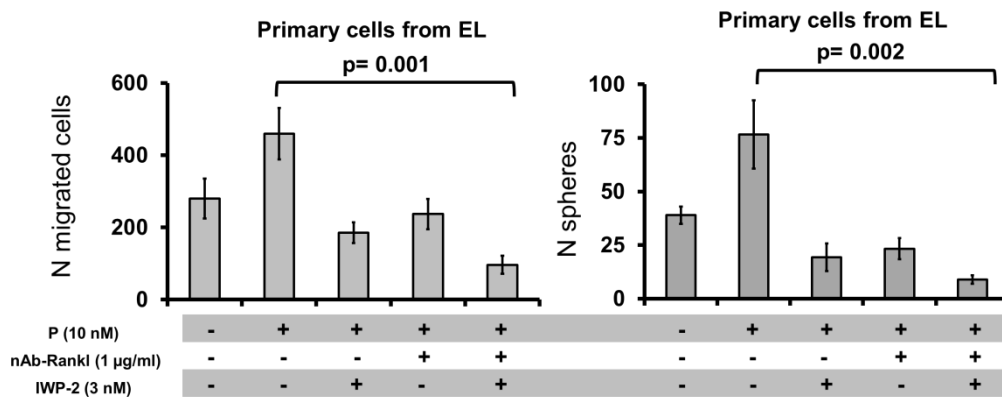
Figure 31. Progesterone. Inhibition of Wnt and Rankl diminished impacts of progesterone on stemness and migration. Abrogation of Wnt by IWP-2 (chemical inhibitor of Wnt production) or nAb-Rankl (neutralizing antibody) reduces migration (left panel) and stemness (right panel) of EL cells. All p values, Student's t-test; all error bars correspond to standard deviation (Mean ±SD).

3.5.2 Her2 expression level defines types of responses to the progestrone signaling

Next, we aimed to check impact of Her2 on *in vitro* proliferation of cancer cells in the context of suggested mechanism. To test that, XTT assay was performed for Her2 transduced cell line and primary cultures of EL and PT cells. We noted that transduction of *Her2* into MM3MG cells increases their basal proliferation. Progesterone induced paracrine signals further stimulated proliferation of Her2 expressing cells but suppressed it in parental Her2 negative cells (Figure 32A). Similarly, Wnt4 and Rankl suppressed proliferation of cells from EL samples, while stimulating proliferation of primary tumor-derived cells (Figure 32 B).
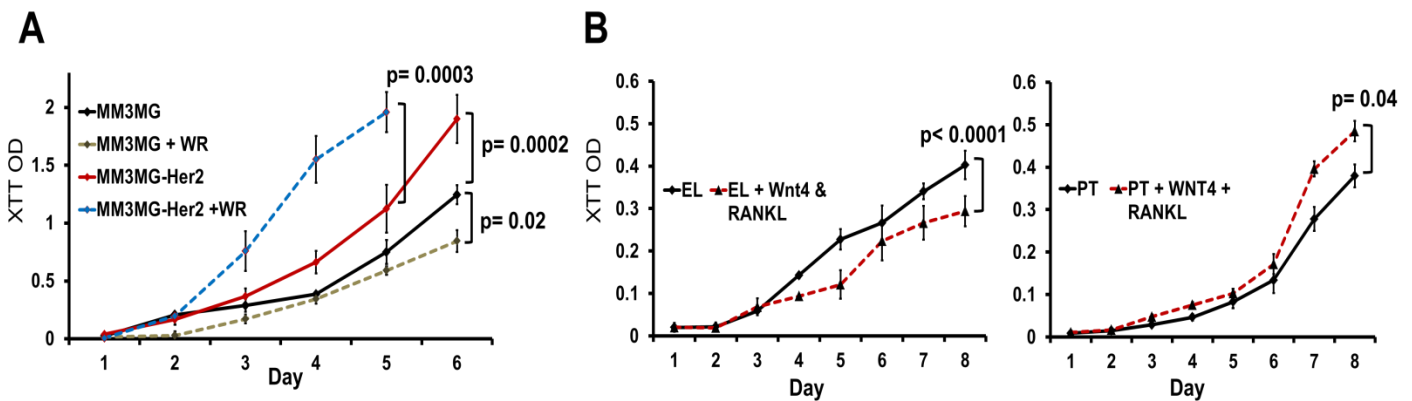
Figure 32. Differential proliferation response of EL and PT cells to Wnt4/Rankl. XTT proliferation assay was done for primary cultures of EL and PT cells. Cells were cultured in 5000 cell/well in 96 well plate. Each single point is result of hexaplicated experiment. Cells were treated every second day with fresh medium contained wnt4/Rankl or vehicle (PBS). (**A**) Overexpression of Her2 increases proliferation of MM3MG cells (MM3MG-Her2). Wnt4 plus Rankl further increase proliferation of MM3MG-Her2 cells, but decrease proliferation of parental (MM3MG) cells. (**B**) Wnt4 plus Rankl treatment induces proliferation of primary cultured PT cells, but reduces it in EL-derived cells. All p-values, linear regression, F-test for slopes; all error bars correspond to standard deviation (Mean ±SD).

We hypothesized that strong expression of Her2 may act as a key mediator for phenotype switching in epithelial cells. Thus, we reduced Her2 signaling by increasing doses of lapatinib (Her2 inhibitor; Figure 33 A) in MM3MG-Her2 cells and noted that intermediate inhibition of Her2 pathway decreased the inhibitory effect of Wnt4 and Rankl on migration (Figure 33 B). These results suggested that depend on the level of Her2 expression, cancer cells translate effects of progesterone induced factors for either proliferation (advanced cancer cells; strong Her2 expression) or dissemination (early cancer cells; weak expression of Her2).
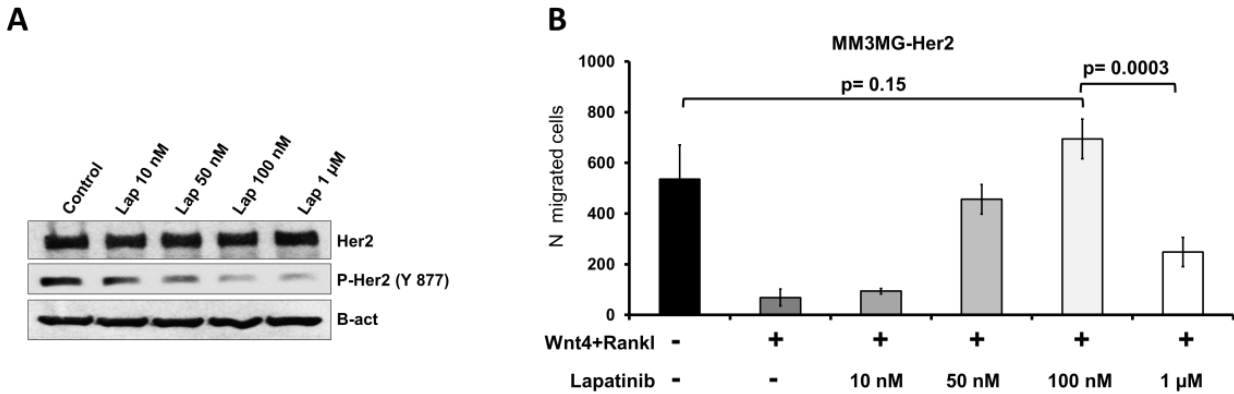
Figure 33. Low-moderate Her2expressing cells respond to progesterone signaling in their migration. (**A**) Protein blotting shows that lapatinib inhibits Her2 signaling by decreasing phosphorylated form. (**B**) Reduction of Her2 signaling overrides the inhibitory effect of Wnt4 and Rankl and increases migration. Note that complete abrogation of Her2 by high lapatinib dosage reduces migration. All p values, Student's t-test; all error bars correspond to standard deviation (Mean ±SD). See supplementary data 4 for the original blotting figures.

3.5.3 Her2 and PgR expression in the migratory cells

To analyze PgR and Her2 status of migratory cells from migration experiments, cells that reached to the other side of inserts were stained for two proteins. While MM3MG-PgR cells strongly suppressed migration of MM3MG-Her2 cells (Figure 30D-F), but those few migratory cells were MM3MG-Her2 cells (Figure 34 A). Moreover, staining revealed EL cells arriving to the other side of migration chambers were negative for PgR expression but weakly expressed Her2 (Figure 34 B).
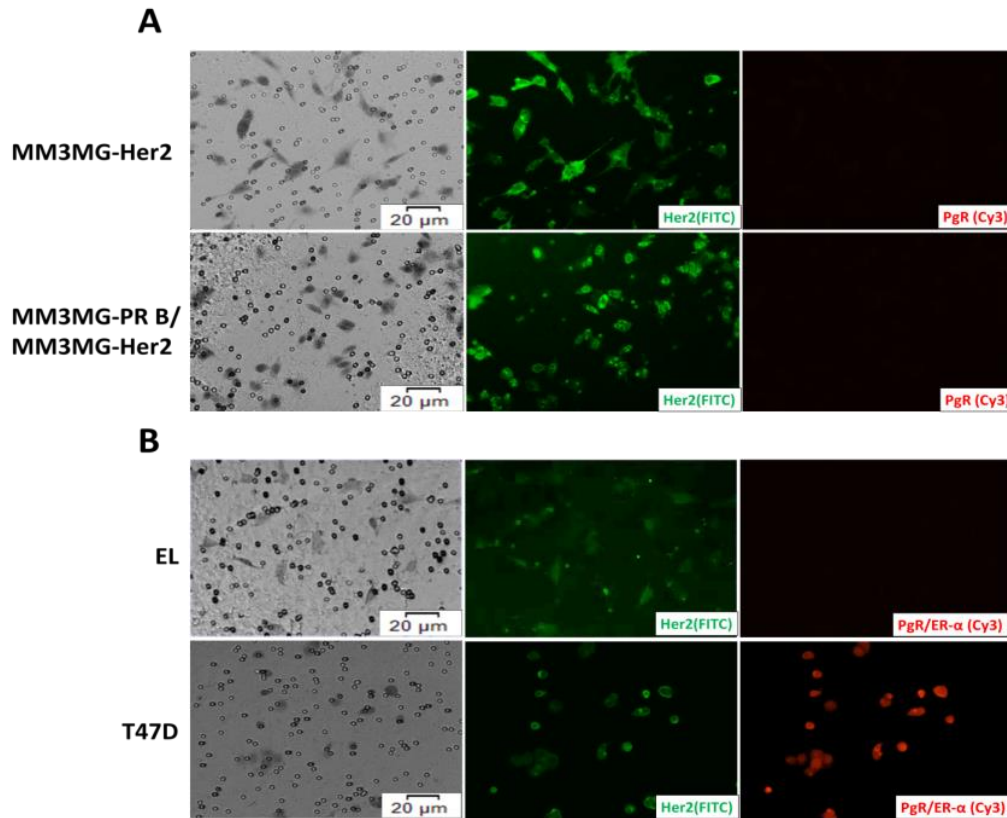
Figure 34. Low-moderate expressing Her2 are the migratory cells in EL. (**A**) Cells that migrated to the other side of the migration chamber were stained for Her2 (FITC green) and PgR/ER-α (Cy3 red). MM3MG-Her2 cells were mixed with the MM3MG-PgRB and they have been checked for presence of Her2 and PgR after migration. None of migrating cells expressed PgR. (**B**) EL cells (upper panel) did not express PgR and displayed faint Her2 staining (brightness of Her2 and PgR staining in EL samples was increased by 50% for better visualization in the picture). Double-positive T47D cells (lower panel) did not migrate but were fixed onto the filter to serve as positive staining control.

We further aimed to characterize *in vitro* migratory cells by staining for other markers including CK8 and CK5. Results showed none of these markers beeing expressed in the migratory cells, which could be due to an activation of EMT program during migration which reprogrames these epithelial cells (Table 10).

Table 10. Summary of IF staining of migratory cells (N.T - not tested).

	PgR	ER-α	Her2	CK8/18	CK5	EpCAM
TUBO	-	-	+	+	weak	+
MM3MG	-	-	-	N.T	N.T	N.T
MM3MG-PgR B	-	-	-	N.T	N.T	N.T
MM3MG-Her2	-	-	+	N.T	N.T	N.T
Primary Tumor	-	-	weak	-	-	-
EL	-	-	weak	-	-	-

3.6 *In vivo* support for the identified mechanism

So far, all *in vitro* results on cell lines and primary cultures suggested an early dissemination program which is mediated by progesterone and fine-tuned by Her2 signaling. Progesterone signaling induced migration and stemness of EL cells which had low Her2 expression and suppressed these traits in PT cells which had strong Her2 expression. In addition, the migration program of early lesion seems to be related to mammary epithelial cell side branching and morphogenesis. Moreover, the migration phenotype was concomitant to stemness characteristics. To further prove these findings *in vivo*, we hypothesized that 1) EL tissues which are enriched in PgR cells, should disseminate more, 2) if the stemness is presented in disseminated cells, EL cells, should be able to form more metastases, 3) PgR expressing cells would provide a favorable environment for dissemination of EL and suppression environment for dissemination of PT cells. For this purpose, a large number of mice in different setting of experiments were used and I got kind help of Milan Obradovic, Christian Werno, Carolin Ehrl and Christian Reimelt for these experiments.

3.6.1 Proliferation and metastasis properties of PT and EL

In the first *in vivo* experiments we transplanted recipient wild type BALB/c mice with either ~1 mm^3 pieces from mammary glands of 4-5 week old Balb-NeuT mice (n=151) or with ~1 mm^3 pieces from an advanced primary tumor (>22 weeks of age; n=34) into the cleared mammary fat pad. This generated a model with a single primary tumor that can be removed by surgery and followed during extended observation periods for metastasis formation. We performed surgery of recipients to remove the resulting primary tumors at a size between 5-10 mm. Thereby; we mimicked clinical stratification of similar T stages that allowed for sufficient follow-up time for metastases to emerge. All details and design of experiment is depicted in figure 35.
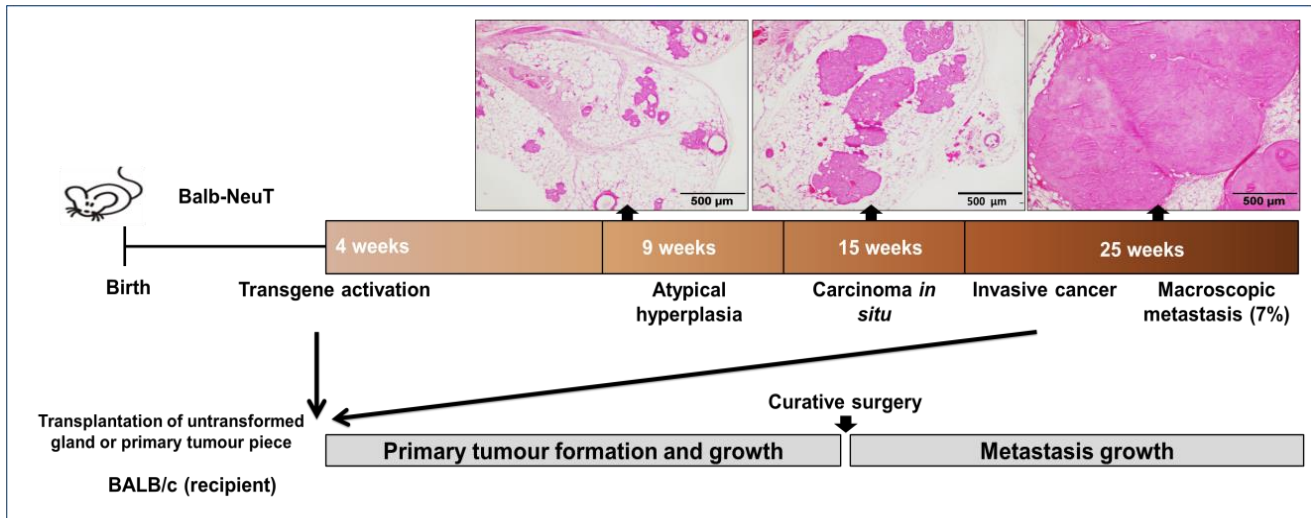
Figure 35. Schematic of the transplantation protocols for mammary gland or PT tissue pieces into wild type recipients. Pieces (~1 mm^3) of 4 week-old mammary glands (i.e. tissue before activation of the Her2-transgene) or PTs of Balb-NeuT mice were transplanted into cleared fourth fat pads of young (4 week old) BALB/c mice. When tumors reached a size of 5-10 mm curative surgery was performed and mice were followed (median 17 weeks), dissected and screened for lung metastases.

Interestingly, the time point for surgical intervention was significantly different for the two groups: primary tumor-derived tumors were resected at a median time point of 12.9 weeks (tumor pieces were perfectly viable, i.e. not necrotic), while gland-derived tumors at week 23 (p< 0.001; Figure 36 A). After surgery, we followed mice from both groups for median of 17 weeks (Figure 36 B), when mice were dissected and inspected for macrometastasis formation in the lungs (Figure 36 C). We noted a significant difference for lung metastasis formation (p<0.0001; chi-square test): about twice as many metastases were generated from EL lesions (101/151 transplanted gland pieces; 66.8%) compared to primary tumor lesions (10/35 transplanted tumor pieces; 28.5%; Figure 36 D). These results indicate that PT cells are more proliferative and less metastatic compared to EL cells.
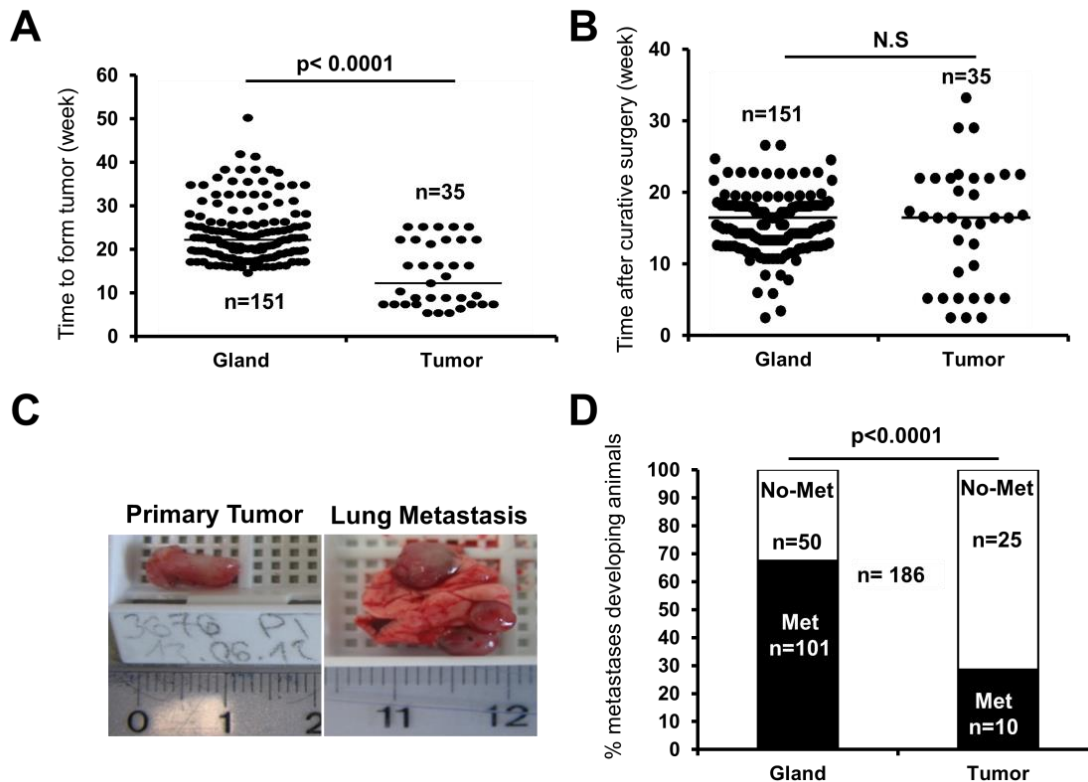
Figure 36. Tumor growth and metastasis of EL and PT (**A**) Tumor formation time after transplantation of tumor pieces or untransformed transgenic mammary glands into wild-type siblings. A curative surgery was done for mice when they developed tumor in size of 5-10 mm. Time to form a big tumor was 23 and 12 weeks for gland and tumor piece, respectively. (**B**) Mice left for a median of 17 weeks after curative surgery until the time they were sacrificed and monitored for macrometastases in their lungs. (**C**) This picture shows examples of tumor and lung metastasis in the analyzed mice. (**D**) Macrometastasis formation in gland- and tumor piece transplanted animals. N.S, not significant; p values, in A and B calculated by Mann-Whitney test, in D calculated by chi-square test; data in A and B presented with median. The transplantation experiments were done by Milan Obradovic, Carolin Ehrl and Christian Reimelt.

3.6.2 Proliferation and metastasis traits are constant phenotypes over the time

We raised two hypotheses for induced metastasis formation by transplanting EL: first, in the gland-derived model the longer period to tumor formation (i.e. to reach 5-10 mm tumors) influences metastases formation; second, there are intrinsic differences between cells disseminating from the gland and the PT-derived models independent of the time period before surgery. To test first hypothesis, we compared metastatic mice with similar kinetic of tumors from both models (Figure 37A) and compared their metastatic success (Figure 36 A). Interestingly, we noted a much higher rate of lung metastases in the gland model than in the PT-derived model (Figure 37B, 67.5% *vs.* 41%; p=0.03; chi-square test). Together, the data suggest that intrinsic differences between the gland- and tumor-derived models are prevailing over time considerations. The criterion which determined how long we kept the mice after curative surgery

was the general health conditions of mice. When a mouse appeared sick, it was dissected and inspected for macrometastasis. Interestingly, when we looked at time when mice were kept after curative surgery until dissection, we saw that mice from tumor model stayed longer compared to the gland model (Figure 37C). These results indicate that ELs have a higher intrinsic metastatic potency compare to PT cells.
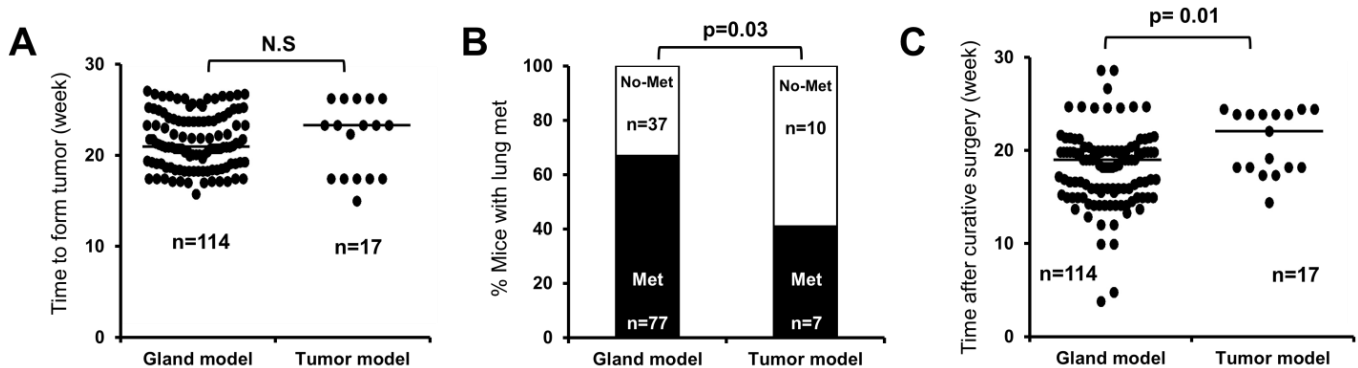
Figure 37. Metastasis phenotype is independent of tumor kinetics. (**A**) Recipient mice were with similar tumor kinetic having been selected (**B**) Macrometastasis formation in gland- and tumor piece transplanted animals. Gland model cause more metastatic mice than tumor model regardless of tumor kinetics. (**C**) Longer time keeping after curative surgery does not result to more metastases for PTs. Mice with similar primary tumor kinetic were compared for the time they have been dissected. N.S, not significant; p values, in A and C calculated by Mann-Whitney test, in B calculated by chi-square test; data in A and C presented with median.

3.6.3 Higher metastatic property of EL cells comes from higher dissemination

The lower rates of metastasis in the tumor model suggested that late cancer cells have a dominant proliferation phenotype, while dissemination is the dominant phenotype in early cancer cells. We hypothesized that the number of disseminated cancer cells of EL should be higher than of PT cells in the same window of time but their tumor forming ability, as reflected by their proliferation rate, should be lower. In order to control number of transplanted cells and to get sure that cells are tumor initiating cells, we used spheres instead of pieces of tissue. Epithelial cells were sorted from fresh tissue and cultured *in vitro* to form spheres, and then 50 spheres were injected to the fourth mammary gland of recipient mice. For the EL model we transplanted 17, for the PT model 23 recipients. After 8 weeks, when the first mouse developed a primary tumor of about 5-10 mm in diameter, all mice were sacrificed and 10^6 bone marrow cells were analyzed for DCCs by CK8/18 staining. The majority of PT-spheres transplanted mice (20/23; 87%) formed tumors, but none of EL transplanted mice developed tumors (Figure 38 A) within this

time window (p<0.0001). However, the number of mice that harbored DCCs in the bone marrow as well as the number of DCCs per positive bone marrow were significantly higher in EL-derived models as compared to PT-derived models (p=0.04; chi-square test for detection rate; p=0.0003 for cell number; Mann-Whitney test; Figure 38 B and C). These results depict a clear difference in proliferation and metastatic dissemination of EL and PT cells.
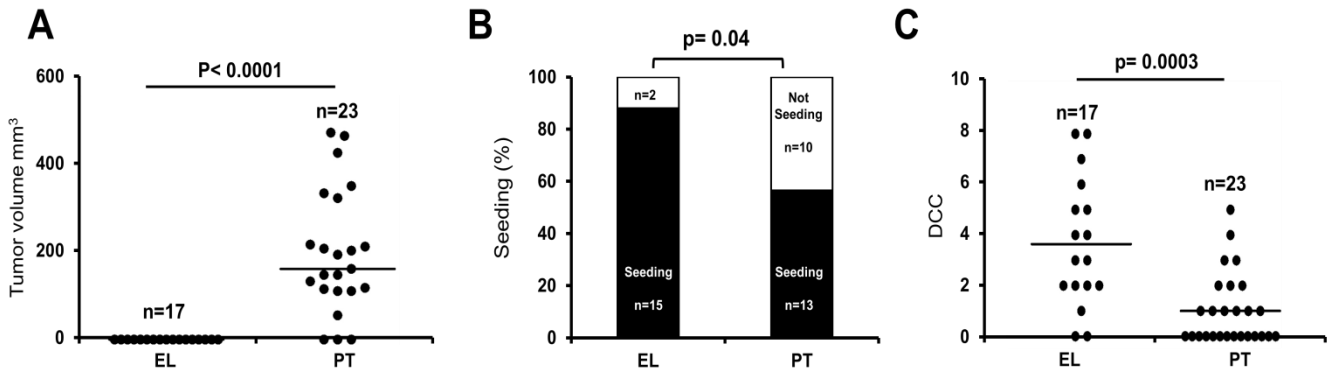
Figure 38. Dissemination and proliferation of PT and EL cells. (**A-B**) Tumor volume and dissemination to BM at week 8 after transplantation of PT or EL-derived spheres. (**C**) Number of DCCs (per 10^6 bone marrow cells) in positive mice at week 8 after transplantation of PT or EL-derived spheres. P values, in A and C calculated by Mann-Whitney test, in B calculated by Fisher exact test; data in A and C presented with median.

3.7 PgR is the distinticive environmantal factor in regulation of dissemination

3.7.1 Impact of mammary gland environment on dissemination of PT and EL cells

The role of paracrine factors of progesterone, Wnt4/Rankl, in the *in vitro* migration and sphere formation experiments suggested that dissemination and metastasis formation can be resulted of intricate interactions of cancer cells and the microenvironment. To get a first glimpse into such microenvironmental impact *in vivo*, we performed transplantation studies of EL and PT cells into young BALB/c recipients and old recipient mice. Mammary glands of 4 week-old wild type BALB/c mice comprise more than twice as many PgR-positive epithelial and fibroblastic cells than glands from 40 week-old mice (Figures 21 E, 22 A, 26 A and B). Furthermore, EL samples express much higher levels of Wnt4 and Rankl compared to PT samples (Figure 22 A). Therefore, we compared the impact of 4 and 40 week-old recipients' microenvironment on tumor formation and dissemination. Dissemination in BM was not significantly different when EL-derived spheres were injected into the forth mammary gland of 4 or 40 week-old BALB/c mice (Figure 39 A). However the PgR-dense microenvironment of young mammary glands suppressed

dissemination from PT spheres (p=0.01; Mann-Whitney test; Figure 39 A). On the other hand, we found that tumors grew faster when PT-cells were transplanted into young recipients (Linear regression, F-test; p = 0.009; Figure 39 B). These results prove that progesterone signaling has inhibitory effect on dissemination of PT cells while induces their proliferation.
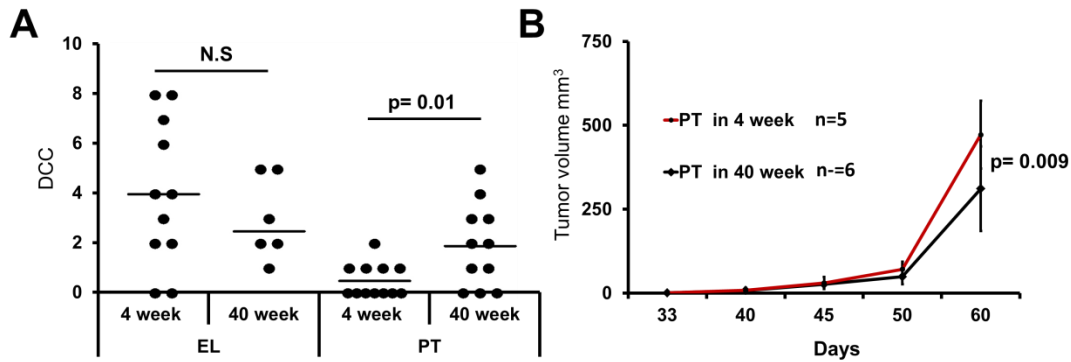
Figure 39. Young mammary gland suppresses dissemination but induce proliferation. (**A**) DCC counting in BM of recipient mice (young= 4-week-old recipient; old= 40-week old recipient) shows a reduction in young recipients of PT cells. (**B**) Tumors grow faster from PT-derived spheres in young (PgR rich environment) *vs.* old recipient mice. P values, in A calculated by t-test, in B calculated for slopes of curves by F-test; data in A presented with median.

However, IHC staining for PgR revealed PgR expression exclusively in lesions resulting from EL transplantation (Figure 40), indicating the generation of a PgR-rich environment in the old recipients by EL cells which may be the reason why EL cells do not disseminate less in the old environment.
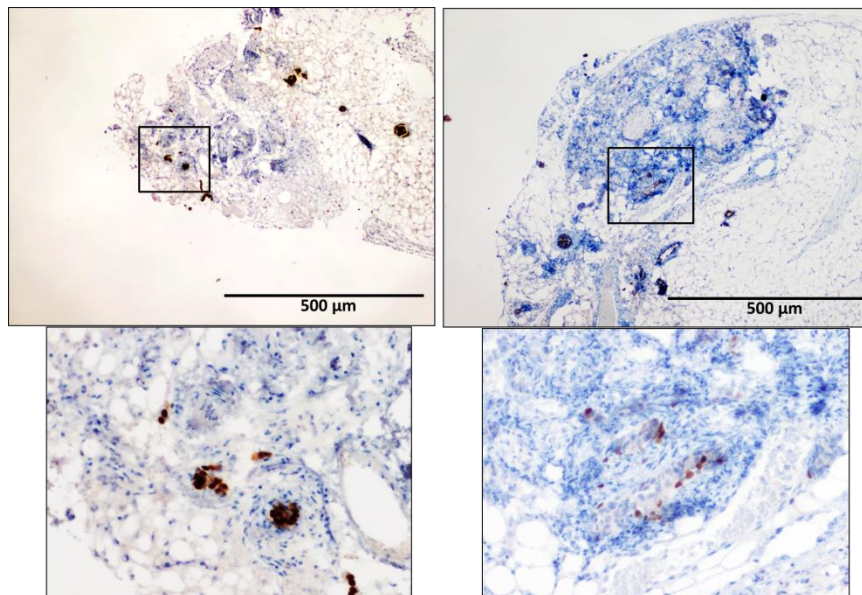
Figure 40. PgR expression in the lesions left after transplantation of EL. EL cells transplanted in old recipient mice (40 weeks) and mice were sacrificed 8 weeks after transplantation. Lesions were stained for PgR which shows PgR expressing cells.

This was further corroborated by demonstrating that only EL but not PT cells could generate PgR-positive cells in 3D culture. That came from the experiments in which epithelial cells were sorted from freshly digested tissue and cultured in either sphere medium for 5 weeks or cultured between two layers of matrigel. Interestingly, Balb-NeuT-derived EL, but not PT cells, could differentiate in matrigel and sphere culture. Acinus-like structures, characteristic of cells with stem-like potential (Debnath et al., 2003; Ghajar and Bissell, 2008), were exclusively observed for EL cells both in matrigel and in sphere cultures and their formation was accelerated by progesterone (p=0.0008; Mann-Whitney test; Figure 41 A).
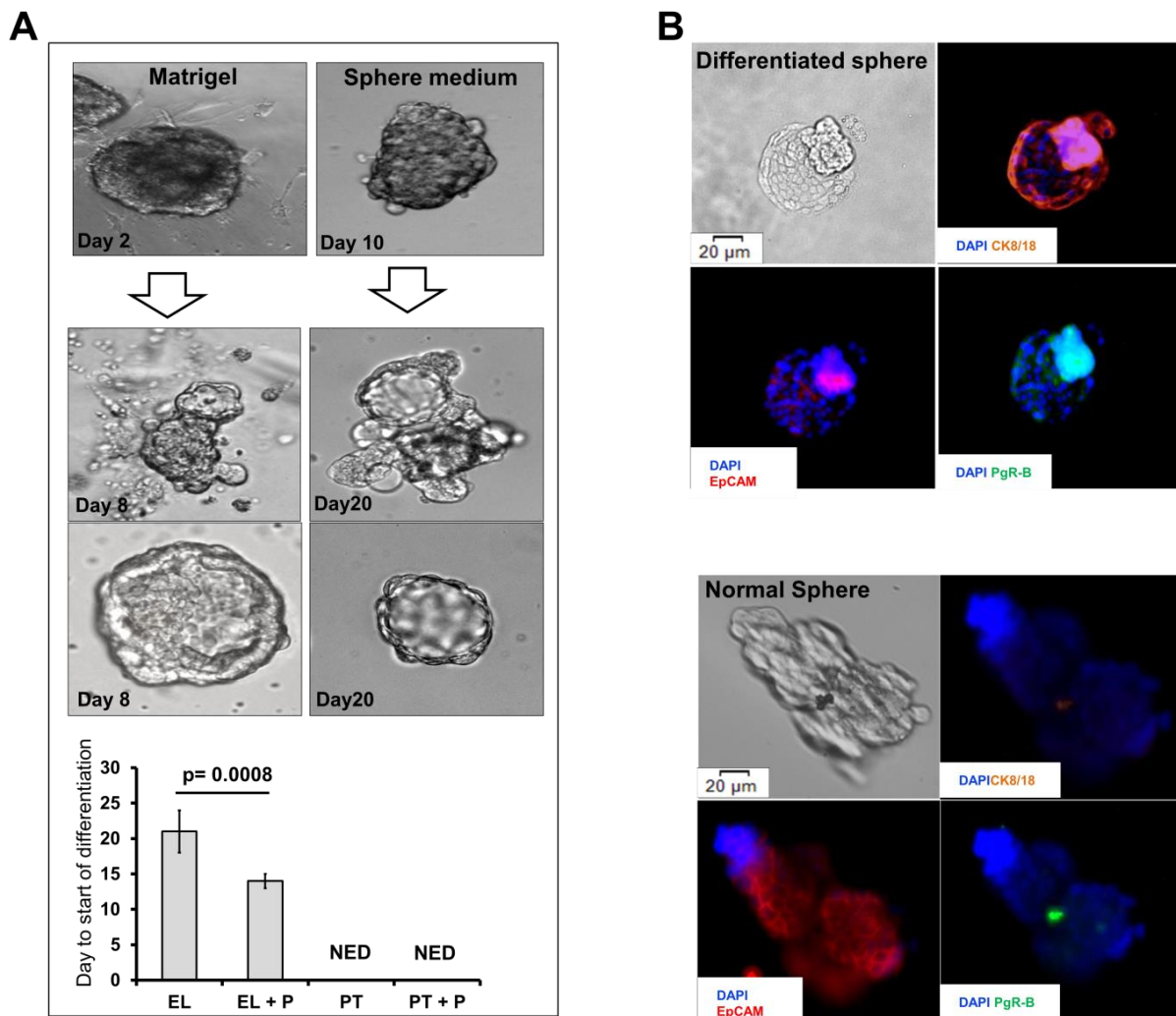
Figure 41. Progesterone accelerate differentiation of EL cells A) Differentiation of mammary epithelial cells from EL or PT cells in sphere culture (up to 35 days) or in matrigel similar to previously published conditions (Debnath et al., 2003). The formation of acinus-like structures is shown in matrigel (left panel) or sphere culture (right panel). No such structures were detected for PT cells during the entire experiment (35 days). Progesterone stimulation accelerated formation of acinus-like structures particularly under mammosphere conditions (NED, no evidence of differentiation; Student t-test). (**B**) Immunofluorescence staining for CK8/18, PgR and EpCAM reveals exclusive expression of PgR and CK8/18 in differentiated structures (Upper panel) as compared to undifferentiated spheres (Lower panel).

Finally, to show that formation of acini-like structures is a consequence of differentiation program, we performed immunofluorescence staining of those acini structures. Spheres and differentiated structures were transferred into the normal cell culture 8 hours before staining to fix them physically to the surface. Then a routine cell culture staining performed for CK8/18, EpCAM, and PgR. Our results revealed that acinus-like spheres from EL samples expressed cytokeratin 18 and PgR as the signs of mammary epithelial differentiation (Figure 41 B). Altogether, these results suggested that EL cell are more migratory and PT cells are more proliferative. The PgR rich environment induces dissemination of EL cells but proliferation of PT cells.

3.7.2 PgR expression changes dissemination behaviour of cancer cells

To test the hypothesis that PgR in the mammary gland microenvironment suppresses dissemination and enhances proliferation, Balb-NeuT PT-spheres were mixed with MM3MG cells with or without overexpression of PgR in a 1:1 ratio and transplanted. We used 40 week-old, largely PgR-depleted mice. Interestingly, the number of DCCs in PT: MM3MG-PgR mice fell to levels seen when PT cells are transplanted into young, PgR-rich recipients (Figure 42 A). Furthermore, transplantation of PT spheres mixed with PgR-B-transduced MM3MG cells into old recipients resulted in increased tumor formation after 4 weeks (5 out of 5 versus 1 out of 5; Figure 42 B). IHC results confirmed the presence of PgR cells as small island in the tumor mass (Figure 42C). In summary, these observations are consistent with our *in vitro* data and *in vivo* results from recipient at varying age, showing that progesterone signaling induces migration from EL lesions but suppressing migration from further advanced lesions. On the other hand, while dissemination of PT cells is suppressed by progesterone signaling, they proliferate and form tumor faster.
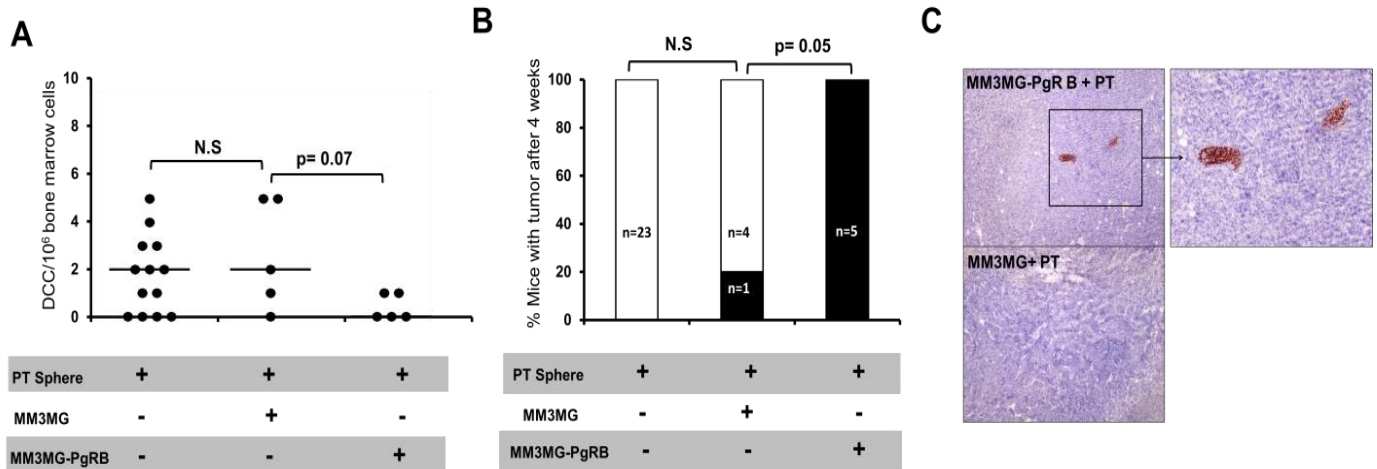
Figure 42. Environmental PgR expression suppresses dissemination from primary tumor cells. (**A**) PT spheres were co-transplanted with and without 50 PgR-transduced MM3MG spheres and DCCs were counted 8 weeks later. To reduce natural PgR mediated signaling only old 40 week BALB/c mice were used as recipients. (**B-C**) PT cells formed more tumors 4 weeks post transplantation when co-transplanted with PgR expressing cells. IHC staining (red/brown) shows small islands of PgR expressing cells in tumors from PT spheres mixed with MM3MG-PgRB. N.S, not significant; p values, in A calculated by student t-test, in B calculated by fisher exact test; A is shown by median for individual values.

3.7.3 Pregnancy induces migration of EL and proliferation of PT cells

Our previous results indicated that progesterone signaling induces dissemination of EL cells. We attempted to investigate the effect of physiologically elevated progesterone levels during pregnancy (10-20 times over normal (Powis and Shapiro, 2015)), on dissemination and proliferation of cancer cells. Female transgenic mice were mated at two time points: at EL (week 7) and at early tumour formation (week 15). At week 7 Balb-NeuT mice display early lesion, thus we could see if progesterone released during pregnancy induce their dissemination. Whereas in week 15 mice usually progress from *in situ* carcinomas to invasive cancers, therefore we can evaluate effect of progesterone signaling on proliferation of advanced cancer cell *in vivo*.

When mice were sacrificed, mice mated at week 7 displayed higher numbers of DCCs (p=0.004; Student's t-test; Figure 43 A), whereas all mice mated at week 15 formed large tumors by week 18, much faster than usual (Figure 43 B-C). In conclusion, this shows that high levels of progesterone exert different effects depending on the age and the PgR status of the tissue. While progesterone induces dissemination in EL, in advanced lesions it enhances proliferation.
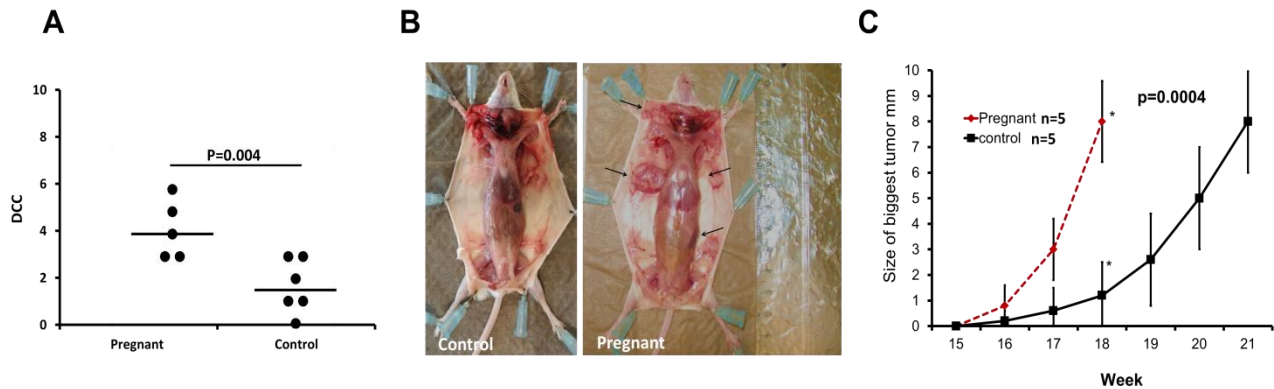
Figure 43. Pregnancy, tumor formation and dissemination. (**A**) Young Balb-NeuT mice entered pregnancy (n=5, pregnant; n=6 control) at the time of early lesion (week 7) and sacrificed at end of pregnancy (week 12). These mice did not formed palpable tumors but showed higher number of DCCs compare to sterile mice as control. Student t-test; shown are median and individual values. (**B-C**) A group of Balb-NeuT mice (n=5, pregnant; n=5 control) entered pregnancy at the time of *in situ* carcinoma (week 15) and sacrificed in the end of pregnancy (week 18). All pregnant mice formed tumors faster (p=0.0004; linear regression, F test for slopes) compared to sterile mice as control. The time for palpable tumors in Balb-NeuT is normally after week 20.

3.8 Cell density regulates proliferation and dissemination phenotypes

Altogether, the *in vivo* results corroborated our *in vitro* findings that EL cells had more dissemination/migration abilities and PT cells proliferate as response to progesterone signaling. We saw that EL is the time point with highest overlap between PgR and Her2 expression. Once, cancer cells progress to more advanced stages PgR disappeared and Her2 expression got stronger. These changes accompanied by a switch from migration to proliferation. The remaining question was how these observations can be mechanistically explained. We further wanted to know how PgR disappeared in advanced tumors and differentiate whether a clonal selection or epigenetic changes governs it.

3.8.1 PgR expression in PT cells regulated by cell density

First, 160 tissues from different stages of Balb-NeuT model were screened and found none of the primary tumors express PgR. Her2 and PgR expression goes to opposite direction from a normal like structure to advanced primary tumors (Figure 44). Therefore, we hypothesized that overexpression of Her2 and loss of PgR apparently marks a switch from a migratory to a proliferative phenotype.
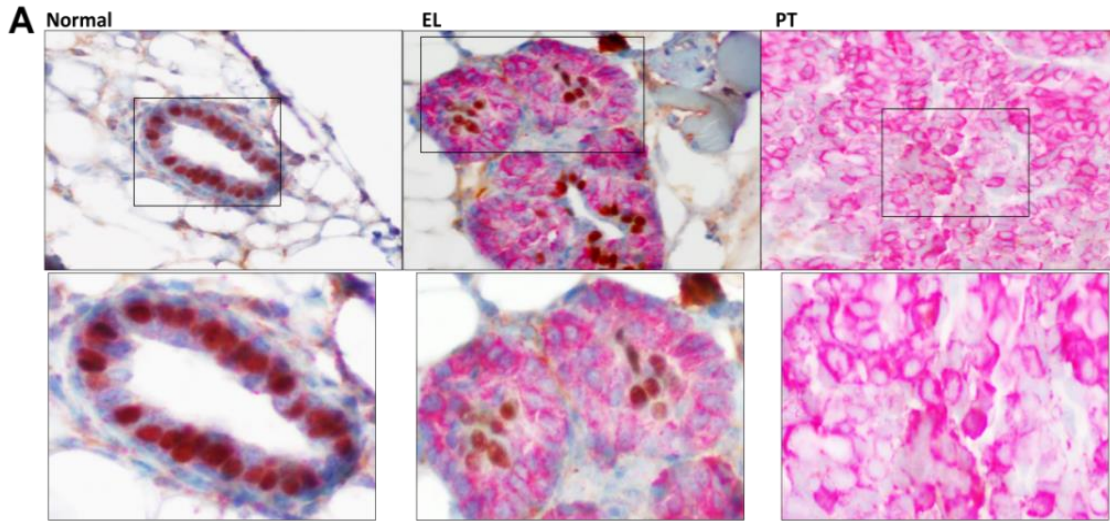
Figure 44. Loss of PgR expression during tumor growth. (**A**) An IHC double staining of Her2 (membrane red/pink) and PgR (nuclear brown) shows diminishing of PgR coincide with gradual upregulation of Her2. (**B**) We found no PgR expressing cells in 102 PT samples of Balb-NeuT.

We noted that PgR expression can be rescued in advanced cancer cells under certain conditions. For example, individual cells re-expressing PgR mRNA and protein in primary tumor cell cultures of only low cellular density (2.2×10^3 cells/cm^2 for low density experiments; Figure 45), but they disappeared again when they transplanted and formed tumors, which always impress morphologically with high cellular density. This raised the question if density of tumor cells in culture or tissue might regulate the expression of PgR.
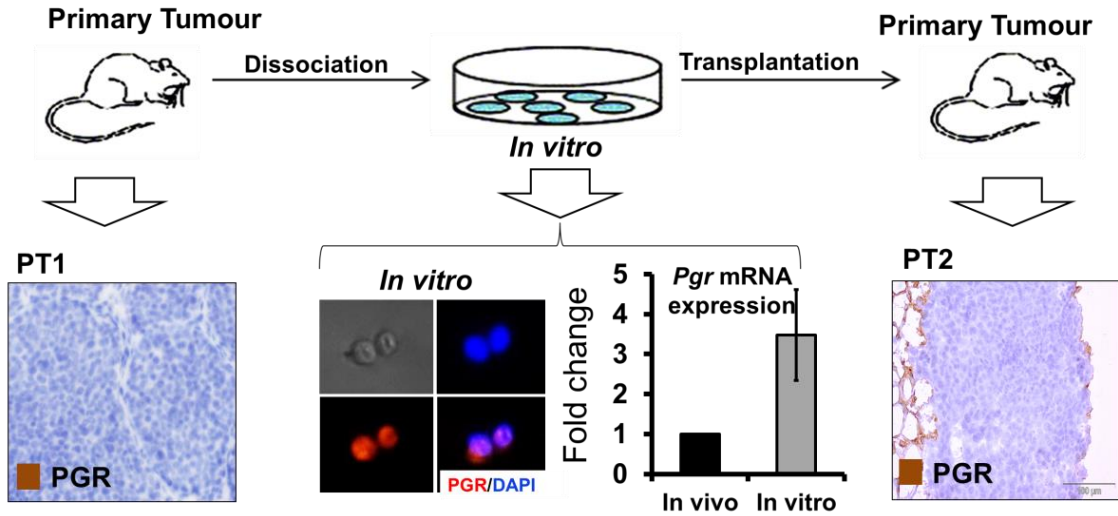
Figure 45. PgR expression is silenced in tumors, can be re-activated in culture and re-silenced in vivo. IHC staining for PgR in PTs (PT1 in right of panel) show the absence of PgR expression. When PT digested and cultured in low densities, some cells start to re-express PgR (middle of panel). We generated spheres from primary cultures derived from PTs (PT1) and transplant them in wild type mice until they form tumors. IHC staining for PgR in the grown tumors (PT2 in left of panel) revealed again absence of PgR expression.

To test this hypothesis, TUBO cells were plated at low and high cellular densities and tested for PgR expression. TUBO cells grown at high density (3×10^4 cells/cm^2) did not express PgR, while $10\pm5\%$ of cells grown under low-density (5.2×10^3 cells/cm^2) conditions did (Figure 46 A). Additionally, frequent medium change of high-density cultures induced PgR re-expression, suggesting involvement of soluble regulators (Figure 46 B).
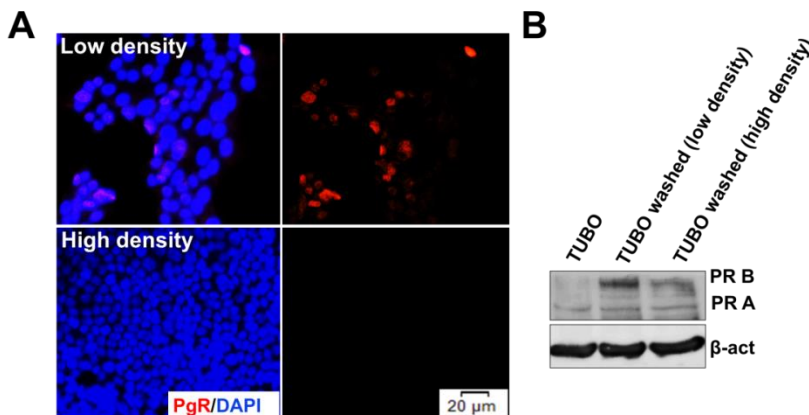
Figure 46. Identification of the PgR regulating activity (A) Immunofluorescent staining for PgR showed that in low-density cell culture of TUBO cells, some cell express PgR, while that could not be seen in high density cultures. **(B)** Frequent medium changes and washing will rescue PgR expression in TUBO cell. See supplementary data 4 for the original blotting figures.

3.8.2 PT cells regulate PgR expression via miRNAs

To further confirm role of soluble component of PgR regulation, we performed two additional experiments. First, in transwell-cultures of primary tumor cells next to EL cells, PgR expression was found greatly reduced in EL cells (Figure 47 A and B). Second, we exposed human PgR-positive T47D breast cancer cells to conditioned medium prepared from TUBO cells which was cultured on high density and 100% confluent at the time of media harvesting. Likewise the transwell assay, PgR expression was reduced to 50% of controls (Figure 47C and D). Therefore, soluble factors are the meditators for PgR knockdown. We hypothesized that these soluble factors either are soluble proteins or they are miRNA containing vesicles. To find out the answer, we separated candidate mediators contained within the supernatant in vesicular and extra-vesicular fractions by ultracentrifugation. Adding both fractions to PgR-positive T47D breast cancer cells, The PgR-regulating activity found exclusively within the vesicular fraction that reduced PgR expression by about 50% (Figure 47 E). Altogether, these results suggested that TUBO and primary tumor cells from Balb-NeuT mice down-regulate the PgR via miRNAs, which act within the cells and are secreted via exosomes.
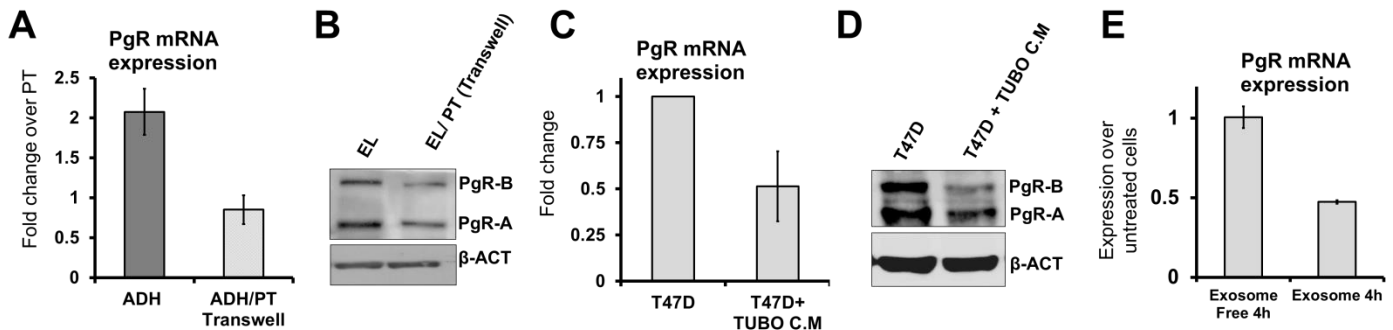
Figure 47. Secretion of exosome is responsible for PgR downregulation. (A-B) A transwell assay was done for PT and EL primary culture cells. The qPCR and western blotting results shows a soluble activity down-regulating PgR message comes from PT. (**C-D**); T47D cells exposed to conditioned medium from TUBO cells reduce PgR expression. TUBO cells were cultured at high density (3 x 10^4 cells/cm^2) and media were collected after 3 days and added to T47D cells for 24 hours. Then mRNA or proteins were checked for PgR expression. (**E**) The down-regulating activity is located in exosomes from high-density TUBO cell culture supernatants. See supplementary data 4 for the original blotting figures.

3.8.3 miR9-5p and miR30a-5P regulate PgR expression in PTs of Balb-NeuT

To identify miRNAs able to regulate PgR expression, we prepared miRNAs for sequencing from TUBO cells, and supernatants of TUBO cells. Since we also observed that PgR expression regulated in the opposite way to Her2 expression in the Balb-NeuT model, we hypothesized that

a Her2 driven miRNA mechanism might also be involved in PgR knockdown mechanism. Therefore, miRNAs were prepared from BALB/c derived immortalized mammary epithelial cells that had been transduced with a Her2-containing retrovirus (MM3MG-Her2). All miRNA sequencing and analyses was performed in collaboration with Gunter Meister at University of Regensburg. Based on miRNA sequencing (Supplementary Data 2) and bioinformatic prediction of PgR regulators (Figure 48 A-C), we searched for miRNAs predicted to bind PgR and miRNAs up-regulated by Her2.

A

Her2 upregulated miRNA (MM3MG-Her2/MM3MG)	Log2 fold
mmu-miR-7a-5p	2.9
mmu-miR-20a-5p	2.3
mmu-miR-92a-3p	1.8
mmu-miR-5099	1.6
mmu-miR-93-5p	1.6
mmu-miR-19a-3p	1.3
mmu-miR-30a-5p	**1.2**
mmu-miR-210-3p	1.2
mmu-miR-378a-3p	1.0
mmu-miR-30e-5p	1.0

B

Top 10 expressed miRNA in TUBO cells and exosomes
mmu-miR-21a-5p
mmu-miR-182-5p
mmu-let-7c-5p
mmu-miR-181a-5p
mmu-miR-9-5p
mmu-miR-143-3p
mmu-miR-25-3p
mmu-let-7f-5p
mmu-miR-92a-3p

C

miRNA prediction for PgR control (miRanda)
mmu-miR-448
mmu-miR-590-3p
mmu-miR-384-5p
mmu-miR-30e
mmu-miR-30b
mmu-miR-30c
mmu-miR-30d
mmu-miR-30a
mmu-miR-32
mmu-miR-92a
mmu-miR-92b
mmu-miR-363
mmu-miR-367
mmu-miR-653
mmu-miR-9
mmu-miR-26a
mmu-miR-26b
mmu-miR-25

Figure 48. miRNA sequencing to identify PgR regulating miRNAs. (**A**) The left table lists the top 10 upregulated miRNAs in Her2 overexpressing cells (MM3MG-Her2) compared to control (MM3MG). (**B**) The middle table presents the top 10 expressed miRNAs in TUBO cells and TUBO cell-derived exosomes. (**C**) The right table displays miRNAs predicted by miRanda to regulate PgR.

Identified candidates were added to T47D cells. The T47D cells were transiently transfected with mimic miRNAs using lipofectamine reagents. After 24 hours of transfection, PgR expression has been checked in the mRNA level by qPCR. We found that miR30a-5P which is a Her2 regulated miRNA and miR9-5P which abundantly expressed in TUBO cells and exosome fraction are concomitantly able to down-regulate PgR in T47D cells (Figure 49 A-B) down to a level of 50%.
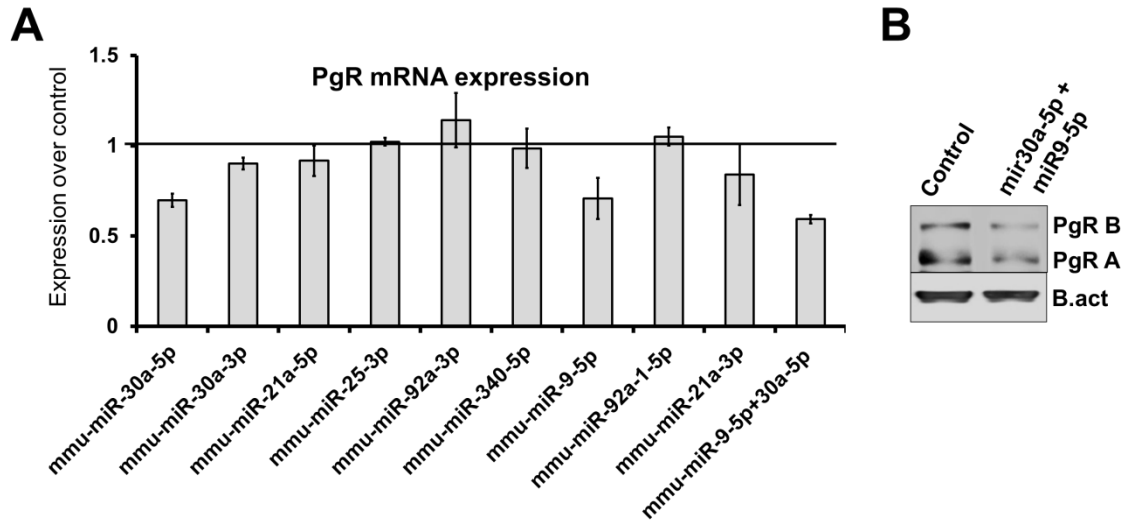
Figure 49. Effect of candidate miRNAs on PgR expression in T47D cells. (**A**) Down-regulation of PgR mRNA by miR30a-5P and 9-5P. (**B**) Western blot of PgR-A and B after addition of miR30a-5P and 9a-5P. See supplementary data 4 for the original blotting figures.

3.8.4 Cell density regulates phenotypic characteristics of cancer cells

Since we saw progesterone expression is regulated by cell density, we speculated these miRNA mechanisms might be regulated by density as well. Interestingly, miR9-5P expression was particularly sensitive to cell density in TUBO cells (Figure 50 A). We speculated that PT lesions are high density of cancer cells and early lesions are low density of cancer cells. Checking expression of miR9-5P in fresh tissue samples, revealed a 15-fold higher expression of this miRNA in PT samples than in EL lesions (Figure 50 B).
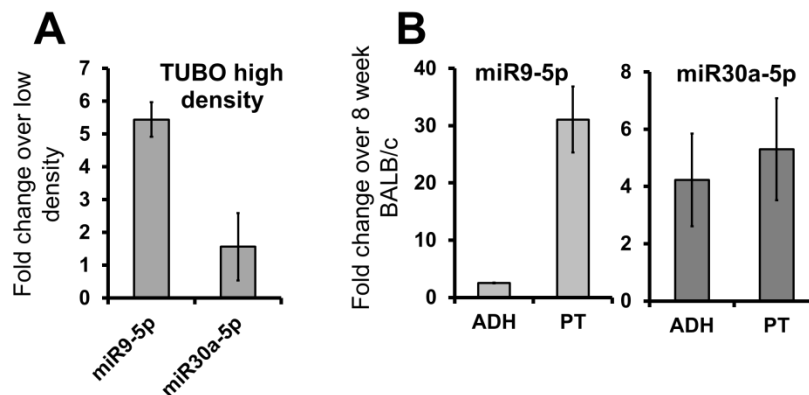
Figure 50. Regulation of miR9-5p by cell density. (**A**) High cell density upregulate miR9-5P in TUBO cells (results of qPCR) (**B**) PT and not EL upregulate miR9-5P in EL compared to 8 week BALB/c mammary glands.

To check whether density might be also able to regulate EL program, we checked the EL gene signature, migration and stemness in high and low densities. First we directly demonstrated the impact of cell density on EL signature by plating TUBO and primary tumor cells at low density, which enabled progesterone-induction of the EL signature (Figure 51).
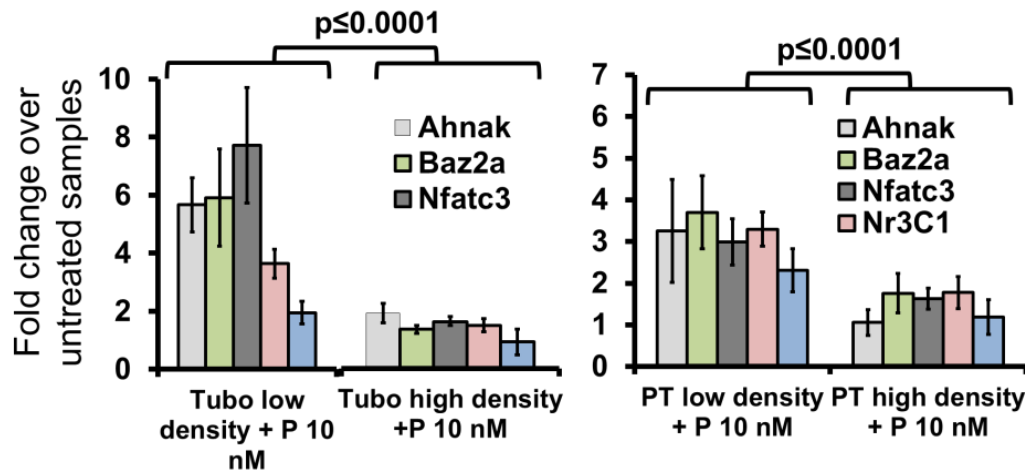
Figure 51. Cell density and EL signature. PT and TUBO cells generate the EL signature only in low density. (Low and high densities for PT: 2.6×10^4 cells/cm^2 vs. 10^5 cells/cm^2; for TUBO cells: 5.2×10^3 cells/cm^2 vs. 3×10^4 cells/cm^2). All p-values, Student's *t*-test and Stouffer's combined probability test; all error bars correspond to standard deviation (Mean ±SD).

Next, we compared sphere formation and migration abilities of TUBO cells at low and high densities. Indeed, progesterone and paracrine signals induced migration and sphere-forming ability of low-density TUBO cells whereas high-density TUBO cells showed the observed repression (Figure 52 A-C). These results suggested that cell density regulates the transition from a migratory to a proliferative phenotype in current model.
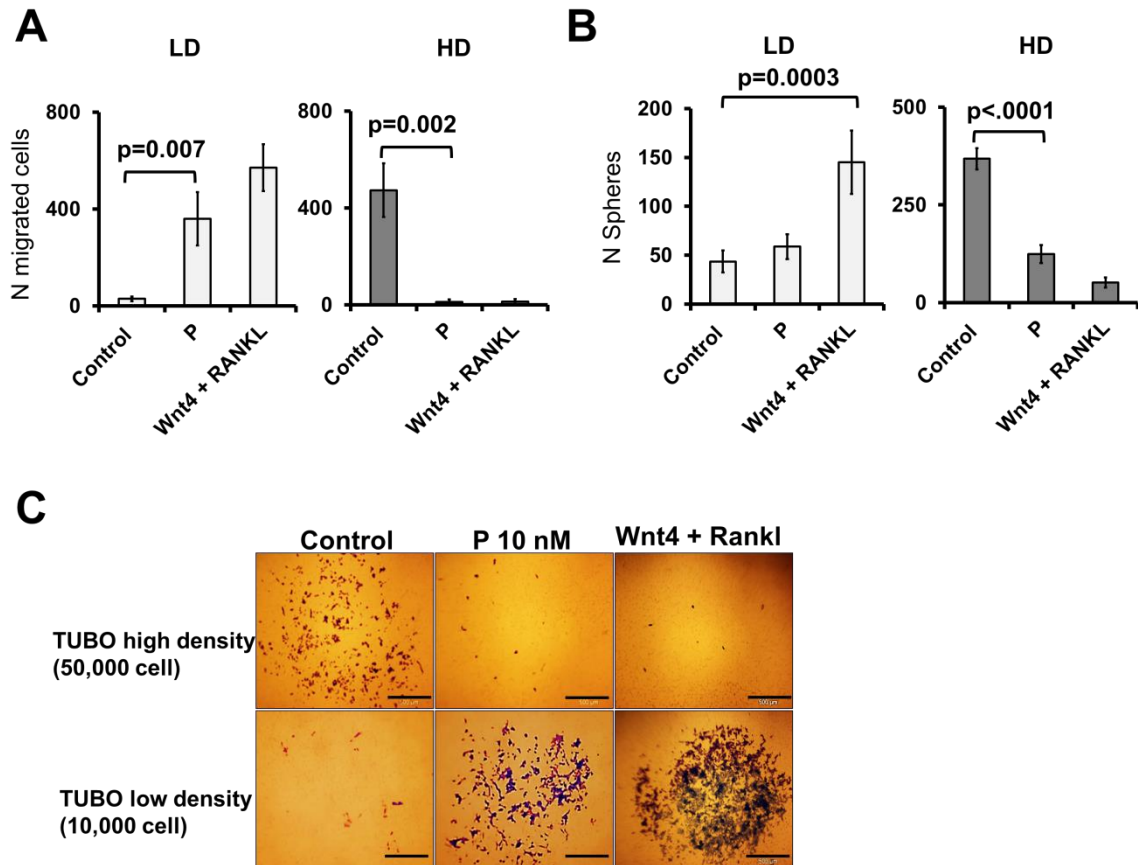
Figure 52. Cell density regulates migration and sphere formation abilities. PT-derived low-density TUBO cells acquire EL phenotype: sphere formation (A) and migration (B-C) in response to progesterone and Wnt4/Rankl. The migration of TUBO cells in low (10000 cells /well) and high density (50000 cells/well). TUBO cells in low cell density positively respond to progesterone and Wnt4+Rankl by increasing migration. All p-values, student's t-test; all error bars correspond to standard deviation (Mean ±SD).

3.8.5 Human cell line model

Finally, we aimed to explore whether human breast cancer cell lines display similar regulatory circuits. We selected 16 cell lines of different breast cancer subtypes (See figure 53A for breast cancer subtypes of cell lines). First, we checked the expression levels of Her2 and miR9-5p. The mRNA expression of Her2 and miR9-5p were evaluated in high density (90-100% cell culture confluency) of cell lines compared to their expression in the hTERT-HME cell line (Figure 53 A-B). Interestingly, these two transcripts were positively correlated in the PgR$^-$/Her2^{strong} expressing cell lines but, as expected, miR9-5p was suppressed in PgR$^+$ cell lines (Figure 53 B). Since miR9-5p suppresses PgR expression and was absent in the PgR positive cell lines, confirming our proposed mechanism for role of this miRNA in regulating expression of PgR.
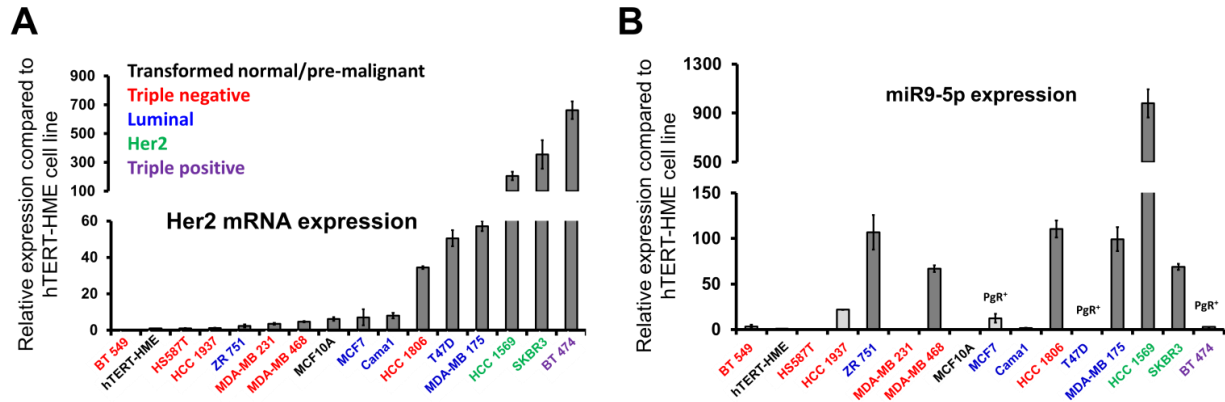
Figure 53. Her2 and miR9-5p expression in human breast cancer cell lines. (**A**) Her2 mRNA expression levels in 15 human cell lines compared to the h-TERT-HME cells. Different colors for name of cell lines indicate subtype of breast cancer. (**B**) The expression of miR9-5p in human breast cancer cell lines compared to h-TERT-HME cells. Note that Her2 strong-expressing cell lines express more miR9-5p except PgR-positive lines, such as BT474 and T47D.

Next, we checked density regulation of Her2 and miR9-5p expression. The density criteria was 90-100% cell culture confluency for high density and 20-30% for low density. We found that *Her2* is upregulated at high cell density in 10/16 cell lines (Figure 54A) and miR9-5p in 4/16 displaying strongest up-regulation at high cell density (Figure 54B). These four cell lines (HCC1937, MCF7, HCC1806, and SKBR3) were also showing Her2 density regulation which indicates recapitulation of Her2-miRNA regulation by cell density what we observed in the mouse model (See figures 48 and 50).
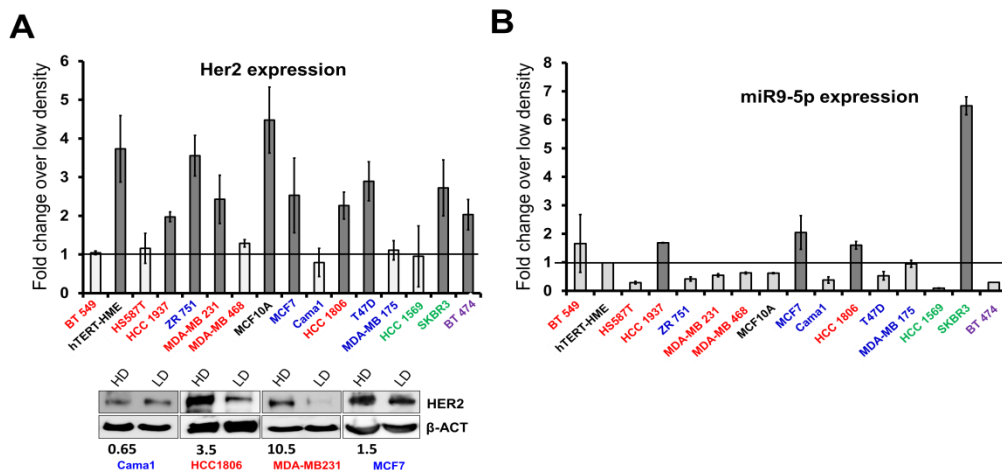
Figure 54. Cell density regulation of Her2 and miR9-5p expression. (**A**) High cell density up-regulates Her2 at mRNA (upper panel) or protein levels (lower panel) in several cell lines. Only four cell lines were checked for protein level (Her2 level not influenced by cell density – Cama1; Her2 level regulated by cell density – HCC1806, MDA-MB-231, and MCF7). Numbers below the blots indicate fold-change of Her2 in high density compared to low density normalized over beta actin. (**B**) Expression of miR9-5p is up-regulated by cell density in SKBR3, HCC1937, HCC1806, and MCF7 cell lines. Key color for the name of cell lines presented in figure 53A. See supplementary data 4 for the original blotting figures.

91

Finally, we tested 10 cell lines for migration and found 7/10 responded positively to Wnt4/Rankl and the remaining three to progesterone when using low-density cells, whereas the same factors suppressed (or unchanged) migration in high-density cells (Figure 55). Similarly, albeit less effectively, sphere formation was induced only in low-density cells (Figure 55).
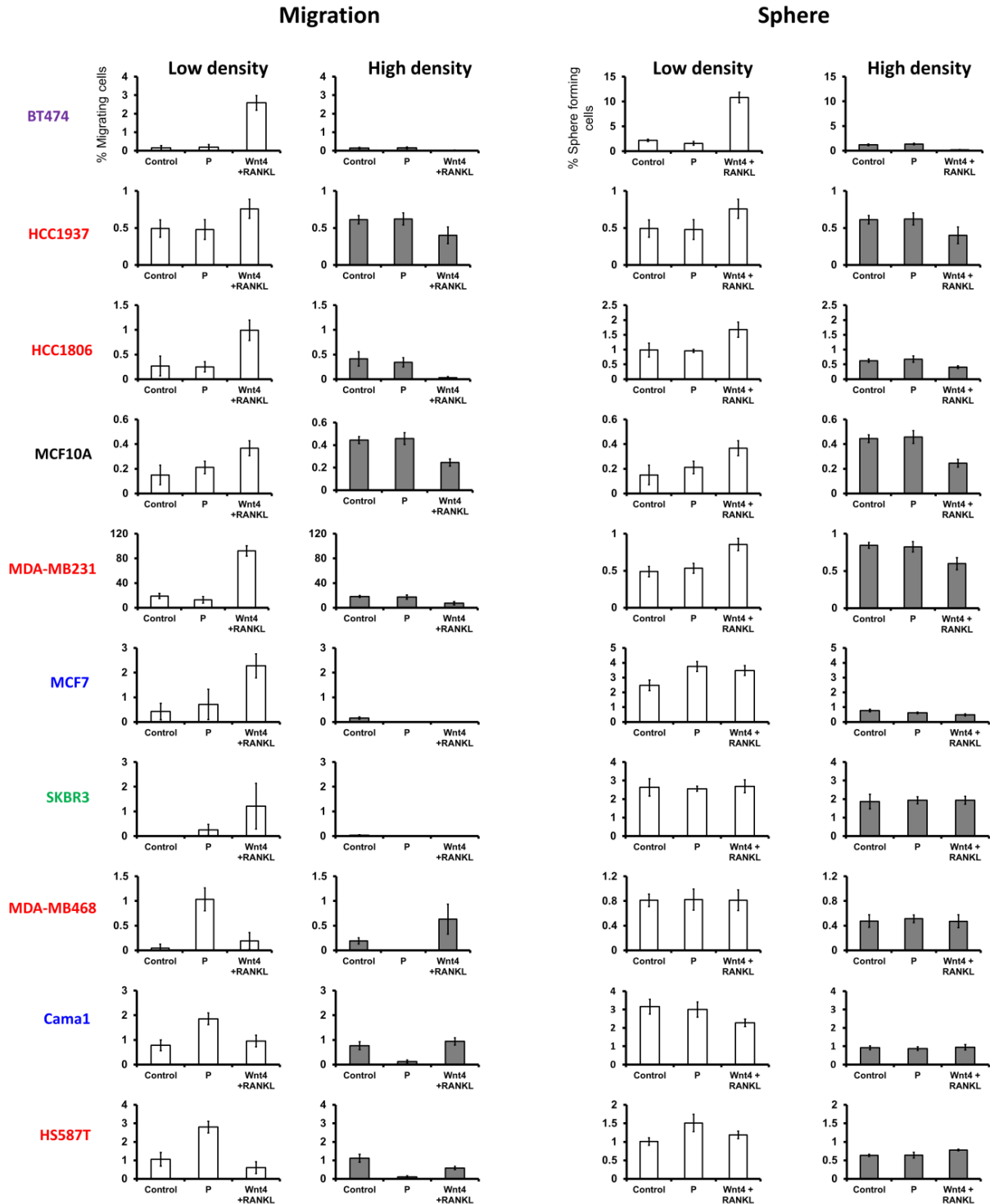
Figure 55. Cell density and regulation of migration and stemness of human breast cancer cell lines. Migration and sphere-forming potential of 10 cell lines grown at low and high densities, and treated with Wnt4/Rankl or progesterone. The first 7 cell lines regulate Her2 by density (see 4L) and their response to PIPS is similar to TUBO cells and primary mammary cell cultures of BALB-NeuT mice. The remaining three cell lines do not regulate Her2 by cell density but respond to progesterone similarly to TUBO cell line and primary mammary cell cultures of BALB-NeuT mice. We did not perform functional assays with BT549 (TN), T47D (luminal, MCF7-like), MDA-MB-175, ZR75-1 (luminal, CAMA1-like), hTERT-HME (transformed normal, similar to MCF-10A) because of breast cancer subtype redundancy or poor growth (HCC1569). Y-axes show the percentage of migrating cells (left) and observed spheres (right) relative to seeded cells. All error bars correspond to standard deviation (Mean ±SD).

In summary, although we note variation among the genetically different human cell lines, we obtained strong support for a model of metastatic dissemination in which cell density, Her2 expression and progesterone signalling play major regulatory roles (Figure 56).
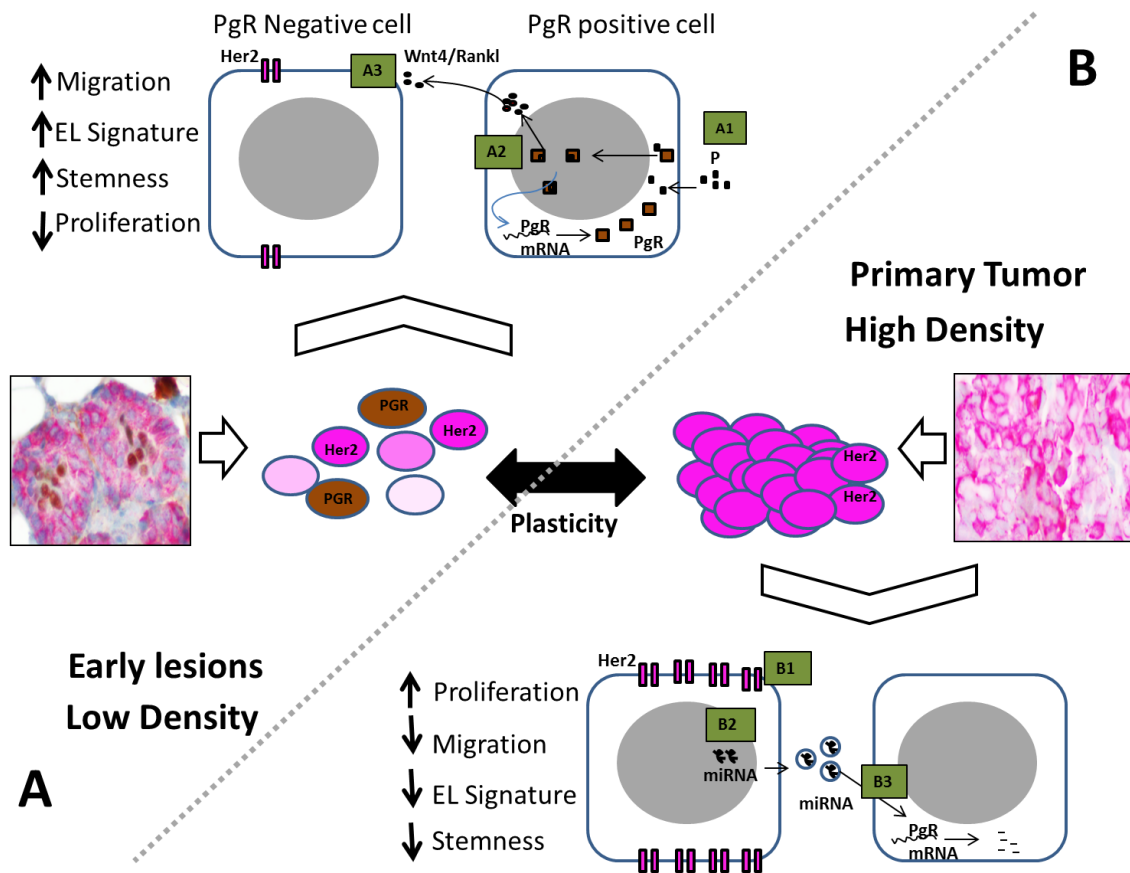
Figure 56. Graphical abstract of our mechanistic findings. In early lesions of Balb-NeuT mice which reflect low density of our *in vitro* condition (A part of graph), PgR activation upon progesterone treatment (A1) will increase PgR, Wnt4/Rankl and slightly Her2 expression (A2). Wnt4 and Rankl will target Her2 weak-moderate expressing cells which increased migration, stemness and gene expression signature of EL (A3). Cells in this state proliferate less but instead are migratory. In the PT which reflects high density of our *in vitro* condition (B part of graph), strong expression of Her2 (B1) activates miRNA transcription and secretion (B2). These miRNAs will shut down PgR expression (B3) and therefore all PgR signaling pathway which resulting in low migration, stemness and EL signature. Her2 strong expressing cells are more proliferative and further increase their proliferation if they receive progesterone-induced paracrine signals. As results a large tumor is forming.

3.9 Human samples and patient data analyses

We examined role of cell density, Her2 and PgR cooperation in human breast cancer. In the Balb-NeuT model PgR expression was lost in 100% of primary tumors (Figure 44) and co-expression of Her2 and PgR was only detectable in pre-malignant lesions (Figure 19 and 44). However, pre-malignant lesions in humans comprise diverse, heterogeneous morphologies, which may or may not progress to malignancy and, in addition, are rarely available. Therefore, mechanism of early dissemination cannot be studied in patients because the event occurs before diagnosis. Instead, we asked if metastatic dissemination in early breast cancer (stage I-III) is correlated to Her2 and PgR expression. Patient data analyses were done in collaboration with Nina Patwary from our department; Andreas Hartkopf, Florin-Andrei Taran, and Sara Y. Brucker from department of gynecology and obstetrics, University of Tübingen; Tanja Fehm form department of Gynecology and Obstetrics, University of Düsseldorf; Brigitte Rack from department of Gynecology and Obstetrics, University Munich; Stefan Buchholz from department of Gynecology and Obstetrics, University Medical Center Regensburg.

3.9.1 Her2 and PgR expression in primary tumors are correlated to cancer cell dissemination

To answer the question if PgR and Her2 expression is correlated to dissemination in patients, we investigated bone marrow samples taken at surgery in UICC stage M0, i.e. without manifest metastasis, of 2239 breast cancer patients for disseminated cancer cells. DCCs were detected by cytokeratin staining (Fehm et al., 2006). We categorized the primary tumors for expression of PgR and Her2 status (Table 11 shows all patients based on pathological scores for PgR and Her2), each into three categories of absent, moderate and high expression (which in the case of Her2 was identified as genetic activation by amplification).

Table 11. Patient data classified based on DCC positivity and PgR/Her2 scores

	Her2 IRS / PR IRS	0	1	2 no-amplification	2 (+) amplification	3	Total
DCC Negative	0	142	74	13	11	74	314
	1	15	12	6	5	10	48
	2	39	28	13	3	18	101
	3	24	22	1	1	8	56
	4	45	39	7	3	16	110
	6	76	70	14	11	17	188
	8	56	49	9	3	10	127
	9	56	30	10	3	3	102
	12	432	168	18	25	26	669
	Total	885	492	91	65	182	1715
DCC positive	0	52	27	4	3	32	118
	1	9	4	0	2	5	20
	2	8	10	5	2	6	31
	3	5	9	1	0	1	16
	4	14	7	3	3	6	33
	6	29	22	5	1	5	62
	8	17	15	5	3	1	41
	9	14	18	1	2	3	38
	12	106	29	7	10	13	165
	Total	254	141	31	26	72	524

Without consideration of the Her2 status, we noted a significant lower dissemination rate for PgR^{high} tumors (p=0.013; chi-square test; Figure 57 A). On the other hand number of DCC positive patients increased with Her2 expression in primary tumors and was highest in Her2-amplified tumors (p0.056; chi-square test; Figure 57 B).
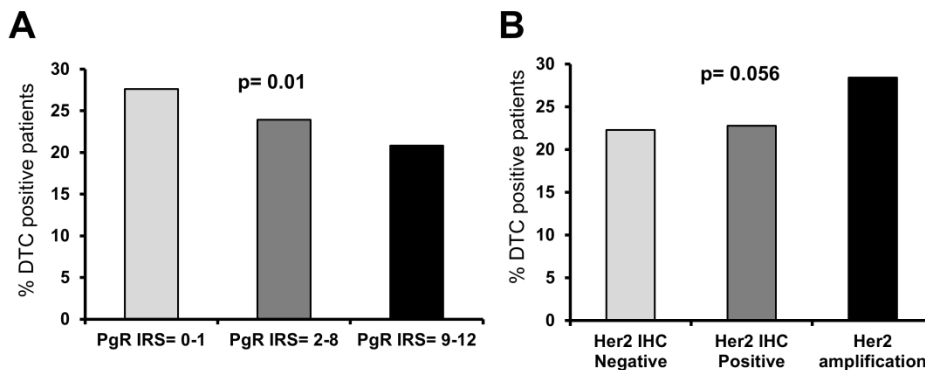
Figure 57. PgR and Her2 status of primary tumors correlated to dissemination. Higher expression of PgR (**A**) correlated with lower DCC positive patients and higher expression of Her2 (**B**) is linked to higher number of DTC positive patients. Based on expression of PgR or Her2, patients were divided in three groups including low or negative (PgR IRS=0-1 and Her2=0), moderate (PgR IRS=2-8 and Her2=1-2 without amplification) and high (PgR IRS=9-12 and Her2=2-3.with amplification). P values, chi-square test.

Strikingly, in breast cancers with high PgR score (9-12), we noted that genetic activation of Her2 increased the dissemination rate (p=0.02; Figure 58), similar to the EL lesions in the Balb-NeuT model.
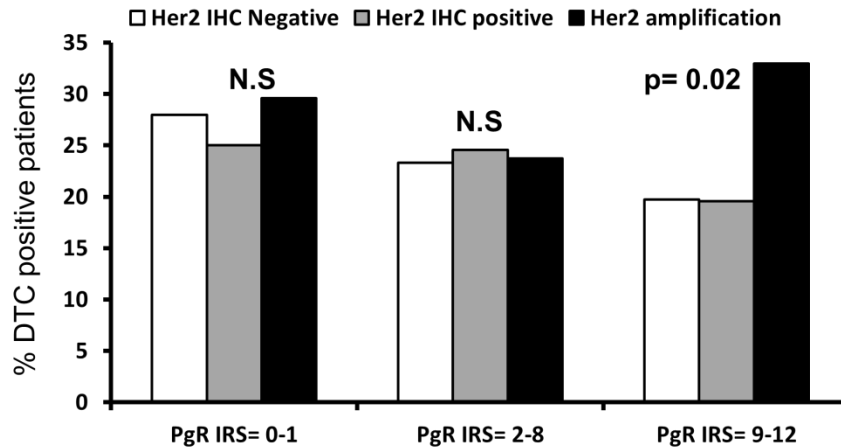
Figure 58. PgR **and Her2 expression identifies Her2^{high}/PgR^{high} subgroup of patients with highest seeding rates.** Based on expression of PgR and Her2, patients were divided in three groups including low or negative (PgR IRS=0-1 and Her2=0), moderate (PgR IRS=2-8 and Her2=1-2 without amplification) and high (PgR IRS=9-12 and Her2=2-3.with amplification). P values calculated by Chi-square test; N.S, not significant.

3.9.2 New subtype of human breast cancer with caractarastics like EL of Balb-NeuT

We had never observed high PgR expression in established primary tumors of the Balb-NeuT model. In humans, we identified this subgroup comprising 3.7% of all patients (85/2239) or 24.6% of Her2-amplified tumors (85/345). We performed IHC double-staining for Her2 and PgR in these samples (Table 12) and found Her2 and PgR single positive cells and also double-negative and double-positive cells in low density invasive regions (Figure 59 A) similar to EL in Balb-NeuT mice. When also noted areas of high cell density without PgR expression and (Figure 59 A and B), providing within the same samples evidence for density-associated PgR regulation.

Table 12. Her2^{amp}/PR^{high} samples used for double staining for PgR and Her2

	ID	DCC	PR	HER2-ICH	FISH
1	788/12X	positive	12	3	n.a.
2	149/03	positive	12	3	n.a.
3	623/10	positive	12	2	positive
4	031/03	positive	12	2	positive
5	210/06	positive	12	2	positive
6	264/06	positive	12	2	positive
7	375/03	positive	9	3	n.a.
8	503/12	positive	12	3	n.a.
9	473/03	positive	12	2	positive
10	106/03	positive	12	2	positive
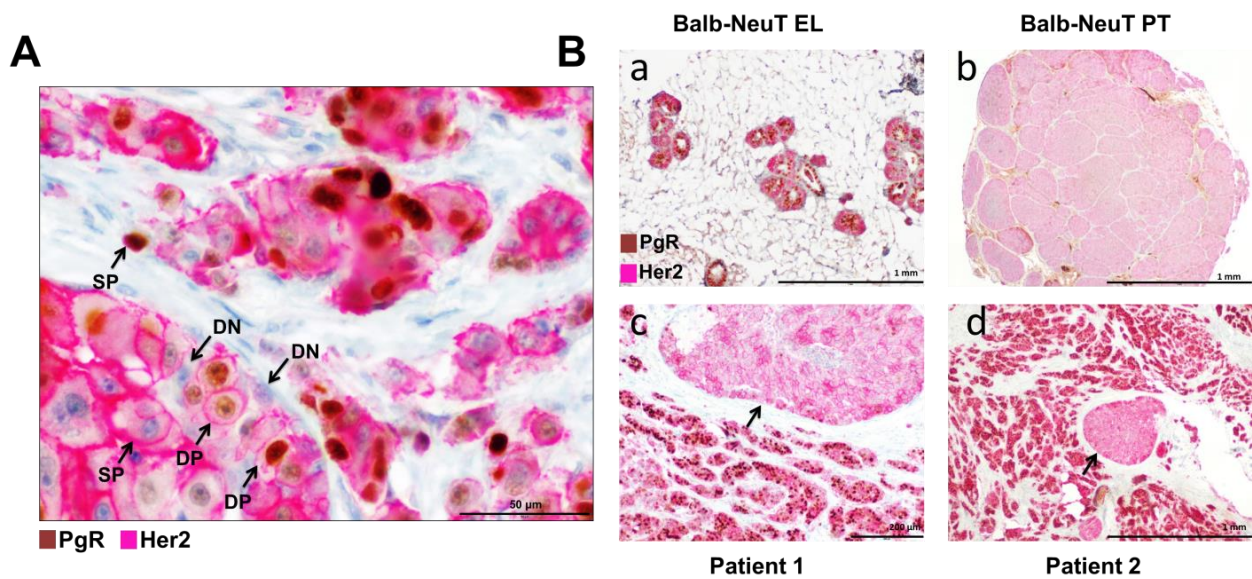
Figure 59. Immunohistochemical double staining of a Her2^{high}/PgR^{high} breast cancer and Balb-NeuT samples. (**A**) Double staining of Her2^{high}/PgR^{high} human breast cancer sample (PgR: brown, nucleus; Her2: red/pink, membrane). Cells with varying expression levels of Her2 and PgR, as well as negative, single- or double-positive cells can be seen (scale bar = 100 μm). Arrows indicate DP, double-positive; DN, double-negative; SP, single-positive. (**B**) Comparison of Her2^{high}/PgR^{high} human breast cancers and primary tumour Balb-NeuT mouse for Her2/PgR staining. (**a**) Early lesion (EL) from Balb-NeuT (10x magnification). (**b**) primary tumour (PT) from Balb-NeuT model. (**c-d**) Human breast cancer. Note in human sample (d) and Balb-NeuT PT (b) high-density regions displaying strong expression of Her2 that lack PgR indicated by arrows. In human sample (c) and EL of Balb-NeuT (a) regions of invasive cells stain strongly positive for PgR and Her2.

3.9.3 miR9-5p and 30a-5p are upregulated in Her2^{high}/PgR^{neg}

Next, we checked the expression level of the miRNAs those found in mouse regulate PgR. We compared miRNA expression in fresh samples of Her2^{amp}/PgR^{high} and Her2^{amp}/PgR^{neg} patients. As reference, classical Her2^{neg}/PgR^{high} luminal breast cancers with high PgR expression were used (Table 13 shows details of samples). Indeed, Her2^{amp}/PgR^{neg} displayed a median 5-fold (miR30a-5p; p=0.04; Mann-Whitney test) to 20-fold (miR9-5p; p=0.006; Mann-Whitney test) up-

regulation over $\text{Her2}^{amp}/\text{PR}^{high}$ tumors, indicating that lack of miRNA-mediated PgR down-regulation enabled the $\text{Her2}^{amp}/\text{PR}^{high}$ phenotype in these patients (Figure 60).

Table 13. Three groups of samples used for miRNA analyses

	Sample ID	PgR IRS	HER2 Score/ amplification
	T 3653	12	0
	T 3441	12	0
	T 3283	12	0
	T 2171	12	1
$\text{PgR}^{high}/\text{Her2}^{neg}$	T 2127	12	0
	T 2376	12	0
	T 2188	12	1
	T 2307	12	0
	T 2355	12	1
	T 3732	0	2/amp*
	T 3744	0	3
	T 3751	0	2/amp
	T 2886	0	3
$\text{PgR}^{neg}/\text{Her2}^{high}$	T 2946	0	3
	T 2312	0	3
	T 2103	0	3
	T 2080	0	3
	T 2504	0	3
	T 4404	12	3
	T 2420	12	3
	T 2670	12	3
$\text{PgR}^{high}/\text{Her2}^{high}$	T 1877	12	2/amp
	T 2299	12	3
	T 2362	12	2/amp
	T 2203	12	3
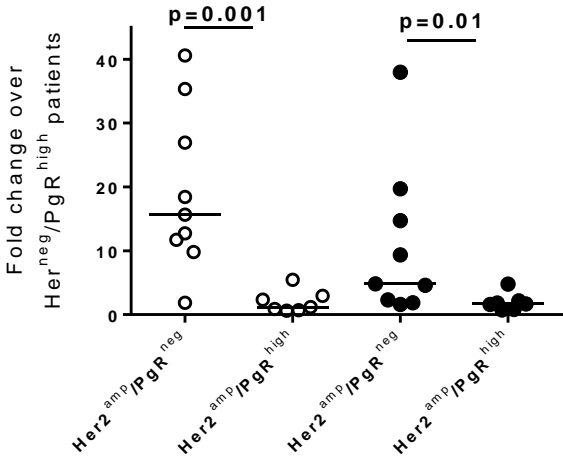
Figure 60. miR9-5p and 30a-5p are upregulated in $\text{Her2}^{high}/\text{PR}^{neg}$ samples of patients. PgR-downregulating miRNAs show lower expression levels in $\text{Her2}^{high}/\text{PgR}^{high}$ human mammary carcinomas compared to $\text{Her2}^{high}/\text{PgR}^{neg}$ carcinomas. Expression of miR9-5p and miR30a-5p is normalized to $\text{Her2}^{-}/\text{PgR}^{high}$ breast cancers (see Table 13 for details on patients). P-values, Mann-Whitney test; shown are median and individual values.

3.9.4 Human DCCs do not express hormone receptors

Finally, we tested whether human DCCs isolated from bone marrow are characterized by the absence of PgR expression as predicted from the Balb-NeuT model, where migrating cells lacked PgR expression (Figure 22). For 27 EpCAM-positive cells, isolated from 19 M0 breast cancer patients, we isolated the genomic DNA and mRNA and performed single cell whole genome (WGA) and transcriptome amplification (WTA) as previously published (Guzvic et al., 2014). After confirmation of the malignant origin by CGH analysis and quality control of the WTA we tested for transcript expression of ER-α, PgR and Her2 by PCR (Figure 61). Indeed, none of the DCCs expressed the ER-α/PgR, but one DCC expressed Her2 consistent with our finding in the mouse model where we found migratory cells are PgR negative and low expressing Her2 (See figure 34).
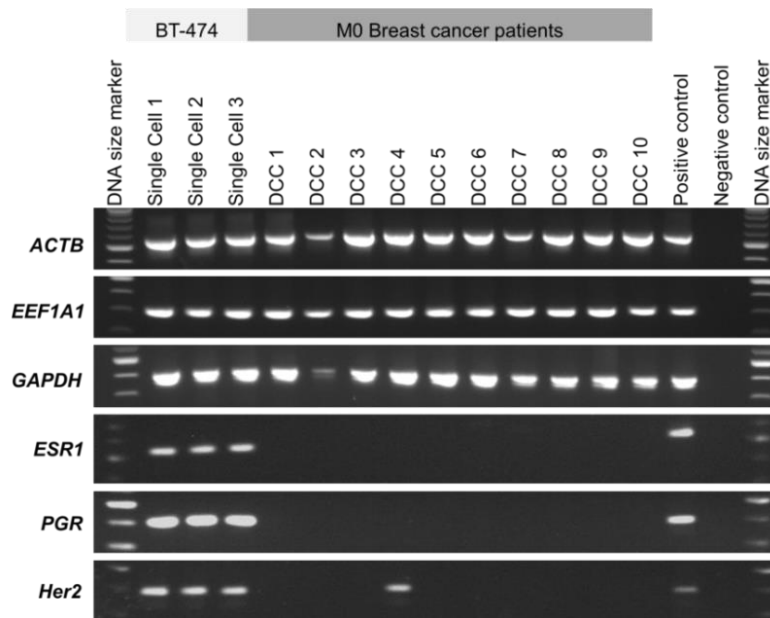
Figure 61. ER and PgR genes are not expressed in human M0 DCCs. Estrogen receptor (*ESR1*) and progesterone receptor (*PGR*) transcripts expression in human breast cancer DCCs (26 DCCs from 19 M0 patients; only 10 samples are shown). One DCC out 26 was Her2 positive which originated from a DCIS patient. *ACTB*, *EEF1A,* and *GAPDH* serve as controls for single cell expression profiling. The first 3 lanes depict results from BT474 single cells which is positive for ESR1, PgR and Her2. This figure generated by Nina Patwary.

3.10 Summary of numbers and type of replications

All statistical tests, calculated p values, and numbers are mentioned in the legends and figures. Numbers for all in vivo experiments are shown in the figure or legends. All experiment on cell lines and primary cultures including sphere assays, migration assays and qPCR are done in at least triplicates (biological). I made a summary table (Table 14) for all numbers and type of

replicates which used in each given figure in the result section. The source data which used to generate all graphs can be found in the supplementary data 3.

Table 14. Summary of numbers and type of replications

Figure	N replication #	N mice	is addressed in
12	Not applicable		
13			In the figure
14			Table 7
15			Table 7
16			Table 7
17	≥3		
18	≥3		
19			Fig 44
20	≥3		
21	Not applicable		
22	A, ≥3; B, ≥3		
23		2 per condition	In the figure
24	≥3		
25			In the figure
26		3 per condition	In the figure
27	≥3		
28	≥3		
29	≥3		
30	≥3		
31	≥3		
32	≥3		
33	≥3		
34	≥3		
35	Not applicable		
36			In the figure
37			In the figure
38			In the figure
39			In the figure
40		4	
41	≥3		
42			In the figure
43			In the figure
44			In the figure
45		6	
46	≥3		
47	≥3		
48	≥3		
49	≥3		
50	≥3		
51	≥3		
52	≥3		
53	≥3		
54	≥3		
55	≥3		
56	Not applicable		
57			Table 11
58			Table 11
59			Table 12
60			Table 13
61			In the figure

I consider all experiments were done in ≥3 biological replicates. The "biological replicates" is based on assumption that all conditions of experiments were constant and the differences measured between ≥3 biological replicates were the result of tested conditions (Blainey et al., 2014).

4 Discussion

In this work we studied the early steps of metastasis. For this we used the Balb-NeuT mouse model of breast cancer and investigated the dissemination of cancer cells in early stages of carcinoma development, which are considered as non-invasive stages by light microscopy. We further addressed why late-stage tumors are less successful in seeding metastases. Our results reveal a mechanism of early dissemination of murine mammary cancer cells that taps into mammary branching morphogenesis programs and thereby enables efficient migration and dissemination of cancer cells from pre-invasive lesions. This mechanism consists of three key players: cell density, PgR, and Her2 signaling, and is shut down as primary tumors grow and overt lesions develop. Our suggested model comprises a stage-dependent interpretation of microenvironmental signals as a function of cell density, and oncogenic signals, which leads to a switch from dissemination to proliferation mode. Moreover, we demonstrate that early disseminated cancer cells are able to complete all steps of metastatic cascade from dissemination to colonization at distant site. Finally, analyses of human samples confirmed the fundamental findings from our mouse model and, interestingly, we found a group of patients (comprising 4% of all breast cancer patients) with higher dissemination rate, whose tumors are morphologically similar to early stages of Balb-NeuT model.

4.1 Mechanisms of early metastatic dissemination

4.1.1 A transient cooperation of progesterone and Her2 signaling in early mammary lesions of Balb-NeuT mice

To identify mechanisms regulating early dissemination of tumor cells, we first investigated the gene expression profile of mammary lesions in the Balb-NeuT mouse model at the time point of maximal relative seeding - around week 7-12, long before tumors are palpable or visible -when mammary lesions morphologically resemble atypical ductal hyperplasia (ADH). We established unique and stage dependent expression profiles of Balb-NeuT model including one characteristic for ELs. The gene expression analyses suggested the putative role of nuclear receptor signaling. A role for steroid hormones as regulators of early dissemination is consistent with their role in breast carcinogenesis and control of postnatal mammary gland development (Brisken and O'Malley, 2010).

The EL-signature was only induced in early lesions and only by progesterone treatment. Lack of PgR in PTs or lack of Her2 in aged matched BALB/c samples abrogated the EL-program. This suggested that PgR signaling has been hijacked in the context of Her2-induced transformation for an EL dissemination program. In support of this, we found that PgR signaling initially increased Her2 expression, which was independent from MMTV-driven Her2 expression. On the other hand, while increased PgR signaling and expression of Her2 were mandatory to generate the EL signature, strong expression of Her2 and high cell density abrogated PgR expression and consequently the EL signature. These results are supported by previous findings that showed progesterone receptor and Her2 participating in a bidirectional cross-talk during breast cancer development (Beguelin et al., 2010). It has been reported that Her2 could migrate into the nucleus where Her2 binds to DNA at specific sequences named Her2 Associated Sequences (HASs) (Wang et al., 2004). In addition, progesterone could activate the HRG (heregulin)/Her2 pathway (Balana et al., 1999; Labriola et al., 2003). Moreover, Her2 expression and its signaling pathway can be regulated by Rankl which is the downstream target of progesterone signaling (Ithimakin et al., 2013; Liu et al., 2010a) indicating links between progesterone and Her2 signaling. These observations are consistent with our findings of a transient window of PgR and Her2 cooperation in a dissemination program of cancer cells from ELs.

4.1.2 A branching morphogenesis program is recruited for migration and dissemination of cancer cells from early lesions

We investigated how progesterone can regulate dissemination of cells from very early lesions. Since progesterone induces side branches by its paracrine signals, Wnt4 and Rankl, from mammary epithelial cells invading into the mammary fat pad (Brisken, 2013; Brisken et al., 2000; Muschler and Streuli, 2010), we evaluated the role of progesterone signaling in this process. Our results indicated that progesterone and its paracrine signals (Rankl and Wnt4) and the EL-signature are upregulated in young mammary glands, which is associated with the migration of EL-derived cells. In addition, we observed higher numbers of PgR$^+$ cells in the anterior sprouting ducts in the normal mammary glands, where differentiation process occurs. Consistently, *in vitro* results revealed higher differentiation ability of EL-derived cells. The differentiated structures of EL-derived cells were able to express PgR in their formed acini,

which were induced by progesterone. Moreover, we found that the B form of PgR is the relevant isoform in early dissemination - in the line with other findings showing that progesterone receptor isoform B is the main player during pregnancy and mammary gland morphogenesis in puberty (Aupperlee et al., 2005; Fernandez-Valdivia et al., 2005; Mulac-Jericevic et al., 2003). Based on these results, we concluded that a normal local invasion program is exploited for early metastatic dissemination in our model. This is in line with notions that biological programs which are used during normal development are also used by carcinoma cells (Yang and Weinberg, 2008). Therefore, all findings are supporting a dual role of progesterone in both metastasis and side branching during normal morphogenesis.

4.1.3 Expression of Her2 regulates the switch from migration to proliferation

We found that changes in the expression level of Her2 are associated with switching from a migratory to proliferative phenotype. In the early lesions of Balb-NeuT mice, lower expression of Her2 was correlated with higher migration and sphere formation ability. Conversely, strong expression of Her2 in MM3MG (by retroviral transduction) and PT-derived cells induced proliferation. Additionally, in the transduced MM3MG-Her2 cell line the Wnt4/Rankl-induced migration phenotype could be rescued by reducing Her2 signaling. Finally, we noted that the up-regulation of Her2 by high cellular density of primary cultures of murine PT and, TUBO cells, and human breast cancer cell lines was correlated with loss of stemness and migratory phenotypes.

Although it is known that overexpression of Her2 in breast cancer cells increases proliferation (Moody et al., 2002; Ursini-Siegel et al., 2007; Yang et al., 2004), not much is known about the correlation between expression level of oncogenes and different phenotypes of cancer cells. However, there are several studies which are consistent with our findings. In one study the authors showed that overexpression of Myc in human metastatic breast cancer cells decreased their metastatic traits, while increasing tumorigenicity of these cells (Liu et al., 2012). Another study found that simultaneous activation of Akt-1 and Her2 strongly increased proliferation and growth of tumors whereas significantly fewer metastatic lesions were observed compared to the activated Her2 strain alone (Hutchinson et al., 2004). Another study in the intestinal adenocarcinoma mouse model ($APC^{-/-}$/K-Ras$^{wt/mut(V12)}$) observed that activation of K-

Ras at the initial stages did not change proliferation. Although K-Ras is a strong mitogenic factor, the authors found no evidence of elevated proliferation in early stages. In contrast, activation of metastasis was dependend on the presence of mutant K-Ras (Sansom et al., 2006). Therefore, proliferation and invasion are not concomitant phenotypes (Evdokimova et al., 2009; Svensson et al., 2003), which is in line with our observations that EL-derived cells migrate more and proliferate less, but PT-derived cells migrate less and proliferate more. This is further supported by other studies in melanoma (Hoek et al., 2008) and glioblastoma (Zhong et al., 2010) which reported that cancer cells switch between proliferative and invasive states, and suggested that a cancer cell has only one of these phenotypes at a given time.

We further observed that cell density may be involved in the phenotypic changes. It has been reported two decades ago by Berner's group that high cell density or non-permissive substrates inhibit cell motility, and favor a more proliferative phenotype(Giese et al., 1996). Conversely, active migration suppresses cell proliferation (Giese et al., 1996).

4.1.4 Migration and stemness are concomitant phenotypes

We found more mammosphere-forming and differentiation potential in EL cells which were able to differentiate and re-express PgR. Comparing sphere formation of BALB/c and Balb-NeuT mammary epithelial cells showed that Her2 expression induced stemness, in line with other reports (Ginestier et al., 2007; Korkaya et al., 2008). We also found that progesterone induced stemness, via paracrine factors. The paracrine mode of action was shown by experiments in which we were exposing MM3MG and MM3MG-Her2 cells to either Wnt4 / Rankl or to co-culture with MM3MG-PgR cells. Both conditions generated similar results. The stemness and migration induction could be ablated by addition of inhibitors of Wnt4 and Rankl. Interestingly, we could not detect PgR expression in migratory cells of cell lines or primary cultures of EL *in vitro*. Consistently, we could not find any expression of PgR in the DCCs of patients with luminal primary tumors. These results supported the concept that paracrine signals of PgR$^+$ cells target PgR$^-$ cells for migration.

Under physiological conditions, the paracrine factors Wnt4/Rankl released after progesterone stimulation activate adult MaSCs (mammary stem cells) in the mammary stem cell

niche during reproductive cycles. Here, MaSCs are important target cells of ovarian hormones and therefore are putative targets for cell transformation events leading to breast cancer (Asselin-Labat et al., 2006; Asselin-Labat et al., 2010; Joshi et al., 2010; Mukherjee et al., 2010; Schramek et al., 2010). Indeed, we observed that cells from young mammary glands of mice formed more spheres indicating activation of stemness features. Young mammary glands in both wild type and transgenic models contained more PgR^+ cells, expressed more paracrine signals, and faintly expressed Her2 compared to older mammary gland, which did not express Her2. Therefore, progesterone induced stemness of $Her2^{low}$ cells which then differentiated in a positive feedback loop and generated PgR^+ cells (See section 3.1.2).

We showed that *in vitro* migrating cells have stemness potential and disseminating cancer cells *in vivo* can colonize and form metastasis. All DCCs from M0 patients were PgR and ER negative despite the fact that the PTs where they were derived from expressed these molecules. This is in line of our previous study and other studies, showing that disseminated cancer cells in breast cancer have stem-like features (Aktas et al., 2011; Balic et al., 2006; Fehm et al., 2009; Hüsemann et al., 2008; Weng et al., 2012). Therefore, stemness traits of cancer cells are tightly correlated to a migration phenotype.

When we compared the number of formed spheres, number of DCC seeding mice, and number of DCCs in BM of mice, we observed a similar ratio of around 2 fold higher in EL compared to PT, which was also found for metastasis outgrowth for transplanted young mammary gland versus of PT. This suggests that colonization success may be similar for different DCCs from PT and EL and that the main reason for different number of metastatic mice transplanted with PT or mammary gland does not reside in a higher/intrinsic propensity of early DCCs to colonize, but rather reflects the higher numbers of DCCs that disseminated from early lesions. One may further speculate that the intratumoral heterogeneity of Her2 expression (Bartlett et al., 2011; Seol et al., 2012), generates cells within the primary tumor with metastatic potential.

Finally, we observed that strong Her2 expression in PTs or high cellular density affected the stemness of cancer cells. As mentioned before, strong expression of Her2 increases proliferation. It has been suggested that increase in proliferation potential yields larger

populations of non-stem cancer cells that compete with CSC and, thus, inhibit CSC division. Conversely, decrease in proliferation potential loosens such inhibition and facilitates frequent CSC division (Morton et al., 2011; Poleszczuk et al., 2015; Sadler et al., 2013).

4.1.5 Loss of PgR and strong expression of Her2 marks the switch from migration to proliferation

Next, we tried to answer why the mechanism of early dissemination is not working in PTs which may explain a decreased seeding rate of PTs. We focused on the regulation of PgR, which is lost in all primary tumors of the Balb-NeuT model. Using PgR expression as a marker, we identified its regulation by cell density-regulated miRNAs. These miRNAs were also abundantly found in exosomes, which could spread the signal for PgR down-regulation among tumor forming cells. We identified a link between cell density and PgR expression via up-regulation of the PgR-targeting miR9-5p, known to be density-regulated (Mori et al., 2014). However, we could not detect regulation of miR30-5p by density, which may due to our inability to specifically target only this member of the miR30 family which all have very similar sequences with only 1-2 nucleotides difference (Chugh and Dittmer, 2012; van Rooij, 2011).

We observed that PT-derived TUBO cells could re-express PgR under conditions of low cell density. The same was true for primary tumors of the Balb-NeuT model. Interestingly, under low cell density TUBO cells displayed all major features of EL cells, including Wnt4/Rankl stimulated migration and sphere formation, and induction of the EL surrogate signature. Increase of cell density was a key factor in this phenotypic change. Density upregulates Her2 expression and miR9-5p and upregulation of Her2 increases miR30a-5p expression. Consequently, these miRNAs decrease PgR expression. Interestingly, progesterone-induced factors induce proliferation of PgR negative PT cells. Therefore, PgR and density in advanced PT cells mark a phenotype of cancer cells that either responses to progesterone-induced cytokines with migration or proliferation. We conclude that higher cell density and upregulation of Her2 turns on proliferative machinery and therefore change the translation of environmental signals.

4.1.6 Early and late lesions of Balb-NeuT represent different subtypes of breast cancer

The mechanism of early dissemination identified in our murine model is also activated in human breast cancer cells. We found that cell lines from all subtypes of breast cancer displayed cell density regulation of stemness and migration in response to progesterone or its induced paracrine factors. We saw that some triple negative and Her2-amplified cell lines displayed migration/stemness phenotypes at lower density under Wnt4/Rankl treatment. The decreasing migration and stemness of triple negative and Her2 cell lines at high density can be explained by following facts. First, progesterone paracrine-induced factors target mammary stem cells(Asselin-Labat et al., 2006; Asselin-Labat et al., 2010; Joshi et al., 2010; Mukherjee et al., 2010; Schramek et al., 2010). Second, since the higher cell density decreases the stemness property of cell, (Morton et al., 2011; Poleszczuk et al., 2015; Sadler et al., 2013) the target cell population of progesterone paracrine-induced factors is diluted at higher cell density. Remarkably, we observed that some of Her2 negative luminal cell lines also displayed phenotype switching which was linked to the changes of Her2 expression level at different densities. This is of interest because an intermediate expression of Her2 confers stemness in luminal breast cancer cells (Ithimakin et al., 2013). Furthermore, gene expression analyses revealed more similarity of Balb-NeuT tumors to human luminal breast tumors[46] which is higher for early lesions compared to advanced tumors(Astolfi et al., 2005; Herschkowitz et al., 2007). Therefore, the Balb-NeuT model may represent a luminal like phenotype in earlier stage of tumor development and Her2-like phenotype in later stages.

4.2 Potential relevance for human breast cancer

4.2.1 Progesterone mechanisms in tumor growth and dissemination can explain pregnancy-associated breast cancers

Pregnancy-associated breast cancer is associated with poor prognosis (Schedin, 2006). During pregnancy high levels of progesterone are secreted which activate proliferation of mammary epithelial cells and induce side branching, a physiological fat pad invasion program[49]. Although PgR signaling induces proliferation and migration of normal mammary epithelial cells, it

prevents their terminal differentiation. Terminal differentiation and lactation start shortly after a sharp decrease of progesterone at the end of pregnancy(Ismail et al., 2003; Ismail et al., 2002). In the Balb-NeuT model, we found that pregnancy during early lesions induced dissemination, while pregnancy during later stages induced proliferation and tumor growth. These results can be explained based by the differential response of EL and PT cells to progesterone. It may also address the question why pregnancy-associated breast cancers develop to a highly metastatic phenotype. During pregnancy mammary epithelial cells undergo many mitotic cycles, and in addition an EL-like dissemination program is activated because of the progesterone surge. If a cancer favoring mutation has already been acquired or happens during pregnancy-induced mammary cell expansion (Pike et al., 1983; Russo and Russo, 2011; Schedin, 2006), it may favor tumor growth and dissemination.

4.2.2 Risk of breast cancer is related to PgR expression, age, and subtypes

We found that PgR expression suppressed dissemination of advanced cancer cells in the mouse model. This was confirmed in patients where we saw less dissemination in PgR^+ tumors. Previous data showed that the presence of PgR in primary breast cancers is an independent marker associated with less invasive phenotype, despite the fact that progesterone induces proliferation and is risk factor for breast cancer(Obr and Edwards, 2012). It was also reported that loss of PgR in ER^+ tumors is associated with a more aggressive tumor phenotype, reduced responsiveness to endocrine therapies, and a shorter overall survival (Liu et al., 2010b; Mohammed et al., 2015).

On the other hand, breast cancer in young women is associated with a higher frequency of metastasis and death (Fredholm et al., 2009; Tjokrowidjaja et al., 2014). Interestingly, $Her2^+$ and basal like breast cancers, which are considered as more stem-like, are more frequent subtypes in young women (Jenkins et al., 2014; Kurian et al., 2010; McGuire et al., 2015; Yankaskas, 2005). Consistently, our observations corroborated that young mammary glands/EL are PgR-rich environment which supports dissemination of EL stem-like cells. We saw that EL lesions have a high dissemination potential and were generating more metastases. The number of dissemination events and metastases from EL were twice as high compared to those from advanced lesions, which are depleted of PgR expressing cells. We speculate that in young women with breast

cancer, cancer stem cells are more abundant, on one hand, and have more PgR^+ cells as a proper mechanism of cancer stem cell dissemination, on the other hand. Therefore, the presence of PgR-expressing cells may be part of the worse of outcome of young women. This conclusion is in line with recent data showing that death from DCIS is significantly higher in young women(Narod et al., 2015).

4.2.3   Early dissemination can explain CUP syndrome

Carcinoma of unknown primary (CUP) is one of the 10 most frequent cancers worldwide. It constitutes 3-5% of all human malignancies. Patients with CUP present with metastases without an established primary site (van de Wouw et al., 2002). The syndrome may be explained by dissemination of cancer cells with metastatic potential whereas cancer cells at the primary lesion fail to progress. We also noted in the transplantation experiments of small pieces of mammary glands or low numbers of spheres that cancer cells disseminate and form metastases while at the primary site no tumor is forming .

4.2.4   Her2-PgR crosstalk in dissemination mechanism and DCC subtypes in

patients

Another debated issue in the field of breast cancer is the disparity between Her2 expression in DCCs, metastases, and primary tumors (Bock et al., 2012; Fehm et al., 2010; Guzvic et al., 2014; Stoecklein et al., 2008). We noted that migrating EL cells display a phenotype comprising low/intermediate expression of Her2, and absence of PgR-expression during migration. In addition, PgR mechanism of EL-dissemination targets low-moderate Her2 expressing stem-like cells. Interestingly, when we tested human DCCs from bone marrow, we could confirm the absence of ER-α and PgR, which suggests that stem-like cells are the main targets of the identified dissemination program. Therefore, these results interpret how Her2 negative DCCs disseminate in patients with Her2 positive breast tumors and, consequently, may explain why Her2-targeted therapies fail in many patients. This may also explain why up-regulation of Her2 (not amplification) is observed frequently in in human *in situ* carcinoma (Ignatiadis et al., 2011) and linked to the detection of CTCs.

4.2.5 New subtype of breast cancer as the most aggressive group of breast cancer is similar to EL of Balb-NeuT

We could not analyze EL in patients since these are only circumstantially diagnosed. Therefore we had to analyze advanced lesions regardless of their pathological stage of tumors. These analyses revealed that human breast cancers follow the suggested mechanism according to which dissemination of advanced cancer cells is decreased by PgR expression, but However, still there is small group of patients which have high expression of PgR and Her2 ($Her2^{high}/PgR^{high}$). This group of patients lacked the PgR-miRNA-regulating mechanism whereas $Her2^{high}/PgR^{neg}$ expressed these miRNAs similar to mouse model. This is highlighting the importance of PgR-regulation by miRNA and suggests that $Her2^{high}/PgR^{high}$ cells found a way to escape the miRNA-mediated PgR-downregulation. The new group of patients comprises 24% of Her2-amplified breast cancers and 4% of total breast patients, and display highest DCC rates among all tested groups. This group shows high similarity in their invasive regions to the EL of Balb-NeuT. Tumors of these patients are composed of some regions lacking PgR expression and have higher cell density similar to PT of Balb-NeuT.

4.3 Significance and conclusion

This study mechanistically addresses metastatic early dissemination in one cancer model. In *vitro, in vivo,* and patient data cohere and suggest a model for metastasis from early lesions. During early stages, all pre-requisites for dissemination are naturally present, i.e. intermediate Her2 expression, presence of PgR expressing cells, and low cell density. In advanced stages the EL dissemination program may become re-activated in areas of lower cell density. Indeed, primary tumor and PT spheres were able to seed and to form metastases, although at much lower rates than EL-derived cells.

Moreover, these results suggest that although progesterone function is necessary for mammary gland morphogenesis and development, it may also provide an error prone mechanism and contribute to cancer cell growth or dissemination. The aberrant engagement of the normal physiological function of progesterone during mammary gland morphogenesis during early stages of breast cancer apparently results in fatal outcome.

The importance of these findings for the understanding of metastasis and development of adjuvant therapies is immediate: systemically spread cancer cells in the adjuvant therapy setting comprise cells that are derived from different stages of primary tumor evolution, including the earliest. DCCs from early and later stages have the potential to progress to metastasis. Therefore, therapies targeting the seed of metastasis need to address this heterogeneity.

5 Summary

Current cancer therapies generally assume cancers to progress linearly from primary to metastatic sites. The model postulates a stepwise accumulation of genetic and epigenetic alterations within the primary tumor, and therefore, primary tumors may be used as surrogate markers for disseminated cancer cells. However, this model is challenged by (i) the insufficient therapy success and (ii) the genomic disparity between disseminated cancer cells (DCCs) and their matched primary tumors when isolated at surgery. The genomic disparity suggests that metastatic dissemination may occur early during tumor formation, however the mechanisms of early metastatic spread are unknown so far.

To uncover mechanisms of early metastatic dissemination we microdissected mammary tissue from a *Her2*-driven mouse model (Balb-NeuT) of breast cancer before and after microscopic invasion and performed gene expression analysis. Identified pathways were tested in a series of *in vitro* and *in vivo* experiments. Finally, the findings were validated in a panel of human breast cancer cell lines and investigation of more than 2000 patient samples.

Gene expression profiling identified a distinct signature at the time point of maximal seeding when only pre-invasive mammary lesions could be identified. The morphology of pre-invasive lesions coincided with a transient time window of progesterone receptor (PgR) and Her2 co-expression. Upon functional testing progesterone-induced signaling triggered migration of stem-like cells from early lesions shortly after Her2 activation, but promoted proliferation in advanced primary tumor cells. The switch from migration to proliferation was regulated by elevated Her2 expression and increased cell density involving miRNA-regulated PgR down-regulation. The combined result was a differential response of cancer cells to progesterone and its paracrine-signal mediators Wnt4 and Rankl imposing stemness and migration at low and proliferation at high cellular density. Exploring human breast cancer cell lines we confirmed the observed phenotypes and mechanisms. Molecular-genetic and transcriptomic analysis of DCCs isolated from the bone marrow of breast cancer patients provided strong support for early metastatic dissemination. Finally, we identified a subtype of breast cancer mimicking the Balb-NeuT model closest.

We identify microenvironmental signaling (PgR signaling), oncogenic signaling (Her2) and cellular density as central regulators of early dissemination and metastasis. In light of the patient-derived data we suggest that (i) dissemination is mostly early and (ii) clones that evolved over time at the primary site and became pre-dominant are less able to disseminate. We predict the findings not only to be relevant for Her2-driven cancers but for many other cancers as well.

6 Bibliography

Adelaide, J., Finetti, P., Bekhouche, I., Repellini, L., Geneix, J., Sircoulomb, F., Charafe-Jauffret, E., Cervera, N., Desplans, J., Parzy, D.*, et al.* (2007). Integrated profiling of basal and luminal breast cancers. Cancer Res *67*, 11565-11575.

Aktas, B., Muller, V., Tewes, M., Zeitz, J., Kasimir-Bauer, S., Loehberg, C.R., Rack, B., Schneeweiss, A., and Fehm, T. (2011). Comparison of estrogen and progesterone receptor status of circulating tumor cells and the primary tumor in metastatic breast cancer patients. Gynecologic oncology *122*, 356-360.

Asselin-Labat, M.L., Shackleton, M., Stingl, J., Vaillant, F., Forrest, N.C., Eaves, C.J., Visvader, J.E., and Lindeman, G.J. (2006). Steroid hormone receptor status of mouse mammary stem cells. Journal of the National Cancer Institute *98*, 1011-1014.

Asselin-Labat, M.L., Vaillant, F., Sheridan, J.M., Pal, B., Wu, D., Simpson, E.R., Yasuda, H., Smyth, G.K., Martin, T.J., Lindeman, G.J.*, et al.* (2010). Control of mammary stem cell function by steroid hormone signalling. Nature *465*, 798-802.

Astolfi, A., Landuzzi, L., Nicoletti, G., De Giovanni, C., Croci, S., Palladini, A., Ferrini, S., Iezzi, M., Musiani, P., Cavallo, F.*, et al.* (2005). Gene expression analysis of immune-mediated arrest of tumorigenesis in a transgenic mouse model of HER-2/neu-positive basal-like mammary carcinoma. Am J Pathol *166*, 1205-1216.

Aupperlee, M.D., Smith, K.T., Kariagina, A., and Haslam, S.Z. (2005). Progesterone receptor isoforms A and B: temporal and spatial differences in expression during murine mammary gland development. Endocrinology *146*, 3577-3588.

Balana, M.E., Lupu, R., Labriola, L., Charreau, E.H., and Elizalde, P.V. (1999). Interactions between progestins and heregulin (HRG) signaling pathways: HRG acts as mediator of progestins proliferative effects in mouse mammary adenocarcinomas. Oncogene *18*, 6370-6379.

Balic, M., Lin, H., Young, L., Hawes, D., Giuliano, A., McNamara, G., Datar, R.H., and Cote, R.J. (2006). Most early disseminated cancer cells detected in bone marrow of breast cancer patients have a putative breast cancer stem cell phenotype. Clin Cancer Res *12*, 5615-5621.

Bartlett, A.I., Starcyznski, J., Robson, T., Maclellan, A., Campbell, F.M., van de Velde, C.J., Hasenburg, A., Markopoulos, C., Seynaeve, C., Rea, D.*, et al.* (2011). Heterogeneous HER2 gene amplification: impact on patient outcome and a clinically relevant definition. American journal of clinical pathology *136*, 266-274.

Beck, B., and Blanpain, C. (2013). Unravelling cancer stem cell potential. Nature reviews Cancer *13*, 727-738.

Beguelin, W., Diaz Flaque, M.C., Proietti, C.J., Cayrol, F., Rivas, M.A., Tkach, M., Rosemblit, C., Tocci, J.M., Charreau, E.H., Schillaci, R.*, et al.* (2010). Progesterone receptor induces ErbB-2 nuclear translocation to promote breast cancer growth via a novel transcriptional effect: ErbB-2 function as a coactivator of Stat3. Molecular and cellular biology *30*, 5456-5472.

Berx, G., and van Roy, F. (2009). Involvement of members of the cadherin superfamily in cancer. Cold Spring Harbor perspectives in biology *1*, a003129.

Blainey, P., Krzywinski, M., and Altman, N. (2014). Points of Significance: Replication. Nat Meth *11*, 879-880.

Bock, C., Rack, B., Kuhn, C., Hofmann, S., Finkenzeller, C., Jager, B., Jeschke, U., and Doisneau-Sixou, S.F. (2012). Heterogeneity of ERalpha and ErbB2 Status in Cell Lines and Circulating Tumor Cells of Metastatic Breast Cancer Patients. Translational oncology *5*, 475-485.

Boggio, K., Nicoletti, G., Di Carlo, E., Cavallo, F., Landuzzi, L., Melani, C., Giovarelli, M., Rossi, I., Nanni, P., De Giovanni, C.*, et al.* (1998). Interleukin 12-mediated prevention of

spontaneous mammary adenocarcinomas in two lines of Her-2/neu transgenic mice. J Exp Med *188*, 589-596.

Bombonati, A., and Sgroi, D.C. (2011). The molecular pathology of breast cancer progression. J Pathol *223*, 307-317.

Brabletz, T., Jung, A., Spaderna, S., Hlubek, F., and Kirchner, T. (2005). Opinion: migrating cancer stem cells - an integrated concept of malignant tumour progression. Nature reviews Cancer *5*, 744-749.

Brisken, C. (2013). Progesterone signalling in breast cancer: a neglected hormone coming into the limelight. Nature reviews Cancer *13*, 385-396.

Brisken, C., Heineman, A., Chavarria, T., Elenbaas, B., Tan, J., Dey, S.K., McMahon, J.A., McMahon, A.P., and Weinberg, R.A. (2000). Essential function of Wnt-4 in mammary gland development downstream of progesterone signaling. Genes & development *14*, 650-654.

Brisken, C., and O'Malley, B. (2010). Hormone action in the mammary gland. Cold Spring Harbor perspectives in biology *2*, a003178.

Cavallaro, U., and Christofori, G. (2004). Cell adhesion and signalling by cadherins and Ig-CAMs in cancer. Nature reviews Cancer *4*, 118-132.

Chaffer, C.L., and Weinberg, R.A. (2011). A perspective on cancer cell metastasis. Science (New York, NY) *331*, 1559-1564.

Chiang, A.C., and Massague, J. (2008). Molecular basis of metastasis. N Engl J Med *359*, 2814-2823.

Chugh, P., and Dittmer, D.P. (2012). Potential pitfalls in microRNA profiling. Wiley interdisciplinary reviews RNA *3*, 601-616.

Ciarloni, L., Mallepell, S., and Brisken, C. (2007). Amphiregulin is an essential mediator of estrogen receptor alpha function in mammary gland development. Proc Natl Acad Sci U S A *104*, 5455-5460.

Clarke, M.F., and Fuller, M. (2006). Stem cells and cancer: two faces of eve. Cell *124*, 1111-1115.

Debnath, J., Muthuswamy, S.K., and Brugge, J.S. (2003). Morphogenesis and oncogenesis of MCF-10A mammary epithelial acini grown in three-dimensional basement membrane cultures. Methods (San Diego, Calif) *30*, 256-268.

Dueck, A., Eichner, A., Sixt, M., and Meister, G. (2014). A miR-155-dependent microRNA hierarchy in dendritic cell maturation and macrophage activation. FEBS letters *588*, 632-640.

Evdokimova, V., Tognon, C., Ng, T., and Sorensen, P.H. (2009). Reduced proliferation and enhanced migration: two sides of the same coin? Molecular mechanisms of metastatic progression by YB-1. Cell Cycle *8*, 2901-2906.

Fehm, T., Braun, S., Muller, V., Janni, W., Gebauer, G., Marth, C., Schindlbeck, C., Wallwiener, D., Borgen, E., Naume, B.*, et al.* (2006). A concept for the standardized detection of disseminated tumor cells in bone marrow from patients with primary breast cancer and its clinical implementation. Cancer *107*, 885-892.

Fehm, T., Hoffmann, O., Aktas, B., Becker, S., Solomayer, E.F., Wallwiener, D., Kimmig, R., and Kasimir-Bauer, S. (2009). Detection and characterization of circulating tumor cells in blood of primary breast cancer patients by RT-PCR and comparison to status of bone marrow disseminated cells. Breast Cancer Res *11*, R59.

Fehm, T., Muller, V., Aktas, B., Janni, W., Schneeweiss, A., Stickeler, E., Lattrich, C., Lohberg, C.R., Solomayer, E., Rack, B.*, et al.* (2010). HER2 status of circulating tumor cells in patients with metastatic breast cancer: a prospective, multicenter trial. Breast cancer research and treatment *124*, 403-412.

Fernandez-Valdivia, R., Mukherjee, A., Mulac-Jericevic, B., Conneely, O.M., DeMayo, F.J., Amato, P., and Lydon, J.P. (2005). Revealing progesterone's role in uterine and mammary gland biology: insights from the mouse. Seminars in reproductive medicine *23*, 22-37.

Fidler, I.J. (2003). The pathogenesis of cancer metastasis: the 'seed and soil' hypothesis revisited. Nature reviews Cancer *3*, 453-458.

Fredholm, H., Eaker, S., Frisell, J., Holmberg, L., Fredriksson, I., and Lindman, H. (2009). Breast cancer in young women: poor survival despite intensive treatment. PloS one *4*, e7695.

Friedl, P., and Alexander, S. (2011). Cancer invasion and the microenvironment: plasticity and reciprocity. Cell *147*, 992-1009.

Friedl, P., and Wolf, K. (2003). Tumour-cell invasion and migration: diversity and escape mechanisms. Nature reviews Cancer *3*, 362-374.

Ghajar, C.M., and Bissell, M.J. (2008). Extracellular matrix control of mammary gland morphogenesis and tumorigenesis: insights from imaging. Histochemistry and cell biology *130*, 1105-1118.

Giese, A., Loo, M.A., Tran, N., Haskett, D., Coons, S.W., and Berens, M.E. (1996). Dichotomy of astrocytoma migration and proliferation. International journal of cancer Journal international du cancer *67*, 275-282.

Ginestier, C., Hur, M.H., Charafe-Jauffret, E., Monville, F., Dutcher, J., Brown, M., Jacquemier, J., Viens, P., Kleer, C.G., Liu, S.*, et al.* (2007). ALDH1 is a marker of normal and malignant human mammary stem cells and a predictor of poor clinical outcome. Cell stem cell *1*, 555-567.

Grange, C., Lanzardo, S., Cavallo, F., Camussi, G., and Bussolati, B. (2008). Sca-1 identifies the tumor-initiating cells in mammary tumors of BALB-neuT transgenic mice. Neoplasia *10*, 1433-1443.

Gupta, P.B., Onder, T.T., Jiang, G., Tao, K., Kuperwasser, C., Weinberg, R.A., and Lander, E.S. (2009). Identification of selective inhibitors of cancer stem cells by high-throughput screening. Cell *138*, 645-659.

Guzvic, M., Braun, B., Ganzer, R., Burger, M., Nerlich, M., Winkler, S., Werner-Klein, M., Czyz, Z.T., Polzer, B., and Klein, C.A. (2014). Combined genome and transcriptome analysis of single disseminated cancer cells from bone marrow of prostate cancer patients reveals unexpected transcriptomes. Cancer Res *74*, 7383-7394.

Hanahan, D., and Weinberg, R.A. (2011). Hallmarks of cancer: the next generation. Cell *144*, 646-674.

Hartmann, C.H., and Klein, C.A. (2006). Gene expression profiling of single cells on large-scale oligonucleotide arrays. Nucleic Acids Res *34*, e143.

Herschkowitz, J.I., Simin, K., Weigman, V.J., Mikaelian, I., Usary, J., Hu, Z., Rasmussen, K.E., Jones, L.P., Assefnia, S., Chandrasekharan, S.*, et al.* (2007). Identification of conserved gene expression features between murine mammary carcinoma models and human breast tumors. Genome biology *8*, R76.

Hoek, K.S., Eichhoff, O.M., Schlegel, N.C., Dobbeling, U., Kobert, N., Schaerer, L., Hemmi, S., and Dummer, R. (2008). In vivo switching of human melanoma cells between proliferative and invasive states. Cancer Res *68*, 650-656.

Hüsemann, Y., Geigl, J.B., Schubert, F., Musiani, P., Meyer, M., Burghart, E., Forni, G., Eils, R., Fehm, T., Riethmüller, G.*, et al.* (2008). Systemic spread is an early step in breast cancer. Cancer Cell *13*, 58-68.

Hutchinson, J.N., Jin, J., Cardiff, R.D., Woodgett, J.R., and Muller, W.J. (2004). Activation of Akt-1 (PKB-alpha) can accelerate ErbB-2-mediated mammary tumorigenesis but suppresses tumor invasion. Cancer Res *64*, 3171-3178.

Hynes, R.O. (2002). Integrins: bidirectional, allosteric signaling machines. Cell *110*, 673-687.

Ignatiadis, M., Rothe, F., Chaboteaux, C., Durbecq, V., Rouas, G., Criscitiello, C., Metallo, J., Kheddoumi, N., Singhal, S.K., Michiels, S.*, et al.* (2011). HER2-positive circulating tumor cells in breast cancer. PloS one *6*, e15624.

Imitola, J., Raddassi, K., Park, K.I., Mueller, F.J., Nieto, M., Teng, Y.D., Frenkel, D., Li, J., Sidman, R.L., Walsh, C.A.*, et al.* (2004). Directed migration of neural stem cells to sites of CNS injury by the stromal cell-derived factor 1alpha/CXC chemokine receptor 4 pathway. Proc Natl Acad Sci U S A *101*, 18117-18122.

Inman, J.L., Robertson, C., Mott, J.D., and Bissell, M.J. (2015). Mammary gland development: cell fate specification, stem cells and the microenvironment. Development (Cambridge, England) *142*, 1028-1042.

Ismail, P.M., Amato, P., Soyal, S.M., DeMayo, F.J., Conneely, O.M., O'Malley, B.W., and Lydon, J.P. (2003). Progesterone involvement in breast development and tumorigenesis--as revealed by progesterone receptor "knockout" and "knockin" mouse models. Steroids *68*, 779-787.

Ismail, P.M., Li, J., DeMayo, F.J., O'Malley, B.W., and Lydon, J.P. (2002). A novel LacZ reporter mouse reveals complex regulation of the progesterone receptor promoter during mammary gland development. Molecular endocrinology (Baltimore, Md) *16*, 2475-2489.

Ithimakin, S., Day, K.C., Malik, F., Zen, Q., Dawsey, S.J., Bersano-Begey, T.F., Quraishi, A.A., Ignatoski, K.W., Daignault, S., Davis, A.*, et al.* (2013). HER2 drives luminal breast cancer stem cells in the absence of HER2 amplification: implications for efficacy of adjuvant trastuzumab. Cancer Res *73*, 1635-1646.

Jenkins, E.O., Deal, A.M., Anders, C.K., Prat, A., Perou, C.M., Carey, L.A., and Muss, H.B. (2014). Age-specific changes in intrinsic breast cancer subtypes: a focus on older women. Oncologist *19*, 1076-1083.

Joshi, P.A., Jackson, H.W., Beristain, A.G., Di Grappa, M.A., Mote, P.A., Clarke, C.L., Stingl, J., Waterhouse, P.D., and Khokha, R. (2010). Progesterone induces adult mammary stem cell expansion. Nature *465*, 803-807.

Joyce, J.A., and Pollard, J.W. (2009). Microenvironmental regulation of metastasis. Nature reviews Cancer *9*, 239-252.

Klein, C.A. (2008). Cancer. The metastasis cascade. Science (New York, NY) *321*, 1785-1787.

Korkaya, H., Paulson, A., Iovino, F., and Wicha, M.S. (2008). HER2 regulates the mammary stem/progenitor cell population driving tumorigenesis and invasion. Oncogene *27*, 6120-6130.

Kurian, A.W., Fish, K., Shema, S.J., and Clarke, C.A. (2010). Lifetime risks of specific breast cancer subtypes among women in four racial/ethnic groups. Breast Cancer Res *12*, R99.

Labriola, L., Salatino, M., Proietti, C.J., Pecci, A., Coso, O.A., Kornblihtt, A.R., Charreau, E.H., and Elizalde, P.V. (2003). Heregulin induces transcriptional activation of the progesterone receptor by a mechanism that requires functional ErbB-2 and mitogen-activated protein kinase activation in breast cancer cells. Molecular and cellular biology *23*, 1095-1111.

Lawson, J.C., Blatch, G.L., and Edkins, A.L. (2009). Cancer stem cells in breast cancer and metastasis. Breast cancer research and treatment *118*, 241-254.

Liao, M.J., Zhang, C.C., Zhou, B., Zimonjic, D.B., Mani, S.A., Kaba, M., Gifford, A., Reinhardt, F., Popescu, N.C., Guo, W.*, et al.* (2007). Enrichment of a population of mammary gland cells that form mammospheres and have in vivo repopulating activity. Cancer Res *67*, 8131-8138.

Liu, H., Radisky, D.C., Yang, D., Xu, R., Radisky, E.S., Bissell, M.J., and Bishop, J.M. (2012). MYC suppresses cancer metastasis by direct transcriptional silencing of alphav and beta3 integrin subunits. Nature cell biology *14*, 567-574.

Liu, M., Sakamaki, T., Casimiro, M.C., Willmarth, N.E., Quong, A.A., Ju, X., Ojeifo, J., Jiao, X., Yeow, W.S., Katiyar, S.*, et al.* (2010a). The canonical NF-kappaB pathway governs mammary tumorigenesis in transgenic mice and tumor stem cell expansion. Cancer Res *70*, 10464-10473.

Liu, S., Chia, S.K., Mehl, E., Leung, S., Rajput, A., Cheang, M.C., and Nielsen, T.O. (2010b). Progesterone receptor is a significant factor associated with clinical outcomes and effect of adjuvant tamoxifen therapy in breast cancer patients. Breast cancer research and treatment *119*, 53-61.

Lucchini, F., Sacco, M.G., Hu, N., Villa, A., Brown, J., Cesano, L., Mangiarini, L., Rindi, G., Kindl, S., Sessa, F.*, et al.* (1992). Early and multifocal tumors in breast, salivary, harderian and epididymal tissues developed in MMTY-Neu transgenic mice. Cancer letters *64*, 203-209.

Mani, S.A., Guo, W., Liao, M.J., Eaton, E.N., Ayyanan, A., Zhou, A.Y., Brooks, M., Reinhard, F., Zhang, C.C., Shipitsin, M.*, et al.* (2008). The epithelial-mesenchymal transition generates cells with properties of stem cells. Cell *133*, 704-715.

May, C.D., Sphyris, N., Evans, K.W., Werden, S.J., Guo, W., and Mani, S.A. (2011). Epithelial-mesenchymal transition and cancer stem cells: a dangerously dynamic duo in breast cancer progression. Breast Cancer Res *13*, 202.

McGuire, A., Brown, J.A., Malone, C., McLaughlin, R., and Kerin, M.J. (2015). Effects of age on the detection and management of breast cancer. Cancers *7*, 908-929.

Micalizzi, D.S., Farabaugh, S.M., and Ford, H.L. (2010). Epithelial-mesenchymal transition in cancer: parallels between normal development and tumor progression. Journal of mammary gland biology and neoplasia *15*, 117-134.

Mimura, K., Kono, K., Hanawa, M., Mitsui, F., Sugai, H., Miyagawa, N., Ooi, A., and Fujii, H. (2005). Frequencies of HER-2/neu expression and gene amplification in patients with oesophageal squamous cell carcinoma. Br J Cancer *92*, 1253-1260.

Mohammed, H., Russell, I.A., Stark, R., Rueda, O.M., Hickey, T.E., Tarulli, G.A., Serandour, A.A., Birrell, S.N., Bruna, A., Saadi, A.*, et al.* (2015). Progesterone receptor modulates ERalpha action in breast cancer. Nature *523*, 313-317.

Moody, S.E., Sarkisian, C.J., Hahn, K.T., Gunther, E.J., Pickup, S., Dugan, K.D., Innocent, N., Cardiff, R.D., Schnall, M.D., and Chodosh, L.A. (2002). Conditional activation of Neu in the mammary epithelium of transgenic mice results in reversible pulmonary metastasis. Cancer Cell *2*, 451-461.

Mori, M., Triboulet, R., Mohseni, M., Schlegelmilch, K., Shrestha, K., Camargo, F.D., and Gregory, R.I. (2014). Hippo signaling regulates microprocessor and links cell-density-dependent miRNA biogenesis to cancer. Cell *156*, 893-906.

Morrison, C., Zanagnolo, V., Ramirez, N., Cohn, D.E., Kelbick, N., Copeland, L., Maxwell, G.L., and Fowler, J.M. (2006). HER-2 is an independent prognostic factor in endometrial cancer: association with outcome in a large cohort of surgically staged patients. J Clin Oncol *24*, 2376-2385.

Morton, C.I., Hlatky, L., Hahnfeldt, P., and Enderling, H. (2011). Non-stem cancer cell kinetics modulate solid tumor progression. Theoretical biology & medical modelling *8*, 48.

Mukherjee, A., Soyal, S.M., Li, J., Ying, Y., He, B., DeMayo, F.J., and Lydon, J.P. (2010). Targeting RANKL to a specific subset of murine mammary epithelial cells induces ordered branching morphogenesis and alveologenesis in the absence of progesterone receptor expression. Faseb j *24*, 4408-4419.

Mulac-Jericevic, B., Lydon, J.P., DeMayo, F.J., and Conneely, O.M. (2003). Defective mammary gland morphogenesis in mice lacking the progesterone receptor B isoform. Proc Natl Acad Sci U S A *100*, 9744-9749.

Muller, W.J., Sinn, E., Pattengale, P.K., Wallace, R., and Leder, P. (1988). Single-step induction of mammary adenocarcinoma in transgenic mice bearing the activated c-neu oncogene. Cell *54*, 105-115.

Muschler, J., and Streuli, C.H. (2010). Cell-matrix interactions in mammary gland development and breast cancer. Cold Spring Harbor perspectives in biology *2*, a003202.

Narod, S.A., Iqbal, J., Giannakeas, V., Sopik, V., and Sun, P. (2015). Breast Cancer Mortality After a Diagnosis of Ductal Carcinoma In Situ. JAMA oncology *1*, 888-896.

Nieto, M.A. (2013). Epithelial plasticity: a common theme in embryonic and cancer cells. Science (New York, NY) *342*, 1234850.

Obr, A.E., and Edwards, D.P. (2012). The biology of progesterone receptor in the normal mammary gland and in breast cancer. Molecular and cellular endocrinology *357*, 4-17.

Palmer, N.P., Schmid, P.R., Berger, B., and Kohane, I.S. (2012). A gene expression profile of stem cell pluripotentiality and differentiation is conserved across diverse solid and hematopoietic cancers. Genome biology *13*, R71.

Petti, L.M., and Ray, F.A. (2000). Transformation of mortal human fibroblasts and activation of a growth inhibitory pathway by the bovine papillomavirus E5 oncoprotein. Cell growth & differentiation : the molecular biology journal of the American Association for Cancer Research *11*, 395-408.

Pike, M.C., Krailo, M.D., Henderson, B.E., Casagrande, J.T., and Hoel, D.G. (1983). 'Hormonal' risk factors, 'breast tissue age' and the age-incidence of breast cancer. Nature *303*, 767-770.

Poleszczuk, J., Hahnfeldt, P., and Enderling, H. (2015). Evolution and phenotypic selection of cancer stem cells. PLoS computational biology *11*, e1004025.

Polyak, K., and Weinberg, R.A. (2009). Transitions between epithelial and mesenchymal states: acquisition of malignant and stem cell traits. Nature reviews Cancer *9*, 265-273.

Powis, K.M., and Shapiro, R.L. (2015). Protease inhibitors and adverse birth outcomes: is progesterone the missing piece to the puzzle? The Journal of infectious diseases *211*, 4-7.

Récamier, J.C. (1829). Recherches sur le traitement du cancer sur la compression methodique simple ou combinee et sur l'histoire generale de la meme maladie. .

Robert, N., Leyland-Jones, B., Asmar, L., Belt, R., Ilegbodu, D., Loesch, D., Raju, R., Valentine, E., Sayre, R., Cobleigh, M.*, et al.* (2006). Randomized phase III study of trastuzumab, paclitaxel, and carboplatin compared with trastuzumab and paclitaxel in women with HER-2-overexpressing metastatic breast cancer. J Clin Oncol *24*, 2786-2792.

Russo, I.H., and Russo, J. (2011). Pregnancy-induced changes in breast cancer risk. Journal of mammary gland biology and neoplasia *16*, 221-233.

Sadler, N.M., Harris, B.R., Metzger, B.A., and Kirshner, J. (2013). N-cadherin impedes proliferation of the multiple myeloma cancer stem cells. American journal of blood research *3*, 271-285.

Sansom, O.J., Meniel, V., Wilkins, J.A., Cole, A.M., Oien, K.A., Marsh, V., Jamieson, T.J., Guerra, C., Ashton, G.H., Barbacid, M.*, et al.* (2006). Loss of Apc allows phenotypic manifestation of the transforming properties of an endogenous K-ras oncogene in vivo. Proc Natl Acad Sci U S A *103*, 14122-14127.

Scadden, D.T. (2006). The stem-cell niche as an entity of action. Nature *441*, 1075-1079.

Schechter, A.L., Stern, D.F., Vaidyanathan, L., Decker, S.J., Drebin, J.A., Greene, M.I., and Weinberg, R.A. (1984). The neu oncogene: an erb-B-related gene encoding a 185,000-Mr tumour antigen. Nature *312*, 513-516.

Schedin, P. (2006). Pregnancy-associated breast cancer and metastasis. Nature reviews Cancer *6*, 281-291.

Schramek, D., Leibbrandt, A., Sigl, V., Kenner, L., Pospisilik, J.A., Lee, H.J., Hanada, R., Joshi, P.A., Aliprantis, A., Glimcher, L.*, et al.* (2010). Osteoclast differentiation factor RANKL controls development of progestin-driven mammary cancer. Nature *468*, 98-102.

Seol, H., Lee, H.J., Choi, Y., Lee, H.E., Kim, Y.J., Kim, J.H., Kang, E., Kim, S.W., and Park, S.Y. (2012). Intratumoral heterogeneity of HER2 gene amplification in breast cancer: its clinicopathological significance. Mod Pathol *25*, 938-948.

Shehata, M., Teschendorff, A., Sharp, G., Novcic, N., Russell, I.A., Avril, S., Prater, M., Eirew, P., Caldas, C., Watson, C.J.*, et al.* (2012). Phenotypic and functional characterisation of the luminal cell hierarchy of the mammary gland. Breast cancer research : BCR *14*, R134-R134.

Sherwood, D.R. (2006). Cell invasion through basement membranes: an anchor of understanding. Trends Cell Biol *16*, 250-256.

Sinn, E., Muller, W., Pattengale, P., Tepler, I., Wallace, R., and Leder, P. (1987). Coexpression of MMTV/v-Ha-ras and MMTV/c-myc genes in transgenic mice: synergistic action of oncogenes in vivo. Cell *49*, 465-475.

Slamon, D.J., Clark, G.M., Wong, S.G., Levin, W.J., Ullrich, A., and McGuire, W.L. (1987). Human breast cancer: correlation of relapse and survival with amplification of the HER-2/neu oncogene. Science (New York, NY) *235*, 177-182.

Slamon, D.J., Godolphin, W., Jones, L.A., Holt, J.A., Wong, S.G., Keith, D.E., Levin, W.J., Stuart, S.G., Udove, J., Ullrich, A.*, et al.* (1989). Studies of the HER-2/neu proto-oncogene in human breast and ovarian cancer. Science (New York, NY) *244*, 707-712.

Sternlicht, M.D. (2005). Key stages in mammary gland development: The cues that regulate ductal branching morphogenesis. Breast Cancer Research *8*, 1-11.

Stoecklein, N.H., Hosch, S.B., Bezler, M., Stern, F., Hartmann, C.H., Vay, C., Siegmund, A., Scheunemann, P., Schurr, P., Knoefel, W.T.*, et al.* (2008). Direct genetic analysis of single disseminated cancer cells for prediction of outcome and therapy selection in esophageal cancer. Cancer Cell *13*, 441-453.

Svensson, S., Nilsson, K., Ringberg, A., and Landberg, G. (2003). Invade or proliferate? Two contrasting events in malignant behavior governed by p16(INK4a) and an intact Rb pathway illustrated by a model system of basal cell carcinoma. Cancer Res *63*, 1737-1742.

Talmadge, J.E., and Fidler, I.J. (2010). AACR centennial series: the biology of cancer metastasis: historical perspective. Cancer Res *70*, 5649-5669.

Thery, C., Amigorena, S., Raposo, G., and Clayton, A. (2006). Isolation and characterization of exosomes from cell culture supernatants and biological fluids. Current protocols in cell biology / editorial board, Juan S Bonifacino [et al] *Chapter 3*, Unit 3.22.

Tjokrowidjaja, A., Lee, C.K., Houssami, N., and Lord, S. (2014). Metastatic breast cancer in young women: a population-based cohort study to describe risk and prognosis. Internal medicine journal *44*, 764-770.

Ursini-Siegel, J., Schade, B., Cardiff, R.D., and Muller, W.J. (2007). Insights from transgenic mouse models of ERBB2-induced breast cancer. Nature reviews Cancer *7*, 389-397.

Valastyan, S., and Weinberg, R.A. (2011). Tumor metastasis: molecular insights and evolving paradigms. Cell *147*, 275-292.

van de Wouw, A.J., Janssen-Heijnen, M.L., Coebergh, J.W., and Hillen, H.F. (2002). Epidemiology of unknown primary tumours; incidence and population-based survival of 1285 patients in Southeast Netherlands, 1984-1992. Eur J Cancer *38*, 409-413.

van Rooij, E. (2011). The art of microRNA research. Circulation research *108*, 219-234.

Velasco-Velazquez, M.A., Popov, V.M., Lisanti, M.P., and Pestell, R.G. (2011). The role of breast cancer stem cells in metastasis and therapeutic implications. Am J Pathol *179*, 2-11.

Visvader, J.E., and Stingl, J. (2014). Mammary stem cells and the differentiation hierarchy: current status and perspectives. Genes & development *28*, 1143-1158.

Wang, S.C., Lien, H.C., Xia, W., Chen, I.F., Lo, H.W., Wang, Z., Ali-Seyed, M., Lee, D.F., Bartholomeusz, G., Ou-Yang, F.*, et al.* (2004). Binding at and transactivation of the COX-2 promoter by nuclear tyrosine kinase receptor ErbB-2. Cancer Cell *6*, 251-261.

Watson, C.J., and Khaled, W.T. (2008). Mammary development in the embryo and adult: a journey of morphogenesis and commitment. Development (Cambridge, England) *135*, 995-1003.

Weigelt, B., Peterse, J.L., and van 't Veer, L.J. (2005). Breast cancer metastasis: markers and models. Nature reviews Cancer *5*, 591-602.

Weng, D., Penzner, J.H., Song, B., Koido, S., Calderwood, S.K., and Gong, J. (2012). Metastasis is an early event in mouse mammary carcinomas and is associated with cells bearing stem cell markers. Breast Cancer Res *14*, R18.

Williams, C., Helguero, L., Edvardsson, K., Haldosen, L.A., and Gustafsson, J.A. (2009). Gene expression in murine mammary epithelial stem cell-like cells shows similarities to human breast cancer gene expression. Breast Cancer Res *11*, R26.

Yang, G., Cai, K.Q., Thompson-Lanza, J.A., Bast, R.C., Jr., and Liu, J. (2004). Inhibition of breast and ovarian tumor growth through multiple signaling pathways by using retrovirus-mediated small interfering RNA against Her-2/neu gene expression. The Journal of biological chemistry *279*, 4339-4345.

Yang, J., and Weinberg, R.A. (2008). Epithelial-mesenchymal transition: at the crossroads of development and tumor metastasis. Developmental cell *14*, 818-829.

Yankaskas, B.C. (2005). Epidemiology of breast cancer in young women. Breast disease *23*, 3-8.

Yano, T., Doi, T., Ohtsu, A., Boku, N., Hashizume, K., Nakanishi, M., and Ochiai, A. (2006). Comparison of HER2 gene amplification assessed by fluorescence in situ hybridization and HER2 protein expression assessed by immunohistochemistry in gastric cancer. Oncol Rep *15*, 65-71.

Zhong, J., Paul, A., Kellie, S.J., and O'Neill, G.M. (2010). Mesenchymal migration as a therapeutic target in glioblastoma. Journal of oncology *2010*, 430142.

7 Supplementary Data

7.1 Supplementary data1

List of 300 differentially expressed genes in EL which are conserved between human and mouse. Complete microarray gene expression data and analyses can be seen in the GEO data base with the accession number: GSE68683.

	Gene Symbol	Description
1	Ahnak	AHNAK nucleoprotein (desmoyokin) [Source:MarkerSymbol;Acc:MGI:1316648]
2	BC035947	cDNA sequence BC035947 [Source:MarkerSymbol;Acc:MGI:2652858]
3	4632404H22Rik	RIKEN cDNA 4632404H22 gene [Source:MarkerSymbol;Acc:MGI:1926005]
4	Fgfr1op	Fgfr1 oncogene partner [Source:MarkerSymbol;Acc:MGI:1922546]
5	LOC635841	-
6	Q7TQ39_MOUSE	Gag protein. [Source:Uniprot/SPTREMBL;Acc:Q7TQ39]
7	Stac3	SH3 and cysteine rich domain 3 [Source:MarkerSymbol;Acc:MGI:3606571]
8	Mreg	melanoregulin [Source:MarkerSymbol;Acc:MGI:2151839]
9	Ptn	pleiotrophin [Source:MarkerSymbol;Acc:MGI:97804]
10	Olfr142	olfactory receptor 142 [Source:MarkerSymbol;Acc:MGI:2177525]
11	Nfatc3	nuclear factor of activated T-cells, cytoplasmic, calcineurin-dependent 3 [Source:MarkerSymbol;Acc:MGI:103296]
12	BC036313	cDNA sequence BC036313 [Source:MarkerSymbol;Acc:MGI:2448573]
13	Acox3	acyl-Coenzyme A oxidase 3, pristanoyl [Source:MarkerSymbol;Acc:MGI:1933156]
14	Zcchc11	zinc finger, CCHC domain containing 11 [Source:MarkerSymbol;Acc:MGI:2445126]
15	Msx1	homeo box, msh-like 1 [Source:MarkerSymbol;Acc:MGI:97168]
16	2310047C04Rik	RIKEN cDNA 2310047C04 gene [Source:MarkerSymbol;Acc:MGI:1917433]
17	LOC635264	-
18	Angptl4	angiopoietin-like 4 [Source:MarkerSymbol;Acc:MGI:1888999]
19	Q78E13_MOUSE	RNA for type IIB intracisternal A-particle (IAP) element encoding integrase, clone 111. (Fragment). [Source:Uniprot/SPTREMBL;Acc:Q78E13]
20	Hapln1	hyaluronan and proteoglycan link protein 1 [Source:MarkerSymbol;Acc:MGI:1337006]
21	Baz2a	bromodomain adjacent to zinc finger domain, 2A [Source:MarkerSymbol;Acc:MGI:2151152]
22	Pstpip1	proline-serine-threonine phosphatase-interacting protein 1 [Source:MarkerSymbol;Acc:MGI:1321396]
23	CN716893	expressed sequence CN716893 [Source:MarkerSymbol;Acc:MGI:3584456]
24	Tnnt1	troponin T1, skeletal, slow [Source:MarkerSymbol;Acc:MGI:1333868]
25	C330007P06Rik	RIKEN cDNA C330007P06 gene [Source:MarkerSymbol;Acc:MGI:1924894]

26	Nox4	NADPH oxidase 4 [Source:MarkerSymbol;Acc:MGI:1354184]
27	Dclre1c	DNA cross-link repair 1C, PSO2 homolog (S. cerevisiae) [Source:MarkerSymbol;Acc:MGI:2441769]
28	6530418L21Rik	RIKEN cDNA 6530418L21 gene [Source:MarkerSymbol;Acc:MGI:1923497]
29	Ankrd26	ankyrin repeat domain 26 [Source:MarkerSymbol;Acc:MGI:1917887]
30	Dcn	decorin [Source:MarkerSymbol;Acc:MGI:94872]
31	Pard3b	par-3 partitioning defective 3 homolog B (C. elegans) [Source:MarkerSymbol;Acc:MGI:1919301]
32	Adam22	a disintegrin and metallopeptidase domain 22 [Source:MarkerSymbol;Acc:MGI:1340046]
33	BC013712	cDNA sequence BC013712 [Source:MarkerSymbol;Acc:MGI:2446213]
34	Ly6d	lymphocyte antigen 6 complex, locus D [Source:MarkerSymbol;Acc:MGI:96881]
35	LOC635297	-
36	Tnpo2	transportin 2 (importin 3, karyopherin beta 2b) [Source:MarkerSymbol;Acc:MGI:2384849]
37	BC053393	cDNA sequence BC053393 [Source:MarkerSymbol;Acc:MGI:3039605]
38	Hist2h3c2	histone cluster 2, H3c2 [Source:MarkerSymbol;Acc:MGI:2448357]
39	Utp14a	UTP14, U3 small nucleolar ribonucleoprotein, homolog A (yeast) [Source:MarkerSymbol;Acc:MGI:1919804]
40	Rhbdd1	rhomboid domain containing 1 [Source:MarkerSymbol;Acc:MGI:1924117]
41	Nup54	nucleoporin 54 [Source:MarkerSymbol;Acc:MGI:1920460]
42	Hs3st2	heparan sulfate (glucosamine) 3-O-sulfotransferase 2 [Source:MarkerSymbol;Acc:MGI:1333802]
43	Vsx1	visual system homeobox 1 homolog (zebrafish) [Source:MarkerSymbol;Acc:MGI:1890816]
44	Defb3	defensin beta 3 [Source:MarkerSymbol;Acc:MGI:1351612]
45	Kcng1	-
46	Asb8	ankyrin repeat and SOCS box-containing protein 8 [Source:MarkerSymbol;Acc:MGI:1925791]
47	Mug4	murinoglobulin 4 [Source:MarkerSymbol;Acc:MGI:101843]
48	Olfr323	olfactory receptor 323 [Source:MarkerSymbol;Acc:MGI:3030157]
49	BC050196	cDNA sequence BC050196 [Source:MarkerSymbol;Acc:MGI:2687329]
50	2810021B07Rik	RIKEN cDNA 2810021B07 gene [Source:MarkerSymbol;Acc:MGI:1913558]
51	4930535B03Rik	RIKEN cDNA 4930535B03 gene [Source:MarkerSymbol;Acc:MGI:1922387]
52	5730593F17Rik	RIKEN cDNA 5730593F17 gene [Source:MarkerSymbol;Acc:MGI:2144564]
53	Mast3	microtubule associated serine/threonine kinase 3 [Source:MarkerSymbol;Acc:MGI:2683541]
54	Col6a2	procollagen, type VI, alpha 2 [Source:MarkerSymbol;Acc:MGI:88460]
55	Galr3	galanin receptor 3 [Source:MarkerSymbol;Acc:MGI:1329003]
56	EG234159	-
57	Rab38	Rab38, member of RAS oncogene family [Source:MarkerSymbol;Acc:MGI:1919683]
58	Pdk1	pyruvate dehydrogenase kinase, isoenzyme 1 [Source:MarkerSymbol;Acc:MGI:1926119]

59	Smc2	structural maintenance of chromosomes 2 [Source:MarkerSymbol;Acc:MGI:106067]
60	1810022C23Rik	RIKEN cDNA 1810022C23 gene [Source:MarkerSymbol;Acc:MGI:1916373]
61	Ptges	prostaglandin E synthase [Source:MarkerSymbol;Acc:MGI:1927593]
62	Prickle2	prickle-like 2 (Drosophila) [Source:MarkerSymbol;Acc:MGI:1925144]
63	Gcap14	granule cell antiserum positive 14 [Source:MarkerSymbol;Acc:MGI:101859]
64	Atp10d	ATPase, Class V, type 10D [Source:MarkerSymbol;Acc:MGI:2450125]
65	Tmem43	transmembrane protein 43 [Source:MarkerSymbol;Acc:MGI:1921372]
66	4930534B04Rik	RIKEN cDNA 4930534B04 gene [Source:MarkerSymbol;Acc:MGI:1922466]
67	Nr3c2	nuclear receptor subfamily 3, group C, member 2 [Source:MarkerSymbol;Acc:MGI:99459]
68	Arrdc3	arrestin domain containing 3 [Source:MarkerSymbol;Acc:MGI:2145242]
69	Mal	myelin and lymphocyte protein, T-cell differentiation protein [Source:MarkerSymbol;Acc:MGI:892970]
70	BC107364	cDNA sequence BC107364 [Source:MarkerSymbol;Acc:MGI:3618860]
71	Topbp1	topoisomerase (DNA) II beta binding protein [Source:MarkerSymbol;Acc:MGI:1920018]
72	4930511J11Rik	RIKEN cDNA 4930511J11 gene [Source:MarkerSymbol;Acc:MGI:1921970]
73	Olfr179	olfactory receptor 179 [Source:MarkerSymbol;Acc:MGI:3030013]
74	Q8C1Z1_MOUSE	Colon RCB-0549 Cle-H3 cDNA, RIKEN full-length enriched library, clone:G430046L24 product:hypothetical protein, full insert sequence. [Source:Uniprot/SPTREMBL;Acc:Q8C1Z1]
75	Qrsl1	glutaminyl-tRNA synthase (glutamine-hydrolyzing)-like 1 [Source:MarkerSymbol;Acc:MGI:1923813]
76	Csk	c-src tyrosine kinase [Source:MarkerSymbol;Acc:MGI:88537]
77	Podxl	podocalyxin-like [Source:MarkerSymbol;Acc:MGI:1351317]
78	Arpp21	cyclic AMP-regulated phosphoprotein, 21 [Source:MarkerSymbol;Acc:MGI:107562]
79	Gm397	gene model 397, (NCBI) [Source:MarkerSymbol;Acc:MGI:2685243]
80	Prkag3	protein kinase, AMP-activated, gamma 3 non-catatlytic subunit [Source:MarkerSymbol;Acc:MGI:1891343]
81	Mbtps2	membrane-bound transcription factor peptidase, site 2 [Source:MarkerSymbol;Acc:MGI:2444506]
82	Mlh3	mutL homolog 3 (E coli) [Source:MarkerSymbol;Acc:MGI:1353455]
83	Cyhr1	cysteine and histidine rich 1 [Source:MarkerSymbol;Acc:MGI:1859320]
84	2310065K24Rik	RIKEN cDNA 2310065K24 gene [Source:MarkerSymbol;Acc:MGI:1919637]
85	Fbxo43	F-box protein 43 [Source:MarkerSymbol;Acc:MGI:1926053]
86	Phgdhl1	phosphoglycerate dehydrogenase like 1 [Source:MarkerSymbol;Acc:MGI:1916139]
87	ENSMUSG00000060559	predicted gene, ENSMUSG00000060559 [Source:MarkerSymbol;Acc:MGI:3642418]
88	P2rxl1	purinergic receptor P2X-like 1, orphan receptor [Source:MarkerSymbol;Acc:MGI:1337113]
89	Olfr1361	olfactory receptor 1361 [Source:MarkerSymbol;Acc:MGI:3031195]
90	Wdr4	WD repeat domain 4 [Source:MarkerSymbol;Acc:MGI:1889002]

91	Shprh	SNF2 histone linker PHD RING helicase [Source:MarkerSymbol;Acc:MGI:1917581]
92	Sgk3	serum/glucocorticoid regulated kinase 3 [Source:MarkerSymbol;Acc:MGI:2182368]
93	6330416L07Rik	RIKEN cDNA 6330416L07 gene [Source:MarkerSymbol;Acc:MGI:2442394]
94	Defcr24	defensin related cryptdin 24 [Source:MarkerSymbol;Acc:MGI:3630383]
95	Srrm2	serine/arginine repetitive matrix 2 [Source:MarkerSymbol;Acc:MGI:1923206]
96	Pex11c	peroxisomal biogenesis factor 11c [Source:MarkerSymbol;Acc:MGI:1920905]
97	Cep290	centrosomal protein 290 [Source:MarkerSymbol;Acc:MGI:2384917]
98	Sec31b	Sec31 homolog B (S. cerevisiae) [Source:MarkerSymbol;Acc:MGI:2685187]
99	Fgd3	FYVE, RhoGEF and PH domain containing 3 [Source:MarkerSymbol;Acc:MGI:1353657]
100	1700025H01Rik	RIKEN cDNA 1700025H01 gene [Source:MarkerSymbol;Acc:MGI:1922781]
101	Dixdc1	DIX domain containing 1 [Source:MarkerSymbol;Acc:MGI:2679721]
102	Atp13a3	ATPase type 13A3 [Source:MarkerSymbol;Acc:MGI:2685387]
103	1110051M20Rik	RIKEN cDNA 1110051M20 gene [Source:MarkerSymbol;Acc:MGI:1915079]
104	Nrxn3	neurexin III [Source:MarkerSymbol;Acc:MGI:1096389]
105	Kctd9	potassium channel tetramerisation domain containing 9 [Source:MarkerSymbol;Acc:MGI:2145579]
106	D930028F11Rik	RIKEN cDNA D930028F11 gene [Source:MarkerSymbol;Acc:MGI:1924792]
107	Prkacb	protein kinase, cAMP dependent, catalytic, beta [Source:MarkerSymbol;Acc:MGI:97594]
108	Neu4	sialidase 4 [Source:MarkerSymbol;Acc:MGI:2661364]
109	Gm817	gene model 817, (NCBI) [Source:MarkerSymbol;Acc:MGI:2685663]
110	Smg6	Smg-6 homolog, nonsense mediated mRNA decay factor (C. elegans) [Source:MarkerSymbol;Acc:MGI:2144117]
111	Kif16b	kinesin family member 16B [Source:MarkerSymbol;Acc:MGI:1098240]
112	Sh3glb2	SH3-domain GRB2-like endophilin B2 [Source:MarkerSymbol;Acc:MGI:2385131]
113	Shmt1	serine hydroxymethyl transferase 1 (soluble) [Source:MarkerSymbol;Acc:MGI:98299]
114	Tram2	translocating chain-associating membrane protein 2 [Source:MarkerSymbol;Acc:MGI:1924817]
115	Nat2	N-acetyltransferase 2 (arylamine N-acetyltransferase) [Source:MarkerSymbol;Acc:MGI:109201]
116	Fmn2	formin 2 [Source:MarkerSymbol;Acc:MGI:1859252]
117	4930486L24Rik	RIKEN cDNA 4930486L24 gene [Source:MarkerSymbol;Acc:MGI:1922258]
118	Ttc13	tetratricopeptide repeat domain 13 [Source:MarkerSymbol;Acc:MGI:2384573]
119	Asb11	ankyrin repeat and SOCS box-containing protein 11 [Source:MarkerSymbol;Acc:MGI:1916104]
120	Tnfrsf22	tumor necrosis factor receptor superfamily, member 22 [Source:MarkerSymbol;Acc:MGI:1930270]

121	Cdh16	cadherin 16 [Source:MarkerSymbol;Acc:MGI:106671]
122	V1rc15	vomeronasal 1 receptor, C15 [Source:MarkerSymbol;Acc:MGI:2159451]
123	IGKV6-17	Immunoglobulin Kappa light chain V gene segment [Source:IMGT/GENE-DB;Acc:IGKV6-17]
124	BC013672	cDNA sequence BC013672 [Source:MarkerSymbol;Acc:MGI:2384570]
125	Ccdc56	coiled-coil domain containing 56 [Source:MarkerSymbol;Acc:MGI:1098757]
126	LOC631256	-
127	Eef2	eukaryotic translation elongation factor 2 [Source:MarkerSymbol;Acc:MGI:95288]
128	Ccdc94	coiled-coil domain containing 94 [Source:MarkerSymbol;Acc:MGI:1920136]
129	Sox15	SRY-box containing gene 15 [Source:MarkerSymbol;Acc:MGI:98363]
130	Apobec3	apolipoprotein B editing complex 3 [Source:MarkerSymbol;Acc:MGI:1933111]
131	Tsr2	TSR2, 20S rRNA accumulation, homolog (S. cerevisiae) [Source:MarkerSymbol;Acc:MGI:1916749]
132	Slc12a5	solute carrier family 12, member 5 [Source:MarkerSymbol;Acc:MGI:1862037]
133	Megf11	multiple EGF-like-domains 11 [Source:MarkerSymbol;Acc:MGI:1920951]
134	Fbxw8	F-box and WD-40 domain protein 8 [Source:MarkerSymbol;Acc:MGI:1923041]
135	Dpysl3	dihydropyrimidinase-like 3 [Source:MarkerSymbol;Acc:MGI:1349762]
136	Mapkbp1	mitogen activated protein kinase binding protein 1 [Source:MarkerSymbol;Acc:MGI:1347004]
137	Cst12	cystatin 12 [Source:MarkerSymbol;Acc:MGI:1916612]
138	Hmgcs2	3-hydroxy-3-methylglutaryl-Coenzyme A synthase 2 [Source:MarkerSymbol;Acc:MGI:101939]
139	Tmem41a	transmembrane protein 41a [Source:MarkerSymbol;Acc:MGI:1913914]
140	Rdh9	retinol dehydrogenase 9 [Source:MarkerSymbol;Acc:MGI:2143528]
141	Ddx58	DEAD (Asp-Glu-Ala-Asp) box polypeptide 58 [Source:MarkerSymbol;Acc:MGI:2442858]
142	Crk	v-crk sarcoma virus CT10 oncogene homolog (avian) [Source:MarkerSymbol;Acc:MGI:88508]
143	Kcnip1	Kv channel-interacting protein 1 [Source:MarkerSymbol;Acc:MGI:1917607]
144	Mier1	mesoderm induction early response 1 homolog (Xenopus laevis [Source:MarkerSymbol;Acc:MGI:1918398]
145	Sbno2	strawberry notch homolog 2 (Drosophila) [Source:MarkerSymbol;Acc:MGI:2448490]
146	Mrpl39	mitochondrial ribosomal protein L39 [Source:MarkerSymbol;Acc:MGI:1351620]
147	Zswim6	zinc finger, SWIM domain containing 6 [Source:MarkerSymbol;Acc:MGI:1914513]
148	5033413D22Rik	RIKEN cDNA 5033413D22 gene [Source:MarkerSymbol;Acc:MGI:1923223]
149	Fpr-rs2	formyl peptide receptor, related sequence 2 [Source:MarkerSymbol;Acc:MGI:1278319]
150	Tnrc6a	trinucleotide repeat containing 6a [Source:MarkerSymbol;Acc:MGI:2385292]
151	Wnt4	wingless-related MMTV integration site 4

		[Source:MarkerSymbol;Acc:MGI:98957]
152	Galnt14	UDP-N-acetyl-alpha-D-galactosamine:polypeptide N-acetylgalactosaminyltransferase 14 [Source:MarkerSymbol;Acc:MGI:1918935]
153	A830007P12Rik	RIKEN cDNA A830007P12 gene [Source:MarkerSymbol;Acc:MGI:2442720]
154	Slc19a2	solute carrier family 19 (thiamine transporter), member 2 [Source:MarkerSymbol;Acc:MGI:1928761]
155	Il1rapl2	interleukin 1 receptor accessory protein-like 2 [Source:MarkerSymbol;Acc:MGI:1913106]
156	Olfr1247	olfactory receptor 1247 [Source:MarkerSymbol;Acc:MGI:3031081]
157	Zfp408	zinc finger protein 408 [Source:MarkerSymbol;Acc:MGI:2685857]
158	Cyb5d2	cytochrome b5 domain containing 2 [Source:MarkerSymbol;Acc:MGI:2684848]
159	ORF28	open reading frame 28 [Source:MarkerSymbol;Acc:MGI:2181053]
160	Man1a	mannosidase 1, alpha [Source:MarkerSymbol;Acc:MGI:104677]
161	Frrs1	ferric-chelate reductase 1 [Source:MarkerSymbol;Acc:MGI:108076]
162	Mtvr2	Sjogren's syndrome/scleroderma autoantigen 1 homolog (human) [Source:MarkerSymbol;Acc:MGI:1913482]
163	Pgbd1	piggyBac transposable element derived 1 [Source:MarkerSymbol;Acc:MGI:2441675]
164	Dna2l	DNA2 DNA replication helicase 2-like (yeast) [Source:MarkerSymbol;Acc:MGI:2443732]
165	Apba2bp	amyloid beta (A4) precursor protein-binding, family A, member 1 binding protein [Source:MarkerSymbol;Acc:MGI:1861721]
166	Rif1	Rap1 interacting factor 1 homolog (yeast) [Source:MarkerSymbol;Acc:MGI:1098622]
167	Cacna1a	calcium channel, voltage-dependent, P/Q type, alpha 1A subunit [Source:MarkerSymbol;Acc:MGI:109482]
168	Wbscr25	Williams Beuren syndrome chromosome region 25 (human) [Source:MarkerSymbol;Acc:MGI:1918554]
169	Zfp62	zinc finger protein 62 [Source:MarkerSymbol;Acc:MGI:99662]
170	Zfp69	zinc finger protein 69 [Source:MarkerSymbol;Acc:MGI:107794]
171	Prnd	prion protein dublet [Source:MarkerSymbol;Acc:MGI:1346999]
172	Golt1a	golgi transport 1 homolog A (S. cerevisiae) [Source:MarkerSymbol;Acc:MGI:1915588]
173	5730406M06Rik	RIKEN cDNA 5730406M06 gene [Source:MarkerSymbol;Acc:MGI:1913875]
174	Zfp454	zinc finger protein 454 [Source:MarkerSymbol;Acc:MGI:2679253]
175	Nut	nuclear protein in testis [Source:MarkerSymbol;Acc:MGI:2661384]
176	Pcbd2	pterin 4 alpha carbinolamine dehydratase/dimerization cofactor of hepatocyte nuclear factor 1 alpha (TCF1) 2 [Source:MarkerSymbol;Acc:MGI:1919812]
177	L3mbtl	l(3)mbt-like (Drosophila) [Source:MarkerSymbol;Acc:MGI:2676663]
178	Elac1	elaC homolog 1 (E. coli) [Source:MarkerSymbol;Acc:MGI:1890495]
179	Lmbrd2	LMBR1 domain containing 2 [Source:MarkerSymbol;Acc:MGI:2444173]
180	Oas1h	2'-5' oligoadenylate synthetase 1H [Source:MarkerSymbol;Acc:MGI:2180853]
181	A930038C07Rik	RIKEN cDNA A930038C07 gene [Source:MarkerSymbol;Acc:MGI:1915419]

182	Leng8	leukocyte receptor cluster (LRC) member 8 [Source:MarkerSymbol;Acc:MGI:2142195]
183	Myo9a	myosin IXa [Source:MarkerSymbol;Acc:MGI:107735]
184	Dnahc1	dynein, axonemal, heavy chain 1 [Source:MarkerSymbol;Acc:MGI:107721]
185	Xmr	Xlr-related, meiosis regulated [Source:MarkerSymbol;Acc:MGI:99543]
186	1700054O19Rik	RIKEN cDNA 1700054O19 gene [Source:MarkerSymbol;Acc:MGI:1921522]
187	LOC673755	-
188	C87436	expressed sequence C87436 [Source:MarkerSymbol;Acc:MGI:2141787]
189	Clca3	chloride channel calcium activated 3 [Source:MarkerSymbol;Acc:MGI:1346342]
190	Nlrp3	NLR family, pyrin domain containing 3 [Source:MarkerSymbol;Acc:MGI:2653833]
191	Fbf1	Fas (TNFRSF6) binding factor 1 [Source:MarkerSymbol;Acc:MGI:1922033]
192	S3-12	plasma membrane associated protein, S3-12 [Source:MarkerSymbol;Acc:MGI:1929709]
193	Snx16	sorting nexin 16 [Source:MarkerSymbol;Acc:MGI:1921968]
194	BC005537	cDNA sequence BC005537 [Source:MarkerSymbol;Acc:MGI:2441726]
195	ENSMUSG00000056606	predicted gene, ENSMUSG00000056606 [Source:MarkerSymbol;Acc:MGI:3641968]
196	2210009G21Rik	RIKEN cDNA 2210009G21 gene [Source:MarkerSymbol;Acc:MGI:1921493]
197	1700020N01Rik	RIKEN cDNA 1700020N01 gene [Source:MarkerSymbol;Acc:MGI:1914942]
198	4933431E20Rik	RIKEN cDNA 4933431E20 gene [Source:MarkerSymbol;Acc:MGI:3584041]
199	Gipr	gastric inhibitory polypeptide receptor [Source:MarkerSymbol;Acc:MGI:1352753]
200	Tm4sf4	transmembrane 4 superfamily member 4 [Source:MarkerSymbol;Acc:MGI:2385173]
201	Ankrd28	ankyrin repeat domain 28 [Source:MarkerSymbol;Acc:MGI:2145661]
202	Abcg3	ATP-binding cassette, sub-family G (WHITE), member 3 [Source:MarkerSymbol;Acc:MGI:1351624]
203	Olfr874	olfactory receptor 874 [Source:MarkerSymbol;Acc:MGI:3030708]
204	Slc9a8	solute carrier family 9 (sodium/hydrogen exchanger), member 8 [Source:MarkerSymbol;Acc:MGI:1924281]
205	Cttn	cortactin [Source:MarkerSymbol;Acc:MGI:99695]
206	Tmem97	transmembrane protein 97 [Source:MarkerSymbol;Acc:MGI:1916321]
207	AI894139	expressed sequence AI894139 [Source:MarkerSymbol;Acc:MGI:2141515]
208	Vbp1	von Hippel-Lindau binding protein 1 [Source:MarkerSymbol;Acc:MGI:1333804]
209	5133401N09Rik	RIKEN cDNA 5133401N09 gene [Source:MarkerSymbol;Acc:MGI:1922981]
210	AI836003	expressed sequence AI836003 [Source:MarkerSymbol;Acc:MGI:2146066]
211	Vegfa	vascular endothelial growth factor A [Source:MarkerSymbol;Acc:MGI:103178]
212	9230110C19Rik	RIKEN cDNA 9230110C19 gene [Source:MarkerSymbol;Acc:MGI:3045346]

213	Mcpt6	mast cell protease 6 [Source:MarkerSymbol;Acc:MGI:96942]
214	Ntn2l	netrin 2-like (chicken) [Source:MarkerSymbol;Acc:MGI:1341188]
215	Spag16	sperm associated antigen 16 [Source:MarkerSymbol;Acc:MGI:1913972]
216	Gpr92	G protein-coupled receptor 92 [Source:MarkerSymbol;Acc:MGI:2685918]
217	Pdcd11	programmed cell death protein 11 [Source:MarkerSymbol;Acc:MGI:1341788]
218	1700069B07Rik	RIKEN cDNA 1700069B07 gene [Source:MarkerSymbol;Acc:MGI:1923863]
219	Olfr1231	olfactory receptor 1231 [Source:MarkerSymbol;Acc:MGI:3031065]
220	Hlx1	H2.0-like homeo box 1 (Drosophila) [Source:MarkerSymbol;Acc:MGI:96109]
221	Itgb2l	integrin beta 2-like [Source:MarkerSymbol;Acc:MGI:1277979]
222	Mcf2l	mcf.2 transforming sequence-like [Source:MarkerSymbol;Acc:MGI:103263]
223	Cav1	caveolin, caveolae protein 1 [Source:MarkerSymbol;Acc:MGI:102709]
224	Q8CDT6_MOUSE	Adult male testis cDNA, RIKEN full-length enriched library, clone:4930415C24 product:hypothetical protein, full insert sequence. [Source:Uniprot/SPTREMBL;Acc:Q8CDT6]
225	4933436C20Rik	RIKEN cDNA 4933436C20 gene [Source:MarkerSymbol;Acc:MGI:1918546]
226	Tpcn1	two pore channel 1 [Source:MarkerSymbol;Acc:MGI:2182472]
227	Uck1	uridine-cytidine kinase 1 [Source:MarkerSymbol;Acc:MGI:98904]
228	Olfr788	olfactory receptor 788 [Source:MarkerSymbol;Acc:MGI:3030622]
229	Adam33	a disintegrin and metallopeptidase domain 33 [Source:MarkerSymbol;Acc:MGI:1341813]
230	4930528F23Rik	RIKEN cDNA 4930528F23 gene [Source:MarkerSymbol;Acc:MGI:1922428]
231	Abi2	abl-interactor 2 [Source:MarkerSymbol;Acc:MGI:106913]
232	Pax4	paired box gene 4 [Source:MarkerSymbol;Acc:MGI:97488]
233	Nod1	nucleotide-binding oligomerization domain containing 1 [Source:MarkerSymbol;Acc:MGI:1341839]
234	V2r4	vomeronasal 2, receptor, 4 [Source:MarkerSymbol;Acc:MGI:1316666]
235	Prkar2a	protein kinase, cAMP dependent regulatory, type II alpha [Source:MarkerSymbol;Acc:MGI:108025]
236	Spon1	spondin 1, (f-spondin) extracellular matrix protein [Source:MarkerSymbol;Acc:MGI:2385287]
237	EG628893	-
238	Aspn	asporin [Source:MarkerSymbol;Acc:MGI:1913945]
239	Trpm6	transient receptor potential cation channel, subfamily M, member 6 [Source:MarkerSymbol;Acc:MGI:2675603]
240	Zfp780b	zinc finger protein 780B [Source:MarkerSymbol;Acc:MGI:2444764]
241	4932438A13Rik	RIKEN cDNA 4932438A13 gene [Source:MarkerSymbol;Acc:MGI:2444631]
242	Olfr513	olfactory receptor 513 [Source:MarkerSymbol;Acc:MGI:3030347]
243	Wwc2	WW, C2 and coiled-coil domain containing 2 [Source:MarkerSymbol;Acc:MGI:1261872]
244	Ppfibp1	PTPRF interacting protein, binding protein 1 (liprin beta 1) [Source:MarkerSymbol;Acc:MGI:1914783]
245	Ela3	elastase 3, pancreatic [Source:MarkerSymbol;Acc:MGI:1915118]
246	Cdh10	cadherin 10 [Source:MarkerSymbol;Acc:MGI:107436]

247	6330569M22Rik	RIKEN cDNA 6330569M22 gene [Source:MarkerSymbol;Acc:MGI:2443884]
248	Si	silver [Source:MarkerSymbol;Acc:MGI:98301]
249	Defb40	defensin beta 40 [Source:MarkerSymbol;Acc:MGI:2672976]
250	Abhd10	abhydrolase domain containing 10 [Source:MarkerSymbol;Acc:MGI:2442422]
251	NP_808532.1	RIKEN cDNA A030013N09 gene (A030013N09Rik), mRNA [Source:RefSeq_dna;Acc:NM_177864]
252	Gsg2	germ cell-specific gene 2 [Source:MarkerSymbol;Acc:MGI:1194498]
253	Msr2	macrophage scavenger receptor 2 [Source:MarkerSymbol;Acc:MGI:1933397]
254	Olfr688	olfactory receptor 688 [Source:MarkerSymbol;Acc:MGI:3030522]
255	1700041C02Rik	RIKEN cDNA 1700041C02 gene [Source:MarkerSymbol;Acc:MGI:1920582]
256	Olfr374	olfactory receptor 374 [Source:MarkerSymbol;Acc:MGI:3030208]
257	A130090K04Rik	RIKEN cDNA A130090K04 gene [Source:MarkerSymbol;Acc:MGI:2444159]
258	Slc33a1	solute carrier family 33 (acetyl-CoA transporter), member 1 [Source:MarkerSymbol;Acc:MGI:1332247]
259	4930458L03Rik	RIKEN cDNA 4930458L03 gene [Source:MarkerSymbol;Acc:MGI:1925374]
260	Med12l	mediator of RNA polymerase II transcription, subunit 12 homolog (yeast)-like [Source:MarkerSymbol;Acc:MGI:2139916]
261	1700063H04Rik	RIKEN cDNA 1700063H04 gene [Source:MarkerSymbol;Acc:MGI:1921519]
262	Cabp2	calcium binding protein 2 [Source:MarkerSymbol;Acc:MGI:1352749]
263	Gsbs	G substrate [Source:MarkerSymbol;Acc:MGI:1333876]
264	8030423J24Rik	RIKEN cDNA 8030423J24 gene [Source:MarkerSymbol;Acc:MGI:1924416]
265	Olfr1446	olfactory receptor 1446 [Source:MarkerSymbol;Acc:MGI:3031280]
266	Ccdc93	coiled-coil domain containing 93 [Source:MarkerSymbol;Acc:MGI:1918079]
267	NP_997045.1	-
268	Nlrp4d	NLR family, pyrin domain containing 4D [Source:MarkerSymbol;Acc:MGI:3056574]
269	Sp5	trans-acting transcription factor 5 [Source:MarkerSymbol;Acc:MGI:1927715]
270	Otor	otoraplin [Source:MarkerSymbol;Acc:MGI:1888678]
271	Cnih3	cornichon homolog 3 (Drosophila) [Source:MarkerSymbol;Acc:MGI:1920228]
272	Scn1b	sodium channel, voltage-gated, type I, beta [Source:MarkerSymbol;Acc:MGI:98247]
273	Evl	Ena-vasodilator stimulated phosphoprotein [Source:MarkerSymbol;Acc:MGI:1194884]
274	Fancd2	Fanconi anemia, complementation group D2 [Source:MarkerSymbol;Acc:MGI:2448480]
275	Rsc1a1	regulatory solute carrier protein, family 1, member 1 [Source:MarkerSymbol;Acc:MGI:3526447]
276	Map2k6	mitogen activated protein kinase kinase 6 [Source:MarkerSymbol;Acc:MGI:1346870]

277	NP_780727.2	RIKEN cDNA D730040F13 gene (D730040F13Rik), mRNA [Source:RefSeq_dna;Acc:NM_175518]
278	Grlf1	glucocorticoid receptor DNA binding factor 1 [Source:MarkerSymbol;Acc:MGI:1929494]
279	Mepe	matrix extracellular phosphoglycoprotein with ASARM motif (bone) [Source:MarkerSymbol;Acc:MGI:2137384]
280	Ankhd1	ankyrin repeat and KH domain containing 1 [Source:MarkerSymbol;Acc:MGI:1921733]
281	E2f8	E2F transcription factor 8 [Source:MarkerSymbol;Acc:MGI:1922038]
282	Tmem106b	transmembrane protein 106B [Source:MarkerSymbol;Acc:MGI:1919150]
283	3222402P14Rik	RIKEN cDNA 3222402P14 gene [Source:MarkerSymbol;Acc:MGI:2442104]
284	Trpm8	transient receptor potential cation channel, subfamily M, member 8 [Source:MarkerSymbol;Acc:MGI:2181435]
285	Mga	MAX gene associated [Source:MarkerSymbol;Acc:MGI:1352483]
286	Dcst1	DC-STAMP domain containing 1 [Source:MarkerSymbol;Acc:MGI:1925022]
287	Arhgap21	Rho GTPase activating protein 21 [Source:MarkerSymbol;Acc:MGI:1918685]
288	Dgat2	diacylglycerol O-acyltransferase 2 [Source:MarkerSymbol;Acc:MGI:1915050]
289	Tmem169	transmembrane protein 169 [Source:MarkerSymbol;Acc:MGI:2442781]
290	Olfr437	olfactory receptor 437 [Source:MarkerSymbol;Acc:MGI:3030271]
291	Trpc3	transient receptor potential cation channel, subfamily C, member 3 [Source:MarkerSymbol;Acc:MGI:109526]
292	Ccdc102a	coiled-coil domain containing 102A [Source:MarkerSymbol;Acc:MGI:2686927]
293	Dtx3l	deltex 3-like (Drosophila) [Source:MarkerSymbol;Acc:MGI:2656973]
294	Rxrb	retinoid X receptor beta [Source:MarkerSymbol;Acc:MGI:98215]
295	Gna12	guanine nucleotide binding protein, alpha 12 [Source:MarkerSymbol;Acc:MGI:95767]
296	5031414D18Rik	RIKEN cDNA 5031414D18 gene [Source:MarkerSymbol;Acc:MGI:2685590]
297	V1rh12	vomeronasal 1 receptor, H12 [Source:MarkerSymbol;Acc:MGI:2159675]
298	Proz	protein Z, vitamin K-dependent plasma glycoprotein [Source:MarkerSymbol;Acc:MGI:1860488]
299	4933417A18Rik	RIKEN cDNA 4933417A18 gene [Source:MarkerSymbol;Acc:MGI:1914011]
300	Esr2	estrogen receptor 2 (beta) [Source:MarkerSymbol;Acc:MGI:109392]

7.2 Supplementary data 2

List of upregulated miRNAs secreted in exosomes and supernatant of TUBO cells compare to non-secretory miRNAs extracted from TUBO cells, exosomes from TUBO, exosome free supernatant from TUBO cells and miRNA extracted from MM3MG-Her2 cell line compare to MM3MG cells are shown respectively in 7.2.1, 7.2.2, 7.2.3 and 7.2.4 sections. Complete miRNA sequencing data and analyses can be seen in the GEO data base with the accession number: GSE68683.

7.2.1 miRNAs upregulated in TUBO

Annotation (miRBase V20; mus musculus; no mismatchess allowed)	Mean RPM$_{annot.}$	relative STDV
mmu-miR-30a-5p	147,314.4	3.4%
mmu-miR-21a-5p	81,163.2	1.6%
mmu-miR-92a-3p	67,084.8	4.3%
mmu-miR-182-5p	57,019.1	11.7%
mmu-miR-9-5p	52,488.0	2.3%
mmu-miR-143-3p	48,617.0	0.3%
mmu-miR-181a-5p	40,799.0	3.2%
mmu-let-7c-5p	32,818.3	4.2%
mmu-let-7f-5p	32,625.4	5.3%
mmu-miR-204-5p	30,492.6	1.8%
mmu-miR-148a-3p	26,058.3	7.0%
mmu-let-7i-5p	25,733.5	3.3%
mmu-miR-25-3p	23,367.2	8.4%
mmu-miR-146b-5p	20,385.7	6.3%
mmu-miR-30d-5p	19,605.8	2.3%
mmu-miR-27b-3p	19,159.4	3.3%
mmu-let-7b-5p	17,033.0	5.7%
mmu-miR-181b-5p	14,912.7	4.0%
mmu-let-7a-5p	11,467.4	6.0%
mmu-let-7g-5p	11,094.2	3.7%
mmu-miR-200a-3p	10,852.1	4.8%
mmu-miR-30e-5p	9,190.7	1.8%
mmu-miR-103-3p	8,410.6	4.3%
mmu-miR-22-3p	8,084.7	4.5%
mmu-miR-378a-3p	7,688.9	2.1%

mmu-miR-26a-5p	7,417.8	8.8%
mmu-miR-181c-5p	7,092.6	1.6%
mmu-miR-183-5p	7,081.8	4.7%
mmu-miR-200b-3p	6,593.4	6.0%
mmu-miR-93-5p	6,296.8	4.5%
mmu-miR-24-3p	5,943.9	3.7%
mmu-miR-99b-5p	5,822.0	5.5%
mmu-miR-101b-3p	5,626.4	6.1%
mmu-miR-30c-5p	5,244.0	3.8%
mmu-miR-31-5p	4,901.2	1.1%
mmu-miR-340-5p	4,606.9	12.0%
mmu-miR-16-5p	4,603.8	5.3%
mmu-miR-19b-3p	4,349.2	15.4%
mmu-miR-200c-3p	4,157.5	8.3%
mmu-let-7e-5p	3,933.2	6.8%
mmu-miR-26b-5p	3,530.7	12.0%
mmu-miR-181d-5p	3,461.7	3.5%
mmu-miR-191-5p	3,376.8	3.3%
mmu-miR-151-3p	3,093.4	7.3%
mmu-miR-222-3p	3,003.6	2.8%
mmu-miR-125b-5p	2,865.3	6.2%
mmu-miR-125a-5p	2,793.6	5.5%
mmu-miR-29a-3p	2,776.6	4.5%
mmu-miR-103-3p, mmu-miR-107-3p	2,388.1	1.4%
mmu-miR-210-3p	2,386.2	5.5%
mmu-miR-532-5p	2,359.7	3.2%
mmu-miR-30a-3p	2,275.4	9.0%
mmu-let-7d-5p	2,228.3	3.0%
mmu-miR-429-3p	2,216.9	12.0%
mmu-miR-141-3p	2,157.8	3.4%
mmu-miR-101a-3p, mmu-miR-101c	2,156.9	2.5%
mmu-miR-20a-5p	2,108.4	6.5%
mmu-miR-151-5p	2,066.2	8.9%
mmu-miR-23b-3p	1,806.6	5.9%
mmu-miR-221-3p	1,513.5	10.8%
mmu-miR-148b-3p	1,467.2	4.7%
mmu-miR-19a-3p	1,437.6	15.1%
mmu-miR-423-3p	1,375.1	1.4%
mmu-miR-140-3p	1,353.8	2.7%
mmu-miR-7a-5p	1,309.6	4.3%
mmu-miR-30c-2-3p	1,191.9	4.1%
mmu-miR-30b-5p	1,146.5	3.1%

mmu-miR-320-3p	1,068.1	10.1%
mmu-miR-27a-3p	1,022.0	3.7%

7.2.2 miRNAs upregulated in exosomes of TUBO

Annotation (miRBase V20; mus musculus; no mismatchess allowed)	Mean RPM$_{annot.}$	relative STDV
mmu-miR-30a-5p	101,037.9	24.9%
mmu-miR-21a-5p	79,956.9	24.5%
mmu-miR-182-5p	65,360.4	34.1%
mmu-let-7c-5p	60,376.5	21.0%
mmu-miR-181a-5p	53,138.5	20.1%
mmu-miR-9-5p	52,779.7	14.4%
mmu-miR-143-3p	44,145.0	3.0%
mmu-miR-25-3p	42,264.8	18.1%
mmu-let-7f-5p	40,074.9	8.8%
mmu-miR-92a-3p	36,845.4	19.2%
mmu-let-7b-5p	29,005.5	21.5%
mmu-miR-148a-3p	27,910.0	7.1%
mmu-miR-146b-5p	19,234.9	8.7%
mmu-let-7a-5p	18,578.6	22.2%
mmu-miR-204-5p	18,356.1	11.8%
mmu-miR-30d-5p	17,317.9	22.6%
mmu-miR-27b-3p	16,752.7	17.7%
mmu-let-7i-5p	15,212.6	22.6%
mmu-miR-93-5p	14,958.7	4.3%
mmu-miR-486-5p, mmu-miR-3107-5p	14,516.7	57.4%
mmu-let-7g-5p	13,193.3	11.8%
mmu-miR-181b-5p	12,524.5	7.8%
mmu-miR-183-5p	10,878.8	15.5%
mmu-miR-103-3p	9,259.9	16.1%
mmu-miR-210-3p	8,820.2	47.5%
mmu-miR-26a-5p	8,479.2	4.0%
mmu-miR-200a-3p	7,215.5	45.0%
mmu-miR-99b-5p	6,454.6	13.0%
mmu-miR-19b-3p	6,306.7	73.0%
mmu-miR-378a-3p	6,273.3	6.5%
mmu-miR-30e-5p	5,982.8	18.4%
mmu-miR-200c-3p	5,867.1	20.2%
mmu-miR-101c	5,853.4	7.0%
mmu-miR-200b-3p	5,355.2	29.4%
mmu-miR-101b-3p	5,308.3	45.2%
mmu-miR-101a-3p, mmu-miR-101c	5,088.0	39.7%
mmu-miR-26b-5p	4,777.3	4.4%

mmu-let-7e-5p	4,762.3	29.7%
mmu-miR-22-3p	4,716.3	0.8%
mmu-miR-30a-3p	4,575.7	0.8%
mmu-miR-181c-5p	4,404.1	42.2%
mmu-miR-30c-5p	4,004.1	21.0%
mmu-miR-151-3p	3,470.0	22.4%
mmu-miR-340-5p	3,014.4	22.6%
mmu-miR-140-3p	2,893.3	5.0%
mmu-miR-181d-5p	2,754.9	12.7%
mmu-miR-16-5p	2,745.3	16.1%
mmu-miR-103-3p, mmu-miR-107-3p	2,636.9	2.4%
mmu-miR-24-3p	2,415.1	11.2%
mmu-miR-19a-3p	2,233.5	66.0%
mmu-miR-221-3p	2,103.4	13.7%
mmu-miR-31-5p	2,075.3	1.3%
mmu-miR-532-5p	1,915.2	7.2%
mmu-miR-429-3p	1,879.2	13.1%
mmu-miR-191-5p	1,868.4	25.5%
mmu-miR-20a-5p	1,721.3	2.6%
mmu-miR-125a-5p	1,693.1	16.1%
mmu-miR-23b-3p	1,605.8	10.0%
mmu-miR-106b-3p	1,536.3	19.4%
mmu-miR-125b-5p	1,522.1	3.3%
mmu-miR-320-3p	1,519.7	32.6%
mmu-let-7d-5p	1,408.2	19.6%
mmu-miR-29a-3p	1,349.3	19.1%
mmu-miR-152-3p	1,168.5	5.3%
mmu-miR-151-5p	1,127.6	14.5%
mmu-miR-148b-3p	1,113.0	5.8%
mmu-miR-98-5p	1,041.1	7.6%
mmu-miR-451a	1,029.4	15.8%
mmu-miR-28a-3p	1,020.5	27.4%
mmu-miR-423-3p	1,018.0	10.7%

7.2.3 miRNAs upregulated in exosomes free supernatant

Annotation (miRBase V20; mus musculus; no mismatchess allowed)	Mean RPM$_{annot.}$	relative STDV
mmu-miR-92a-3p	258,291.5	2.3%
mmu-let-7c-5p	103,634.7	10.0%
mmu-miR-25-3p	96,367.3	32.8%
mmu-miR-204-5p	64,322.1	18.6%
mmu-let-7b-5p	62,914.1	20.6%
mmu-miR-30a-5p	37,861.5	34.7%
mmu-miR-143-3p	25,682.0	17.1%
mmu-miR-182-5p	25,516.2	44.4%
mmu-miR-148a-3p	23,133.4	38.6%
mmu-miR-30d-5p	23,078.6	6.6%
mmu-miR-99b-5p	19,835.4	16.2%
mmu-miR-151-3p	16,998.1	49.5%
mmu-miR-27b-3p	14,599.3	13.7%
mmu-miR-146b-5p	13,376.1	15.6%
mmu-miR-320-3p	11,345.1	27.1%
mmu-miR-181a-5p	11,037.6	28.0%
mmu-miR-423-5p	10,519.9	9.7%
mmu-miR-92b-3p	10,320.7	26.0%
mmu-miR-21a-5p	9,944.6	38.8%
mmu-let-7d-3p	8,498.2	15.6%
mmu-miR-328-3p	5,933.5	27.1%
mmu-miR-24-3p	5,760.0	6.5%
mmu-miR-378a-3p	4,979.8	21.4%
mmu-miR-200c-3p	4,844.9	25.2%
mmu-miR-9-5p	4,822.3	53.1%
mmu-miR-125b-5p	4,574.9	10.2%
mmu-miR-22-3p	4,541.7	12.5%
mmu-miR-486-5p, mmu-miR-3107-5p	4,369.6	56.2%
mmu-miR-181b-5p	4,313.2	25.1%
mmu-miR-204-3p	4,057.6	31.4%
mmu-miR-125a-5p	3,739.5	17.6%
mmu-miR-210-3p	3,387.3	59.3%
mmu-let-7i-5p	3,381.8	20.7%
mmu-miR-191-5p	3,375.5	6.1%
mmu-miR-532-5p	3,355.9	33.0%
mmu-miR-183-5p	3,161.7	15.8%
mmu-miR-423-3p	3,134.5	21.8%
mmu-miR-16-5p	3,079.6	12.0%

mmu-miR-200a-3p	2,861.5	39.7%
mmu-miR-103-3p, mmu-miR-107-3p	2,715.0	35.6%
mmu-miR-106b-3p	2,621.6	25.0%
mmu-miR-93-5p	2,525.1	31.0%
mmu-miR-200b-3p	2,382.0	19.4%
mmu-miR-30a-3p	2,377.9	5.6%
mmu-miR-28a-3p	2,327.5	22.7%
mmu-miR-140-3p	2,315.5	18.2%
mmu-miR-221-3p	1,927.7	49.2%
mmu-let-7g-5p	1,878.7	27.9%
mmu-let-7a-5p	1,702.2	15.6%
mmu-miR-181c-5p	1,695.4	64.1%
mmu-miR-484	1,682.1	13.0%
mmu-miR-26a-5p	1,647.5	32.0%
mmu-let-7f-5p	1,523.3	28.1%
mmu-miR-744-5p	1,492.8	27.7%
mmu-miR-30e-5p	1,403.0	32.8%
mmu-miR-429-3p	1,373.5	38.2%
mmu-miR-27b-3p, mmu-miR-27a-3p	1,234.4	22.5%
mmu-miR-23a-3p	1,211.3	56.0%
mmu-miR-339-5p	1,091.5	34.4%
mmu-miR-100-5p	1,039.2	42.3%
mmu-miR-425-5p	1,013.8	33.3%
mmu-miR-222-3p	994.9	22.4%

7.2.4 miRNAs upregulated in MM3MG v.s MM3MG-Her2

Annotation (miRBase V20; mus musculus; no mismatchess allowed)	Mg-Her2 vs. Mg		
	log2fold	p-value	Mean RPM$_{annot.}$
mmu-miR-6539	4.62608112	4.24E-05	204.8487
mmu-miR-212-3p	4.274491594	0.005134	50.9419
mmu-miR-7a-1-3p	4.138220121	9.04E-05	6.596053
mmu-miR-3061-3p	3.790244502	0.019721	5.258391
mmu-miR-7224-3p	3.718086363	0.062192	5.019148
mmu-miR-452-5p	3.521375935	0.014839	4.424576
mmu-miR-297a-5p	3.464715541	0.037902	4.267825
mmu-miR-210-5p	3.40185678	0.004171	37.8121
mmu-let-7c-1-3p	3.297099799	0.031674	21.93988
mmu-miR-196b-3p	3.2969582	0.080797	3.838237
mmu-miR-690	3.273103337	0.136218	3.781107
mmu-miR-1983	3.083593576	0.002583	15.63564
mmu-miR-7a-5p	2.943694597	0.000201	1306.558
mmu-miR-378c	2.715538135	0.095227	2.682688
mmu-miR-200c-3p	2.657471536	0.119915	6.235515
mmu-miR-155-5p	2.655630038	0.002794	136.1589
mmu-miR-3473b, mmu-miR-3473e	2.647932711	0.02839	102.4302
mmu-let-7a-2-3p	2.614982157	0.124958	5.051873
mmu-miR-344d-3-5p	2.545498483	0.008699	19.30172
mmu-miR-503-5p	2.54147329	2.17E-06	767.175
mmu-miR-92a-1-5p	2.46578573	0.000207	205.8652
mmu-miR-365-2-5p	2.313435576	0.030522	7.209907
mmu-miR-20a-5p	2.299275147	1.52E-05	2307.254
mmu-miR-16-1-3p	2.28650958	7.23E-05	83.85507
mmu-miR-125a-3p	2.273308841	0.014181	49.5699
mmu-miR-17-5p	2.266316675	0.000114	880.4865
mmu-miR-132-3p	2.256061722	1.79E-05	816.1163
mmu-miR-32-5p	2.237717635	0.067868	21.71276
mmu-miR-466b-3p, mmu-miR-466c-3p, mmu-miR-466p-3p	2.187907156	0.011651	7.510836
mmu-miR-18a-5p	2.125343722	0.000549	171.0609
mmu-miR-130b-3p	2.122259019	0.09352	17.1257
mmu-miR-466a-3p, mmu-miR-466e-3p	2.08381048	0.249185	1.857105
mmu-miR-98-3p	2.07857562	0.139045	8.912993
mmu-miR-342-5p	2.006791425	0.203736	5.886448
mmu-miR-450b-5p	2.004122807	0.000482	69.00143
mmu-miR-3066-5p	1.984634566	0.061548	15.59532
mmu-miR-3473b	1.974768892	0.048508	26.96948

mmu-miR-466d-3p	1.959831932	0.170054	3.466735
mmu-miR-1949	1.941609367	0.030431	4.828149
mmu-miR-297c-5p	1.916019507	0.258314	1.692122
mmu-miR-219a-1-3p	1.892354829	0.010959	12.78566
mmu-miR-669b-5p	1.878099512	0.176875	4.663165
mmu-miR-92a-3p	1.844125287	3.42E-05	70965.04
mmu-miR-378d	1.804588392	0.145893	2.240526
mmu-miR-25-5p	1.796506325	0.020939	13.52529
mmu-miR-1198-5p	1.784300287	4.02E-05	169.7109
mmu-miR-101a-5p	1.765769707	0.045183	3.119639
mmu-miR-99b-3p	1.760776708	0.000242	481.3809
mmu-miR-30c-2-3p	1.760757945	0.001387	149.685
mmu-miR-190a-5p	1.743930358	0.015927	17.52934
mmu-miR-3470b	1.726852158	0.143094	4.676699
mmu-miR-5099	1.584678446	0.000759	5143.971
mmu-miR-423-3p	1.572599265	9.2E-05	939.0329
mmu-miR-19b-1-5p	1.570618666	0.170527	2.32832
mmu-miR-93-5p	1.552112998	7.71E-05	3430.599
mmu-miR-8103	1.551286744	0.219176	3.920075
mmu-miR-15b-3p	1.550998968	0.03241	57.10887
mmu-miR-421-3p	1.544448889	0.020502	49.80006
mmu-let-7f-1-3p	1.528560532	0.148337	4.691335
mmu-let-7b-3p	1.523207222	0.052386	32.78266
mmu-miR-1940	1.509983154	0.174761	1.918791
mmu-miR-3470a	1.509983154	0.174761	1.918791
mmu-miR-6909-5p	1.509983154	0.174761	1.918791
mmu-miR-6952-3p	1.509983154	0.174761	1.918791
mmu-miR-21a-3p	1.503160876	0.000178	346.4298
mmu-miR-7666-3p	1.500625299	0.183028	2.245828
mmu-miR-344d-3p	1.485913518	0.013329	82.45667
mmu-miR-122-5p	1.482630667	0.289026	1.345026
mmu-miR-3058-3p	1.482630667	0.289026	1.345026
mmu-miR-466i-5p	1.482630667	0.289026	1.345026
mmu-miR-669f-3p	1.482630667	0.289026	1.345026
mmu-miR-7226-3p	1.482630667	0.289026	1.345026
mmu-miR-16-2-3p	1.471583421	0.002997	55.50337
mmu-miR-342-3p	1.459345346	0.096285	21.38055
mmu-miR-8106	1.365839664	0.172506	4.835512
mmu-miR-374b-5p, mmu-miR-374c-5p	1.356063824	0.000213	95.94959
mmu-miR-378a-5p	1.322062016	0.009582	17.476
mmu-miR-125b-1-3p	1.317253386	0.003779	454.232
mmu-miR-466a-3p, mmu-miR-466b-3p, mmu-miR-466c-3p, mmu-miR-466e-3p, mmu-miR-466p-3p	1.309680974	0.157139	6.54647

mmu-miR-374c-5p	1.276013427	0.20889	2.006585
mmu-miR-19a-3p	1.27166894	0.005896	2638.734
mmu-miR-30a-5p	1.227517313	0.000108	23128.29
mmu-miR-30a-3p	1.226770005	5.71E-05	285.4946
mmu-miR-615-5p	1.222249784	0.008006	25.09964
mmu-miR-210-3p	1.212624766	0.000217	1144.554
mmu-miR-219a-5p	1.20698337	0.195125	6.412509
mmu-miR-1291	1.189679972	0.317062	1.924093
mmu-miR-27a-5p	1.175758452	0.026276	97.59772
mmu-miR-15b-5p	1.163148336	0.001009	284.5802
mmu-miR-3082-3p	1.147621839	0.31082	3.882881
mmu-miR-148a-5p	1.118546948	0.000112	203.933
mmu-miR-30e-3p	1.116502698	0.004374	260.8848
mmu-miR-872-5p	1.115864816	0.000751	267.1922
mmu-miR-93-3p	1.11519183	0.133401	17.21911
mmu-miR-221-5p	1.091415003	0.000596	168.8836
mmu-miR-744-5p	1.090102342	0.02334	404.5584
mmu-miR-100-3p	1.08381048	0.328891	1.105783
mmu-miR-103-2-5p	1.08381048	0.328891	1.105783
mmu-miR-141-3p	1.08381048	0.328891	1.105783
mmu-miR-3102-5p	1.08381048	0.328891	2.211565
mmu-miR-429-3p	1.08381048	0.328891	1.105783
mmu-miR-466n-3p	1.08381048	0.328891	1.105783
mmu-miR-505-3p	1.08381048	0.328891	1.105783
mmu-miR-5132-5p	1.08381048	0.328891	1.105783
mmu-miR-130b-5p	1.071234426	0.212126	4.192043
mmu-miR-99a-3p	1.068339823	3.88E-05	361.3195
mmu-miR-128-1-5p	1.049854942	0.020805	10.37061
mmu-miR-378a-3p	1.046407625	2.88E-05	8418.672
mmu-miR-671-3p	1.040971392	0.024018	85.24312
mmu-miR-30e-5p	1.039290003	0.000313	7437.372
mmu-miR-10a-3p	1.035551677	0.052008	30.43866
mmu-miR-301a-5p	1.025573786	0.078221	5.712655
mmu-miR-3057-5p	1.024415599	0.026686	28.09093
mmu-miR-92b-5p	1.006014799	0.268423	5.132842
mmu-miR-17-3p	1.003328581	0.002057	110.3944
mmu-miR-7068-3p	0.999216525	0.111076	5.74735
mmu-miR-467e-5p	0.997372038	0.078978	3.618277
mmu-miR-181b-1-3p	0.997126242	0.054216	22.46717
mmu-miR-3962	0.99026086	0.340141	1.489204
mmu-miR-130a-5p	0.97340369	0.096571	17.22134
mmu-miR-30c-1-3p	0.960660809	0.151955	12.72342

7.3 Supplementary data3

All source data which used to generate graphs and statistical material are listed here for each figure independently.

7.3.1 Source data for Figure 13

Age in week	Mean number of DCC / Tumor area	S.D	Number of mice per data point
4	42.5	28.61381	3
7	48	37.62978	5
9	45	22.91288	4
11	30	2.5	2
18	2.336083	2.86053	4
22	0.390671	0.476405	5
28	0.144011	0.009985	4

7.3.2 Source data for Figure 15

	Transcript	EL	PT	Met
Ava. Fold changes over normal	AR	76.86451	1.643832	0.175492
STDV		57.6713	1.5247	0
		EL	Tumor	Meta
Ava. Fold changes over normal	Nr3c1	12.92824	2.97704	1.536018
STDV		9.592439	3.072271	1.625111
		EL	Tumor	Met
Ava. Fold changes over normal	ER-α	43.10078	49.42275	13.31518
STDV		79.96272	125.1211	0
		EL	Tumor	Meta
Ava. Fold changes over normal	Nr3C2	3.43781	1.08	1.03
STDV		2.30952	1.00214	0
		EL	Tumor	Met
Ava. Fold changes over normal	ER-β	166.5792	16.44682	8.033571
STDV		87.79785	14.87284	4.275056
		EL	Tumor	Meta
Ava. Fold changes over normal	PgR A&B	3.375428	0	0
STDV		2.775341	0	0
		EL	Tumor	Meta
Ava. Fold changes over normal	PgR B	208.6187	0	0
STDV		29.721	0	0

7.3.3 Source data for Figure 16

		Ahnak	Nfatc3	Baz2a	Nr3c1	Nr3c2
Fold change	**EL**	3.70928	62.36703	76.14834	14.46	44.49096
	Avarage of other stages	0.930677	14.07462	18.25849	2.755	20.10031

		Ahnak	Nfatc3	Baz2a	Nr3c1	Nr3c2
Fold change	**EL/Other Stages**	3.985572	4.431169	4.170571	5.248639	2.213447

7.3.4 Source data for Figure 17

	Ahnak			Baz2a			Nfatc3			Nr3c1			Nr3c2		
	F.C	Ava	S.D	F.C	Ava	S.D	F.C	Ava	S.D	F.C	Ava	S.D	F.C	Ava	S.D
P 1n	3.10			2.84			3.87			4.35			2.48		
P 1n	4.02	3.86	0.70	3.05	3.27	0.56	4.06	4.22	0.45	2.01	3.66	1.43	3.37	3.53	1.14
P 1n	4.46			3.91			4.73			4.60			4.74		
P 10n	7.15			4.09			7.24			5.88			2.94		
P 10n	5.22	6.35	1.01	3.47	3.71	0.33	5.06	5.70	1.34	4.77	4.57	1.43	4.56	3.58	0.87
P 10n	6.69			3.58			4.80			3.05			3.23		
P 100n	2.81			2.83			2.30			4.99			2.92		
P 100n	2.69	2.68	0.13	2.06	2.37	0.41	2.21	2.21	0.09	3.39	4.46	0.92	2.39	2.52	0.35
P 100n	2.56			2.22			2.13			4.99			2.26		
E 1n	2.07			2.64			1.96			0.60			1.79		
E 1n	0.56	1.00	0.93	0.91	1.35	1.13	0.73	1.04	0.81	0.13	0.68	0.59	0.99	1.11	0.63
E 1n	0.38			0.50			0.42			1.29			0.56		
E 10n	0.35			0.84			0.92			0.45			0.88		
E 10n	0.26	0.32	0.05	0.49	0.80	0.29	0.70	0.83	0.12	0.67	0.74	0.33	0.47	0.80	0.30
E 10n	0.34			1.07			0.88			1.10			1.06		
E 100n	0.43			0.87			0.88			4.72			0.77		
E 100n	0.49	0.53	0.12	0.95	1.00	0.16	0.82	0.89	0.07	0.67	4.73	4.06	1.06	1.00	0.21
E 100n	0.67			1.18			0.96			8.80			1.16		
C 1n	0.97			1.92			1.05			2.10			1.54		

C 1n	0.67	0.61	0.39	1.19	1.16	0.78	1.30	0.91	0.48	1.59	1.39	0.84	1.54	1.18	0.63
C 1n	0.20			0.36			0.37			0.46			0.45		
C 10n	2.13			1.88			1.63			1.03			2.78		
C10 n	0.99	1.30	0.73	1.63	1.67	0.19	1.38	1.30	0.37	0.35	1.64	1.68	2.74	2.26	0.86
C 10n	0.77			1.50			0.90			3.54			1.27		
C 100n	0.73			1.00			1.57			1.71			1.98		
C 100n	0.68	0.67	0.05	0.87	1.19	0.45	1.32	1.64	0.35	4.73	2.19	2.33	1.65	1.50	0.57
C 100n	0.62			1.71			2.01			0.14			0.87		
A 1n	0.37			0.47			0.68			1.91			1.02		
A 1n	0.43	0.38	0.05	0.57	0.77	0.44	0.55	0.68	0.12	0.90	1.04	0.81	1.12	1.08	0.05
A 1n	0.34			1.28			0.80			0.30			1.10		
A 10 n	0.59			0.71			1.27			1.44			0.92		
A 10 n	0.49	0.48	0.12	0.82	0.83	0.12	0.91			0.12	0.78	0.66	1.03	1.03	0.12
A 10n	0.36			0.95			0.54	0.91	0.37	0.78			1.15		
A 100n	0.24			0.35			0.32			2.15			0.43		
A 100n	0.78	0.50	0.27	1.06	0.74	0.36	1.46	0.84	0.57	2.08	1.61	0.87	1.09	0.80	0.34
A 100 n	0.49			0.81			0.74			0.60			0.89		
T 1n	0.15			0.33			0.29			1.41			0.56		
T 1n	1.07	0.54	0.47	1.16	0.65	0.45	1.11	0.66	0.42	2.88	2.72	1.23	1.20	0.78	0.37
T 1n	0.40			0.46			0.57			3.85			0.57		
T 10n	0.46			0.85			0.61			1.15			0.76		
T 10n	0.72	0.74	0.30	1.03	1.10	0.29	3.09	1.71	1.27	10.63	4.40	5.40	0.90	1.10	0.46
T 10n	1.05			1.42			1.42			1.42			1.63		
T 100n	0.63			1.20			1.08			0.90			1.56		
T 100n	0.40	0.68	0.32	1.12	1.53	0.65	0.69	1.31	0.76	7.73	7.55	6.56	0.71	1.50	0.76
T 100n	1.03			2.28			2.16			14.01			2.23		

7.3.5 Source data for Figure 18

		F.C	F.C	F.C	Ava	S.D
EL + P 10 nM	**Ahnak**	6.75	7.95	5.87	6.86	1.04
	Baz2a	3.99	4.82	5.41	4.74	0.72
	Nfatc3	7.81	8.35	5.64	7.27	1.43
	Nr3c1	4.69	4.13	5.50	4.78	0.69
	Nr3c2	3.32	4.18	5.16	4.22	0.92
PT + P 10 nM	**Ahnak**	0.75	1.12	1.34	1.07	0.30
	Baz2a	2.31	1.47	1.49	1.76	0.48
	Nfatc3	1.91	1.44	1.60	1.65	0.24
	Nr3c1	1.70	1.38	2.17	1.75	0.40
	Nr3c2	1.54	0.73	1.31	1.19	0.42
BALB/c 9 week + P 10 nM	**Ahnak**	0.63	1.53	0.35	0.84	0.62
	Baz2a	1.08	1.17	0.62	0.96	0.30
	Nfatc3	0.87	0.85	1.23	0.98	0.21
	Nr3c1	1.32	0.94	0.99	1.08	0.20
	Nr3c2	1.22	0.80	2.25	1.42	0.75

7.3.6 Source data for Figure 20

		Ahnak	Baz2a	Nfatc3	Nr3c1	Nr3c2
4T1 + P 10 nM	**F.C**	4.16	2.26	3.22	2.85	6.34
	F.C	3.46	3.96	3.98	3.65	3.91
	F.C	6.07	3.32	4.91	2.57	6.31
	Avarage	4.56	3.18	4.03	3.03	5.52
	STDV	1.35	0.86	0.85	0.56	1.40
67 NR + P 10 nM	**F.C**	0.52	1.36	0.88	0.85	2.27
	F.C	1.68	0.36	1.63	0.21	1.96
	F.C	1.23	1.17	0.20	1.85	0.70
	Avarage	1.15	0.96	0.90	0.97	1.64
	STDV	0.58	0.53	0.72	0.83	0.83
MM3MG + P 10 nM	**F.C**	0.85	1.35	0.79	1.88	1.19
	F.C	0.42	0.98	0.28	1.29	0.20
	F.C	1.12	0.28	1.19	1.15	1.99
	Avarage	0.80	0.87	0.75	1.44	1.13
	STDV	0.36	0.55	0.45	0.39	0.90

7.3.7 Source data for Figure 22A

		RANKL	PR-B	RANK	PR-AB	Wnt4
PT	F.C over BALB/c 8 weeks	0.073379	0.047211	5.801532	0.073954	0.282293
	F.C over BALB/c 8 weeks	0.060608	0.018318	3.059312	0.045026	0.423197
	F.C over BALB/c 8 weeks	0.065862	0.021409	3.513204	0.076778	0.346117
	F.C over BALB/c 8 weeks	0.057023	0.004176	4.36578	0.012949	0.040008
	F.C over BALB/c 8 weeks	0.06581	0.002233	3.36532	0.005121	0.025176
	F.C over BALB/c 8 weeks	0.048834	0.003552	4.53501	0.009891	0.031748
	Average	0.061919	0.01615	4.106693	0.037286	0.191423
	STDV	0.008473	0.017279	1.01212	0.032685	0.179982
BC25	F.C over BALB/c 8 weeks	1.047678	0.066336	2.559649	0.253217	1.537883
	F.C over BALB/c 8 weeks	1.629696	0.07048	3.793036	0.25452	1.781822
	F.C over BALB/c 8 weeks	1.144393	0.368142	1.30888	0.618066	0.935191
	F.C over BALB/c 8 weeks	0.726294	0.428503	1.081007	0.397734	0.73835
	Average	1.137016	0.233365	2.185643	0.380884	1.248311
	STDV	0.373926	0.192071	1.253332	0.172052	0.492135
EL	F.C over BALB/c 8 weeks	1.257038	1.197372	1.213167	1.985999	1.970796
	F.C over BALB/c 8 weeks	0.407788	1.917504	0.685221	1.097554	1.681374
	F.C over BALB/c 8 weeks	0.410486	1.141827	1.520089	1.660511	2.77821
	F.C over BALB/c 8 weeks	0.704514	1.326455	3.601131	1.004109	2.400692
	Average	0.694957	1.39579	1.754902	1.437043	2.207768
	STDV	0.399757	0.356305	1.278201	0.466896	0.481619

7.3.8 Source data for Figure 22B

		AHNAK	Baz2a	Nfatc3	Nr3c1	Nr3c2
P (10 nM)	F.C over untreated samples	3.242072	3.506522	3.984192	3.203381	3.335428
Wnt4 (5 ng)	F.C over untreated samples	2.697961	3.285782	2.914412	2.6797	3.381309
RANKL (50 ng)	F.C over untreated samples	3.302766	3.268202	3.216782	2.677282	3.736106
Wnt4 + RANKL	F.C over untreated samples	5.713623	4.85313	4.241014	3.870453	5.859924
P (10 nM)	STDV	0.35047	0.573533	0.186473	0.63028	0.169092
Wnt4 (5 ng)	STDV	0.246244	0.081637	0.616441	0.590552	0.171418
RANKL (50 ng)	STDV	0.49816	0.177999	0.091672	0.180908	0.414212
Wnt4 + RANKL	STDV	2.470851	0.085592	0.061453	0.224216	0.565216

7.3.9 Source data for Figure 23B

%PgR+ cells in ductal structures of 12 weeks old FVB mouse		%PgR+ cells in ductal structures of 5 weeks old FVB mouse	
PgR in Proximal	PgR in Distal	PgR in Proximal	PgR in Distal
13.2	37.5	16.5	36.6
9.4	18.5	23	41.1
10.6	22.6	24	40.6
5.6	33.3	22.7	29.2
5.1	23.5	25.3	40.7
21.7	43.5	18.7	36.6
16.7	45.5	18.1	27.8
9.8	69.2	12.5	32.3
20.5	34.8	4.3	21
19.2	30.2	5.6	30.1
9.6	22.3	22.8	22
2.6	33.3	2.3	36.8
9.9	41.4	39.3	37.2
5.8	21.1	29.2	39.3
12.8	29.1	29.5	37.3
13	22.7	21.1	40.4
9.9	32.8	29.2	36.5
17.9	28.7	41.3	48.5
44.4	63.2	42.9	43.8
	42.7	29	36.6
		32.3	24.5
			44.7

Average	13.56315789	34.795	23.31428571	35.61818182
SEM	2.112	3.002	2.451	1.55

7.3.10 Source data for Figure 24B

EL	Migration assay for cells isolated from spheres (sphere digestion)				
	Repli 1	Repli 2	Repli 3	Ava	S.D
Control	128	119	100	115.7	14.29
PR 10 nm	390	340	380	370	26.46
Wnt4 5ng	270	200	240	236.7	35.12
RANKL 50ng	250	200	280	243.3	40.41
Wnt4+RANKL	340	430	460	410	62.45

PT	Repli 1	Repli 2	Repli 3	Average	STDV
Control	18	25	13	18.67	6.028
PR 10 nm	15	14	11	13.33	2.082
Wnt4 5ng	13	10	4	9	4.583
RANKL 50ng	6	8	10	8	2
Wnt4+RANKL	0	0	0	0	0

7.3.11 Source data for Figure 24D

EL	Migration assay for cells isolated from primary cells				
	Repli 1	Repli 2	Repli 3	Ava	S.D
Control	67	33	45	48.33333	17.24336
PR 10 nm	109	110	89	102.6667	11.84624
Wnt4 5ng	84	110	100	98	13.11488
RANKL 50ng	186	113	153	150.6667	36.55589
Wnt4+RANKL	198	289	240	242.3333	45.54485
PT	Repli 1	Repli 2	Repli 3	Average	STDV
Control	66	72	80	72.66667	7.023769
PR 10 nm	36	24	30	30	6
Wnt4 5ng	30	22	25	25.66667	4.041452
RANKL 50ng	33	53	40	42	10.14889
Wnt4+RANKL	9	8	7	8	1

7.3.12 Source data for Figure 25A

	Sphere number	Ava	S.D
Balb-C 9W	1000	870.4	135.7509
	965		
	937		
	750		
	700		
Balb-C 25W	600	515.8333	65.60615
	460		
	500		
	575		
	530		
	430		
Balb-NeuT 9weeks	1280	1357.273	116.6114
	1410		
	1440		
	1230		
	1460		
	1250		
	1250		
	1530		
	1250		
	1530		
	1300		
Balb-NeuT PT	750	692.2222	136.178
	670		
	600		
	490		
	620		
	600		
	950		
	800		
	750		

7.3.13 Source data for Figure 26B

EL	PT	Week 4	Week 8	Week 25	Week 40
40.3	0	28.2051	42.3	15.7	2.8
39.7	0	27.2727	59.2	27.4	5.5
56.7	0	29.8507	50.5	31.1	4.3
64.3	0	32.7273	54.2	16.9	18.5
55.1	0	27.2727	35.7	19.2	13.7
42.2	0	15.5556	45	29.4	4.6
58.7	0	21.0526	38.8	37.3	2.5
48.2	0	40	49.1	12.7	9.3
46.1	0	21.0526	34.4	22.5	5.4
42.8	0	24.3902	42.6	20.6	3.6
51.7	0	20.4	56.9	25.8	5.8
49	0	27.8	39.3	28.1	4.1
45.5	0	32.6	35.4	19.5	8.4
47.4	0	26.3	54.5	22.4	4.6
53.7	0		43.6	22.6	2.1
47.6	0		49.2	26.7	12.4
39.1	0		38.4	17.3	3.8
	0		49.4	25.2	9.9
	0		45.1	24.1	
	0		42.3		
	0				
	0				
	0				
	0				
	0				
	0				
	0				
	0				
Ava 48.7	0	26.7485	45.295	23.39	6.73889
S.D 7.17	0	6.17204	7.35659	5.978	4.45832

	EL	Average	STDV	PT	Average	STDV
Control	1320	1367.667	160.8861	630	706.6667	83.11638
	1236			695		
	1547			795		
PR	1920	2133.333	265.0157	650	673.3333	68.06859
	2430			620		
	2050			750		
Wnt4	1725	1748.333	121.6895	370	443.3333	114.2731
	1640			385		
	1880			575		
RANKL	1930	2385	417.3428	300	343.3333	83.86497
	2750			290		
	2475			440		
W+R	2720	2906.667	573.2655	180	240	65.57439
	2450			230		
	3550			310		

7.3.15 Source data for Figure 28c

	PT	PT + P 10 nM	EL	EL + P 10 nM
Sphere	0	2	32	60
	3	1	45	65
	1	0	40	69
Avarage	1.333333	1	39	64.66666667
STDV	1.527525	1	6.557439	4.509249753

single cell migration	25	35	125	225
	30	37	101	210
	35	34	110	260
Avarage	30	35.33333333	112	231.6666667
STDV	5	1.527525232	12.12436	25.6580072

7.3.16 Source data for Figure 29B

	Replication	Average	STDV
	220		
	240	250	29.4392
	250		
MM3MG	290		
	160	135	21.79449
	120		
MM3MG-PgR B	125		
	125		
MM3MG-PgR B +P 10 nM	170	145	22.91288
	140		
	580		
	410	536.6667	111.5049
MM3MG-Her2	620		

7.3.17 Source data for Figure 29C

	Replication	Average	STDV
	47		
	49		
MM3MG	43	47	5.477226
	55		
	41		
	29		
	25		
MM3MG-PgR	19	22.2	4.604346
	19		
	19		
	7		
	6		
MM3MG-PgR + P (10 nM)	17	12	5.147815
	14		
	16		
	126		
	98		
MM3MG-Her2	93	109.75	16.66083
	122		

155

7.3.18 Source data for Figure 30B

	Control	P (10 nM)	Wnt4 + Rankl	MM3MG-PgR B
	220	450	900	755
	240	430	840	970
	250	385	730	650
	290		1100	1000
Average	250	421.6666667	892.5	843.75
STDV	29.43920289	33.29164059	155.2149048	169.0845449

7.3.19 Source data for Figure 30C

	Replication	Average	STDV
Control	47	47	5.477226
	49		
	43		
	55		
	41		
P 10 nM	63	61.4	6.580274
	55		
	58		
	72		
	59		
W+R	85	85.6	15.46932
	96		
	64		
	104		
	79		

7.3.20 Source data for Figure 30E

	Control	P (10 nM)	Wnt4 + Rankl	MM3MG-PgR B
	580	280	30	100
	410	330	50	90
	620	450	70	70
Average	536.6666667	353.3333333	50	86.66666667
STDV	111.5048579	87.36894948	20	15.27525232

156

7.3.21 Source data for Figure 30F

	Replication	Average	STDV
MM3MG-Her2	126	109.75	16.66083
	98		
	93		
	122		
MM3MG-Her2 + P	93	94	7.245688
	102		
	84		
	100		
	91		
MM3MG-Her2 + Wnt4+RANKL	45	44.2	8.467585
	39		
	58		
	43		
	36		

7.3.22 Source data for Figure 31

	Migration assay and inhibitors				
	Cont	P	P+Wi	P+Ri	P+Wi+Ri
Progesterone (10 nM)		√	√	√	√
nAB-Rankl (1 µg/ml)				√	√
IWP-2 (3 nM)			√		√
Replicate 1	340	456	156	245	125
Replicate 2	270	390	213	275	79
Replicate 3	230	532	187	192	85
Average	280	459.3333	185.3333	237.3333	96.33333
STDV	55.67764	71.05866	28.53653	42.02777	25.00667

	Sphere culture and inhibitors				
	Cont	P 10 nM	P+Wi	P+Ri	P+Wi+Ri
Progesterone 10 nM		√	√	√	√
nAB-Rankl 1 µg/ml				√	√
IWP-2 3 nM			√		√
Replicate 1	39	66	13	29	9
Replicate 2	43	69	19	20	7
Replicate 3	35	95	26	21	11
Average	39	76.66667	19.33333	23.33333	9
STDV	4	15.94783	6.506407	4.932883	2

7.3.23 Source data for Figure 32A

Day	MM3MG				MM3MG + WR				MM3MG-Her2				MM3MG-Her2 + WR			
1	0.03	0.02	0.04	0.02	0.02	0	0.02	0.01	0.04	0.04	0.025	0.05	0.01	0	0.01	0.01
2	0.22	0.18	0.23	0.2	0.08	0	0.01	0.01	0.16	0.11	0.21	0.19	0.23	0.17	0.21	0.19
3	0.23	0.34	0.25	0.33	0.18	0.1	0.21	0.18	0.37	0.3	0.455	0.35	0.54	0.76	0.95	0.79
4	0.39	0.37	0.42	0.36	0.34	0.3	0.39	0.36	0.66	0.64	0.795	0.57	1.72	1.27	1.57	1.65
5	0.7	0.64	0.87	0.79	0.61	0.6	0.56	0.63	1.2	0.98	1.38	0.94	2.15	1.85	2.06	1.78
6	1.35	1.15	1.25	1.23	0.96	0.8	0.85	0.73	2.15	1.95	1.85	1.65				

7.3.24 Source data for Figure 32B

Days	EL							
	Control				Wnt4 & RANKL			
1	23	20	28	13	19	17	22	14
2	10	26	18	33	24	14	22	16
3	50	66	60	55	40	74	70	100
4	150	142	136	140	90	104	96	85
5	235	208	258	208	86	115	116	167
6	232	248	327	259	195	253	271	175
7	320	368	327	347	320	266	226	253
8	392	383	468	402	268	323	256	290

Days	PT							
	Control				+ Wnt4 & RANKL			
1	0.009	0.011	0.003	0.006	0.005	0.015	0.012	0.01
2	0.013	0.009	0.01	0.014	0.018	0.011	0.016	0.012
3	0.028	0.036	0.024	0.026	0.045	0.055	0.06	0.04
4	0.055	0.04	0.053	0.045	0.062	0.075	0.065	0.065
5	0.075	0.08	0.092	0.1	0.097	0.108	0.096	0.099
6	0.122	0.161	0.118	0.14	0.21	0.156	0.16	0.16
7	0.294	0.276	0.295	0.286	0.4	0.36	0.37	0.43
8	0.356	0.396	0.355	0.409	0.507	0.487	0.5	0.48

7.3.25 Source data for Figure 33B

	Replication	Average	STDV
Control	685	535.3333	134.9308
	498		
	423		
WR	107	68.66667	33.38163
	46		
	53		
WR+LAP 10 nM	108	94	10.55146
	83		
	95		
	90		
WR+LAP 100 nM	470	456.25	57.93315
	430		
	530		
	395		
WR+LAP 100 nM	783	694.6667	78.25812
	634		
	667		
WR+LAP 1 µM	164	248.5	57.84174
	265		
	295		
	270		

7.3.26 Source data for Figure 36A

Time to form Tumor (week)	
Gland Model	Tumor Model
15.29	6
16.57	6
16.57	6
16.71	7
16.71	8
16.71	8
16.71	8
16.71	8
17	8
17	8
17	8
17	9.5
17	9.5
17.86	9.5
17.86	9.5
17.86	10
17.86	11
17.86	12.9
17.86	14.5
18	17
18	17
18	17
18	17
18.14	17
18.29	22
18.29	23
18.29	23
18.71	23
18.71	23
18.71	23
18.71	26
18.86	26
18.9	26
18.86	26
19	26
19.29	

19.57
19.71
19.71
19.71
19.71
20
20
20
20.4
20.4
20.4
20.4
20.4
20.4
20.4
20.57
20.57
20.57
20.57
20.57
20.57
20.7
20.7
20.86
21
21
21
21.43
21.43
21.43
21.57
21.57
21.57
21.71
21.86
22
22
22.71
23
23
23
23

23.43
23.43
23.43
23.43
23.43
23.5
23.5
23.5
23.7
23.86
23.86
24
24.43
24.43
24.7
24.9
24.9
24.86
25
25
25.14
25.14
25.43
25.43
26
26
26
26
26.29
26.29
26.29
26.29
26.43
26.5
26.5
26.86
27
27.14
27.14
27.14
28.43
29

29
29
29.71
29.86
30.71
31.43
31.57
32
32
33.5
33.5
33.5
33.5
33.5
35.43
35.7
35.7
35.7
35.7
36.43
36.57
36.57
37.43
38.57
39.29
39.29
39.29
39.29
42.29
42.86
51.29

7.3.27 Source data for Figure 36B

Time after curative surgery (week)	
Gland Model	Tumor Model
3.14	3.14
4.14	3.14
6.71	3.14
6.86	18.3
8.71	35.57
9.43	6
9.43	6
11.57	6
11.57	6
11.86	6
11.86	6
11.86	31.14
11.86	14.57
11.86	31.14
12	21.29
12.43	10.86
12.71	18
12.71	9.9
12.71	14
12.71	17.9
12.86	17.9
13.29	17.9
13.29	17.9
13.43	23.71
13.43	24.29
13.43	21.86
13.71	23.71
13.71	23.71
13.71	23.71
13.71	23.71
13.71	17
13.71	24.29
13.71	17
13.86	18.86
13.86	24.29
14.14	
14.57	

14.57
14.57
14.57
14.57
14.57
14.57
14.57
14.86
15.14
15.14
15.57
15.57
15.57
15.57
15.57
15.57
15.57
15.57
15.57
15.57
15.57
16
16
16.3
16.29
16.29
16.29
16.29
16.57
16.57
16.57
16.86
16.86
16.86
16.86
16.86
16.86
17.9
17.9
17.9
17.9
18

18.14
18.14
18.71
18.71
18.7
18.71
18.71
18.71
18.71
18.71
18.71
18.7
19.43
19.43
19.43
19.43
19.57
19.57
19.57
19.57
19.57
19.57
19.57
19.57
19.57
19.57
19.57
19.57
19.57
19.71
19.71
19.71
19.71
19.71
19.71
19.71
19.71
19.71
19.71
19.71
19.71

19.71
19.71
20.1
20.14
20.14
20.3
21
21
21
21
21
21.14
21.14
21.14
21.3
21.43
23.43
23.43
24.43
24.43
24.43
24.57
24.57
24.57
24.57
24.57
26.43
26.57
28.57
28.57

7.3.28 Source data for Figure 36D

	Gland model	Tumor Model
Number of Met+ mice	101	10
Number of Met- mice	50	25

	Gland model	Tumor Model
% of Met+ mice	67	29
% of Met- mice	33	71

7.3.29 Source data for Figure 37A

Time to tumor formation (Week)	
Gland Model	Tumor Model
15.29	14.5
16.57	17
16.57	17
16.71	17
16.71	17
16.71	17
16.71	22
16.71	23
17	23
17	23
17	23
17	23
17	26
17.86	26
17.86	26
17.86	26
17.86	26
17.86	
17.86	
18	
18	
18	
18	

18.14
18.29
18.29
18.29
18.71
18.71
18.71
18.71
18.86
18.9
18.86
19
19.29
19.57
19.71
19.71
19.71
19.71
20
20
20
20.4
20.4
20.4
20.4
20.4
20.4
20.4
20.57
20.57
20.57
20.57
20.57
20.57
20.7
20.7
20.86
21
21
21
21.43
21.43

21.43
21.57
21.57
21.57
21.71
21.86
22
22
22.71
23
23
23
23
23.43
23.43
23.43
23.43
23.43
23.5
23.5
23.5
23.7
23.86
23.86
24
24.43
24.43
24.7
24.9
24.9
24.86
25
25
25.14
25.14
25.43
25.43
26
26
26
26
26.29

26.29
26.29
26.29
26.43
26.5
26.5
26.86

7.3.30 Source data for Figure 37B

	Gland model	Tumor Model
Number of Met+ mice	77	7
Number of Met- mice	37	10

	Gland model	Tumor Model
% of Met+ mice	67.5	41.2
% of Met- mice	32.5	58.8

7.3.31 Source data for Figure 37c

Time after curative surgery (week)	
Gland Model	Tumor Model
15.57	14
11.57	17.9
19.57	17.9
19.57	17.9
19.71	17.9
19.71	23.71
19.71	24.29
26.57	21.86
9.43	23.71
14.57	23.71
14.57	23.71
14.57	23.71
14.57	17

11.57	24.29
16.57	17
19.57	18.86
19.57	24.29
19.57	
19.57	
14.57	
18.71	
18.71	
21.3	
21.14	
13.86	
15.57	
15.57	
13.71	
15.14	
15.14	
19.71	
14.57	
18.7	
24.43	
20.3	
16.86	
15.57	
12.43	
13.29	
19.57	
19.57	
18.71	
18.71	
18.71	
3.14	
13.71	
13.71	
13.71	
13.71	
13.71	
13.71	
14.57	
19.57	
19.57	
19.57	

19.71
19.71
21
21
18
19.43
19.43
19.43
4.14
14.86
21.14
12.86
21
21
28.57
21.43
18.14
18.14
14.57
13.29
16.3
16.57
19.43
19.57
24.57
24.57
24.57
24.57
18.71
18.71
18.71
17.9
24.43
24.43
21.14
15.57
15.57
17.9
17.9
17.9
19.71
18.7

20.1
16
16
15.57
15.57
9.43
14.14
16.29
16.29
19.57
20.14
20.14
28.57
19.71
16.29
16.29
16.57

7.3.32 Source data for Figure 38A

Size of Tumors 8 weeks after transplantation of 50 spheres	
EL	**PT**
0	462
0	225
0	350
0	230
0	380
0	220
0	210
0	0
0	160
0	175
0	362
0	60
0	144
0	128
0	0
0	504
0	0
	120
	125
	160
	235
	512
	120

7.3.33 Source data for Figure 38

	EL (number)	PT (number)
DCC+	15	13
DCC-	2	10

	EL	PT
%Seeding	88	56
%non-seeding	12	44

7.3.34 Source data for Figure 38C

Number of DCCs/1 milion bone marrow cells	
EL	**PT**
8	1
4	1
4	1
7	2
2	2
3	1
2	1
1	3
2	5
3	4
5	3
5	2
8	1
6	0
2	0
0	0
0	0
	0
	0
	0
	0
	0
	0

7.3.35 Source data for Figure 39A

Number of DCCs/1 milion bone marrow cells			
EL in 4 Week	EL in 40 Week	PT in 4 Week	PT in 40 Week
8	2	2	1
4	1	1	3
4	2	1	5
7	3	1	2
3	5	1	4
2	5	0	3
8		0	2
6		0	1
2		0	0
0		0	0
0		0	0
		0	

7.3.36 Source data for Figure 39B

Day	PT in 4 Weeks					
33	1	0	0	1	0	1
40	12	2	1	12	1	18
45	27	24	4	45	8	48
50	72	60	18	60	24	60
60	462	225	350	230	380	220

	PT in 40 Weeks					
33	0	0	0	0	0	0
40	1	0	1	0	2	0
45	2	0	2	6	15	0
50	12	0	12	18	60	30
60	210	0	160	175	362	60

7.3.37 Source data for Figure 41A

	Day until start of differentiation			
	EL	**EL + P**	**PT**	**PT + P**
	25	13	0	0
	21	14	0	0
	22	14	0	0
	17	16	0	0
	20	15	0	0
Average	21	14.4	0	0
STDV	2.91548	1.1402	0	0

7.3.38 Source data for Figure 42A

Number of DCC in 10^6 BM 4 weeks after transplantation		
PT	**PT + MM3MG**	**PT + MM3MG-Pgr-B**
2	5	0
0	1	0
1	2	0
0	5	1
3	0	1
5		
0		
4		
3		
2		
2		
1		
0		

7.3.39 Source data for Figure 42B

	Number of mice with tumor 4 week after transplantation (mice from ED Fig 6h)		
	PT	**PT + MM3MG-PgR B**	**PT + MM3MG**
No-Tumor	23	0	4
Tumor	0	5	1

7.3.40 Source data for Figure 43A

Number of DCC in 10^6 BM cells at the end of prgnancy or age matched controls	
Pregnant	Control
3	1
3	2
6	3
5	0
4	1
	3

7.3.41 Source data for Figure 43C

Week	Pregnant					Control				
15	0	0	0	0	0	0	0	0	0	0
16	0	1	2	0	1	0	0	1	0	0
17	2	3	5	2	3	0	0	2	0	1
18	6	8	10	7	9	1	0	3	0	2
19						2	1	5	1	4
20						5	3	7	3	7
21						8	6	10	6	10

7.3.42 Source data for Figure 47A

	Ava. of F.C over PT	
	PgR expression	STDV
EL	2.075048328	0.289
EL/PT Transwell	0.851787162	0.18

7.3.43 Source data for Figure 47B

	PgR expression in T47D cell line	STDV
T47D	1	0
T47D+ TUBO C.M	0.512747447	0.18918074

7.3.44 Source data for Figure 47C

	Ava. of F.C over untreated samples	
	PR expression in T47D	**STDV**
Exosome Free	1.006617111	0.068550279
Exosome	0.473436482	0.009902528

7.3.45 Source data for Figure 49A

	Fold change over control	
	PR expression	**STDV**
mmu-miR-30a-5p	0.698423688	0.036945
mmu-miR-30a-3p	0.901668247	0.033377
mmu-miR-21a-5p	0.916871994	0.08526
mmu-miR-25-3p	1.022307605	0.021711
mmu-miR-92a-3p	1.141797736	0.15066
mmu-miR-340-5p	0.98533219	0.108733
mmu-miR-9-5p	0.70764369	0.114005
mmu-miR-92a-1-5p	1.050305835	0.049744
mmu-miR-21a-3p	0.840751989	0.16917
mmu-miR-9-5p+30a-5p	0.593328938	0.024271

7.3.46 Source data for Figure 50A

	Fold change over LD	
	TUBO Cells H.D	**STDV**
miR9-5p	5.438969491	0.528617966
miR30a-5p	1.561933827	1.030378309

7.3.47 Source data for Figure 50B

	Fold change over BALB/c 8 weeks	
	miR9-5p	**STDV**
EL	2.525896176	0.041212
PT	31.07053776	5.753632

	Fold change over BALB/c 8 weeks	
	miR30a-5p	**STDV**
EL	4.227355831	1.616353
PT	5.303869328	1.784827

7.3.48 Source data for Figure 51

	TUBO low and high density (replication of F.C)				
	Ahnak	**Baz2a**	**Nfatc3**	**Nr3c1**	**Nr3c2**
Tubo low density + P 10 nM	5.49	6.47	5.61	3.26	2.36
	4.83	7.21	9.51	3.55	1.60
	6.67	4.12	8.06	4.25	1.87
avarage	5.66	5.93	7.73	3.69	1.94
STDV	0.93	1.62	1.97	0.51	0.38
	Ahnak	**Baz2a**	**Nfatc3**	**Nr3c1**	**Nr3c2**
Tubo high density + P 10 nM	2.09	1.08	1.64	1.26	0.51
	1.51	1.30	1.30	1.25	1.31
	1.62	1.29	1.52	1.62	0.71
avarage	1.74	1.23	1.49	1.38	0.84
STDV	0.31	0.12	0.17	0.21	0.41

	PT low and high density (replication of F.C)				
	Ahnak	**Baz2a**	**Nfatc3**	**Nr3C1**	**Nr3C2**
PT LD + P 10 nM	3.03	4.71	2.64	2.86	1.74
	4.60	3.33	2.71	3.66	2.74
	2.14	3.07	3.63	3.41	2.52
avarage	3.26	3.70	2.99	3.31	2.34
STDV	1.25	0.88	0.55	0.41	0.53
	Ahnak	**Baz2a**	**Nfatc3**	**Nr3c1**	**Nr3c2**
PT HD + P 10 nM	0.71	1.38	1.90	2.07	1.45
	1.32	1.54	1.54	1.32	1.42
	1.12	2.28	1.44	1.95	0.71
avarage	1.05	1.73	1.63	1.78	1.19
STDV	0.31	0.48	0.24	0.40	0.42

7.3.49 Source data for Figure 52A

High Density migration assay				Low Density migration assay			
50000/well	Replicates	Average	STDV	10,000/well	Replicates	Average	STDV
Control	460			Control	40		
Control	370			Control	21		
Control	590	473.3333	110.6044	Control	27	29.33333	9.712535
P 10 nM	20			P 10 nM	264		
P 10 nM	15	11.66667	10.40833	P 10 nM	480		
P 10 nM	0			P 10 nM	335	359.6667	110.0924
W+R	25			W+R	480		
W+R	10	13.33333	10.40833	W+R	560	570.6667	96.44342
W+R	5			W+R	672		

7.3.50 Source data for Figure 52B

High Density migration assay				Low Density migration assay			
10,000/ml	Replication	Average	STDV	1000/ml	Replication	Average	STDV
Control	347			Control	38		
Control	400			Control	53		
Control	368	368.2	27.26	Control	43	43.6	11.371
Control	336			Control	56		
Control	390			Control	28		
P 10 nM	119			P 10 nM	50		
P 10 nM	116			P 10 nM	58		
P 10 nM	105	124.25	22.65	P 10 nM	77	58.75	12.7377
P 10 nM	157			P 10 nM	50		
W+R	47			W+R	120		
W+R	70			W+R	165		
W+R	41	51.5	12.71	W+R	115	145	32.4037
W+R	48			W+R	180		

7.3.51 Source data for Figure 53A

	Ava of F.C of Her2 over HME cells	STDV
BT549	0.439825198	0.001078
HME	1	0
HS 578T	1.013147581	0.174786
HCC1937	1.274073581	0.093585
ZR751	2.42645187	0.833344
MDA-MB-231	3.55316947	0.48593
MDA MB 468	4.692809347	0.367636
MCF10A	6.229922992	1.068481
MCF7	7.127599989	4.372407
Cama1	8.064003248	1.482832
HCC1806	34.41797381	0.787163
T47D	50.54810834	4.459325
MDA MB175	57.177583	2.708012
HCC 1569	205.485518	29.43602
SKBR3	354.8043092	99.24162
BT474	662.4819615	60.59161

7.3.52 Source data for Figure 53B

	Ava. of F.C of miR9-5p over HME	STDV
BT549	3.332729133	2.037336
HME	1	0
HS 578T	0.226085392	0.036505
HCC1937	21.83154001	0.107002
ZR751	106.872075	18.93185
MDA-MB-231	0.391158887	0.041634
MDA MB 468	66.76928103	3.706991
MCF10A	0.093280954	0.003002
MCF7	12.39652289	4.906299
Cama1	1.607976502	0.480337
HCC1806	110.4093464	9.278767
T47D	0.216578678	0.060437
MDA MB175	99.25929019	13.25799
HCC 1569	979.4099291	114.3389
SKBR3	68.72797286	3.371164
BT474	2.782005856	0.015207

7.3.53 Source data for Figure 54A

	Ava. F.C of Her2 in HD over LD	STDV
BT549	1.04303084	0.048548
HME	3.733749588	0.860825
HS 578T	1.15832182	0.3872
HCC1937	1.974467715	0.125722
ZR751	3.553361794	0.524979
MDA-MB-231	2.427640738	0.625865
MDA MB 468	1.291626798	0.096228
MCF10A	4.47689248	0.854279
MCF7	2.529896913	0.967495
Cama1	0.793578071	0.366488
HCC1806	2.26539331	0.345621
T47D	2.891377052	0.505508
MDA MB175	1.110787107	0.249401
HCC 1569	0.953091487	0.788232
SKBR3	2.722359114	0.722432
BT474	2.030684445	0.393527

7.3.54 Source data for Figure 54B

	miR9-5p fold change over LD	STDV
BT549	1.660599383	1.015143
HME	0.985094022	0
HS 578T	0.285673612	0.046127
HCC1937	1.687641728	0.008272
ZR751	0.419887416	0.074381
MDA-MB-231	0.545881602	0.058102
MDA MB 468	0.625368851	0.03472
MCF10A	0.620309314	0.01996
MCF7	2.04520326	0.592239
Cama1	0.375941388	0.112302
HCC1806	1.601272114	0.13457
T47D	0.531741309	0.148385
MDA MB175	0.948660357	0.126712
HCC 1569	0.091272532	0.010655
SKBR3	6.490731411	0.318376
BT474	0.293437561	0.001604

7.3.55 Source data for Figure 55

			Migration assay				Ava	S.D			Sphere assay				Ava	S.D
BT474	LD	Control	4	5	0	9	4.5	3.7	HD	Control	68	64	72	56	65	6.83
		WR	65	76	75	94	77.5	12.1		WR	320	325	287	364	324	31.5
		P	5	0	10	7	5.5	4.2		P	59	36	45		46.7	11.6
	HD	Control	54	37	49	30	42.5	11	HD	Control	359	330	307	410	352	44.4
		WR	10	8	0	6	6	4.32		WR	48	65	58	36	51.8	12.6
		P	33	45	60		46	13.5		P	360	395	450		402	45.4
HCC1937	LD	Control	11	16	13	19	14.8	3.5	HD	Control	11	16	13	19	14.8	3.5
		WR	21	28	19	23	22.8	3.86		WR	21	28	19	23	22.8	3.86
		P	10	18	15		14.3	4.04		P	10	18	15		14.3	4.04
	LD	Control	202	180	169		184	16.8	HD	Control	202	180	169		184	16.8
		WR	85	123	153		120	34.1		WR	85	123	153		120	34.1
		P	193	159	207		186	24.7		P	193	159	207		186	24.7
HCC1806	LD	Control	3	3	15	11	8	6	HD	Control	32	22	26	38	29.5	7
		WR	28	38	30	23	29.8	6.24		WR	40	49	54	58	50.3	7.76
		P	5	12	7	6	7.5	3.11		P	29	27	30		28.7	1.53
	LD	Control	153	95	79	168	124	43.4	HD	Control	188	163	195	203	187	17.3
		WR	0	6	15	14	8.75	7.09		WR	127	115	109	138	122	12.9
		P	96	137	109	69	103	28.3		P	168	209	232		203	32.4
MCF10A	LD	Control	6	3	7	2	4.5	2.38	HD	Control	6	3	7	2	4.5	2.38
		WR	10	13	12	9	11	1.83		WR	10	13	12	9	11	1.83
		P	5	8	6		6.33	1.53		P	5	8	6		6.33	1.53
	LD	Control	121	139	142	132	134	9.33	HD	Control	121	139	142	132	134	9.33
		WR	70	63	85	76	73.5	9.33		WR	70	63	85	76	73.5	9.33
		P	132		125	155	137	15.7		P	132		125	155	137	15.7
HS587T	LD	Control	19	38	38		31.7	11	HD	Control	33	31	27		30.3	3.06
		WR	12	13	29		18	9.54		WR	33	35	39		35.7	3.06
		P	75	83	94		84	9.54		P	53	44	39		45.3	7.09
	LD	Control	343	393	267		334	63.4	HD	Control	198	191	180		190	9.07
		WR	204	152	166		174	26.9		WR	233	228	240		234	6.03
		P	28	52	17		32.3	17.9		P	167	199	211		192	22.7
Cama1	LD	Control	29	25	16		23.3	6.66	HD	Control	107	83	94		94.7	12
		WR	22	28	36		28.7	7.02		WR	75	67	63		68.3	6.11
		P	55	63	49		55.7	7.02		P	81	104	85		90	12.3
	LD	Control	243	176	269		229	48	HD	Control	304	278	240		274	32.2
		WR	236	323	287		282	43.7		WR	236	323	287		282	43.7
		P	54	15	39		36	19.7		P	265	232	287		261	27.7
MDA-	LD	Control	700	550	450		567	126	HD	Control	17	14	13		14.7	2.08

Cell		Treatment					Mean	SD		Treatment					Mean	SD
MB231		**WR**	3000	2500	2800		2767	252		**WR**	26	23	28		25.7	2.52
		P	500	450	200		383	161		**P**	14	16	18		16	2
	LD	**Control**	5400	6000	5000		5467	503	**HD**	**Control**	240	257	262		253	11.5
		WR	2000	3000	1500		2167	764		**WR**	176	157	205		179	24.2
		P	6000	5500	4000		5167	1041		**P**	238	271	233		247	20.6
MDA-MB468	**LD**	**Control**	4	0	0		1.33	2.31	**HD**	**Control**	25	21	27		24.3	3.06
		WR	10	7	0		5.67	5.13		**WR**	29	25	19		24.3	5.03
		P	39	28	26		31	7		**P**	29	19	26		24.7	5.13
	LD	**Control**	78	50	43		57	18.5		**Control**	112	173	142		142	30.5
		WR	293	153	123		190	90.7	**HD**	**WR**	106	152	166		141	31.4
		P	0	0	0		0	0		**P**	132	169	159		153	19.1
MCF7	**LD**	**Control**	5	9	24		12.7	10		**Control**	72	86	65		74.3	10.7
		WR	83	54	68		68.3	14.5	**HD**	**WR**	95	103	115		104	10.1
		P	42	6	16		21.3	18.6		**P**	112	103	123		113	10
	LD	**Control**	40	38	63		47	13.9		**Control**	203	243	251		232	25.7
		WR	0	0	0		0	0	**HD**	**WR**	139	166	129		145	19.1
		P	0	0	0		0	0		**P**	189	198	167		185	15.9
SKBR3	**LD**	**Control**	0	0	0		0	0		**Control**	90	84	63		79	14.2
		WR	67	13	29		36.3	27.7	**HD**	**WR**	92	71	79		80.7	10.6
		P	15	4	3		7.33	6.66		**P**	81	76	73		76.7	4.04
	LD	**Control**	11	8	14		11	3		**Control**	673	437	566		559	118
		WR	0	0	0		0	0	**HD**	**WR**	634	511	599		581	63.4
		P	0	0	0		0	0		**P**	518	598	627		581	56.5

7.3.56 Source data for Figure 57A

	DTC-	DTC+	total	ratio
PR (IRS0-1)	362	138	500	0.276
PR (IRS2-8)	582	183	765	0.239216
PR (IRS9-12)	771	203	974	0.208419

7.3.57 Source data for Figure 57B

	DTC-	DTC+	total	ratio
Her2 (0-1)	885	254	1139	0.223003
Her2 (2)	583	172	755	0.227815
Her2 (+2/3)	247	98	345	0.284058

7.3.58 Source data for Figure 58

PGR IRS	HER2 IHC Negative	HER2 IHC positive	Her2 amplification
0-1	61	35	42
2-8	73	82	28
9-12	120	55	28
	Total	Total	Total
PGR IRS	HER2 IHC Negative	HER2 IHC positive	Her2 amplification
0-1	218	140	142
2-8	313	334	118
9-12	608	281	85

7.3.59 Source data for Figure 60

Fold changes over HER2^{neg}/PGR^{high}			
miR9-5p		miR30a-5p	
HER2^{amp}/PGR^{neg}	HER2^{amp}/PGR^{high}	HER2^{amp}/PGR^{neg}	HER2^{amp}/PGR^{high}
9.800163	0.893665	19.72178	1.812007
40.58306	2.325927	1.861951	2.148928
26.96107	2.959927	9.366719	4.774659
35.32961	0.618912	37.95895	0.732072
18.41495	5.474798	14.70425	1.585505
12.72738	1.162963	1.58832	1.668068
1.869164	0.708483	4.803932	0.80778
15.6664		2.322775	
11.71772		4.593411	

7.4 Supplementary data4

All source figures of protein blotting which used to generate figures for result section are listed here for each figure separately.
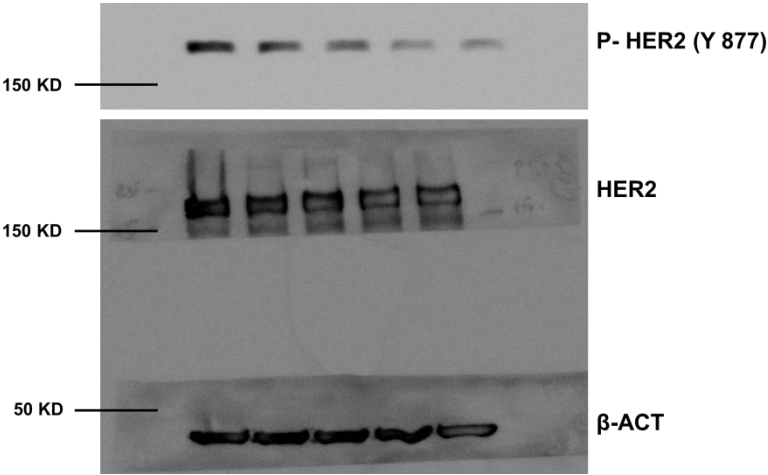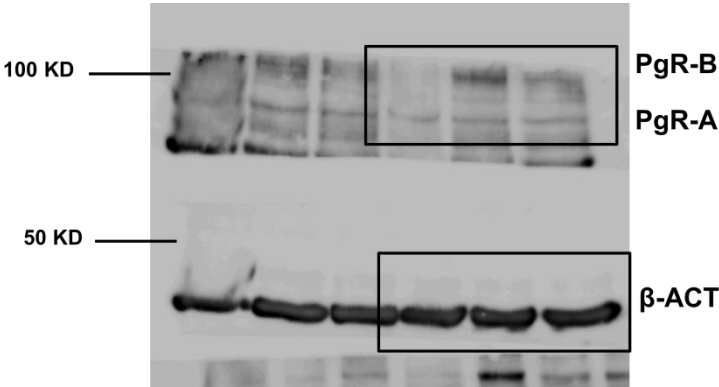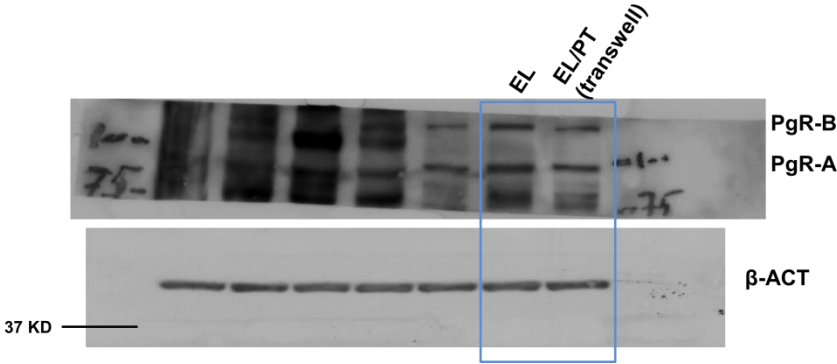
7.4.1 Source blotting figure 21A
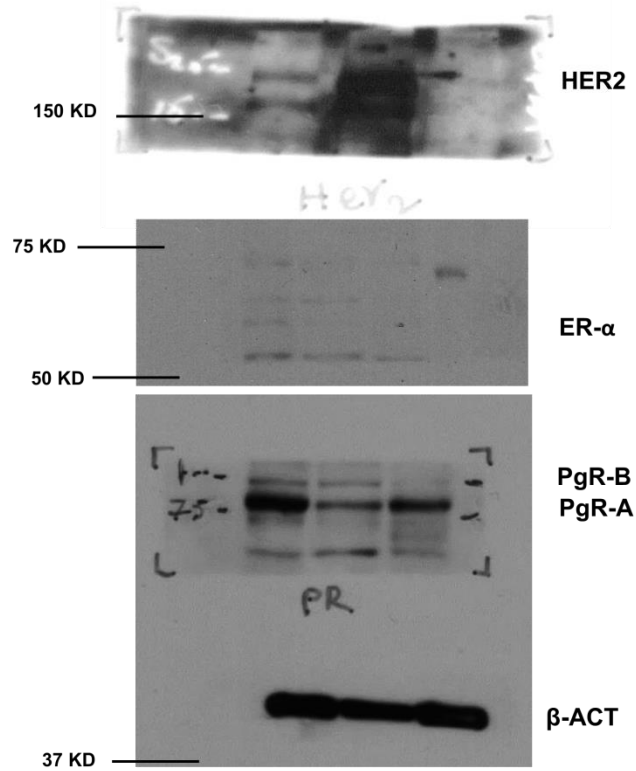
7.4.2 Source blotting figure 21B
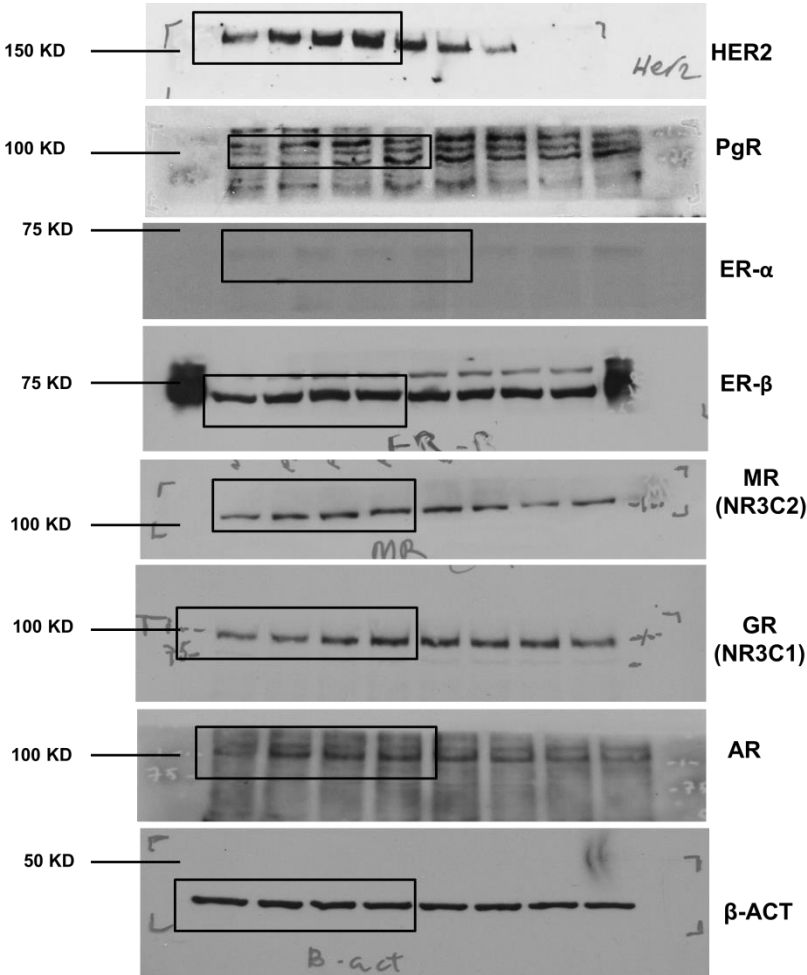
7.4.3 Source blotting figure 21C

7.4.4 Source blotting figure 21D

150 KD ——————   HER2

100 KD ——————   PgR-B
                       PgR-A

β-ACT

37 KD ——————

7.4.5 Source blotting figure 21E

150 KD ——————   HER2

100 KD ——————   PgR-B
                       PgR-A

β-ACT

37 KD ——————
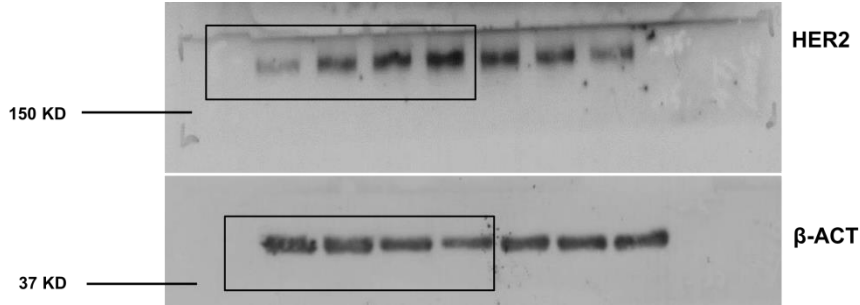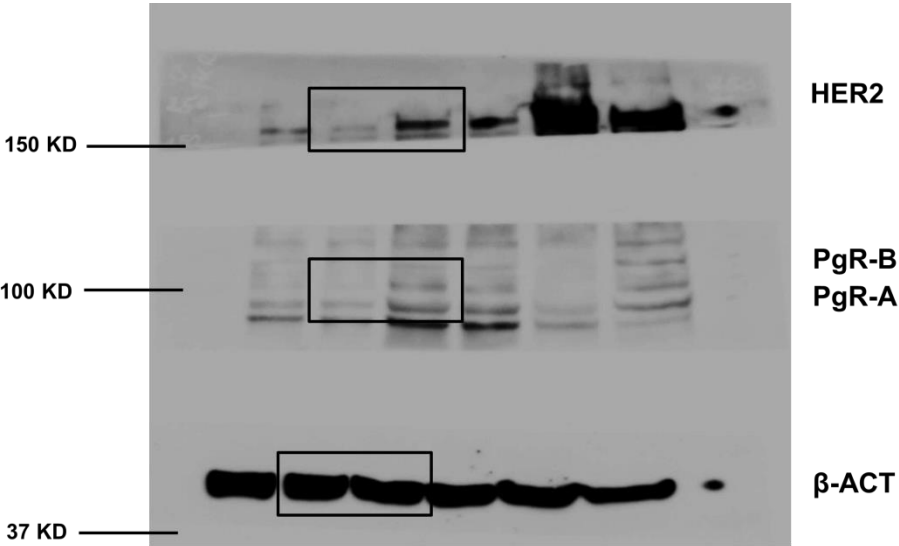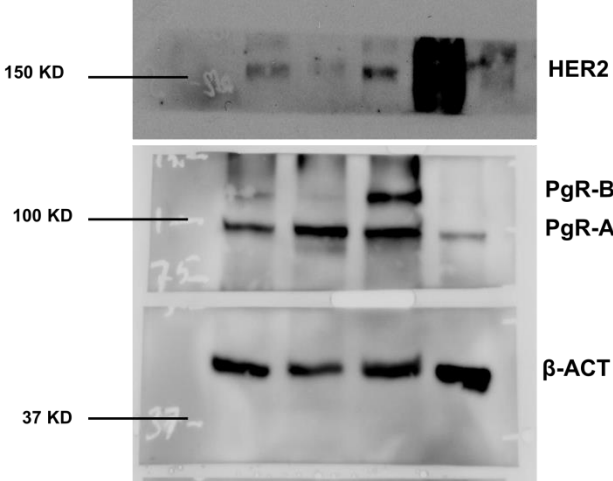
7.4.6 Source blotting figure 33A

P- HER2 (Y 877)

150 KD

HER2

150 KD

50 KD

β-ACT

7.4.7 Source blotting figure 46B

100 KD

PgR-B

PgR-A

50 KD

β-ACT

7.4.8 Source blotting figure 47B

EL   EL/PT (transwell)

PgR-B

PgR-A

β-ACT

37 KD

7.4.9   Source blotting figure 47D

PGR-B
PGR-A
100 KD
50 KD
β-ACT
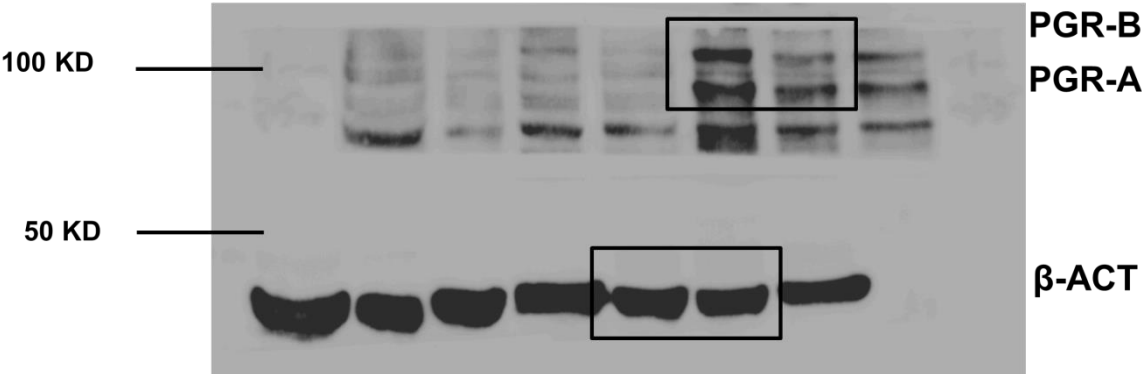
7.4.10 Source blotting figure 49B

PgR-B
PgR-A
100 KD
50 KD
β-ACT
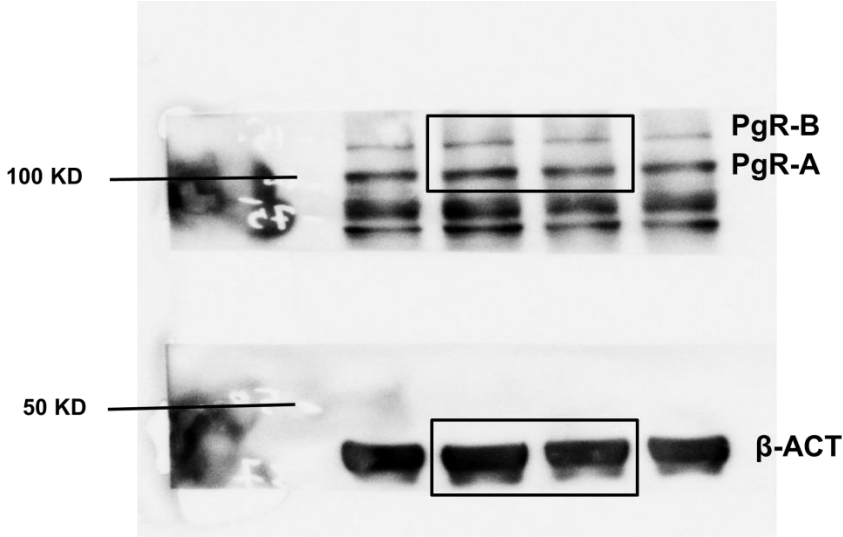
7.4.11 Source blotting figure 54A
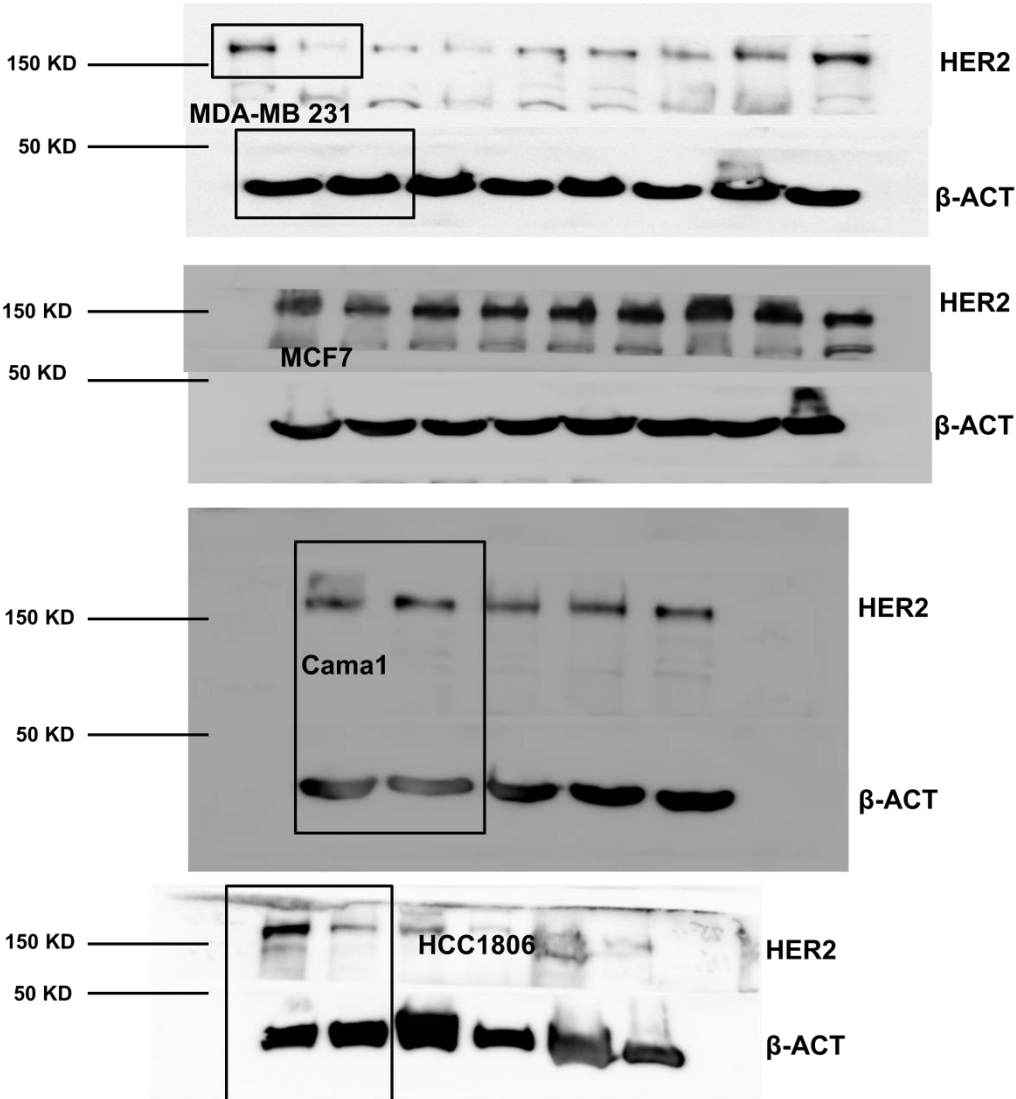
8 Acknowledgment

Firstly, I would like to express my sincere gratitude to my advisor Prof. Christoph A. Klein for the continuous support of my Ph.D study and related research, for his patience, motivation, and immense knowledge. His guidance helped me in all the time of research and writing of this thesis. I could not have imagined having a better advisor and mentor for my Ph.D study.

Besides my advisor, I would like to thank the rest of my thesis committee: Prof. Gunter Meiste and Prof. Peter Nelson for their insightful comments and encouragement, but also for the hard question which incented me to widen my research from various perspectives. Also, I thank my fellow labmates for the stimulating discussions, for the all technical helps, and for all the fun we have had in the last six years. Dr. Lahiri Kanth Nanduri generously helped me at the start of project and shared all his experiences. Dr. Milan Obradovic, Dr. Christian Werno, Carolin Ehrl, and Christian Reimelt helped me with in vivo experiments. Dr. Martin Hoffmann and Dr. Matthias Maneck helped me with the bioinformatic analyses. Nina Patwary and Dr. Gundula Haunschild helped me with the in house pateint data analyses. Dr. Florian Weber and Rudolf Jung kindly helped me with immunohistochemistry stainings. Dr. Andreas Hartkopf, Dr. Florin-Andrei Taran, provided me pateint data. Thanks to Prof. Gunter Meister's lab and specially Norbert Eichner for miRNA sequencing experiment. Thanks to Dr. Kathryn Harpe and Dr. Maria Soledad Sosa from Prof. Julio A. Aguirre-Ghiso's lab for analysing role of PgR on morphogenesis experiments. Special thanks to Dr. Christian Werno and Dr. Miodrag Guzvic for their usfol comments and suggestion for this thesis.

Last but not the least, I would like to dedidicate this work to my family the best of univers: Nikoo, Rayan and Hannah for the love they created on my heart, supporting me spiritually throughout all steps of this thesis and all momments of my life.

Curriculum Vitae

Hedayatollah Hosseini

Date of birth: **30.05.1979**   Place of birth: **Ramhormoz, Iran**
Citizenship: **Iranian**
Phone: **+49 (0)941 944 6718**   Fax: **+49 (0)941 944 6719**
E-mail: Hedayatollah.Hosseini@ukr.de

Academic degrees and Education

2011 - 09/2016 Ph.D. student (Biomedicine) at the Faculty of Biology, University of Regensburg, Germany

09/2003 - 02/2006 MSc. (Molecular Biology and Genetic) at the Faculty of Biology, University of Shahid Chamran, Ahwaz, Iran

09/1998 - 06/2003 Undergraduate student (Molecular Biology and Genetic), at the Faculty of Biology, University of Shahid Chamran, Ahwaz, Iran

Publications

1. Hosseini H, Ahani A, Galehdari H, Foroughmand. Frequent loss of heterozygosity at 8p22 chromosomal region in diffuse type of gastric cancer **WJGNET 2007- volume 13; issue 24: 3354-3358**

2. **Hosseini H**, Obradovic M, Harper K, Sosa MS, Kanth Nanduri L, Werno C, Hoffmann M, Ehrl C, Maneck M, Patway N, Haunschild G, Gužvić M, Werner-Klein M, Reimelt C, Eichner N, Weber F, Hartkopf A, Taran FA, Brucker SY, Fehm T, Rack B, Buchholz S, Meister G, Aguirre-Ghiso JA, Klein CA. **Cell density, Her2 and progesterone signalling regulate dissemination of breast cancer cells. DOI 10.1038/nature20785**

3. Harper K. L, Soledad Sosa M, Entenberg D, **Hosseini H**, Avivar-Valderas A, Nagi C, Davis R.J, Farias E.F, Condeelis J, Klein C.A, and Aguirre-Ghiso J.A. **Mechanism of early dissemination and metastasis during early stages of HER2+ mammary cancer. DOI 10.1038/nature20609.**

Awards & scholarships

2003 11th position between >8000 participants in the 8th Olympiad of Biology in IRAN

2005 Research grant from gastroenterology research center of Shahid beheshti university, Tehran, Iran

2007 Research Grant from Jundi shapour University of Ahwaz, Iran

2009 Research fellow from Japan science administration

2016 Proffered paper presentation at 24th EACR meeting at Manchester

Abstracts, posters Conferences

17.09.2011 - 20.09.2011; 3rd SPP1190 The tumor-vessel Interface, Kloster Seeon Meeting
Poster presentation: Molecular mechanism of early metastatic dissemination in breast cancer.

12.05.2012 - 16.05.2012; 4th SPP1190 The tumor-vessel Interface, Usedom.

03.10.2013 - 06.10.2013; Advances in Breast Cancer Research: Genetics, Biology, and Clinical Applications, Sand Diago USA. **Poster** presentation: Molecular mechanism of early metastatic dissemination in breast cancer.

26.12.2013 - 27.12.2013; Iranian Cancer Genetics Congress, Hematology-Oncology and Stem Cell Transplantation Research Centre. Title of **talk**: Parallel progression of primary tumor and metastasis.

08.06.2014 - 13.06.2014; Gordon Research Conference on Mammary Gland Biology. **Poster** presentation: Molecular Mechanism of Early Dissemination in Breast Cancer

27.06.2014 - 01.07.2014; 15th International Biennial Congress of the Metastasis Research Society. **Poster** presentation: Molecular Mechanism of Early Dissemination in Breast Cancer

01.06.2016 - 03.06.2016; Selection and adaptation during cancer progress. Title of **talk**: Cell density, Her2 and progesterone signalling regulate dissemination of breast cancer cells

09.07.2016 - 12.07.2016; 24th Biennial Congress of the European Association for Cancer Research (EACR24).Title of **talk**: Cell density, Her2 and progesterone signalling regulate dissemination of breast cancer cells

Referees

Prof. Christoph Klein
Chair of Experimental Medicine and
Therapy Research
Department of Pathology
University Hospital Regensburg
University of Regensburg, Regensburg, Germany
E-mail: christoph.klein@klinik.uni-regensburg.de

Prof. Gunter Meister
Biochemistry Center Regensburg (BZR),
Laboratory for RNA Biology,
University of Regensburg,
Regensburg, Germany
gunter.meister@vkl.uni-regensburg.de

Two related papers to this work.

ARTICLE

Early dissemination seeds metastasis in breast cancer

Hedayatollah Hosseini[1], Milan M. S. Obradović[1]†, Martin Hoffmann[2], Kathryn L. Harper[3], Maria Soledad Sosa[3]†, Melanie Werner-Klein[4], Lahiri Kanth Nanduri[1]†, Christian Werno[2], Carolin Ehrl[1], Matthias Maneck[1], Nina Patwary[1], Gundula Haunschild[1], Miodrag Gužvić[1], Christian Reimelt[1], Michael Grauvogl[5], Norbert Eichner[6], Florian Weber[7], Andreas D. Hartkopf[8], Florin-Andrei Taran[8], Sara Y. Brucker[8], Tanja Fehm[9], Brigitte Rack[10], Stefan Buchholz[11], Rainer Spang[5], Gunter Meister[6], Julio A. Aguirre-Ghiso[3] & Christoph A. Klein[1,2]

Accumulating data suggest that metastatic dissemination often occurs early during tumour formation, but the mechanisms of early metastatic spread have not yet been addressed. Here, by studying metastasis in a HER2-driven mouse breast cancer model, we show that progesterone-induced signalling triggers migration of cancer cells from early lesions shortly after HER2 activation, but promotes proliferation in advanced primary tumour cells. The switch from migration to proliferation was regulated by increased HER2 expression and tumour-cell density involving microRNA-mediated progesterone receptor downregulation, and was reversible. Cells from early, low-density lesions displayed more stemness features, migrated more and founded more metastases than cells from dense, advanced tumours. Notably, we found that at least 80% of metastases were derived from early disseminated cancer cells. Karyotypic and phenotypic analysis of human disseminated cancer cells and primary tumours corroborated the relevance of these findings for human metastatic dissemination.

LETTER

Mechanism of early dissemination and metastasis in Her2+ mammary cancer

Kathryn L. Harper[1]*, Maria Soledad Sosa[1]*, David Entenberg[2], Hedayatollah Hosseini[3], Julie F. Cheung[1], Rita Nobre[1], Alvaro Avivar-Valderas[1], Chandandaneep Nagi[1], Nomeda Girnius[4], Roger J. Davis[4], Eduardo F. Farias[1], John Condeelis[2], Christoph A. Klein[3,5] & Julio A. Aguirre-Ghiso[1]

Metastasis is the leading cause of cancer-related deaths and these lesions develop from disseminated cancer cells (DCCs) that can remain dormant[1]. Metastasis-initiating cells are thought to originate from a subpopulation present in progressed, invasive tumours[2]. However, DCCs detected in patients before the manifestation of breast-cancer metastasis contain fewer genetic abnormalities than primary tumours or than DCCs from patients with metastases[3–5]. These findings, and those in pancreatic cancer[6] and melanoma[7] models, indicate that dissemination might occur during the early

for β-catenin (Fig. 1c). Overall, these results suggest that Her2+ cells display a loss of E-cadherin- and β-catenin-based junctions and are p-ATF2^{lo}.

Overt MMTV–Her2 tumours showed low levels of E-cadherin, phosphorylated p38 (p-p38) and p-ATF2, while maintaining high p-ERK1/2 (p-ERK1 and p-ERK2) levels (Extended Data Fig. 2b–d), suggesting that a Her2+p-ATF2^{lo}E-cad[lo] profile is present in early lesions and primary tumours. We found that only HER2− human ductal carcinoma *in situ* (DCIS) lesions retained both high p-ATF2 expression levels and